Ministry of Education and Science of the Russian Federation
Saint Petersburg National Research University of Information Technologies, Mechanics, and Optics

NANOSYSTEMS:

PHYSICS, CHEMISTRY, MATHEMATICS

2013, volume 4(4)

Special Issue

INTERNATIONAL CONFERENCE "MATHEMATICAL CHALLENGE OF QUANTUM TRANSPORT IN NANOSYSTEMS - 2013. PIERRE DUCLOS WORKSHOP"

Наносистемы: физика, химия, математика
2013, том 4, № 4

NANOSYSTEMS:

PHYSICS, CHEMISTRY, MATHEMATICS

Address: University ITMO, Kronverkskiy pr., 49, St. Petersburg 197101, Russia.
Phone: +7(812)232-67-65, **Journal site:** http://nanojournal.ifmo.ru/,
E-mail: popov1955@gmail.com

AIM AND SCOPE

The scope of the journal includes all areas of nano-sciences. Papers devoted to basic problems of physics, chemistry, material science and mathematics inspired by nanosystems investigations are welcomed. Both theoretical and experimental works concerning the properties and behavior of nanosystems, problems of its creation and application, mathematical methods of nanosystem studies are considered.
The journal publishes scientific reviews (up to 30 journal pages), research papers (up to 15 pages) and letters (up to 5 pages). All manuscripts are peer-reviewed. Authors are informed about the referee opinion and the Editorial decision.

Content

FROM THE EDITORIAL BOARD

In this issue we publish the Proceedings of the International Conference **Mathematical Challenge of Quantum Transport in Nanosystems. "Pierre Duclos Workshop"** organized by Saint Petersburg National Research University of Information Technologies, Mechanics, and Optics in March 2013. This workshop was the eighth of a series which has the aim to bring together specialists in nanosystem modeling, mathematicians and condensed matter physicists

PROGRAM COMMITTEE

Vladimir N. Vasilyev (University ITMO, Russia) – Chairman
Igor Yu. Popov (University ITMO, Russia) – Vice-Chairman
Sergey N. Naboko (St. Petersburg State University, Russia)
Boris S. Pavlov (Massey University, New Zealand)
George P. Miroshnichenko (University ITMO, Russia)

LOCAL ORGANIZING COMMITTEE

Leonid M. Studenikin – Chairman
Igor Yu. Popov – Vice-Chairman
Igor S. Lobanov
Ekaterina S. Trifanova
Irina V. Blinova
Alexander I. Trifanov
Maxim A. Skryabin
Anton I. Popov

INVITED SPEAKERS

Pavel Exner (Prague, Czech Republic)
Horia Cornean (Aalborg, Denmark)
Hagen Neidhardt (Berlin, Germany)
Valentin Zagrebnov (Marseille, France)
Konstantin Pankrashkin (Paris, France)
Mikhail Belishev (St. Petersburg, Russia)
Jaroslav Dittrich (Rez, Czech Republic)
Paul Tackley (Zurich, Switzerland)

THE MAIN TOPICS OF THE CONFERENCE:

Spectral theory
Scattering
Quantum transport
Quantum communications and computations

NANOSYSTEMS: PHYSICS, CHEMISTRY, MATHEMATICS, 2013, 4 (4), P. 446–466

DIFFUSION AND LAPLACIAN TRANSPORT FOR ABSORBING DOMAINS

Ibrahim Baydoun[1], Valentin A. Zagrebnov[2]

[1]École Centrale Paris
2 Avenue Sully Prudhomme, 92290 Chtenay-Malabry, France
[2]Département de Mathématiques - Université d'Aix-Marseille
Laboratoire d'Analyse, Topologie et Probabilités (UMR 7353)
CMI - Technopôle Château-Gombert,
39, rue F. Joliot Curie, 13453 Marseille Cedex 13, France
ib_baydoun1985@hotmail.com, Valentin.Zagrebnov@univ-amu.fr

PACS 47A55, 47D03, 81Q10

We study (stationary) Laplacian transport by the Dirichlet-to-Neumann formalism. Our results concern a *formal* solution of the *geometrically* inverse problem for localisation and reconstruction of the form of absorbing domains. Here, we restrict our analysis to the one- and two-dimensional cases. We show that the last case can be studied by the conformal mapping technique. To illustrate this, we scrutinize the constant boundary conditions and analyze a numeric example.

Keywords: Laplacian transport, Dirichlet-to-Neumann operators, Conformal mapping.

1. Introduction

1. Is is known (see e.g. [8]) that the problem of determining a *conductivity matrix* field $\gamma(p) = [\gamma_{i,j}(p)]_{i,j=1}^{d}$, for p in a bounded open domain $\Omega \subset \mathbb{R}^d$, is related to "measuring" the elliptic *Dirichlet-to-Neumann* map for the associated conductivity equation. Notice that the solution to this problem has numerous practical applications in various domains: geophysics, electrochemistry etc. It is also an important diagnostic tool in medicine, e.g. in the *electrical impedance tomography*; the tissue in the human body is an example of highly anisotropic conductor [1].

Assuming there are no current sources or sinks, the potential $v(p),\ p \in \Omega$, for a given voltage $f(\omega),\ \omega \in \partial\Omega$, on the (smooth) boundary $\partial\Omega$ of Ω is a solution of the Dirichlet problem:

$$(\mathbf{P1}) \qquad \begin{cases} \mathrm{div}(\gamma \nabla v) = 0 \quad \text{in } \Omega, \\ v|_{\partial\Omega} = f \quad \text{on } \partial\Omega. \end{cases}$$

Then, the corresponding (**P1**) Dirichlet-to-Neumann map (operator) $\Lambda_{\gamma,\partial\Omega}$ is (*formally*) defined by [16]

$$\Lambda_{\gamma,\partial\Omega} : f \mapsto \partial v_f/\partial\nu_\gamma := \nu \cdot \gamma\ \nabla v_f\ |_{\partial\Omega}\ . \tag{1.1}$$

Here, ν is the unit *outer-normal* vector to the boundary at $\omega \in \partial\Omega$ and the function $v := v_f$ is a solution of the Dirichlet problem (**P1**).

The Dirichlet-to-Neumann operator (1.1) is also called the *voltage-to-current* map, since the function $\Lambda_{\gamma,\partial\Omega} f$ gives the induced current flux trough the boundary $\partial\Omega$. The key (*inverse*) problem is whether one can determine the conductivity matrix γ by knowing the electrical boundary measurements, i.e. the corresponding Dirichlet-to-Neumann operator. In general, this operator does not determine the matrix γ uniquely, see e.g. [4].

The main question in this context is to find sufficient conditions insuring that the inverse problem is uniquely soluble.

2. The problem of electrical current flux in the form (**P1**) is an example of so-called *diffusive* Laplacian transport [17]. Besides the voltage-to-current problem, the motivation to study of this kind of transport comes for instance from the transfer across *biological membranes*, see e.g. [13], [3].

Let some "species" of concentration $C(p)$, $x \in \mathbb{R}^d$, diffuse stationary in the *isotropic* bulk ($\gamma = I$) from a (distant) source localised on the closed boundary $\partial\Omega$ towards a *semipermeable* compact interface ∂B of the *cell* $B \subset \Omega$, where they disappear at a given rate $W \geq 0$. Then, the *steady* field of concentrations (Laplacian transport with a diffusion coefficient $D \geq 0$) obeys the set of equations:

$$(\mathbf{P2})^* \quad \begin{cases} \Delta C = 0, \ p \in \Omega \setminus \overline{B} \ , \\ C \mid_{\partial\Omega} (p) = C_0, \ \text{a constant concentration at the source } \partial\Omega \ , \\ -D \ \partial_\nu C \mid_{\partial B} (\omega) = W \ (C - C^*) \mid_{\partial B} (\omega), \ \text{on the interface } \omega \in \partial B \end{cases}$$

Usually, one assumes that $C(p) = C^* \geq 0$, $p \in \overline{B}$, is a constant concentration of the "species" inside the cell $\overline{B}$.

This example motivates the following abstract *stationary* diffusive Laplacian transport problem with *absorption* on the surface ∂B:

$$(\mathbf{P2}) \qquad \begin{cases} \Delta u = 0, \ p \in \Omega \setminus \overline{B} \ , (u(p) = Const \, , \ p \in \overline{B}), \\ u \mid_{\partial\Omega} (p) = f(p), \quad p \in \partial\Omega \ , \\ (\alpha \ u + \partial_\nu u) \mid_{\partial B} (\omega) = h(\omega), \quad \omega \in \partial B \ . \end{cases}$$

This is the Dirichlet problem for the domain $\Omega \supset B$ with the Dirichlet-Neumann (or Robin [6]) boundary conditions on the absorbing surface ∂B. Varying α between $\alpha = 0$ and $\alpha = +\infty$ one recovers respectively the Neumann and the Dirichlet boundary conditions.

Now, similar to (1.1), we can associate with the problem **(P2)** a Dirichlet-to-Neumann operator

$$\Lambda_{\gamma=I,\partial\Omega} : f \mapsto \partial_\nu u_f \mid_{\partial\Omega} =: g \ . \tag{1.2}$$

Domain $\mathrm{dom}(\Lambda_{I,\partial\Omega})$ belongs to a certain *Sobolev* space of functions on the boundary $\partial\Omega$, which contains $u_f := U_f^{(\alpha,h)}$, the solutions of the problem **(P2)** for given f and for the Robin boundary condition on ∂B fixed by α and h.

Then, there are at least two (in fact related) *geometrical* inverse problems that are of interest:

(a) Given the Dirichlet data f and the corresponding (measured) Neumann data g (1.2) on the accessible *outer* boundary $\partial\Omega$, to reconstruct the shape of the interior

boundary ∂B.
(b) A simpler inverse problem concerns the localisation of the domain (cell) B of a *given shape* and fixed parameters α and h.

3. The aim of the present paper is to study the above problems (a) and (b) in the framework of application outlined in the problem **(P2)*** and to work out the corresponding formalism based on the Dirichlet-to-Neumann operators.

In Section 2.1 we formulate the mathematical setup of the these problems, and we consider uniqueness of the forward boundary value problem **(P2)** solution. There, we illustrate our strategy by an explicit example of one-dimensional inverse problem for $\Omega \subset \mathbb{R}^1$ and $B = (a, b)$.

Our main results (Section 3) concern the two-dimensional case, when the compact $\Omega \subset \mathbb{R}^2$. Notice that there are three points that need particular attention. The first is that the problems **(P2)*** and **(P2)** are formulated for *non-simply* connected domains $\Omega \setminus \overline{B}$. The second point concerns the peculiarity of the combination of Dirichlet and Robin boundary conditions. As a third point, one has to mention that the *geometrically* inverse problem is *poorly formulated*.

The present paper first presents the *formal* solution for the case when $\alpha = +\infty$, i.e. the Dirichlet boundary conditions $u\,|_{\partial B}\,(\omega) = 0$, $\omega \in \partial B$. For this case, our approach is motivated by important papers [9], [12]. Here we refine their results in the framework of the Dirichlet-to-Neumann formalism and add certain observations in the case of a fixed geometry of domains B and Ω following [2].

In Section 4 we consider an explicit example and give numerical calculation for constant external boundary conditions $f = 1$ to illustrate abstract results for $\alpha = +\infty$.

For finite $\alpha \geq 0$ and $h = 0$ we restrict the discussion to a few remarks, (Section 5) as a more thorough investigation will be presented in future publications. The same concerns our formal scheme for $d = 2$, since the corresponding inverse problem is *ill-posed*.

The case $d = 1$ allows explicit calculations and serves to illustrate of our main ideas, whereas, for solution of the inverse Problems, i.e. for $d = 2$, we use a method of conformal mappings for harmonic functions in doubly connected domains $\Omega \setminus B$.

2. Setup of the Problems and Uniqueness

1. Below, we suppose that Ω and $B \subset \Omega$ be open bounded domains in $\mathbb{R}^d$ with C^2-smooth disjoint boundaries $\partial\Omega$ and ∂B, that is $\partial(\Omega \setminus \overline{B}) = \partial\Omega \cup \partial B$ and $\partial\Omega \cap \partial B = \emptyset$.

Then, the unit *outer-normal* to the boundary $\partial(\Omega\setminus\overline{B})$ vector-field $\nu(p)_{p\in\partial(\Omega\setminus B)}$ is well-defined, and we consider the normal derivative in **(P2)** as the *interior* limit:

$$(\partial_\nu u)\,|_{\partial B}\,(\omega) := \lim_{p\to\omega} \nu(\omega)\cdot(\nabla u)(p)\ ,\ p \in \Omega \setminus \overline{B}\ . \tag{2.1}$$

The existence of the limit (2.1) as well as the restriction $u\mid_{\partial B}(\omega) := \lim_{p\to\omega} u(p)$ is insured since u has to be a harmonic solution of the problem **(P2)** for C^2-smooth boundaries $\partial(\Omega\setminus\overline{B})$, [15].

Now, we introduce some indispensable standard notations and definitions [5]. Let $\mathcal{H}$ be Hilbert space $L^2(M)$ on domain $M\subset\mathbb{R}^d$ and $\partial\mathcal{H} := L^2(\partial M)$ denote the corresponding *boundary space*. By $W_2^s(M)$, we denote the Sobolev space of $L^2(M)$-functions, whose s-derivatives are also in $L^2(M)$, and similar, $W_2^s(\partial M)$ is the Sobolev space of $L^2(\partial M)$-functions on the C^2-smooth boundary ∂M.

Proposition 2.1. *Let $f,h\in W_2^{1/2}(\partial\Omega)$ for C^2-smooth boundaries $\partial(\Omega\setminus B)$. If $\alpha\geq 0$, then the Dirichlet-Robin problem* **(P2)** *has a unique (harmonic) solution in domain $\Omega\setminus\overline{B}$.*

Proof. For existence, we refer to [15]. To prove the uniqueness, we consider the problem **(P2)** for $f=0$ and $h=0$. Then, by the Gauss-Ostrogradsky theorem, the corresponding solution u yields:

$$\int_{\Omega\setminus\overline{B}} dp\ (\nabla\overline{u(p)}\cdot\nabla u)(p)) = \int_{\Omega\setminus\overline{B}} dp\ \mathrm{div}(\overline{u(p)}\ (\nabla u)(p)) =$$
$$\int_{\partial B} d\sigma(\omega)\ \overline{u(\omega)}\ (\partial_\nu u)(\omega) = -\alpha\int_{\partial B} d\sigma(\omega)\ |u(\omega)|^2 \leq 0\ . \qquad (2.2)$$

The estimate (2.2) implies that $u(x\in\Omega\setminus\overline{B}) = Const$. Hence, by the Robin boundary conditions, $(\alpha\, u)\mid_{\partial B}(\omega)=0$, and by virtue of $u\mid_{\partial\Omega}(p) = f(x\in\partial\Omega) = 0$, we obtain that for $\alpha\geq 0$ the harmonic function $u(p)=0$ for $x\in\Omega\setminus\overline{B}$. □

The next statement is key for the analysis of inverse geometrical problems (a) and (b). Since we use it below in the case $\mathbb{R}^2$, our formulation is two-dimensional.

Proposition 2.2. *Consider two problems* **(P2)** *corresponding to a bounded domain $\Omega\subset\mathbb{R}^2$ with C^2-smooth boundary $\partial\Omega$ and to two subsets B_1 and B_2 with the same smoothness of the boundaries ∂B_1, ∂B_2. If for solutions $u^{(1)}_{f,h}$, $u^{(2)}_{f,h}$ of these problems one has*

$$\partial_\nu u^{(1)}_{f,h}\mid_{\partial\Omega} = \partial_\nu u^{(2)}_{f,h}\mid_{\partial\Omega}\ , \qquad (2.3)$$

then $\partial B_1 = \partial B_2$.

Proof. By virtue of $u^{(1)}_{f,h}\mid_{\partial\Omega} = u^{(2)}_{f,h}\mid_{\partial\Omega} = f$ and by condition (2.3), the problem **(P2)** has two solutions for identical external (on $\partial\Omega$) and internal (on ∂B_1 and ∂B_2) Robin boundary conditions. Then, by the standard arguments based on the Holmgren uniqueness theorem [14] for harmonic functions on $\mathbb{R}^2$, one obtains that $\partial B_1 = \partial B_2$. □

2. We finish this section by a simple illustration of the explicit solution of the Inverse Problems (a) and (b) in the one-dimensional case. Motivated by the Laplace transport **(P2)*** we consider the case: $f = c_0$, $h = \alpha\, c^*$, and $\alpha = W/D \geq 0$, for

$\Omega := (-R, R) \subset \mathbb{R}^1$ and $B := (a, b)$:

$$(\mathbf{P_{d=1}}) \qquad \begin{cases} \Delta u = 0, \ x \in (-R, R) \setminus [a, b] \ , \\ u \mid_{\partial\Omega} (x = \mp R) = f(\mp R) =: c_{\mp}, \\ (\alpha \ u + \partial_\nu u) \mid_{\partial[a,b]} (a) = (\alpha \ u + \partial_\nu u) \mid_{\partial[a,b]} (b) = \alpha \, c^* \ , \end{cases}$$

where $R > 0$ and $-R < a < b < R$.

The solution of the problem (a) is straightforward, since in the one-dimensional case, the shape of absorbing cell is trivial: it is the interval $B := (a, b)$.

Now notice that a general solution of the problem $(\mathbf{P_{d=1}})$ is a combination of linear functions supported in domain $\Omega := (-R, R) \setminus [a, b]$ and a constant c^* in the interval $[a, b]$:

$$-R < x < a : \qquad u(x) = -\frac{c_- - c^*}{(R + a) + \alpha^{-1}}(R + x) + c_- \ , \tag{2.4}$$

$$a \leq x \leq b : \qquad u(x) = c^* \ ,$$

$$b < x < R : \qquad u(x) = -\frac{c_+ - c^*}{(R - b) + \alpha^{-1}}(R - x) + c_+ \ . \tag{2.5}$$

Given Dirichlet data c_0 on the boundary $\partial\Omega$ and *measuring* on this boundary the Neumann data in the form of the flux currents:

$$j_- := -\partial_\nu u \mid_{\partial\Omega} (x = -R) = \frac{c_- - c^*}{(R + a) + \alpha^{-1}}$$

$$j_+ := -\partial_\nu u \mid_{\partial\Omega} (x = +R) = -\frac{c_+ - c^*}{(R - b) + \alpha^{-1}},$$

one can explicitly solve both problems (a) and (b).

In the one-dimensional case the *shape* of the cell is defined by its *size*: $(b - a)$, whereas localization is fixed by the points:

$$a = (c_- - c^*)/j_- - R - \alpha^{-1} \ ,$$

$$b = (c_+ - c^*)/j_+ + R + \alpha^{-1} \ .$$

3. Two-Dimensional Inverse Problem: Conformal Mapping and the Shape of ∂B

1. The relevance of the conformal mapping in the study of the boundary value problems for harmonic functions (solutions of the Laplace equation) is well-known, see e.g. [7] (Ch.III), or [11] (Ch.13).

Recall that if the complex function $w : z \mapsto \mathbb{C}$ is holomorphic in the open domain $\{\Omega \subset \mathbb{C} : z = x + i\, y \in \Omega\}$, then by the Cauchy-Riemann conditions the functions $u(x, y) := (\mathrm{Re}\, w)(x, y)$ and $v(x, y) := (\mathrm{Im}\, w)(x, y)$ are harmonic in Ω. Here, $w(z) = u(x, y) + i\, v(x, y)$.

Remark 3.1. *There is an elementary inverse problem of the complex analysis : given a harmonic function $u(x, y)$ in Ω to construct in this domain the harmonic function $v(x, y)$ (harmonic conjugate to u) such that the complex function $w =$*

$u + i\,v$ is holomorphic. In fact, one finds the harmonic conjugate from the Cauchy-Riemann conditions,

$$\partial_x u = \partial_y v \quad , \quad \partial_y u = -\partial_x v \ , \tag{3.1}$$

since for a given u this is a system of partial differential equations for v. Notice that for a simply connected domain Ω, the solution of this system always exists and it is unique up to a constant, whereas in non-simply connected domains the harmonic conjugate may not be a single-valued function. Conversely, in any simply connected subset $\Omega_0 \subset \Omega$, one can select a single-valued branch of this function. Consequently this means a selection of the single-valued branch of the total complex function w.

Application of conformal mappings to the analysis of harmonic functions and the Laplace equation are based on the following observations:

Proposition 3.2. *Let $\zeta : z \mapsto \zeta(z)$ be a conformal mapping $\zeta(z) : N \to M$ by a holomorphic function $\zeta(z) = \xi(x,y) + i\eta(x,y)$. If the function $\widetilde{u}(\xi,\eta)$ is harmonic in M, then the composition*

$$u(x,y) := (\widetilde{u} \circ \zeta)(x,y) = \widetilde{u}(\xi(x,y), \eta(x,y)) \ , \tag{3.2}$$

is a harmonic function of x, y in N.

In particular one obtains:

$$(\Delta_z u)(x,y) = |\partial_z \zeta(z)|^2 \ (\Delta_\zeta \widetilde{u})(\xi(x,y), \eta(x,y)) \ . \tag{3.3}$$

(Here we explicitly distinguish Laplacians in different coordinates, $\Delta_z := \partial_x^2 + \partial_y^2$ and $\Delta_\zeta := \partial_\xi^2 + \partial_\eta^2$, but we ignore these subindexes below, in order to avoid any confusion.) Notice that this statement is based only on a straightforward application of the Cauchy-Riemann conditions for the mapping $\zeta(z)$, i.e. it *does not* assume the existence of a harmonic conjugate neither for $\widetilde{u}$, nor for u. Although, for a simply connected $N_0 \subset N$, one can show that every harmonic function is a *real part* of a branch of holomorphic in N_0 function.

The second observation is related to the Dirichlet-to-Neumann formalism and makes clear the importance of the notion of the *harmonic conjugate* function, [7], Ch.III.

Proposition 3.3. *Let Ω be open simply connected bounded domain in $\mathbb{R}^2$ with a C^2-smooth boundary $\partial\Omega$. Then the solution of the Neumann problem*

$$(\mathbf{P_N}) \qquad \begin{cases} \Delta u = 0, \ p \in \Omega \setminus \overline{B} \ , \\ \partial_\nu u \mid_{\partial\Omega} (p) = g(p), \quad p \in \partial\Omega \ , \end{cases}$$

reduces to the Dirichet problem for the function v, which is harmonic conjugate to the function u.

To make this evident, notice first that the normal derivative here is defined in the sense of (2.1). Let the boundary $\partial\Omega$ be parameterized by the natural parameter of

its arc-length: $\partial\Omega = \{\Gamma(\tau) \in \mathbb{C}\}_{\tau\in[0,l)}$. Then, the Cauchy-Riemann conditions (3.1) imply that

$$\partial_\tau v \mid_{\partial\Omega}(p) = \partial_\nu u \mid_{\partial\Omega}(p) = g(p). \tag{3.4}$$

Since by integration along the contour Γ, one obtains

$$v(p_1) = v(p_0) + \int_{\tau_0}^{\tau_1} d\tau\ \partial_\tau v(\Gamma(\tau)) = v(p_0) + \int_{\tau_0}^{\tau_1} ds\ g(\Gamma(\tau)) =: f(p_1)\ ,$$

the solution of $(\mathbf{P_N})$ is equivalent to the Dirichlet problem $(\mathbf{P_D})$ for v and the boundary conditions f.

2. To outline the main steps in reconstructing the unknown boundary ∂B, we consider first the problem **(P2)** for the Dirichlet case $\alpha = +\infty$:

$$(\mathbf{P}^{\infty}_{\mathbf{d=2}}) \qquad \begin{cases} \Delta u = 0,\ p \in \Omega \setminus \overline{B}\ , \\ u \mid_{\partial\Omega}(p) = f(p), \quad p \in \partial\Omega\ , \\ u \mid_{\partial B}(\omega) = 0, \quad \omega \in \partial B\ . \end{cases}$$

It is well-known, see e.g. [7], [10], that the doubly connected bounded domain $\Omega \setminus \overline{B}$ is the image of a conformal mapping of an annulus

$$A_B := \{z \in \mathbb{C} : 0 < \rho_B < |z| < 1\} \tag{3.5}$$

produced by a bijective holomorphic function $\zeta(z)$. This function maps boundaries to boundaries: $\zeta : C_{\rho_B} \to \partial B$ and $\zeta : C_{r=1} \to \partial\Omega$.

(i) The first step is to find the trace $\zeta \mid_{C_1}$ of the unknown function $\zeta(z)$ on the external unit circle $C_{r=1}$.

(ii) Then the next step is to reconstruct the function $\zeta(z)$ in the whole annulus A_B, which solves the geometrical inverse problem (see Introduction 1.2 (a)) by tracing the boundary ∂B as the limit of ζ from inside: $\partial B = \{\zeta(z)\} \mid_{z\to C_{\rho_B}} := \zeta(C_{\rho_B})$.

(i) Let external boundary in the problem $(\mathbf{P}^{\infty}_{\mathbf{d=2}})$ be parameterized by the natural parameter of its arc-length: $\partial\Omega = \{\Gamma(\tau) \in \mathbb{C}\}_{\tau\in[0,l)}$. Then the trace of the conformal mapping $\zeta : C_1 \to \partial\Omega$ defines by the equation:

$$\zeta(e^{i\phi}) = \Gamma(\tau) \quad , \quad \text{for } \phi \in [0, 2\pi)\ , \tag{3.6}$$

with the condition $\zeta(e^{i\phi}) \mid_{\phi=0} = \Gamma(0)$, a bijective function $\phi : \tau \mapsto \phi(\tau) \in [0, 2\pi)$.

Therefore, to calculate the trace of the function $\zeta(z)$ on the external unit circle $C_{r=1}$ is equivalent to finding a solution $\phi(\tau)$ of (3.6), or the corresponding inverse function $\tau(\phi)$.

To this end, let u_f be a solution of the problem $(\mathbf{P}^{\infty}_{\mathbf{d=2}})$. Then, by Proposition 3.2, the function $\widetilde{u}_{\widetilde{f}} := u_f \circ \zeta$ is harmonic in the annulus A_B and is a solution of the Dirichlet problem

$$(\widetilde{\mathbf{P}}^{\infty}_{\mathbf{d=2}}) \qquad \begin{cases} \Delta\widetilde{u} = 0,\ p \in A_B\ , \\ \widetilde{u} \mid_{C_1}(p) = \widetilde{f}(p)\ , \quad p \in C_1\ , \\ \widetilde{u} \mid_{C_{\rho_B}}(\omega) = 0, \quad \omega \in C_{\rho_B}\ . \end{cases}$$

Here $\widetilde{f}(p) = (f \circ \zeta)(p) = f(\zeta(p)) = f(\xi(x,y), \eta(x,y))$ and $p = (x,y) \in C_1$.

Consider the solution u_f of the Dirichlet problem $(\mathbf{P}^{\infty}_{\mathbf{d=2}})$. Then, the Dirichlet-to-Neumann operator $\Lambda_{\partial\Omega}$ for the external boundary $\partial\Omega$ is defined similarly to (1.2):

$$\Lambda_{\partial\Omega} f = \partial_\nu u_f \mid_{\partial\Omega} =: g \ . \tag{3.7}$$

Let v_f be harmonic conjugate to u_f. Then by (3.4) we obtain that for external boundary $\partial\Omega$

$$\begin{aligned} &\partial_\tau v_f \mid_{\partial\Omega} (\tau) = \partial_\tau v_f(\Gamma(\tau)) = \partial_\nu u_f(\Gamma(\tau)) = (\Lambda_{\partial\Omega} f)(\Gamma(\tau)) = \\ &(\Lambda_{\partial\Omega} f)(\zeta(e^{i\phi(\tau)})) = (\Lambda_{\partial\Omega} f \circ \zeta)(e^{i\phi(\tau)}) \ . \end{aligned} \tag{3.8}$$

With conformal mapping ζ, the relation (3.8) can be rewritten as:

$$\partial_\tau v_f(\Gamma(\tau)) = \partial_\tau v_f(\zeta(e^{i\phi(\tau)})) = \partial_\phi (v_f \circ \zeta)(e^{i\phi(\tau)})) \partial_\tau \phi(\tau) \ . \tag{3.9}$$

Since $\widetilde{u}_{\widetilde{f}} := u_f \circ \zeta$ and $\widetilde{v}_{\widetilde{f}} := v_f \circ \zeta$, see $(\widetilde{\mathbf{P}}^{\infty}_{\mathbf{d=2}})$, by (3.4), we obtain

$$\partial_\phi (v_f \circ \zeta)(e^{i\phi})) = \partial_\phi \widetilde{v}_{\widetilde{f}}(\phi) = \partial_\nu \widetilde{u}_{\widetilde{f}} \mid_{C_1} (\phi) = \Lambda_{C_1}(f \circ \zeta)(e^{i\phi}) \ , \tag{3.10}$$

with a usual convention about the normal derivative $\partial_\nu(\cdot) \mid_{C_1}$ on the unit circle C_1. Here, $\Lambda_{C_1} : \widetilde{f} \mapsto \partial_\nu \widetilde{u}_{\widetilde{f}} \mid_{C_1}$ is the Dirichlet-to-Neumann operator corresponding to the problem $(\widetilde{\mathbf{P}}^{\infty}_{\mathbf{d=2}})$.

Relations (3.8)-(3.10) yield the following differential equation for $\phi = \phi(\tau)$:

$$\partial_\tau \phi = \frac{(\Lambda_{\partial\Omega} f \circ \zeta)(e^{i\phi})}{\Lambda_{C_1}(f \circ \zeta)(e^{i\phi})} \ . \tag{3.11}$$

For a given boundary Γ, the solution $\phi(\tau)$ of equation (3.11) gives a trace of the function $\zeta(z)$ on the circle C_1. Indeed, by (3.6), we obtain that on C_1 it is defined by:

$$\zeta(e^{i\phi}) = \Gamma(\tau(\phi)) \quad , \quad \text{for } \phi \in [0, 2\pi) \ , \tag{3.12}$$

where $\tau(\phi)$ is the function, which is inverse to $\phi(\tau)$.

3. Hence, for a fixed boundary Γ, one can in principle find the trace $\zeta(z) \mid_{C_1}$ using the scheme outlined above. To this end, let $\widetilde{f} \in W_2^1(C_1)$, where we identify C_1 with $[0, 2\pi]$, see problem $(\widetilde{\mathbf{P}}^{\infty}_{\mathbf{d=2}})$. Then, the solution of this problem takes the form:

$$\begin{aligned} &\widetilde{u}_{\widetilde{f}}(\rho, \phi) = a_0 \ln \rho + b_0 + \\ &\sum_{n=1}^{\infty} \left[(a_n \rho^n + b_n \rho^{-n}) \cos n\phi + (c_n \rho^n + d_n \rho^{-n}) \sin n\phi \right] \ , \end{aligned} \tag{3.13}$$

The coefficients in expansion (3.13) are equal to the following:

$$a_n = \frac{\widetilde{f}_{1,n}}{(1 - \rho_B^{2n})} \ , \ b_n = -\frac{\rho_B^{2n} \widetilde{f}_{1,n}}{(1 - \rho_B^{2n})} \ , \ a_0 = -\frac{\widetilde{f}_{1,0}}{\ln \rho_B} \ , \quad b_0 = \widetilde{f}_{1,0} \ , \tag{3.14}$$

$$c_n = \frac{\widetilde{f}_{2,n}}{(1 - \rho_B^{2n})} \ , \ d_n = -\frac{\rho_B^{2n} \widetilde{f}_{2,n}}{(1 - \rho_B^{2n})} \ . \tag{3.15}$$

They are related to the Fourier series coefficients for $\widetilde{f}(\phi)$:

$$\widetilde{f}_{1,0} = \frac{1}{2\pi}\int_0^{2\pi} d\phi \widetilde{f}(\phi),\ \widetilde{f}_{1,n} = \frac{1}{\pi}\int_0^{2\pi} d\phi \widetilde{f}(\phi)\cos n\phi,\ \widetilde{f}_{2,n} = \frac{1}{\pi}\int_0^{2\pi} d\phi \widetilde{f}(\phi)\sin n\phi.$$

Then, the corresponding Dirichlet-to-Neumann operator (3.10) acts as a bounded operator from $W_2^1(C_1)$ to $L^2(C_1)$:

$$\Lambda_{C_1}\widetilde{f}(\phi) = \partial_\nu \widetilde{u}_{\widetilde{f}}\,|_{C_1}\,(\phi) = \tag{3.16}$$
$$-\frac{\widetilde{f}_{1,0}}{\ln \rho_B} + \sum_{n=1}^{\infty}\, n\left[(a_n - b_n)\cos n\phi + (c_n - d_n)\sin n\phi\right]\ .$$

By (3.10) and (3.16), we obtain the identity:

$$\int_0^{2\pi} d\phi \Lambda_{C_1}\widetilde{f}(\phi) = -\frac{1}{\ln \rho_B}\int_0^{2\pi} d\phi \widetilde{f}(\phi)\ ,$$

which implies by (3.8)-(3.10) that the radius of the *internal* circle is defined as

$$\rho_B = \exp\left\{-\left(\int_0^{2\pi} d\phi\,(f\circ\zeta)(e^{i\phi})\right)\left(\int_{\partial\Omega} d\tau\,\partial_\tau\phi(\tau)\partial_\phi(v_f\circ\zeta)(e^{i\phi(\tau)})\right)^{-1}\right\}$$
$$= \exp\left\{-\left(\int_0^{2\pi} d\phi\,(f\circ\zeta)(e^{i\phi})\right)\left(\int_{\partial\Omega} d\tau\,\partial_\nu u_f(\Gamma(\tau))\right)^{-1}\right\}\ . \tag{3.17}$$

Relation (3.17) allows the calculation of ρ_B if one knows the trace $\zeta(z)\,|_{C_1}$, but by (3.12), we have $\zeta(e^{i\phi(\tau)}) = \Gamma(\tau)$, the first equation to solve is (3.11). Notice that by definition $\partial\Omega = \{\Gamma(\tau)\in\mathbb{C}\}_{\tau\in[0,l)}$ and by (3.6),(3.11) one notes this constraint:

$$l = \int_0^{2\pi} d\phi\,\frac{\Lambda_{C_{\rho_B},C_1}(f\circ\zeta)(e^{i\phi})}{(\Lambda_{\partial B,\partial\Omega}f\circ\zeta)(e^{i\phi})}\ , \tag{3.18}$$

as well as that the solution $\tau(\phi)$ of (3.11) must be a 2π-periodic function of ϕ. Here, we explicitly recall the second boundary dependence for the both Dirichlet-to-Neumann operators: $\Lambda_{C_1} = \Lambda_{C_{\rho_B},C_{\rho=1}}$ and $\Lambda_{\partial\Omega} = \Lambda_{\partial B,\partial\Omega}$.

Example 3.4. *We illustrate the above by a trivial example of the round Dirichlet absorbing cell. Let boundaries $\partial\Omega = C_R$ and $\partial B = C_{r_B}$ be two concentric circles with radius r_B, which the only unknown parameter that should be defined as a solution of the inverse geometrical problem. Following our scheme, the domain $\Omega\setminus\overline{B}$ is the image of a conformal mapping of an annulus*

$$A_B := \{z\in\mathbb{C} : 0 < \rho_B < |z| < 1\} \tag{3.19}$$

produced by a bijective holomorphic function $\zeta(z)$. This function maps boundaries to other boundaries: $\zeta : C_{\rho_B}\to\partial B$ and $\zeta : C_{r=1}\to\partial\Omega$.

By virtue of the rotational symmetry, one can try to solve this problem for ∂B via $(\mathbf{P}^{\infty}_{\mathbf{d=2}})$ with boundary conditions $u\,|_{\partial\Omega}\,(p) = f$ independent of $\arg(p)$. Then solution of the direct problem $(\mathbf{P}^{\infty}_{\mathbf{d=2}})$ is given by the $n=0$ version of (3.13): $u_f(\rho,\phi) = a\ \ln\rho + b$ for $r_B < \rho < R$. Taking into account boundary conditions

one finds a and b and the explicit form of the corresponding Dirichlet-to-Neumann operator:

$$\Lambda_{\partial B,\partial\Omega} : f \mapsto \partial_\nu u_f \mid_{C_R} = \frac{1}{R\ (\ln R - \ln r_B)}\ f\ . \tag{3.20}$$

(*Note that our example is so simple that the one-measure of the "voltage-current" data $\{f, j := \Lambda_{\partial B,\partial\Omega} f\}$ is enough to uniquely define the operator $\Lambda_{\partial B,\partial\Omega}$ that solves the problem of r_B explicitly.*)

Since the conformal mapping for the exterior boundaries gives $\zeta(e^{i\phi}) = R\ e^{i\phi}$, for $p \in C_1$ (trace $\zeta\ \mid_{C_1}$), one gets $\widetilde{f}(p) := (f \circ \zeta)(p) = f(\zeta(e^{i\phi})) = f(Re^{i\phi}) = f$. Then, by (3.13), the Dirichlet-to-Neumann operator for the problem $(\widetilde{\mathbf{P}}^{\infty}_{\mathbf{d=2}})$ has the form:

$$\Lambda_{C_{\rho_B},C_{\rho=1}} : \widetilde{f} \mapsto \partial_\nu \widetilde{u}_{\widetilde{f}} \mid_{C_1} = -\ \frac{1}{\ln \rho_B}\ \widetilde{f}\ . \tag{3.21}$$

Then, by (3.20), we get for the numerator in (3.11):

$$(\Lambda_{\partial B,\partial\Omega} f \circ \zeta) = \frac{1}{R\ (\ln R - \ln r_B)}\ f \circ \zeta = \left\{ R\ \ln \frac{R}{r_B} \right\}^{-1} \widetilde{f}, \tag{3.22}$$

and by (3.21) one obtains for denominator in (3.11):

$$\Lambda_{C_{\rho_B},C_{\rho=1}}(f \circ \zeta) = -\ \frac{1}{\ln \rho_B}\ \widetilde{f}\ . \tag{3.23}$$

Inserting (3.22) and (3.23) into (3.17) (or into (3.18), where $l = 2\pi\, R$) we obtain that $\rho_B = r_B/R$, i.e. for internal boundaries, the conformal mapping gives: $\zeta(\rho_B e^{i\phi}) = r_B e^{i\phi} = R\ \rho_B e^{i\phi}$. This implies that the mapping is $\zeta(z) = R\ z$ (see (ii)), and also the evident final result about the form of the boundary ∂B as the trace of $\zeta(z)$ on the C_{ρ_B}.

4. This example shows that $\tau(\phi)$ is a 2π-periodic extension of the *linear* function

$$\tau_0(\phi) := \frac{l}{2\pi}\,\phi\ , \quad \phi \in [0, 2\pi)\ . \tag{3.24}$$

The result is a simple linear form of the corresponding conformal mapping. Any deviation from concentric domains $\partial\Omega = C_R$ and $\partial B = C_{r_B}$ makes the function $\tau(\phi)$ non-linear, but still obeying condition (3.18).

A less trivial application of the scheme presented above is the example of non-concentric domains $\partial\Omega = C_R$ and $\partial B = C_{r_B}$. In this case the conformal mapping ζ is *a priori* known: it is the Möbius transformation, and one can proceed with this trial ζ along the same line of reasoning as in Example 3.4, see [2]. Illustration of the inverse geometrical problem solution needs a complete application of the above formalism, since now, one has to solve two coupled equations (3.11) and (3.17) with condition (3.18). (ii) We rewrite these equations (incorporating the

constraint (3.18)) in the following form:

$$\rho_B = \exp\left\{-\left(\int_0^{2\pi} d\phi\,(f\circ\zeta)(e^{i\phi})\right)\left(\int_{\partial\Omega} d\tau\,\partial_\nu u_f(\Gamma(\tau))\right)^{-1}\right\}, \quad (3.25)$$

$$\partial_\phi\tau = \frac{l}{2\pi} + \frac{\Lambda_{C_{\rho_B},C_1}(f\circ\zeta)}{(\Lambda_{\partial B,\partial\Omega}f\circ\zeta)} - \frac{1}{2\pi}\int_0^{2\pi} d\phi\,\frac{\Lambda_{C_{\rho_B},C_1}(f\circ\zeta)(e^{i\phi})}{(\Lambda_{\partial B,\partial\Omega}f\circ\zeta)(e^{i\phi})}\ . \quad (3.26)$$

Notice that by (3.22) and (3.23) for concentric domains $\partial\Omega = C_R$ and $\partial B = C_{r_B}$ the last two terms in (3.26) cancel. Therefore, one can consider this case as the *zero-order* approximation $\tau = \tau_0(\phi)$ for the solution of (3.26) with $\zeta = \zeta_0(z) := z$ and $\rho_B = \rho_0 := r_B/R$. This observation implies that one can consider equations (3.25) and (3.26), together with relations $\zeta_n(e^{i\phi}) = \Gamma(\tau_n(\phi))$, see (3.12), as a non-linear iterative scheme to obtain ρ_B and the function $\tau(\phi)$ (or $\zeta(z)$), cf [9]:

$$\rho_n = \exp\left\{-\left[\int_0^{2\pi} d\phi(f\circ\zeta_n)(e^{i\phi})\right]\left[\int_{\partial\Omega} d\tau\partial_\nu u_f(\Gamma(\tau))\right]^{-1}\right\}, \quad (3.27)$$

$$\partial_\phi\tau_{n+1} = \frac{l}{2\pi} + \frac{\Lambda_{C_{\rho_n},C_1}(f\circ\zeta_n)}{(\Lambda_{\partial B,\partial\Omega}f\circ\zeta_n)} - \frac{1}{2\pi}\int_0^{2\pi} d\phi\,\frac{\Lambda_{C_{\rho_n},C_1}(f\circ\zeta_n)(e^{i\phi})}{(\Lambda_{\partial B,\partial\Omega}f\circ\zeta_n)(e^{i\phi})}, \quad (3.28)$$

$$\zeta_n(e^{i\phi}) = \Gamma(\tau_n(\phi))\ . \quad (3.29)$$

Remark 3.5. *Suppose that for $n\to\infty$ the iterations converge: $\rho_n\to\rho_B$, $\tau_n(\phi)\to\tau(\phi)$ and for given Γ: $\zeta_n(z)\to\zeta(z)$. Then, the function $\Gamma(\tau(\phi))$ can be presented as the Fourier series:*

$$\Gamma(\tau(\phi)) = \sum_{s\in\mathbb{Z}}\gamma_s e^{is\phi}\ . \quad (3.30)$$

Since $\Gamma(\tau(\phi))$ is the image of the external boundary C_1 by the seeking function $\zeta(z)$, the coefficients γ_s are the same as in the Laurent series for this function in the annulus A_B:

$$\zeta(z) = \sum_{s\in\mathbb{Z}}\gamma_s z^s\ . \quad (3.31)$$

Now, the final step is to observe that the unknown internal boundary ∂B coincides with the conformal image $\{\Gamma_{\partial B}(\phi)\}_{0\le\phi<2\pi} = \zeta(C_{\rho_B})$ of the internal A_B-circle C_{ρ_B} with the radius $\rho_B<1$ calculated by iterations (3.27):

$$\Gamma_{\partial B}(\phi) = \sum_{s\in\mathbb{Z}}(\rho_B)^s\ \gamma_s e^{is\phi}\ . \quad (3.32)$$

The relation (3.32) *formally* solves the inverse geometrical problem for Dirichlet boundary conditions on the unknown contour $\partial B = \{\Gamma_{\partial B}(\phi)\}_{0\le\phi<2\pi}$.

4. Constant boundary conditions

1.1 Problem $(P_{f_\pm=1,0})$**.** Below we suppose that Ω and $B\subset\Omega$ are open bounded domains in $\mathbb{R}^2$ with C^2-smooth disjoint boundaries $\partial\Omega$ and ∂B, that is, $\partial(\Omega\setminus\overline{B}) = \partial\Omega\cup\partial B$ and $\partial\Omega\cap\partial B = \emptyset$.

The *unknown internal boundary* ∂B should be found from the solution u of the Dirichlet problem:

$$(\mathbf{P}_{\mathbf{f}_{\pm}=\mathbf{1},\mathbf{0}}) \qquad \begin{cases} \Delta u = 0, \ p \in \Omega \setminus \overline{B} \ , \\ u \mid_{\partial\Omega} (p) = f_+(p) = 1, \quad p \in \partial\Omega \ , \\ u \mid_{\partial B} (p) = f_-(p) = 0, \quad p \in \partial B \ , \end{cases}$$

with help of the *given* (measured) Neumann data: $g(p) = \partial_\nu u \mid_{\partial\Omega} (p)$, *exterior* normal derivative on the external boundary $p \in \partial\Omega$.

Remark 4.1. *Notice that one can always find a conformal mapping that transforms domain* Ω *into a unit disc. Therefore, we put for simplicity* $\Omega = D_{r=1}$*, the unit disc, i.e.* $\partial\Omega = C_1$*, is the unit circle.*

Remark 4.2. *Since below we use a conformal map approach to the localization of the internal boundary* ∂B*, we identify the* $\mathbb{R}^2$*-points* $p = (x, y)$ *with those of the complex plane* $\mathbb{C}$ *by:* $p \mapsto z(p) := x + iy \in \mathbb{C}$*. Then it is known, see e.g. [7], that the harmonic function solving* $(\mathbf{P}_{\mathbf{f}_{\pm}=\mathbf{1},\mathbf{0}})$ *can be viewed as the real part of a holomorphic in domain* $\Omega \setminus \overline{B}$ *function* $\widehat{u}(z)$ *, i.e.,* $u(p) = \mathrm{Re}\ \widehat{u}(z(p))$*. We put* $\widehat{u}(z) = u(x, y) + iv(x, y)$*, where* $v(x, y)$ *is harmonic conjugate to* $u(x, y)$*, [7]. Recall that for a doubly-connected domain, the function* $\widehat{u}(z)$ *may be multi-valued. Then, we consider for* $\widehat{u}(z)$ *only one (principle) branch.*

Remark 4.3. *Recall that in polar coordinates* $z = re^{i\phi} \in \mathbb{C}$ *the measured Neumann data* g *on* C_1 *take the form:*

$$\begin{aligned} g(\phi) &= e_r \cdot \nabla u \mid_{z\in C_1} = (\cos\phi \ \partial_x u + \sin\phi \ \partial_y u) \mid_{z\in C_1} = \\ &= \partial_r u(r\cos\phi, r\sin\phi) \mid_{r=1} \ . \end{aligned} \tag{4.1}$$

We also recall that the Cauchy-Riemann conditions in these coordinates can be written as:

$$\partial_r u = \frac{1}{r} \ \partial_\phi v \quad , \quad \frac{1}{r} \ \partial_\phi u = -\partial_r v \ . \tag{4.2}$$

1.2 Problem $(P^*_{f_{\pm}=1,0})$**.** Let the holomorphic function $w : z = (x+iy) \mapsto (w_1+iw_2)$ Map the doubly-connected bounded domain $D_1 \setminus \overline{B} \subset \mathbb{C}$ into annulus

$$A_B := \{w \in \mathbb{C} : 0 < \rho_B < |w| < 1\} \ . \tag{4.3}$$

This function maps boundaries to other boundaries: $w : \partial B \to C_{\rho_B}$ and $w : \partial\Omega = C_1 \to C_1$ and define the function $U(w_1, w_2)$ by

$$u(x, y) = (U \circ w)(x, y) = U(w_1(x, y), w_2(x, y)) \ . \tag{4.4}$$

Then, the problem $(P_{f_{\pm}=1,0})$ transfers into

$$(\mathbf{P}^*_{\mathbf{f}_{\pm}=\mathbf{1},\mathbf{0}}) \qquad \begin{cases} \Delta U = 0, \ p \in D_1 \setminus \overline{D_{\rho_B}} \ , \\ U \mid_{C_1} (p) = 1, \quad p \in C_1 \ , \\ U \mid_{C_{\rho_B}} (p) = 0, \quad p \in C_{\rho_B} \ , \end{cases}$$

with the exterior normal derivative:

$$\partial_\nu U\mid_{z\in C_1}(w(z)) = \left(\frac{1}{|w'(z)|}\, g(z)\right)\Big|_{z\in C_1} . \tag{4.5}$$

Notice that the value of the normal derivative (4.5) is B-dependent via conformal mapping w.

1.3 Solution of the Problem $(P^*_{f_\pm=1,0})$**.** For the general solution, one easily finds a representation in the (complex) polar coordinates $w=\rho ei\varphi$:

$$U(\rho,\varphi) = a + b\ln\rho + \sum_{n\in\mathbb{Z}\setminus 0}\left(a_n\rho^n e^{in\varphi} + b_n\rho^{-n}e^{-in\varphi}\right) ,$$

which is simply the standard Fourier-series representation. By virtue of the boundary conditions, we obtain:

$$a=1\ ,\ b=-\frac{1}{\ln\rho_B}\ ,\ a_n=b_n=0\ .$$

Then, Consequently, we get for the solution the explicit form:

$$U(w_1,w_2)=U(\rho,\varphi)=\frac{\ln(\rho/\rho_B)}{\ln(1/\rho_B)}=\frac{1}{\ln(1/\rho_B)}\ \ln\frac{|w|}{\rho_B}\ , \tag{4.6}$$

and the corresponding B-dependent normal derivative on the external boundary C_1, cf. (4.5):

$$\partial_\nu U\mid_{C_1}(w)=\partial_\rho U(\rho,\varphi)\mid_{\rho=1}=\frac{1}{\ln(1/\rho_B)}\ . \tag{4.7}$$

Notice that in contrast to the Problem $(P_{f_\pm=1,0})$, the Neumann data (4.7) for the Problem $(P^*_{f_\pm=1,0})$ are *isotropic* and they depend on B only via radius ρ_B.

It is clear that to proceed with localization of the internal boundary ∂B, one has to find the conformal mapping $w(z)$. The relations (4.5) and (4.7) yield the functional equation:

$$\frac{1}{\ln(1/\rho_B)}=\left(\frac{1}{|w'(z)|}\, g(z)\right)\Big|_{z\in C_1} \tag{4.8}$$

for w. This equation is insufficient, since it is localized only on the boundary C_1. To overcome this difficulty, we use complex extensions of $(P_{f_\pm=1,0})$ and $(P^*_{f_\pm=1,0})$ indicated in Remark 4.2.

2.1 Complex extension. Let us define the complex extension of (4.6) by

$$\widehat{U}(w=w_1+iw_2):=\frac{1}{\ln(1/\rho_B)}\ln\frac{w}{\rho_B}=(U+iV)(w)\ , \tag{4.9}$$

where $V=\arg w$ is the harmonic conjugate to $U=\ln|w|$ and corresponds to the principle branch of the logarithm. Hence, one can similarly introduce the function

$$\widehat{u}(z):=\widehat{U}(w(z))=(u+iv)(z)=\frac{1}{\ln(1/\rho_B)}\ln\frac{w(z)}{\rho_B}\ , \tag{4.10}$$

where v is the harmonic conjugate to u.

2.2 Complex extension and the Problem $(P_{f_\pm=1,0})$. By (4.10), one gets

$$u(x,y) = \mathrm{Re}\ \widehat{u}(z) = \frac{1}{\ln(1/\rho_B)} \ln \frac{|w(z)|}{\rho_B} \ .$$

Let $z = re^{i\phi}$. Then by virtue of (4.1), (4.10) and

$$\partial_r \widehat{u}(z) = (\partial_r u + i\partial_r v)(z) = \widehat{u}^{\,'}(z)\, e^{i\phi} = \frac{1}{\ln(1/\rho_B)} \frac{w^{'}(z)}{w(z)}\ e^{i\phi} \ , \tag{4.11}$$

we obtain the following equation:

$$\partial_r u\ |_{C_1} = \mathrm{Re}\left\{ \frac{1}{\ln(1/\rho_B)} \frac{w^{'}(e^{i\phi})}{w(e^{i\phi})}\ e^{i\phi} \right\} = g(\phi) \ . \tag{4.12}$$

Notice that the Cauchy-Riemann conditions (4.2) implies:

$$\partial_r v(z = re^{i\phi}) = -\frac{1}{r}\ \partial_\phi u(re^{i\phi}) = -\frac{1}{r\ \ln(1/\rho_B)}\ \partial_\phi \ln|w(re^{i\phi})| \ . \tag{4.13}$$

Since for $r = 1$, we have $|w(e^{i\phi})| = 1$, one gets $\partial_r v(z)\ |_{C_1} = 0$, i.e. the condition Re in (4.12) is superfluous as soon as we stick to the external boundary C_1:

$$\frac{1}{\ln(1/\rho_B)} \frac{w^{'}(e^{i\phi})}{w(e^{i\phi})}\ e^{i\phi} = g(\phi) \ . \tag{4.14}$$

2.3 Solution for conformal mapping $w(z)$. Motivated by (4.14), we define a continuation of (4.12) from the external boundary C_1 into domain $\Omega \setminus \overline{B}$. To this end, we introduce a holomorphic in $\Omega \setminus \overline{B}$ function F with the corresponding Laurent series:

$$F(z) := \frac{1}{\ln(1/\rho_B)} \frac{w^{'}(z)}{w(z)}\ z = F_0 + \sum_{n=1}^{\infty} (F_n\ z^n + F_{-n}\ z^{-n}) \ . \tag{4.15}$$

Then by periodicity of g and by (4.14), (4.33) we obtain the relation

$$g(\phi) = \sum_{n\in\mathbb{Z}} g_n e^{in\phi} = F(z = e^{i\phi}) \ , \tag{4.16}$$

which implies $F_n = g_n$ and $\overline{g_n} = g_{-n}$, for $n \in \mathbb{Z}$, as well as equation

$$\frac{1}{\ln(1/\rho_B)} \frac{w^{'}(z)}{w(z)}\ z = g_0 + \sum_{n=1}^{\infty} (g_n z^n + g_{-n} z^{-n}) \ . \tag{4.17}$$

Therefore, one has

$$\partial_z \ln w(z) = \ln(1/\rho_B) \left[\frac{g_0}{z} + \sum_{n=1}^{\infty} (g_n z^{n-1} + g_{-n} z^{-n-1}) \right] \ . \tag{4.18}$$

Hence, we obtain:

$$w(z) = w_0\ z^{g_0 \ln(1/\rho_B)} \exp\left[\ln(1/\rho_B) \sum_{n=1}^{\infty} (g_n z^n - g_{-n} z^{-n})/n \right] \ . \tag{4.19}$$

Since $w : C_1 \to C_1$, one obviously gets

$$w(e^{i\phi}) = e^{i\varphi(\phi)} \quad \text{and} \quad w(e^{i(\phi+2\pi)}) = e^{i\varphi(\phi+2\pi)} = e^{i\varphi(\phi)} \ , \tag{4.20}$$

which implies that $g_0 \ln(1/\rho_B) = 1$ and

$$\rho_B = e^{-1/g_0} \ , \tag{4.21}$$

i.e., we *must* put $g_0 > 0$. Notice that $|w(e^{i\phi})| = 1$ and (4.21) yield $|w_0| = 1$, which we can choose to be real. Therefore, one finally obtains for the conformal mapping w the expression:

$$w(z) = z \ \exp\left[(1/g_0)\sum_{n=1}^{\infty}(g_n z^n - g_{-n}z^{-n})/n\right] \ , \tag{4.22}$$

which is completely defined by the measured Neumann data $g(p)$ on the external boundary C_1.

Remark 4.4. *In spite of the obvious remark:* $\partial_\phi|w(e^{i\phi})| = 0$*, which we used to establish (4.14), the derivative* $\partial_\phi w(e^{i\phi}) = e^{i\varphi(\phi)}\,\partial_\phi\varphi(\phi) \neq 0$*. This means that* $\varphi(\phi)$ *is a nontrivial periodic function on* C_1 *, see (4.20).*

3.1 Inverse conformal mapping. According to our construction (see 1.2), the inverse function $z(w)$ maps C_{ρ_B} into the contour ∂B, i.e. formally $\partial B = \{z(w = \rho_B e^{i\varphi})\}_{\varphi\in[0,2\pi)}$.

Note that by using (4.33), we can introduce the holomorphic function:

$$G(w) := F(z(w))^{-1} = \ln(1/\rho_B)\ \frac{z^{'}(w)}{z(w)}\ w = G_0 + \sum_{n=1}^{\infty}(G_n w^n + G_{-n}w^{-n}) \ , \tag{4.23}$$

where the last sum is the corresponding Laurent series. Hence, following the same line of reasoning as in Section 2, we obtain:

$$z(w) = z_0\ w^{G_0/\ln(1/\rho_B)} \exp\left[(\ln(1/\rho_B))^{-1}\sum_{n=1}^{\infty}(G_n w^n - G_{-n}w^{-n})/n\right] \ . \tag{4.24}$$

Notice that on the circle C_1 the function $z(w = e^{i\varphi})$ is periodic. Then, the same is true for G. By arguments similar to those in Section 2, this function has the Fourier coefficients satisfying the same properties as g_n in (4.16), i.e. by (4.23) one gets:

$$G_n = \overline{G_{-n}} = \frac{1}{2\pi}\int_{-\pi}^{\pi} d\varphi\ G(e^{i\varphi})\ e^{-in\varphi} \ . \tag{4.25}$$

3.2 Localization of ∂B**.** Since $z : C_1 \to C_1$, then similar to Section 2, the representation (4.24) for this periodic function implies that we can choose $z_0 = 1$ and that $G_0/\ln(1/\rho_B) = 1$, or $G_0 = 1/g_0$. By virtue of (4.16) and (4.23) the other coefficients are given by

$$G_m = \frac{1}{2\pi i}\int_{C_1} dw\ \frac{1}{w^{m+1}}\ \frac{1}{F(z(w))} = \frac{1}{2\pi}\int_0^{2\pi} d\phi\ \frac{e^{i\phi}}{g(\phi)}\frac{w'(e^{i\phi})}{w^{m+1}(e^{i\phi})} \ . \tag{4.26}$$

Since the conformal mapping w has been already calculated in (4.22) for given Neumann data g, formulae (4.26) solve the problem of inversion $z(w)$, see (4.24).

Hence in the cases $f_+ = 1$ and $f_- = 0$, the position of unknown boundary ∂B is defined for a given Neumann data g as a set:

$$\partial B = \{z(w = \rho_B e^{i\varphi})\}_{\varphi\in[0,2\pi)} \ , \tag{4.27}$$

which is uniquely defined by (4.24),(4.26) and auxiliary radius $\rho_B = e^{-1/g_0}$.

3.3 Existence and uniqueness. Notice that existence and uniqueness of the solution (4.27) follow from the explicit construction in the above subsection 3.2. This statement is not *unconditional*. The first necessary condition is:

(i) $g_0 > 0$, see (4.21).

Another restriction follows directly from the $f_\pm$-boundary conditions for the Problem $(P_{f_\pm=1,0})$:

(ii) $g(\phi) > 0$, see (4.5) and (4.7).

(iii) A more subtle constraint for the given Neumann data $g(\phi)$ follows from the conditions insuring the invertibility of the conformal mapping w. We study this restriction first for the particular example in the next subsection 4.1.

4.1 Let $g_0 > 0$ and $g_1 > 0$. By (4.22) one gets

$$w(z) = z \ \exp\left[(g_1/g_0)(z - z^{-1})\right] \ , \tag{4.28}$$

but our aim is to inverse the function $w(z)$, i.e. to find (4.24) and then to calculate the unknown boundary ∂B (4.27).

It is worth noting that despite $|w(z = e^{i\phi})| = 1$, the conformal mapping (4.28) acts nontrivially on C_1 since, see (4.20):

$$w(e^{i\phi}) = e^{i\phi}\exp\left[2i(g_1/g_0)\sin\phi\right] = e^{i\varphi(\phi)} \ . \tag{4.29}$$

Equation (4.29) yields for the function $\varphi(\phi)$ the expression:

$$\varphi(\phi) = \phi + 2(g_1/g_0)\sin\phi \ . \tag{4.30}$$

4.2 Notice first that the general conditions on $g(\phi)$ imply: $g_0 > 0$ and $g_0 > 2g_1$, see (i) and (ii). For example, the importance of $g_0 > 2g_1$ is directly related to *monotonicity* of the function (4.30).

A more delicate condition (iii) requires that $w : \partial B \to C_{\rho_B}$ and in particular:

$$w(z = r(\phi)) \mid_{\phi=0} = r(\phi) \ \exp\left[(g_1/g_0)(r(\phi) - r(\phi)^{-1})\right] \mid_{\phi=0} = \rho_B \tag{4.31}$$

$$w(z = -r(\phi)) \mid_{\phi=\pi} = -r(\phi) \ \exp\left[(g_1/g_0)(-r(\phi) + r(\phi)^{-1})\right] \mid_{\phi=\pi} = -\rho_B \tag{4.32}$$

Notice that for given $g_0 > 0$ and $g_0 > 2g_1$, the solution of (4.31) for $r(\phi = 0)$ always exists and is unique. Whereas for $r(\phi = \pi)$, this is not true. Indeed, for any $r < 1$, the function defined by the left side of (4.32):

$$F_\varepsilon(r) := r \ \exp\left[\varepsilon(-r + r^{-1})\right] > 0 \ \ , \ \ \varepsilon := g_1/g_0 < 1/2 \ , \tag{4.33}$$

is monotonously increasing, for increasing ε. Hence, there is a critical value ε_{cr} : $0 < \varepsilon_{cr} < 1/2$, corresponding to condition

$$\min_{r\le 1} F_{\varepsilon_{cr}}(r) = \rho_B \ , \tag{4.34}$$

and there are no solutions $r(\phi = \pi) < 1$ of (4.32) for $\varepsilon > \varepsilon_{cr}$. Let $g_0 = 1$. Then, one obtains from (4.34) the equation for ε_{cr} in the form:

$$\ln[(1 - \sqrt{1 - 4\varepsilon^2})/2\varepsilon] + \sqrt{1 - 4\varepsilon^2} + 1 = 0 \ . \tag{4.35}$$

Equation (4.35) implies that a solution for $r(\phi = \pi)$ does not exist, when $1/2 > g_1$, but $g_1 > g_{cr} = 0,13796148...$. This means that for $g_1 > g_{cr}$, the conformal map w is not invertible, i.e. the image ∂B is not correctly defined.

We illustrate this evolution of conformal mapping and the form of the internal absorbing boundary ∂B as a function of g_1 for $g_0 = 1$ by Figures 1-5.

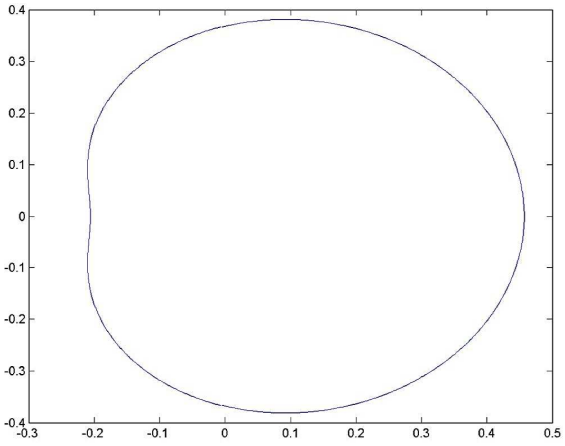

FIG. 1. Internal boundary ∂B for $g_0 = 1$ and $g_1 = 0,125 < g_{cr}$

On the last two figures, one observes that the boundary ∂B is not closed because of small gaps for $\varphi(\phi = \pi) = \pi$, see (4.30). This is a numerical indication that the conformal map w is not invertible for $g_1 > g_{cr}$.

5. Concluding remarks

1. First, we comment the case $\alpha = 0$, i.e. the Neumann boundary conditions on the absorbing cell ∂B, see **(P2)**. Then, $(\mathbf{P}^{\infty}_{\mathbf{d=2}})$ is transformed into the following problem:

$$(\mathbf{P}^{\alpha=\mathbf{0}}_{\mathbf{d=2}}) \qquad \begin{cases} \Delta u = 0, \ p \in \Omega \setminus \overline{B} \ , \\ u \mid_{\partial\Omega} (p) = f(p), \quad p \in \partial\Omega \ , \\ \partial_\nu u \mid_{\partial B} (\omega) = g(\omega), \quad \omega \in \partial B \ . \end{cases}$$

To map domain $\Omega \setminus \overline{B}$ onto annulus (4.3), we use the same holomorphic function $\zeta(z)$. Since conformal mappings preserve angles, the corresponding problem

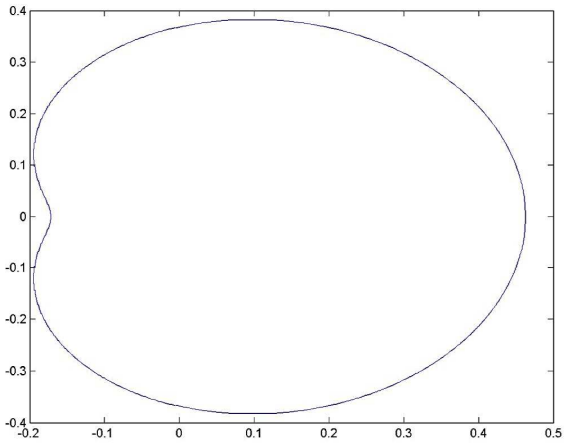

FIG. 2. Internal boundary ∂B for $g_0 = 1$ and $g_1 = 0,135 < g_{cr}$

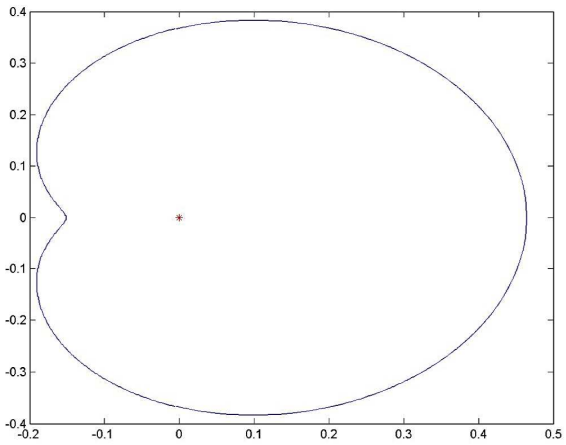

FIG. 3. Internal boundary ∂B for $g_0 = 1$ and $g_1 = 0,13796148 < g_{cr}$

assumes the form:

$$(\widetilde{\mathbf{P}}^{\alpha=\mathbf{0}}_{\mathbf{d}=\mathbf{2}}) \qquad \begin{cases} \Delta\widetilde{u} = 0, \ p \in A_B \ , \\ \widetilde{u} \mid_{C_1} (p) = \widetilde{f}(p) \ , \quad p \in C_1 \ , \\ \partial_\nu \widetilde{u} \mid_{C_{\rho_B}} (\omega) = |\partial_z \zeta(\omega)| \widetilde{g}(\omega), \quad \omega \in C_{\rho_B} \ . \end{cases}$$

Here $\partial_\nu(\cdot) \mid_{C_{\rho_B}}$ is the external *normal* derivative at the point $\omega \in C_{\rho_B} = \zeta(\partial B)$ for a value proportional to $\widetilde{g}(\omega) = (g \circ \zeta)(\omega)$.

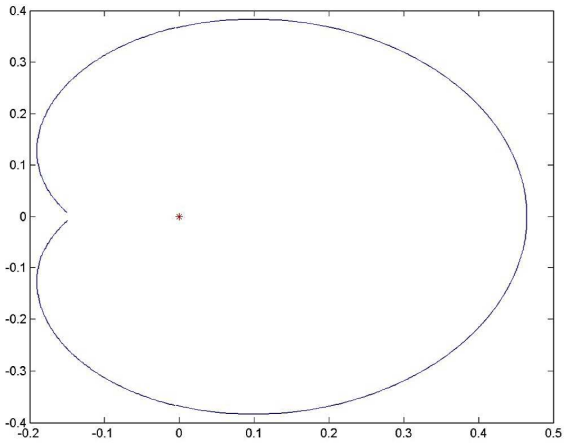

FIG. 4. Internal boundary ∂B for $g_0 = 1$ and $g_1 = 0,13815648 > g_{cr}$

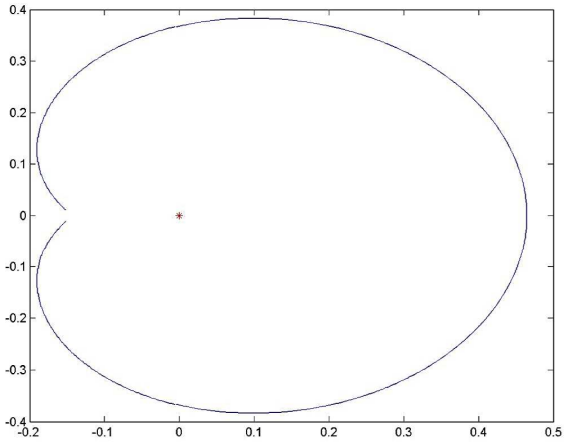

FIG. 5. Internal boundary ∂B for $g_0 = 1$ and $g_1 = 0,13824948 > g_{cr}$

It is clear now that our scheme must be considerably modified (simplified), since the actual boundary conditions depend on an *unknown* conformal mapping ζ. Note that this cannot be aided by Proposition 3.3 to reduce the Neumann boundary condition to Dirichlet, since our domain is not simply connected. The external data for solving the inverse geometrical problem correspond to $\widetilde{f}(p)$, so we prefer to simplify the conditions on the cell surface ∂B and set $g = 0$, which excludes the annoying dependence of the Neumann boundary conditions on derivative $\partial_z \zeta$.

2. Consider the problem $(\widetilde{\mathbf{P}}^{\alpha=\mathbf{0}}_{\mathbf{d=2}})$ for $\widetilde{g}=0$.

$$(\widetilde{\mathbf{P}}^{\mathbf{0}}_{\mathbf{d=2}}) \qquad \begin{cases} \Delta\widetilde{u}=0,\ p\in A_B\ , \\ \widetilde{u}\mid_{C_1}(p)=\widetilde{f}(p)\ ,\quad p\in C_1\ , \\ \partial_\nu\widetilde{u}\mid_{C_{\rho_B}}(\omega)=0\ ,\quad \omega\in C_{\rho_B}\ . \end{cases}$$

Example 5.1. *As above (see Example 3.4) we first illustrate a possible strategy to solve* $(\widetilde{\mathbf{P}}^{\mathbf{0}}_{\mathbf{d=2}})$ *by a simple example of the round Neumann absorbing cell.*

Let boundaries $\partial\Omega=C_R$ *and* $\partial B=C_{r_B}$ *be two concentric circles with radius* r_B*, which is the only unknown parameter that should be defined as a solution of the inverse geometrical problem. Moreover, since* $\zeta: C_{\rho_B}\to\partial B=C_{r_B}$ *and* $\zeta: C_{r=1}\to\partial\Omega=C_R$*, we find this conformal mapping coincides with the same linear mapping,* $\zeta(z)=R\,z$*, as in Example 3.4, i.e.* $\rho_B=r_B/R$*.*

Notice that the constant external condition $\widetilde{f}(p)=(f\circ\zeta)(p)=f(Re^{i\phi})=f$*,* $p\in C_1$*, implies a trivial constant solution* $u_f=\widetilde{u}_f=f$*. Therefore, we consider the one-mode boundary condition defined by* $\widetilde{f}(e^{i\phi})=(f\circ\zeta)(e^{i\phi})=f(Re^{i\phi})=f(\phi):=\mathrm{f}\cos\phi$*. Then by general solution (3.13) in annulus one obtains for the Dirichlet-to-Neumann operator,* $(\mathbf{P}^{\alpha=\mathbf{0}}_{\mathbf{d=2}})$ *with* $g=0$*:*

$$\Lambda_{\partial B,\partial\Omega}: f(\phi)\mapsto\partial_\nu u_f\mid_{C_R}=\frac{R^2-r_B^2}{R\,(R^2+r_B^2)}f(\phi)\ . \tag{5.1}$$

Similarly one obtains for for the problem $(\widetilde{\mathbf{P}}^{\mathbf{0}}_{\mathbf{d=2}})$*:*

$$\Lambda_{C_{\rho_B},C_{\rho=1}}: f(\phi)\mapsto\partial_\nu\widetilde{u}_{\widetilde{f}}\mid_{C_1}=\ \frac{1-\rho_B^2}{(1+\rho_B^2)}\ f(\phi)\ . \tag{5.2}$$

By virtue of $\rho_B=r_B/R$*, (5.1) and (5.2) imply that relations (3.17) and (3.18), where* $l=2\pi\,R$*, are valid with solution (3.24):* $\tau_0(\phi):=(l/2\pi)\,\phi\ ,\ \phi\in[0,2\pi)$ *.*

This example shows that following along verbatim through the arguments of Section 3.4, one obtains the same iterative scheme (3.27)-(3.29), but with Dirichlet-to-Neumann operators that are defined by the Neumann problems $(\mathbf{P}^{\alpha=\mathbf{0}}_{\mathbf{d=2}})$ and $(\widetilde{\mathbf{P}}^{\mathbf{0}}_{\mathbf{d=2}})$. Example 5.1 gives the zero-order approximation for solution. **3.** Recall that the aim of present note is to advocate a *formal* solution of some $d=2$ inverse geometrical problems, see e.g. Remark 3.5. Since the error in calculations of the coefficients $\{\gamma_s\}_{s\in\mathbb{Z}}$, see (3.30), can be exponentially amplified in expression (3.32) for the boundary ∂B, it is clear that the problem is ill-posed, i.e. it demands further analysis.

We plan to return to numerical implementations of this formal iterative scheme elsewhere. The cut-offs and regularizations, as well as their possible generalizations to Robin boundary conditions need to be studied.

Acknowledgements

During his visit of Indiana University - Purdue University Indianapolis, V.A.Z. benefited of numerous useful suggestions and comments concerning the present paper from discussions with Pavel Bleher.

V.A.Z is most grateful Pavel Bleher and Department of Mathematical Sciences of IUPUI for kind invitation and for warm hospitality extended him at the Indiana University (Indianapolis).

References

[1] D.C. Barber, B.H. Brown, Applied potential tomography. *J.Phys. E*, **17**, P. 723–733 (1984).
[2] I. Baydoun, V.A. Zagrebnov. Diffusion and Laplacian Transport. *Theor.Math.Phys.*, **168**, P. 1180–1191 (2011).
[3] D.S. Grebenkov, M. Filoche, B. Sapoval. Mathematical basis for a general theory of Laplacian transport towards irregular interfaces. *Phys.Rev. E*, **73**, P. 021103–9 (2006).
[4] A. Greenleaf, G. Uhlmann. Local uniqueness for the Dirichelet-to-Neumann map via the two plane transform. *Duke Math.J.*, **108**, P. 559–617 (2001).
[5] J.K. Hunter, B. Nachtergaele. *Applied Analysis*. World Scientific, Singapore, 2001.
[6] O. Kellog. *Foundation of Potential Theory*. Dover, New-York, 1954.
[7] M.A. Lavrentiev, B.V. Chabat, *Méthodes de la théorie des fonctions d'une variable complexe*. Mir, Moscow, 1972.
[8] J. Lee, G. Uhlmann. Determining anisotropic real-analytic conductivities by boundary measurement. *Comm.Pure Appl.Math.*, **42**, P. 1097–1112 (1989).
[9] Jia-qi Liu, Ying-Wei Lu, A new algorithm for solving the geometrical inverse problems for a partial differential equation and its numerical semulation. *Proc. 11th IMACS Congress (Oslo)*, **1**, P. 221–224 (1985).
[10] A. I. Markushevich. *Theory of Functions of a Complex Variable: Second Edition* AMS Chelsea Publishing, 1977.
[11] S.G. Mihlin. *Mathematical Physics: An advanced course* North-Holland, Amsterdam, 1970 (S. G. Mihlin. *Lectures on Mathematical Physics*, 2nd ed. Lan' Publishing, St.Petersbourg, 2002.)
[12] A.G. Ramm. A geometrical inverse problem. *Inverse Probl.*, **2**, P. L19–L21 (1986).
[13] B. Sapoval. General formulation of Laplacian transfer across irregular sufaces. *Phys.Rev.Lett.*, **73**, P. 3314–3316 (1994).
[14] D. Tataru. Unique continuation for solutions to PDE's: between Hörmander's theorem and Holmgren's theorem. *Comm. Partial Differential Equations*, **20**, P. 855–884 (1995).
[15] M.E. Taylor. *Partial Differential Equations II: Qualitative Studies of Linear Equations.* Springer-Verlag, Berlin, 1996.
[16] M.E. Taylor. *Preudodifferential Operators.* Princeton University Press, New Jersey. 1996.
[17] V.A. Zagrebnov. From Laplacian transport to Dirichlet-to-Neumann (Gibbs) semigroups. *J.Math.Phys.(Analysis, Geometry)*, **4**, P. 551–568 (2008).

NANOSYSTEMS: PHYSICS, CHEMISTRY, MATHEMATICS, 2013, 4 (4), P. 467–473

ON SPECTRAL GAPS IN GRAPHENE IN A WEAK CONSTANT MAGNETIC FIELD

M. H. Brynildsen, H. D. Cornean

Aalborg University, Department of Mathematics, Aalborg, Denmark
mikkelhb@math.aau.dk, cornean@math.aau.dk

We present a mathematical introduction to a widely used discrete tight-binding model for graphene. We also introduce the "Peierls substitution," modelling the Hamiltonian of a 2d crystal in a perpendicular uniform magnetic field in this setting. We consider a discrete single-cone Hamiltonian closely related to the (double-cone) graphene Hamiltonian. Finally, we announce in this paper a result concerning an opening of gaps in the spectrum of this single-cone Hamiltonian, when the Peierls phase-factor arises from a weak, but non-zero, external magnetic field. Full proofs will be given elsewhere.

1. Introduction

Graphene, carbon atoms arranged in a flat honeycomb lattice, possesses many interesting electronic properties [1, 9]. After the realization of large graphene crystals in the laboratory [10] the interest, theoretical and experimental, has been intense. One of the main features is what physicists call the "relativistic behavior" of electrons in graphene, electrons in graphene can be viewed as massless fermions living in a 2d space, with their dynamics generated by a Weyl Hamiltonian, i.e., a Dirac Hamiltonian with zero rest mass.

We present here a standard analysis of graphene which shows the Weyl fiber, a discrete treatment of graphene which dates back to [13], if not earlier.

We have for some time been interested in the electronic properties of a graphene sheet subjected to a perpendicular uniform magnetic field. We model this situation by multiplying the Hamiltonian integral kernel by unimodular phase factors, this technique is known as "Peierls substitution" [6, 7, 11].

2. The Setting and Main Result

2.1. A Crystal Structure in the XY-plane

We will now introduce our notation for the set of atom-sites of a two-dimensional crystal lying in the XY-plane. A crystal structure is constructed by the indefinite periodic repetition of a crystallographic basis[1]. The honeycomb structure of a graphene monolayer is an example of such a crystal structure. More generally, consider a two-dimensional crystal structure embedded in the XY-plane of $\mathbb{R}^3$. The set of primitive vectors $\{\mathfrak{a}, \mathfrak{b}\}$, where we denote $\mathfrak{a} = (\mathfrak{a}_1, \mathfrak{a}_2)$ and $\mathfrak{b} = (\mathfrak{b}_1, \mathfrak{b}_2)$, generates the Bravais lattice:

$$\Gamma = \text{Bravais lattice} := \{\gamma = (\gamma_1, \gamma_2) \in \mathbb{R}^2 \ : \ \gamma = m\mathfrak{a} + n\mathfrak{b}, \ m, n \in \mathbb{Z}\}. \tag{2.1}$$

A primitive unit cell of Γ is given by

$$\Omega = \text{unit cell} := \left\{ x = (x_1, x_2) \in \mathbb{R}^2 \ : \ x = \theta_1\mathfrak{a} + \theta_2\mathfrak{b}, -\frac{1}{2} < \theta_1, \theta_2 \leq \frac{1}{2} \right\}. \tag{2.2}$$

[1]We will use the crystallographic nomenclature to distinguish between a Bravais lattice and a general crystal structure. This nomenclature unfortunately includes the word "basis" for the entity which is being repeated in definitely to generate the crystal.

We choose the order of the primitive vectors such that the ordered set of vectors $(\mathfrak{a}, \mathfrak{b}, \hat{z})$ defines a right-handed coordinate system. Then the area of the unit cell is given by $|\Omega| = |\mathfrak{a} \wedge \mathfrak{b}| = |\mathfrak{a}_1\mathfrak{b}_2 - \mathfrak{a}_2\mathfrak{b}_1|$. In our model $\mathscr{B}$ contains two vectors:

$$\mathscr{B} = \text{crystallographic basis} = \{\underline{\boldsymbol{\xi}}, \underline{\boldsymbol{\zeta}}\},$$

it is no restriction to put $\underline{\boldsymbol{\xi}} = 0$. The crystal structure now has the form

$$\Lambda = \Gamma + \mathscr{B}. \tag{2.3}$$

An element $x \in \Lambda$ is the position, or site, of an nucleus of an atom in the two-dimensional crystal filling the XY plane. The reciprocal lattice Γ^* is generated by the primitive vectors $\{\mathfrak{a}^*, \mathfrak{b}^*\}$ that satisfies the identities:

$$\mathfrak{a} \cdot \mathfrak{a}^* = \mathfrak{b} \cdot \mathfrak{b}^* = 2\pi, \qquad \mathfrak{a} \cdot \mathfrak{b}^* = \mathfrak{b} \cdot \mathfrak{a}^* = 0, \tag{2.4}$$

where $v \cdot w$ denotes the euclidean scalar product between vectors v, w in $\mathbb{R}^n$. One can easily see that this fixes $\{\mathfrak{a}^*, \mathfrak{b}^*\}$ from $\{\mathfrak{a}, \mathfrak{b}\}$:

$$\mathfrak{a}^* = \frac{2\pi}{|\Omega|}(\mathfrak{b}_2, -\mathfrak{b}_1), \qquad \mathfrak{b}^* = \frac{2\pi}{|\Omega|}(-\mathfrak{a}_2, \mathfrak{a}_1). \tag{2.5}$$

The reciprocal lattice is regarded as a subset of $\mathbb{R}^2$:

$$\Gamma^* = \text{reciprocal lattice} := \{\gamma^* = (\gamma_1^*, \gamma_2^*) \in \mathbb{R}^2 \ : \ \gamma^* = m\mathfrak{a}^* + n\mathfrak{b}^*, \ m, n \in \mathbb{Z}\}. \tag{2.6}$$

The first Brillouin zone is the Wigner-Seitz primitive cell of the reciprocal lattice:

$$\Omega^* := \{k = (k_1, k_2) \ : \ \|k\| \leq \|k - \gamma^*\|, \text{ for all } \gamma^* \in \Gamma\}, \tag{2.7}$$

that is, Ω^* is the closure of all the points of $\mathbb{R}^2$ that are closer to zero than any other point in the reciprocal lattice. Note that

$$|\Omega||\Omega^*| = (2\pi)^2, \tag{2.8}$$

where $|S|$ denotes the Lebesgue measure of a Borel set $S \subset \mathbb{R}^2$.

We work in a one-electron setting, neglecting electron-electron interactions. Our Hilbert space is $\ell^2(\Lambda)$, in which the Kronecker-basis $\{\delta_x\}_{x\in\Lambda}$;

$$\delta_x(x') := \begin{cases} 1 & \text{if } x' = x, \\ 0 & \text{if } x' \neq x, \end{cases}$$

is a total orthonormal set. We denote the inner product between two vectors ψ, ψ' of $\ell^2(\Lambda)$ by $\langle \psi, \psi' \rangle$.

2.2. Bloch–Floquet Decomposition, Version 1

Suppose a Γ-periodic (Hamilton) integral operator

$$H_0 : \ell^2(\Lambda) \to \ell^2(\Lambda), \tag{2.9}$$

is given. We define Γ-periodicity to mean that that the integral kernel of H_0 satisfies

$$H_0(x, y) := \langle \delta_x, H_0\delta_y \rangle = H_0(x + \gamma, y + \gamma) \qquad (x, y \in \Lambda, \quad \forall \gamma \in \Gamma).$$

The periodicity allows for Bloch-Floquet decomposition; $\ell^2(\Lambda)$ is unitarily equivalent with the constant fiber Hilbert space $\int_{\Omega^*}^{\oplus} \mathbb{C}^2 \, dk$ by a unitary operator, which is the extension of $\tilde{U} : \ell_c^2 \to \int_{\Omega^*}^{\oplus} \mathbb{C}^2 \, dk$ defined by

$$(\tilde{U}\psi)(k; \underline{x}) := \frac{1}{\sqrt{|\Omega^*|}} \sum_{\gamma\in\Gamma} e^{-ik\cdot\gamma}\psi(\gamma + \underline{x}) \quad (\psi \in \ell_c^2(\Lambda), \ k \in \Omega^*, \ \underline{x} \in \mathscr{B}). \tag{2.10a}$$

where every $f(k)$ in the fiber spaces $\mathbb{C}^2$, $k \in \Omega^*$ has the form

$$f(k) = \begin{bmatrix} f(k;\underline{\boldsymbol{\xi}}) \\ f(k;\underline{\boldsymbol{\zeta}}). \end{bmatrix}$$

Note that we use $\tilde{U}$ for the extension of $\tilde{U}$ also. The variable k is often called the crystal-momentum or quasi-momentum. H_0 is a fibered operator $\tilde{U}H_0\tilde{U}^* = \int_{\Omega^*} \tilde{h}_0(k)\ dk$ with fibers $\tilde{h}_0(k) = \begin{bmatrix} \tilde{h}_0(k;\underline{\boldsymbol{\xi}},\underline{\boldsymbol{\xi}}) & \tilde{h}_0(k;\underline{\boldsymbol{\xi}},\underline{\boldsymbol{\zeta}}) \\ \tilde{h}_0(k;\underline{\boldsymbol{\zeta}},\underline{\boldsymbol{\xi}}) & \tilde{h}_0(k;\underline{\boldsymbol{\zeta}},\underline{\boldsymbol{\zeta}}) \end{bmatrix}$ satisfying

$$\begin{aligned} H_0(\gamma + \underline{x},\underline{x}') &= \frac{1}{|\Omega^*|}\int_{\Omega^*} dk\ e^{i\,k\cdot\gamma}\tilde{h}_0(k;\underline{x},\underline{x}') \quad (\underline{x},\underline{x}' \in \mathscr{B};\ \gamma \in \Gamma), \\ \tilde{h}_0(k;\underline{x},\underline{x}') &= \sum_{\gamma\in\Gamma} e^{-ik\cdot\gamma}H_0(\underline{x}+\gamma,\underline{x}') \quad (\underline{x},\underline{x}' \in \mathscr{B};\ k \in \Omega^*). \end{aligned} \tag{2.10b}$$

The main result of this article concerns two isolated energy bands touching in "Dirac"-cones, for instance, when Λ is the honeycomb lattice (graphene), and H_0 is a tight-binding Hamiltonian. We briefly remind the reader of a nearest-neighbour tight-binding calculation of the graphene band structure, not essentially different from the one presented in [13]. The nearest-neighbour tight-binding band structure is one the simplest band structure calculations for graphene. Note that the Dirac-cones is a general artifact of the honeycomb lattice, not a property of the nearest-neighbour tight-binding approximations, see [4].

2.3. A Calculation of the Energy Spectrum of Graphene

First, fix the length-scale such that the nearest-neighbour distance is 1. For graphene a standard choice of Bravais lattice is $\mathfrak{a} = \frac{1}{2}(\sqrt{3},3)$, $\mathfrak{b} = \frac{1}{2}(-\sqrt{3},3)$, see Fig. 1, leading to the dual lattice vectors $\mathfrak{a}^* = 2\pi(\frac{1}{\sqrt{3}},\frac{1}{3})$, $\mathfrak{b}^* = 2\pi(-\frac{1}{\sqrt{3}},\frac{1}{3})$. We choose the

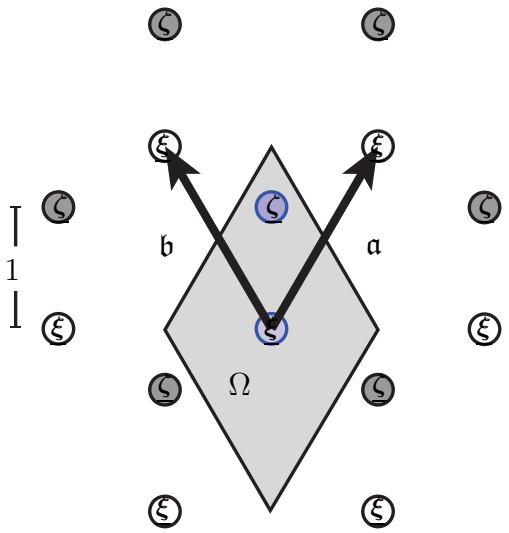

Fig. 1. Graphene crystal structure. The vectors $\mathfrak{a}$ and $\mathfrak{b}$ generates the Bravais lattice Γ. We choose the length-scale such that the nearest neighbour distance is 1.

graphene basis, see Fig. 1,

$$\mathscr{B}^G = \{(0,0),(0,1)\}. \tag{2.11}$$

A simple discrete Hamiltonian for graphene is the often used nearest-neighbour model:

$$H_0^G(x,x') = \begin{cases} 1 & \text{if } \|x-x'\| = 1, \\ 0 & \text{if } \|x-x'\| \neq 1 \end{cases} \qquad (x,x' \in \Lambda). \tag{2.12}$$

In this model, the fiber matrix, found by inserting (2.11) and (2.12) into formula (2.10b) is

$$\tilde{h}_0^G(k) = \begin{bmatrix} 0 & 2e^{-i\frac{3}{2}k_2}\cos(\frac{\sqrt{3}}{2}k_1)+1 \\ 2e^{i\frac{3}{2}k_2}\cos(\frac{\sqrt{3}}{2}k_1)+1 & 0 \end{bmatrix} \tag{2.13}$$

and the famous band functions are given by the eigenvalues of (2.13) as function of $k = (k_1, k_2) \in \Omega^*$:

$$\begin{aligned} \lambda_1(k_1,k_2) &= -\sqrt{3+2\cos\left(\sqrt{3}k_2\right)+4\cos\left(\frac{\sqrt{3}}{2}k_2\right)\cos\left(\frac{3}{2}k_1\right)}, \\ \lambda_2(k_1,k_2) &= \sqrt{3+2\cos\left(\sqrt{3}k_2\right)+4\cos\left(\frac{\sqrt{3}}{2}k_2\right)\cos\left(\frac{3}{2}k_1\right)}, \end{aligned} \tag{2.14}$$

plotted in Fig. 2. At the Dirac points

$$K_\pm = \left(\pm\frac{2\pi}{3}, \frac{2\pi}{3\sqrt{3}}\right) \tag{2.15}$$

see Fig. 2, the bands touch; $\lambda_1(K_\pm) = \lambda_2(K_\pm) = 0$. All other values of k where $\lambda_1(k) \geq 0$, or $\lambda_2(k) \leq 0$ can be reached by adding integer multiples of $\mathfrak{a}^*$ and $\mathfrak{b}^*$ to $K_\pm$. In this sense $K_\pm$ are the only distinct zeros of λ_ν, $\nu = 1, 2$. By symmetry of the two energy bands and half-filling, $\lambda_1(K_\pm) = \lambda_2(K_\pm) = 0$ is also the Fermi energy for this model, and the Fermi surface consists of isolated points.

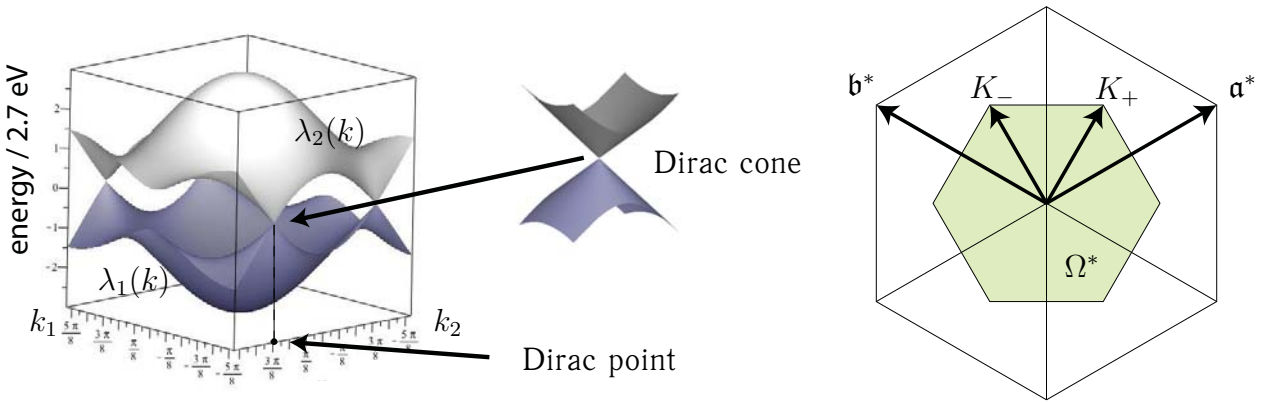

Fig. 2. Electron-energies of isolated graphene as a function of the crystal momentum $k \in \Omega^*$ (in units of the nearest neighbour hopping constant $\sim 2,7eV$). Of special interest are the "Dirac" points, K, where the two bands touch conically.

When expanding the fiber component functions $h_0^G(\,\cdot\,;\underline{x},\underline{x}')$, $\underline{x},\underline{x}' \in \mathscr{B}$ around K_+, one gets

$$h_0^G(\tilde{k}_1,\tilde{k}_2) = \frac{3}{2}\begin{bmatrix} 0 & \tilde{k}_1 - i\tilde{k}_2 + \sum_{|\alpha|\geq 2} C_\alpha \tilde{k}^\alpha \\ \tilde{k}_1 + i\tilde{k}_2 + \ldots & 0 \end{bmatrix}, \qquad \tilde{k} = k - K_+.$$

which to first order in k_1 and k_2 is the fiber of the Dirac Hamiltonian for massless fermions, also known as the *Weyl Hamiltonian*.

2.3.1. The uniform external magnetic field. Now consider a general one-electron Hilbert space $\ell^2(\Lambda)$, where Λ is a crystal structure of atom-sites in the XY-plane.

An uniform orthogonal magnetic field B is incorporated into the model by Peierls substitution [6, 8, 11]; we thus define a magnetic Hamiltonian with the integral kernel

$$H_b(\gamma + \underline{x}, \gamma' + \underline{x}') := e^{iB(\gamma_1\gamma_2' - \gamma_2\gamma_1')} H_0(\gamma + \underline{x}, \gamma' + \underline{x}') \quad (\gamma, \gamma' \in \Gamma, \quad \underline{x}, \underline{x} \in \mathscr{B}), \tag{2.16}$$

where $B(\gamma_1\gamma_2' - \gamma_2\gamma_1')$ is the flux of the magnetic field B through the triangle generated by origin, γ and γ'.

2.3.2. Bloch-Floquet decomposition, version 2. It is convenient to introduce an operator U defined on $\ell^2(\Lambda)$ by extension of

$$(U\psi)(k, \underline{x}) := \frac{1}{\sqrt{|\Omega^*|}} \sum_{\gamma \in \Gamma} e^{-ik\cdot(\gamma + \underline{x})} \psi(\gamma + \underline{x}) \qquad (\psi \in \ell_c^2(\Lambda),\ k \in \Omega^*,\ \underline{x} \in \mathscr{B}) \tag{2.17}$$

(compare with (2.10).) U associates a vector $\psi \in \ell^2(\Lambda)$ with a vector $U\psi \in \int_{\Omega^*}^{\oplus} \mathbb{C}^2\, dk$. The crystal Hamiltonian is again unitarily equivalent with a fibered operator acting in $\int_{\Omega^*}^{\oplus} \mathbb{C}^2\, dk$:

$$UH_0U^* = \int_{\Omega^*}^{\otimes} dk\ h_0(k), \tag{2.18}$$

where each fiber can be represented as a self-adjoint 2×2 matrix

$$h_0(k) = \begin{bmatrix} h_0(k; \underline{\boldsymbol{\xi}}, \underline{\boldsymbol{\xi}}) & h_0(k; \underline{\boldsymbol{\xi}}, \underline{\boldsymbol{\zeta}}) \\ h_0(k; \underline{\boldsymbol{\zeta}}, \underline{\boldsymbol{\xi}}) & h_0(k; \underline{\boldsymbol{\zeta}}, \underline{\boldsymbol{\zeta}}) \end{bmatrix} \qquad (\mathscr{B} = \{\underline{\boldsymbol{\xi}}, \underline{\boldsymbol{\zeta}}\}). \tag{2.19}$$

The unitary U fixes the integral kernel of the fibers $h_0(k)$ from the kernel of H_0, and vice versa:

$$h_0(k; \underline{x}, \underline{x}') = \frac{1}{|\Omega^*|} \sum_{\gamma \in \Gamma} e^{-ik\cdot(\underline{x} + \gamma - \underline{x}')} H_0(\underline{x} + \gamma, \underline{x}') \qquad (k \in \Omega^*, \quad \underline{x}, \underline{x}' \in \mathscr{B}), \tag{2.20a}$$

$$H_0(x, x') = \frac{1}{|\Omega^*|} \int_{\Omega^*} dk\ e^{ik\cdot(x - x')} h_0(k; \underline{x}, \underline{x}') \qquad (x = \underline{x} + \gamma \in \Lambda, \quad x' = \underline{x}' + \gamma' \in \Lambda). \tag{2.20b}$$

2.4. The Main Result

We will now consider a simpler situation than graphene. We suppose that the fibered zero-field Hamiltonian has a dispersion relation with a single Dirac-cone situated at the origin.

Theorem 2.1. *Let $\mathcal{L}(\mathbb{C}^2)$ denote the space of 2×2 matrices with complex components. Consider a matrix valued mapping $h_0 : \mathbb{R}^2 \supset \Omega^* \to \mathcal{L}(\mathbb{C}^2)$, where $h_0(k)$ is self-adjoint for all k. Let $H_0 : \ell^2(\Lambda) \to \ell^2(\Lambda)$ be a zero-field crystal Hamiltonian generated by h_0 by* (2.19) *and* (2.20b). *Furthermore assume that*

- **(a):** *for fixed $\underline{x}, \underline{x}' \in \mathscr{B}$, the function $\Omega^* \ni k \mapsto e^{ik\cdot(\underline{x} - \underline{x}')} h_0(k; \underline{x}, \underline{x}') \in \mathbb{C}$ has an extension which is $C^\infty(\mathbb{R}^2)$ and Γ^*-periodic*;
- **(b):** *0 is an eigenvalue of $h_0(0)$ with degeneracy* 2;
- **(c):** *for $k \neq 0$, $h_0(k)$ has two distinct eigenvalues $\lambda_1(k) < 0 < \lambda_2(k)$*;

(d): $h_0(k) = h_0^{[1]}(k) + h_0^{Rem}(k)$, *where*

$$h_0^{[1]}(k_1, k_2) = \begin{bmatrix} 0 & k_1 - ik_2 \\ k_1 + ik_2 & 0 \end{bmatrix}, \tag{2.21}$$

and that there exists a constant $C_1 > 0$ *such that*

$$\|h_0^{Rem}(k)\| \leq C_1 \|k\|^2 \qquad (k \in \Omega^*). \tag{2.22}$$

Then the spectrum of the magnetic Hamiltonian $H_b : \ell^2(\Lambda) \to \ell^2(\Lambda)$, *defined by* (2.20b) *and* (2.16) *above, develops gaps proportional to* $\sqrt{b}$ *around the origin. To be precise*: *for fixed* $M = 0, 1, 2, 3, \ldots$, *choose* c_1, c_2 *such that*

$$\sqrt{2M} < c_1 < c_2 < \sqrt{2(M+1)}. \tag{2.23}$$

Then there exists $b_0 > 0$ *such that for all* $0 < b < b_0$ *we have*

$$[c_1\sqrt{b}, c_2\sqrt{b}] \subset \rho(H_b). \tag{2.24}$$

(*see Fig.* 3).

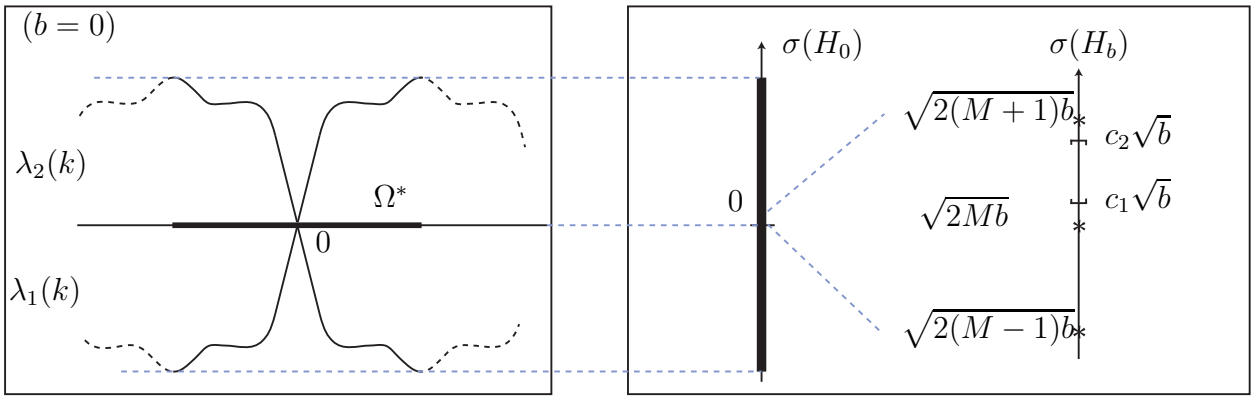

Fig. 3. *Left*: The two energy band functions λ_1 and λ_2, in the zero field case, qualitatively sketched (in reality, the functions are real-valued functions om $\Omega^* \subset \mathbb{R}^2$, of the type like Fig. 2, but only with one Dirac point at the origin). *Right*: The energy spectrum in two situations; no external magnetic field $b = 0$ (left vertical axis, a continuous energy band), and constant external magnetic field, $b > 0$ (right vertical axis). Gaps $[c_1\sqrt{b}, c_2\sqrt{b}]$ between the low Landau levels $\sqrt{2Mb}$, $M = 0, 1, 2, \ldots$ (marked by stars) appear in the spectrum of H_b when b is sufficiently small bur non-zero. $\sqrt{2M} < c_1 < c_2 < \sqrt{2(M+1)}$ for some $M \in \mathbb{N}_0$ small enough. Note that the right vertical axis only covers a tiny portion of the energy values which are inside the zero-field energy band, the two vertical axis are not of same scale!

2.5. About the Proof

Full proofs will be given in another paper of M. H. Brynildsen, H. D. Cornean, and I. Herbst. We construct aa approximation for $(H_b - z)^{-1}$, using a cut-and-paste method. The main idea is to treat fibers $h_0(k)$, with k near the Dirac points, with the continuous Dirac-resolvent, this is where the Landau levels come into play. The proof heavily relies on the $\sqrt{B}$-behaviour of the Hausdorff distance between spectra of Hamiltonians which differ only by a Peierls phase, as proven in [2].

3. Conclusions

Our result can be extended to the double-cone situation. The fact that there are gaps near the Dirac points is in agreement with the numerical calculations of Hofstadter-type [5], which were applied to the honeycomb-lattice in [12] and expanded in [3]. They plot the spectrum for values of B for which the relative flux of the external magnetic field through one unit cell has rational values.

For small intensities of the external magnetic field the Hofstadster-Rammal plot becomes increasingly computationally heavy to produce, so the more modern articles with better access to computer-power have extended the "Hofstadter-Rammal butterfly" spectrum plot to lower field-strengths (compare, for instance, our result with [3, Fig. 2a]).

Our method does not distinguish between rational or irrational fluxes, since we do not concern ourselves with the nature of the spectrum, we only want to show the existence of gaps in the spectrum. Also, our result holds for all B in a small neighborhood of zero, whereas the Hofstadter approach requires more computations, the smaller B is.

4. Acknowledgments

The authors acknowledge partial support from the Danish FNU grant *Mathematical Analysis of Many-Body Quantum Systems*. The authors wish to thank the organizers of the conference *Mathematical Challenge of Quantum Transport in Nanosystems, St. Petersburg,* 2013.

References

[1] A. H. Castro Neto, F. Guinea, N. M. R. Peres, K. S. Novoselov, and A. K. Geim. The electronic properties of graphene. *Reviews of Modern Physics*, **81**, P. 109–162 (2009).

[2] H. D. Cornean, R. Purice. On the regularity of the Hausdorff distance between spectra of perturbed magnetic Hamiltonians. *Spectral Analysis of Quantum Hamiltonians*, P. 55–66 (2012).

[3] P. Dietl, F. Piéchon, and G. Montambaux. New magnetic field dependence of Landau levels in a graphenelike structure. *Physical review letters*, **100** (23), P. 236405 (2008).

[4] C. L. Fefferman, M. I. Weinstein. Honeycomb lattice potentials and Dirac points. *J. Amer. Math. Soc*, **25**, P. 1169–1220 (2012).

[5] D. R. Hofstadter. Energy levels and wave functions of bloch electrons in rational and irrational magnetic fields. *Physical review B*, **14** (6), P. 2239 (1976).

[6] J. M. Luttinger. The effect of a magnetic field on electrons in a periodic potential. *Phys. Rev.*, **84** (4) P. 814–817 (1951).

[7] G. Nenciu. Bloch electrons in a magnetic field: Rigorous justification of the Peierls-Onsager effective Hamiltonian. *Letters in mathematical physics*, **17** (3), P. 247–252 (1989).

[8] G. Nenciu. Dynamics of band electrons in electric and magnetic fields: rigorous justification of the effective Hamiltonians. *Rev. Mod. Phys.*, **63** (1), P. 91–127 (1991).

[9] K. S. Novoselov, A. K. Geim, et al. Two-dimensional gas of massless Dirac fermions in graphene. *Nature*, **438** (7065), P. 197–200 (2005).

[10] K. S. Novoselov, A. K. Geim, et al. Electric field effect in atomically thin carbon films. *Science*, **306** (5696), P. 666–669 (2004).

[11] R. Peierls. Zur theorie des diamagnetismus von leitungselektronen. *Zeitschrift für Physik A Hadrons and Nuclei*, **80** (11), P. 763–791 (1933).

[12] R. Rammal. Landau level spectrum of Bloch electrons in a honeycomb lattice. *Journal de Physique*, **46** (8), P. 1345–1354 (1985).

[13] P. R. Wallace. The band theory of graphite. *Physical Review*, **71** (9), P. 622 (1947).

NANOSYSTEMS: PHYSICS, CHEMISTRY, MATHEMATICS, 2013, 4 (4), P. 474–483

ON THE ASYMPTOTICS OF THE PRINCIPAL EIGENVALUE FOR A ROBIN PROBLEM WITH A LARGE PARAMETER IN PLANAR DOMAINS

Konstantin Pankrashkin

Laboratoire de mathématiques – UMR 8628, Université Paris-Sud,
Bâtiment 425, 91405 Orsay Cedex, France

konstantin.pankrashkin@math.u-psud.fr
http://www.math.u-psud.fr/∼pankrash/

PACS 41.20.Cv, 02.30.Jr, 02.30.Tb

Let $\Omega \subset \mathbb{R}^2$ be a domain having a compact boundary Σ which is Lipschitz and piecewise C^4 smooth, and let ν denote the inward unit normal vector on Σ. We study the principal eigenvalue $E(\beta)$ of the Laplacian in Ω with the Robin boundary conditions $\partial f/\partial\nu + \beta f = 0$ on Σ, where β is a positive number. Assuming that Σ has no convex corners, we show the estimate $E(\beta) = -\beta^2 - \gamma_{\max}\beta + O\big(\beta^{\frac{2}{3}}\big)$ as $\beta \to +\infty$, where $\gamma_{\max}$ is the maximal curvature of the boundary.

Keywords: eigenvalue, Laplacian, Robin boundary condition, curvature, asymptotics.

1. Introduction

Let $\Omega \subset \mathbb{R}^2$ be an open connected set having a compact Lipschitz piecewise smooth boundary Σ. For $\beta > 0$ consider the operator H_β which is the Laplacian $f \mapsto -\Delta f$ with the Robin boundary conditions,

$$\frac{\partial f}{\partial \nu} + \beta f = 0 \text{ on } \Sigma,$$

where ν is the inward unit normal vector. More precisely, H_β is the self-adjoint operator in $L^2(\Omega)$ associated with the sesquilinear form

$$h_\beta(f,g) = \iint_\Omega \overline{\nabla f}\nabla g \,\mathrm{d}x - \beta\int_\Sigma \overline{f}\, g \,\mathrm{d}\sigma, \quad \operatorname{dom} h_\beta = H^1(\Omega); \tag{1}$$

here σ denotes the one-dimensional Hausdorff measure on Σ. The operator H_β is semibounded from below. If Ω is bounded, then H_β has a compact resolvent, and we denote by $E_j(\beta)$, $j \in \mathbb{N}$, its eigenvalues taken according to their multiplicities and enumerated in the non-decreasing order. If Ω is unbounded, then the essential spectrum of H_β coincides with $[0,+\infty)$, and the discrete spectrum consists of a finite number of eigenvalues, which we denote again by $E_j(\beta)$, $j \in \{1,\dots,N_\beta\}$, and enumerate them in the non-decreasing order taking into account the multiplicities. In the both cases, the principal eigenvalue $E(\beta) := E_1(\beta)$ may be defined through the Rayleigh quotients

$$E(\beta) = \inf_{0\neq f\in\operatorname{dom} h_\beta} \frac{h_\beta(f,f)}{\|f\|^2_{L^2(\Omega)}}.$$

It is easy to check that $E(\beta) < 0$: for bounded Ω one can test on $f = 1$, and for unbounded Ω, one may use $f(x) = \exp\big(-|x|^\alpha/2\big)$ with small $\alpha > 0$.

The study of the principal eigenvalue arises in several applications: work [1] discusses the stochastic meaning of the Robin eigenvalues, paper [2] shows that the eigenvalue problem

appears in the study of long-time dynamics related to some reaction-diffusion processes, and a discussion of an interplay between the eigenvalues and the estimate of the critical temperature in a problem of superconductivity may be found in [3].

In the present note, we are interested in the asymptotic behavior of $E(\beta)$ for large values of β. For bounded Ω, this question was already addressed in numerous papers. It was conjectured and partially proven in [2] that one has the asymptotics

$$E(\beta) = -C_\Omega \beta^2 + o(\beta^2) \text{ as } \beta \to +\infty, \tag{2}$$

for some constant $C_\Omega > 0$. It seems that the paper [4] contains the first rigorous proof of the above equality for the case of a C^1 smooth Σ, and in that case one has $C_\Omega = 1$, as predicted in [2]. Under the same assumption, it was shown in [5] that the asymptotics $E_j(\beta) = -\beta^2 + o(\beta^2)$, $\beta \to +\infty$, hold for any fixed $j \in \mathbb{N}$. The paper [6] proved the asymptotics (2) for domains whose boundary is C^∞ smooth with the possible exception of a finite number of corners. If the corner opening angles are $\alpha_j \in (0,\pi) \cup (\pi, 2\pi)$, $j = 1, \dots, m$, and $\theta := \min \alpha_j/2$, then $C_\Omega = (\sin\theta)^{-2}$ if $\theta < \pi/2$, otherwise $C_\Omega = 1$. We remark that the paper [6] formally deals with bounded domains, but the proofs can be easily adapted to unbounded domains with compact boundaries. It should pointed out that domains with cusps need a specific consideration, and the results are different [6, 7]. Various generalizations of the above results and some related questions concerning the spectral theory of the Robin Laplacians were discussed in [7–12]. The aim of the present note is to refine the asymptotics (2) for a class of two-dimensional domains. More precisely, we calculate the next term in the asymptotic expansion for piecewise C^4 smooth domains whose boundary has no convex corners, i.e. we assume that either the boundary is smooth or that all corner opening angles are larger than π; due to the above cited result of [6] we have $C_\Omega = 1$ in the both cases.

Let us formulate the assumptions and the result more carefully. Let Σ_k, $k = 1, \dots, n$, be non-intersecting C^4 smooth connected components of the boundary Σ such that $\Sigma = \bigcup_{k=1}^n \overline{\Sigma}_k$. Denote by ℓ_k the length of Σ_k and consider a parametrization of the closure $\overline{\Sigma}_k$ by the arc length, i.e. let $[0, \ell_k] \ni s \mapsto \Gamma_k(s) \equiv \big(\Gamma_{k,1}(s), \Gamma_{k,2}(s)\big) \in \overline{\Sigma}_k$ be a bijection with $|\Gamma_k'| = 1$, such that $\Gamma_k \in C^4\big([0,\ell_k], \mathbb{R}^2\big)$, and we assume that the orientation of each Γ_k is chosen in such a way that $\nu_k(s) := \big(-\Gamma_{k,2}'(s), \Gamma_{k,1}'(s)\big)$ is the inward unit normal vector at the point $\Gamma_k(s)$ of the boundary. If two components Σ_j, Σ_k meet at some point $P := \Gamma_j(\ell_j) = \Gamma_k(0)$, then two options are allowed: either $\overline{\Sigma_j \cup \Sigma_k}$ is C^4 smooth near P or the corner opening angle at P measured inside Ω belongs to $(\pi, 2\pi)$.

We denote by $\gamma_k(s)$ the signed curvature of the boundary at the point $\Gamma_k(s)$ and let $\gamma_{\max}$ denote its global maximum:

$$\gamma_k(s) := \Gamma_{k,1}'(s)\Gamma_{k,2}''(s) - \Gamma_{k,1}''(s)\Gamma_{k,2}'(s), \quad \gamma_{\max} := \max_{k\in\{1,\dots,n\}} \max_{s\in[0,\ell_k]} \gamma_k(s);$$

note that the decomposition of the boundary Σ into the pieces Σ_k is non-unique, but the value $\gamma_{\max}$ is uniquely determined. Our result is as follows:

Theorem 1. *Under the preceding assumptions there holds*

$$E(\beta) = -\beta^2 - \gamma_{\max}\beta + O\big(\beta^{\frac{2}{3}}\big) \text{ as } \beta \to +\infty.$$

We believe that it is hard to improve the asymptotics without any additional information on the set at which the curvature attains its maximal value. For example, one may expect that the case of a curvature having isolated maxima and the case of a piecewise constant curvature should give different resolutions of the remainder, and we hope to progress in this direction in subsequent works.

At first sight, the Robin eigenvalue problem may look rather similar to the eigenvalue problem for δ-potentials supported by curves, see e.g. [13–15]. This first impression is wrong, and the result of Theorem 1 concerning the secondary asymptotic term is very different from the one obtained in the papers [13, 14] for strong δ-potentials; nevertheless, a part of the machinery of [13] plays an important role in our considerations. On the other hand, the asymptotic behavior of the principal Robin eigenvalue shows some analogy with the lowest eigenvalue of the Neumann magnetic Laplacian studied in the theory of superconductivity [16–18].

2. Dirichlet-Neumann bracketing on thin strips

In this section we introduce and study an auxiliary eigenvalue problem, and the results obtained will be used in the next section to prove theorem 1.

Let $\ell > 0$ and let $\Gamma : [0,\ell] \to \mathbb{R}^2$, $s \mapsto \Gamma(s) = \big(\Gamma_1(s), \Gamma_2(s)\big) \in \mathbb{R}^2$, be an injective C^4 map such that $\big|\Gamma'(s)\big| = 1$ for all $s \in (0,\ell)$. We denote

$$S := \Gamma\big((0,\ell)\big), \quad \kappa(s) := \Gamma_1'(s)\Gamma_2''(s) - \Gamma_1''(s)\Gamma_2'(s), \quad \kappa_{\max} := \max_{s\in[0,\ell]} \kappa(s),$$
$$K := \max_{s\in[0,\ell]} \big|\kappa(s)\big| + \max_{s\in[0,\ell]} \big|\kappa'(s)\big| + \max_{s\in[0,\ell]} \big|\kappa''(s)\big|.$$

Due to $\kappa \in C^2\big([0,\ell]\big)$, the above quantity K is finite.

For $a > 0$, consider the map

$$\Phi_a : (0,\ell)\times(0,a) \to \mathbb{R}^2, \quad \Phi_a(s,u) = \begin{pmatrix} \Gamma_1(s) - u\Gamma_2'(s) \\ \Gamma_2(s) + u\Gamma_1'(s) \end{pmatrix}.$$

As shown in [13, Lemma 2.1], for any $a \in (0, a_0)$, $a_0 := (2K)^{-1}$, the map Φ_a defines a diffeomorphism between the domains $\square_a := (0,\ell)\times(0,a)$ and $\Omega_a := \Phi_a(\square_a)$. In what follows, we always assume that $a \in (0,a_0)$ and we will work with the usual Sobolev space $H^1(\Omega_a)$ and its part $\widetilde{H}^1_0(\Omega_a) := \big\{ f \in H^1(\Omega_a) : f\restriction_{\partial\Omega_a\setminus\overline{S}} = 0\big\}$; here the symbol $\restriction$ means the trace of the function on the indicated part of the boundary.

Here, we introduce two sesquilinear forms in $L^2(\Omega_a)$. The first one, $h_\beta^{N,a}$, is defined on $\operatorname{dom} h_\beta^{N,a} := H^1(\Omega_a)$ by the expression

$$h_\beta^{N,a}(f,g) = \iint_{\Omega_a} \overline{\nabla f}\nabla g \,\mathrm{d}x - \beta\int_S \overline{f} g \,\mathrm{d}\sigma,$$

and the second one, $h_\beta^{D,a}$, is its restriction to $\operatorname{dom} h_\beta^{D,a} := \widetilde{H}^1_0(\Omega_a)$. Both forms are densely defined, symmetric, closed and semibounded from below, and we denote

$$E_{N/D}(\beta,a) = \inf_{0\neq f\in\operatorname{dom} h_\beta^{N/D,a}} \frac{h_\beta^{N/D,a}(f,f)}{\|f\|^2_{L^2(\Omega_a)}}. \tag{3}$$

We show the following results:

Lemma 2. *There exists $a_1 > 0$ such that for any $a \in (0,a_1)$ one has the estimate $E_{N/D}(\beta,a) = -\beta^2 - \kappa_{\max}\beta + O(\beta^{\frac{2}{3}})$ as $\beta \to +\infty$.*

The rest of this section is devoted to the proof of lemma 2. We first introduce a suitable decomposition of Ω_a and then provide two-side eigenvalue estimates using operators with separated variables.

Define $U_a : L^2(\Omega_a) \to L^2(\square_a)$ by $\big(U_a f\big)(s,u) = \sqrt{1-u\kappa(s)}f\big(\Phi_a(s,u)\big)$. Clearly, U_a is a unitary operator, and one has $U_a\big(H^1(\Omega_a)\big) = H^1(\square_a)$ and

$$U_a\big(\widetilde{H}^1_0(\Omega_a)\big) = \widetilde{H}^1_0(\square_a) := \big\{f \in H^1(\square_a) :\ f(0,\cdot) = f(\ell,\cdot) = 0 \text{ and } f(\cdot,a) = 0\big\},$$

where the restrictions should be again understood as the traces. Using integration by parts, one may easily check that for any $f, g \in H^1(\Omega_a)$, one has $h^{N,a}_\beta(f,g) = q^{N,a}_\beta(U_a f, U_a g)$, where the form $q^{N,a}_\beta$ is defined on the domain $\operatorname{dom} q^{N,a}_\beta := H^1(\square_a)$ by the expression

$$\begin{aligned} q^{N,a}_\beta(f,g) = &\iint_{\square_a} \frac{1}{\big(1-u\kappa(s)\big)^2}\,\overline{\frac{\partial f}{\partial s}}\frac{\partial g}{\partial s}\,\mathrm{d}s\,\mathrm{d}u + \iint_{\square_a}\overline{\frac{\partial f}{\partial u}}\frac{\partial g}{\partial u}\,\mathrm{d}s\,\mathrm{d}u \\ &- \iint_{\square_a} V(s,u)\overline{f}\,g\,\mathrm{d}s\,\mathrm{d}u - \beta\int_0^\ell \overline{f(s,0)}g(s,0)\,\mathrm{d}s \\ &- \frac{1}{2}\int_0^\ell \kappa(s)\,\overline{f(s,0)}g(s,0)\,\mathrm{d}s + \frac{1}{2}\int_0^\ell \frac{\kappa(s)}{1-a\kappa(s)}\,\overline{f(s,a)}g(s,a)\,\mathrm{d}s \\ &+ \frac{1}{2}\kappa'(\ell)\int_0^a \frac{u}{\big(1-u\kappa(\ell)\big)^3}\,\overline{f(\ell,u)}g(\ell,u)\,\mathrm{d}u \\ &- \frac{1}{2}\kappa'(0)\int_0^a \frac{u}{\big(1-u\kappa(0)\big)^3}\,\overline{f(0,u)}g(0,u)\,\mathrm{d}u \end{aligned} \tag{4}$$

with

$$V(s,u) := \frac{u\kappa''(s)}{2\big(1-u\kappa(s)\big)^3} + \frac{5u^2\kappa'(s)^2}{4\big(1-u\kappa(s)\big)^4} + \frac{\kappa(s)^2}{4\big(1-u\kappa(s)\big)^2}.$$

Similarly, for any $f, g \in \widetilde{H}^1_0(\Omega_a)$, one has $h^{D,a}_\beta(f,g) = q^{D,a}_\beta(U_a f, U_a g)$, where $q^{D,a}_\beta$ is the restriction of $q^{N,a}_\beta$ to the domain $\operatorname{dom} q^{D,a}_\beta := \widetilde{H}^1_0(\square_a)$; note that for $f, g \in \operatorname{dom} q^{D,a}_\beta$ the three last terms on the right-hand side of (4) vanish. Using the unitarity of U_a we may rewrite the equalities (3) in the form:

$$E_{N/D}(\beta,a) = \inf_{0\neq f\in\operatorname{dom} q^{N/D,a}_\beta} \frac{q^{N/D,a}_\beta(f,f)}{\|f\|^2_{L^2(\square_a)}}. \tag{5}$$

We would like to reduce the estimation of these quantities to the study of the eigenvalues of certain one-dimensional operators.

Using the one-dimensional Sobolev inequality on $(0,\ell)$ we see that one can find a constant $C > 0$ independent of a, such that for all $f \in H^1(\square_a)$, one has

$$\int_0^a \big|f(0,u)\big|^2\,\mathrm{d}u + \int_0^a \big|f(\ell,u)\big|^2\,\mathrm{d}u \le C\Big(\iint_{\square_a}\Big|\frac{\partial f}{\partial s}\Big|^2\mathrm{d}s\,\mathrm{d}u + \iint_{\square_a}|f|^2\mathrm{d}s\,\mathrm{d}u\Big).$$

One can also find a constant $v > 0$, such that $\big|V(s,u)\big| \le v$ for all $(s,u) \in \square_a$ and all $a \in (0,a_0)$. Furthermore, again for $(s,u) \in \square_a$ and any $a \in (0,a_0)$, we have

$$\Big|\frac{\kappa(s)}{1-a\kappa(s)}\Big| \le 2K, \quad \frac{2}{3} \le \frac{1}{1-u\kappa(s)} \le 2.$$

For any $M \in \mathbb{N}$, we denote

$$\delta := \frac{\ell}{M}, \quad I_M^j := (j\delta - \delta, j\delta), \quad \square_{a,M}^j := I_M^j \times (0,a),$$
$$\kappa_{M,j}^- := \inf_{s \in I_M^j} \kappa(s), \quad \kappa_{M,j}^+ := \sup_{s \in I_M^j} \kappa(s), \quad j = 1, \dots, M,$$

and introduce functions $\kappa_M^\pm : (0,\ell) \to \mathbb{R}$ as follows: $\kappa_M^\pm(s) := \kappa_{M,j}^\pm$ if $s \in I_M^j$, and $\kappa_M^\pm(j\delta) := 0$ for $j = 1, \dots, M-1$. In addition, we assume that $0 < a < (10KC)^{-1}$. Now, we introduce two new sesquilinear forms which will be used to obtain a two-side estimate for $E_{N/D}(\beta, a)$. The first one, $t_\beta^{-,M,a}$, is defined by

$$\begin{aligned}
\operatorname{dom} t_\beta^{-,M,a} &= H^1\big(\bigcup_{j=1}^M \square_{a,M}^j\big) \simeq \bigoplus_{j=1}^M H^1\big(\square_{a,M}^j\big),\\
t_\beta^{-,M,a}(f,g) &= \Big(\frac{4}{9} - 4aKC\Big) \iint_{\square_a} \frac{\overline{\partial f}}{\partial s}\frac{\partial g}{\partial s}\,\mathrm{d}s\,\mathrm{d}u + \iint_{\square_a} \frac{\overline{\partial f}}{\partial u}\frac{\partial g}{\partial u}\,\mathrm{d}s\,\mathrm{d}u\\
&\quad - (v + 4aKC) \iint_{\square_a} \overline{f} g\,\mathrm{d}s\,\mathrm{d}u - \int_0^\ell \Big(\beta + \frac{\kappa_M^+(s)}{2}\Big)\,\overline{f(s,0)} g(s,0)\,\mathrm{d}s\\
&\quad - K\int_0^\ell \overline{f(s,a)} g(s,a)\,\mathrm{d}s.
\end{aligned}$$

The second one, $t_\beta^{+,M,a}$, is defined on the domain $\operatorname{dom} t_\beta^{+,M,a} = \bigoplus_{j=1}^M \widetilde{H}_0^1(\square_{a,M}^j)$,

$$\widetilde{H}_0^1(\square_{a,M}^j) := \big\{ f \in H^1(\square_{a,M}^j) :\ f(j\delta - \delta, \cdot) = f(j\delta, \cdot) = 0 \text{ and } f(\cdot, a) = 0 \big\},$$

through

$$\begin{aligned}
t_\beta^{+,M,a}(f,g) &= 4\iint_{\square_a} \frac{\overline{\partial f}}{\partial s}\frac{\partial g}{\partial s}\,\mathrm{d}s\,\mathrm{d}u + \iint_{\square_a} \frac{\overline{\partial f}}{\partial u}\frac{\partial g}{\partial u}\,\mathrm{d}s\,\mathrm{d}u\\
&\quad + v\iint_{\square_a} \overline{f} g\,\mathrm{d}s\,\mathrm{d}u - \int_0^\ell \Big(\beta + \frac{\kappa_M^-(s)}{2}\Big)\,\overline{f(s,0)} g(s,0)\,\mathrm{d}s.
\end{aligned}$$

One clearly has the inclusions $\operatorname{dom} t_\beta^{+,M,a} \subset \operatorname{dom} q_\beta^{D,a} \subset \operatorname{dom} q_\beta^{N,a} \subset \operatorname{dom} t_\beta^{-,M,a}$ and the inequalities

$$\begin{aligned}
t_\beta^{-,M,a}(f,f) &\le q_\beta^{N,a}(f,f), && f \in \operatorname{dom} q_\beta^{N,a},\\
q_\beta^{N,a}(f,f) &= q_\beta^{D,a}(f,f), && f \in \operatorname{dom} q_\beta^{D,a},\\
q_\beta^{D,a}(f,f) &\le t_\beta^{+,M,a}(f,f), && f \in \operatorname{dom} t_\beta^{+,M,a},
\end{aligned}$$

which justify the estimates

$$E_M^-(\beta,a) \le E_N(\beta,a) \le E_D(\beta,a) \le E_M^+(\beta,a), \tag{6}$$

where we denote

$$E_M^\pm(\beta,a) := \inf_{0 \ne f \in \operatorname{dom} t_\beta^{\pm,M,a}} \frac{t_\beta^{\pm,M,a}(f,f)}{\|f\|^2_{L^2(\square_a)}}.$$

Now, we are going to estimate $E_M^\pm(\beta,a)$ using separation of variables. Note that the forms $t_\beta^{\pm,M,a}$ are densely defined, semibounded from below and closed in $L^2(\square_a)$, therefore, they define some self-adjoint operators $T_\beta^{\pm,M,a}$ in $L^2(\square_a)$, and $E_M^\pm(\beta,a) = \inf \operatorname{spec} T_\beta^{\pm,M,a}$. On the

other hand, due to the fact that the domains $\square^j_{a,M}$ are disjoint and isometric to one another , we can identify $T^{\pm,M,a}_\beta \simeq \bigoplus_{j=1}^M T^{\pm,M,a}_{\beta,j}$, where $T^{\pm,M,a}_{\beta,j}$ are self-adjoint operators acting in $L^2(\square_{\delta,a})$, $\square_{\delta,a} := (0,\delta)\times(0,a)$, and associated respectively with the sesqulinear forms $t^{\pm,M,a}_{\beta,j}$,

$$\begin{aligned}
t^{-,M,a}_{\beta,j}(f,g) &= \Big(\frac{4}{9} - 4aKC\Big)\int_0^\delta\int_0^a \overline{\frac{\partial f}{\partial s}}\frac{\partial g}{\partial s}\mathrm{d}u\,\mathrm{d}s + \int_0^\delta\int_0^a \overline{\frac{\partial f}{\partial u}}\frac{\partial g}{\partial u}\mathrm{d}u\,\mathrm{d}s \\
&\quad - (v+4aKC)\int_0^\delta\int_0^a \overline{f}g\,\mathrm{d}u\,\mathrm{d}s - \Big(\beta + \frac{\kappa^+_{M,j}}{2}\Big)\int_0^\delta \overline{f(s,0)}g(s,0)\,\mathrm{d}s \\
&\quad - K\int_0^\delta \overline{f(s,a)}g(s,a)\,\mathrm{d}s, \quad \operatorname{dom} t^{-,M,a}_{\beta,j} = H^1(\square_{\delta,a}), \\
t^{+,M,a}_{\beta,j}(f,g) &= 4\int_0^\delta\int_0^a \overline{\frac{\partial f}{\partial s}}\frac{\partial g}{\partial s}\mathrm{d}u\,\mathrm{d}s + \int_0^\delta\int_0^a \overline{\frac{\partial f}{\partial u}}\frac{\partial g}{\partial u}\mathrm{d}u\,\mathrm{d}s \\
&\quad + v\int_0^\delta\int_0^a \overline{f}g\,\mathrm{d}u\,\mathrm{d}s - \Big(\beta + \frac{\kappa^-_{M,j}}{2}\Big)\int_0^\delta \overline{f(s,0)}g(s,0)\,\mathrm{d}s, \\
&\operatorname{dom} t^{+,M,a}_{\beta,j} = \big\{f\in H^1(\square_{\delta,a}):\ f(0,\cdot) = f(\delta,\cdot) = 0 \text{ and } f(\cdot,a) = 0\big\}.
\end{aligned}$$

It is routine to check that $T^{\pm,M,a}_{\beta,j} = Q^\pm_M\otimes 1 + 1\otimes L^{\pm,j}_{\beta,a}$, where $Q^\pm_M$ are the operators acting in $L^2(0,\delta)$ as follows:

$$\begin{aligned}
Q^-_M f &= -\left(\frac{4}{9} - 4aKC\right) f'' - (v+4aKC)\,f, \\
\operatorname{dom} Q^-_M &= \Big\{f\in H^2(0,\delta) : f'(0) = f'(\delta) = 0\Big\}, \\
Q^+_M f &= -4f'' + vf, \\
\operatorname{dom} Q^-_M &= \Big\{f\in H^2(0,\delta) : f(0) = f(\delta) = 0\Big\},
\end{aligned}$$

and $L^{\pm,j}_{\beta,a}$ are the self-adjoint operators in $L^2(0,a)$ both acting as $L^{\pm,j}_{\beta,a} f = -f''$ on the domains

$$\begin{aligned}
\operatorname{dom} L^{-,j}_{\beta,a} &= \Big\{f\in H^2(0,a):\ f'(0) + \Big(\beta + \frac{\kappa^+_{M,j}}{2}\Big)f(0) = 0,\ f'(a) - Kf(a) = 0\Big\}, \\
\operatorname{dom} L^{+,j}_{\beta,a} &= \Big\{f\in H^2(0,a):\ f'(0) + \Big(\beta + \frac{\kappa^-_{M,j}}{2}\Big)f(0) = 0,\ f(a) = 0\Big\}.
\end{aligned}$$

The spectra of $Q^\pm_M$ can be calculated explicitly; in particular, one has

$$\inf\operatorname{spec} Q^-_M = -v - 4aKC, \quad \inf\operatorname{spec} Q^+_M = \frac{4\pi^2}{\delta^2} + v \equiv \frac{4\pi^2M^2}{\ell^2} + v.$$

Therefore, denoting $E^{\pm,j}(\beta,a) := \inf\operatorname{spec} L^{\pm,j}_{\beta,a}$, we arrive at

$$\begin{aligned}
E^-_M(\beta,a) &= \min_j\big(\inf\operatorname{spec} T^{-,M,a}_{\beta,j}\big) = -v - 4aKC + \min_j E^{-,j}(\beta,a), \\
E^+_M(\beta,a) &= \min_j\big(\inf\operatorname{spec} T^{+,M,a}_{\beta,j}\big) = \frac{4\pi^2M^2}{\ell^2} + v + \min_j E^{+,j}(\beta,a).
\end{aligned} \tag{7}$$

To study the lowest eigenvalues of $L^{\pm,j}_{\beta,a}$, we prove two auxiliary estimates.

Lemma 3. *For $a,\beta,\gamma > 0$, let $\Lambda_{a,\beta,\gamma}$ denote the self-adjoint operator in $L^2(0,a)$ acting as $f\mapsto -f''$ on the functions $f\in H^2(0,a)$ satisfying the boundary conditions*

$f'(0)+\beta f(0)=f'(a)-\gamma f(a)=0$, and let $E(a,\beta,\gamma)$ be its lowest eigenvalue. Let $\beta>2\gamma$ and $\beta a>1$, then $\beta^2<-E(a,\beta,\gamma)<\beta^2+123\beta^2e^{-2\beta a}$.

Proof. Let $k>0$. Clearly, $E=-k^2$ is an eigenvalue of $\Lambda_{a,\beta,\gamma}$ if one can find $(C_1,C_2)\in\mathbb{C}^2\setminus\big\{(0,0)\big\}$ such that the function $f:x\mapsto C_1e^{kx}+C_2e^{-kx}$ belongs to the domain of $\Lambda_{a,\beta,\gamma}$. The boundary conditions give

$$0=f'(0)+\beta f(0)=(\beta+k)C_1+(\beta-k)C_2,$$
$$0=f'(a)-\gamma f(a)=(k-\gamma)e^{ka}C_1-(k+\gamma)e^{-ka}C_2,$$

and one has a non-zero solution if the determinant of this system vanishes, i.e. if k satisfies the equation $(k+\beta)(k+\gamma)e^{-ka}=(k-\beta)(k-\gamma)e^{ka}$. Let us look for solutions $k\in(\beta,+\infty)$. One may rewrite the preceding equation as

$$g(k)=h(k),\quad g(k)=\frac{k+\beta}{k-\beta},\quad h(k)=\frac{k-\gamma}{k+\gamma}e^{2ka}. \tag{8}$$

Both functions g and h are continuous. It is readily seen that the function g is strictly decreasing on $(\beta,+\infty)$ with $g(\beta+)=+\infty$ and $g(+\infty)$=1. Conversely, for $\beta>2\gamma$, the function h is strictly increasing in $(\beta,+\infty)$, being the product of two strictly increasing positive functions, and we have $h(\beta+)=e^{2\beta a}(\beta-\gamma)/(\beta+\gamma)<+\infty$ and $h(+\infty)=+\infty$. These properties of g and h show that there exists a unique solution $k=k(a,\beta,\gamma)\in(\beta,+\infty)$ of (8) and that $E(a,\beta,\gamma)=-k(a,\beta,\gamma)^2$.

To obtain the required estimate we use again the monotonicity of h on $(\beta,+\infty)$ and the inequality $\beta>2\gamma$. We have

$$\frac{k+\beta}{k-\beta}=g(k)=h(k)>h(\beta+)=\frac{\beta-\gamma}{\beta+\gamma}e^{2\beta a}\geq\frac{e^{2\beta a}}{3},$$

which gives $(1-3e^{-2\beta a})k<(1+3e^{-2\beta a})\beta$. The assumption $\beta a>1$ gives the inequality $3e^{-2\beta a}<1/2$, and we arrive at

$$k<\frac{1+3e^{-2\beta a}}{1-3e^{-2\beta a}}\,\beta<(1+3e^{-2\beta a})(1+15e^{-2\beta a})\beta<(1+41e^{-2\beta a})\beta$$

and $k^2<(1+41e^{-2\beta a})^2\beta^2<(1+123e^{-2\beta a})\beta^2$. Together with the inclusion $k\in(\beta,+\infty)$ this gives the result. □

Lemma 4. *For $a,\beta>0$, let $\Pi_{a,\beta}$ denote the self-adjoint operator in $L^2(0,a)$ acting as $f\mapsto -f''$ on the functions $f\in H^2(0,a)$ satisfying the boundary conditions $f'(0)+\beta f(0)=f(a)=0$, and let $E(a,\beta)$ be its lowest eigenvalue. Assume that $\beta a>4/3$, then $\beta^2-4\beta^2e^{-\beta a}<-E(a,\beta)<\beta^2$.*

Proof. Let $k>0$. Proceeding as in the proof of lemma 3, we see that $E=-k^2$ is an eigenvalue of $\Pi_{a,\beta}$ if k satisfies the equation $(\beta+k)e^{-ka}=(\beta-k)e^{ka}$. As the left sideof the equation is strictly positive, the right side must be positive as well, which means that all solutions k belong to $(0,\beta)$. Let us rewrite the equation in the form $g(k)=0$ with $g(k):=\log(\beta+k)-\log(\beta-k)-2ka$. One has $g(0)=0$, the function g is strictly decreasing in $(0,k_0)$ and strictly increasing in (k_0,β), with $k_0:=\sqrt{\beta^2-\beta/a}$. Moreover, $g(\beta-)=+\infty$. Therefore, the equation $g(k)=0$ has a unique solution in (k_0,β). It follows from the assumption $\beta a>4/3$ that $k_0>\beta/2$, and we can represent $k=\beta-s$ with some $s\in(0,\beta/2)$. Using again the condition $g(k)=0$, we arrive at the inequality $\log s=\log(2\beta-s)-2\beta a+2sa<\log(2\beta)-\beta a$, which gives $s<2\beta e^{-\beta a}$ and $k=\beta-s>\beta(1-2e^{-\beta a})$. Finally, $-E(a,\beta)=k^2>\beta^2(1-2e^{-\beta a})^2>\beta^2(1-4e^{-\beta a})$. Together with the first inequality $k<\beta$ this gives the desired estimate . □

Let us complete the proof of lemma 2. Denote $a_1 := \min\{a_0, (10KC)^{-1}\}$ and pick any $a \in (0, a_1)$, and let $\beta > 3K + 1 + 4/(3a)$. Applying lemma 3 to each of the operators $L^{-,j}_{\beta,a}$ and lemma 4 to each of the operators $L^{+,j}_{\beta,a}$, we arrive at the estimates

$$E^{-,j}(\beta,a) > -\Big(\beta + \frac{\kappa^+_{M,j}}{2}\Big)^2 - 123\Big(\beta + \frac{\kappa^+_{M,j}}{2}\Big)^2 \exp\Big[-2a\Big(\beta + \frac{\kappa^+_{M,j}}{2}\Big)\Big],$$
$$E^{+,j}(\beta,a) < -\Big(\beta + \frac{\kappa^-_{M,j}}{2}\Big)^2 + 4\Big(\beta + \frac{\kappa^-_{M,j}}{2}\Big)^2 \exp\Big[-a\Big(\beta + \frac{\kappa^-_{M,j}}{2}\Big)\Big].$$

To simplify the form of the remainders, we choose $\beta_a > 0$ sufficiently large such that for $\beta > \beta_a$ we have

$$\Big(\beta + \frac{K}{2}\Big)^2 \exp\Big[-2a\Big(\beta - \frac{K}{2}\Big)\Big] + 4\Big(\beta + \frac{K}{2}\Big)^2 \exp\Big[-a\Big(\beta - \frac{K}{2}\Big)\Big] \le \frac{1}{\beta},$$

then for $\beta > \beta_a + 3K + 1 + 4/(3a)$ and all $j = 1, \dots, M$, we have

$$E^{-,j}(\beta,a) > -\beta^2 - \kappa^+_{M,j}\beta - \frac{K^2}{4} - \frac{1}{\beta}, \quad E^{+,j}(\beta,a) < -\beta^2 - \kappa^-_{M,j}\beta + \frac{1}{\beta}.$$

Using the inequality $\kappa^+_{M,j} \le \kappa_{\max}$, we obtain

$$\min_j E^{-,j}(\beta,a) > -\beta^2 - \kappa_{\max}\beta - \frac{K^2}{4} - \frac{1}{\beta}. \tag{9}$$

Conversely, let $l \in \{1, \dots, M\}$ be such that $\kappa^+_{M,l} = \kappa_{\max}$. This means that there exists $s \in \overline{I^l_M}$ such that $\kappa(s) = \kappa_{\max}$. Using the Taylor expansion near s, we obtain

$$\kappa^-_{M,l} \ge \kappa^+_{M,l} - K\delta = \kappa_{\max} - K\delta \equiv \kappa_{\max} - \frac{K\ell}{M}. \tag{10}$$

In the previous considerations the number M was arbitrary, and now we pick $M \in \big[\beta^{\frac13}, 2\beta^{\frac13}\big] \cap \mathbb{N}$, then

$$\begin{aligned}\min_j E^{+,j}(\beta,a) \le E^{+,l}(\beta,a) &< -\beta^2 - \kappa^-_{M,l}\beta + \frac{1}{\beta} \\ &= -\beta^2 - \kappa_{\max}\beta + \frac{K\ell}{M}\beta + \frac{1}{\beta} \le -\beta^2 - \kappa_{\max}\beta + K\ell\beta^{\frac23} + \frac{1}{\beta}. \end{aligned} \tag{11}$$

Substituting the estimates (9) and (11) into (7) we arrive at

$$\begin{aligned} E^+_M(\beta,a) &\le -\beta^2 - \kappa_{\max}\beta + K\ell\beta^{\frac23} + \frac{1}{\beta} + \frac{4\pi^2M^2}{\ell^2} + v \\ &= -\beta^2 - \kappa_{\max}\beta + \Big(K\ell + \frac{16\pi^2}{\ell^2}\Big)\beta^{\frac23} + v + \frac{1}{\beta}, \\ E^-_M(\beta,a) &\ge -\beta^2 - \kappa_{\max}\beta - \frac{K^2}{4} - v - 4aKC - \frac{1}{\beta}, \end{aligned}$$

and the assertion of lemma 2 follows from the two-side estimates (6) .

3. Proof of Theorem 1

We continue using the notation introduced just before theorem 1. For $a > 0$, consider the maps

$$\Phi_{k,a} : (0, \ell_k) \times (0, a) \to \mathbb{R}^2, \quad \Phi_{k,a}(s, u) = \begin{pmatrix} \Gamma_{k,1}(s) - u\Gamma'_{k,2}(s) \\ \Gamma_{k,2}(s) + u\Gamma'_{k,1}(s) \end{pmatrix}, \quad k = 1, \dots, n.$$

As in section 2, we can find $a_0 > 0$ such that for any $a \in (0, a_0)$ these maps are diffeomorphic between $\square_{k,a} := (0, \ell_k) \times (0, a)$ and $\Omega_{k,a} := \Phi_{k,a}(\square_{k,a})$, that $\Omega_{k,a} \subset \Omega$, and that $\Omega_{j,a} \cap \Omega_{k,a} = \emptyset$ for $j \neq k$. Note that the last property follows from the fact that the opening angles of the boundary corners (if any) are reflex. In addition, we set $\Omega_{0,a} := \Omega \setminus \Big(\bigcup_{k=1}^n \overline{\Omega_{k,a}} \Big)$. Denote $\widetilde{H}^1_0(\Omega_{k,a}) := \big\{ f \in H^1(\Omega_{k,a}) : f\restriction_{\partial\Omega_{k,a} \setminus \overline{\Sigma}_k} = 0 \big\}$, $k = 1, \dots, n$, and introduce two new sesquilinear forms $h_\beta^{N/D,a}$ in $L^2(\Omega)$, both defined by the same expression as h_β on the domains

$$\operatorname{dom} h_\beta^{N,a} = \bigoplus_{k=0}^n H^1(\Omega_{k,a}), \quad \operatorname{dom} h_\beta^{D,a} = H^1_0(\Omega_{0,a}) \cup \bigg(\bigoplus_{k=1}^n \widetilde{H}^1_0(\Omega_{k,a}) \bigg),$$

and define

$$E_{N/D}(\beta, a) := \inf_{0 \neq f \in \operatorname{dom} h_\beta^{N/D,a}} \frac{h_\beta^{N/D,a}(f, f)}{\|f\|^2_{L^2(\Omega)}}.$$

Due to the inclusions $\operatorname{dom} h_\beta^{D,a} \subset \operatorname{dom} h_\beta \subset \operatorname{dom} h_\beta^{N,a}$, we have the inequalities

$$E_N(\beta, a) \leq E(\beta) \leq E_D(\beta, a). \tag{12}$$

Furthermore, due to the fact that the parts $\Omega_{k,a}$ are disjoint and that the set $\Sigma \cap \partial\Omega_{0,a}$ is finite (this is exactly the set of the corners), we have the equality $E_{N/D}(\beta, a) = \min_{k \in \{0,\dots,n\}} E_{k,N/D}(\beta, a)$, with

$$\begin{aligned}
E_{0,N}(\beta, a) &:= \inf_{0 \neq f \in H^1(\Omega_{0,a})} \frac{\|\nabla f\|^2_{L^2(\Omega_{0,a})}}{\|f\|^2_{L^2(\Omega_{0,a})}}, \\
E_{k,N}(\beta, a) &:= \inf_{0 \neq f \in H^1(\Omega_{k,a})} \frac{\|\nabla f\|^2_{L^2(\Omega_{k,a})} - \beta\|f\|^2_{L^2(\Sigma_k)}}{\|f\|^2_{L^2(\Omega_{k,a})}}, \quad k = 1, \dots, n, \\
E_{0,D}(\beta, a) &= \inf_{0 \neq f \in H^1_0(\Omega_{0,a})} \frac{\|\nabla f\|^2_{L^2(\Omega_{0,a})}}{\|f\|^2_{L^2(\Omega_{0,a})}}, \\
E_{k,D}(\beta, a) &:= \inf_{0 \neq f \in \widetilde{H}^1_0(\Omega_{k,a})} \frac{\|\nabla f\|^2_{L^2(\Omega_{k,a})} - \beta\|f\|^2_{L^2(\Sigma_k)}}{\|f\|^2_{L^2(\Omega_{k,a})}}, \quad k = 1, \dots, n.
\end{aligned}$$

We have clearly $E_{0,N/D}(\beta, a) \geq 0$. Furthermore, in virtue of lemma 2 we can find $a > 0$ such that for each $k \in \{1, \dots, n\}$ for $\beta \to +\infty$ we have

$$E_{k,N/D}(\beta, a) = -\beta^2 - \gamma_{k,\max}\beta + O\big(\beta^{\frac{2}{3}}\big), \quad \gamma_{k,\max} := \max_{s \in [0,\ell_k]} \gamma_k(s),$$

which gives $E_{N/D}(\beta, a) = -\beta^2 - \gamma_{\max}\beta + O\big(\beta^{\frac{2}{3}}\big)$, and the assertion of theorem 1 follows from the two-side estimate (12).

Remark 5. A more detailed asymptotic analysis is beyond the scope of the present note, but we mention one case in which the remainder estimate can be slightly improved with minimal efforts. Namely, assume that one of the following conditions is satisfied:

- the boundary Σ is of class C^4 (i.e. there are no corners),
- the curvature does not attain its maximal value $\gamma_{\max}$ at the corners,

then

$$E(\beta) = -\beta^2 - \gamma_{\max}\beta + O\big(\sqrt{\beta}\,\big) \text{ as } \beta \to +\infty. \tag{13}$$

Indeed, let us pick any $k \in \{1, \dots, n\}$ such that $\gamma_{k,\max} = \gamma_{\max}$ and revise the proof of lemma 2 with $\Gamma := \Gamma_k$, $\kappa := \gamma_k$ and $\ell := \ell_k$. For any $s \in [0, \ell]$ with $\kappa(s) = \kappa_{\max}$ we have then $\kappa'(s) = 0$, and we may replace the inequality (10) with

$$\kappa^-_{M,l} \geq \kappa^+_{M,l} - K\delta^2 = \kappa_{\max} - K\delta^2 \equiv \kappa_{\max} - \frac{K\ell^2}{M^2},$$

and by choosing $M \in \big[\sqrt[4]{\beta},\, 2\sqrt[4]{\beta}\,\big] \cap \mathbb{N}$ we arrive at the estimate $E_{N/D}(\beta, a) = -\beta^2 - \kappa_{\max}\beta + O(\sqrt{\beta}\,)$ as $\beta \to +\infty$, which in turn gives the asymptotics (13).

Acknowledgments

The research was partially supported by ANR NOSEVOL and GDR Dynamique quantique.

References

[1] G. Del Grosso, M. Campanino. A construction of the stochastic process associated to heat diffusion in a polygonal domain. *Bolletino Unione Mat. Ital.*, **13**-B, P. 876–895 (1976).
[2] A.A. Lacey, J.R. Ockendon, J. Sabina. Multidimensional reaction diffusion equations with nonlinear boundary conditions. *SIAM J. Appl. Math.*, **58**, P. 1622–1647 (1998).
[3] T. Giorgi, R. Smits. Eigenvalue estimates and critical temperature in zero fields for enhanced surface superconductivity. *Z. Angew. Math. Phys.*, **57**, P. 1–22 (2006).
[4] Y. Lou, M. Zhu. A singularly perturbed linear eigenvalue problem in C^1 domains. *Pacific J. Math.*, **214**, P. 323–334 (2004).
[5] D. Daners, J.B. Kennedy. On the asymptotic behaviour of the eigenvalues of a Robin problem. *Differential Integr. Equ.*, **23**, P. 659–669 (2010).
[6] M. Levitin, L. Parnovski. On the principal eigenvalue of a Robin problem with a large parameter. *Math. Nachr.*, **281**, P. 272–281 (2008).
[7] H. Kovařík. Eigenvalue asymptotic of Robin Laplace operators on two-dimensional domains with cusps. *J. London Math. Soc.*, **83**, P. 256–271 (2011).
[8] E. Colorado, J. García-Melián. The behavior of the principal eigenvalue of a mixed elliptic problem with respect to a parameter. *J. Math. Anal. Appl.*, **377**, P. 53–69 (2010).
[9] D.Daners.Principal eigenvalues for generalised indefinite Robin problems.*Potent.Anal.* **38**,P.1047-1069(2013)
[10] R.L. Frank, L. Geisinger. Semi-classical analysis of the Laplace operator with Robin boundary conditions. *Bull. Math. Sci.*, **2**, P. 281–319 (2012).
[11] T. Giorgi, R. Smits. Bounds and monotonicity for the generalized Robin problem. *Z. Angew. Math. Phys.*, **58**, P. 1–19 (2007).
[12] H. Kovařík, A. Laptev. Hardy inequalities for Robin Laplacians. *J. Funct. Anal.*, **262**, P. 4972–4985 (2012).
[13] P. Exner, K. Yoshitomi. Asymptotics of eigenvalues of the Schrödinger operator with a strong δ-interaction on a loop. *J. Geom. Phys.*, **41**, P. 344–358 (2002).
[14] P. Exner, K. Pankrashkin. Strong coupling asymptotics for a singular Schrödinger operator with an interaction supported by an open arc. Submitted, preprint `http://arxiv.org/abs/1207.2271`.
[15] V. Lotoreichik. Note on 2D Schrödinger operators with δ-interactions on angles and crossing lines. *Nanosystems: Phys. Chem. Math.*, **4** (2), P. 166–172 (2013).
[16] B. Helffer, A. Morame. Magnetic bottles in connection with superconductivity. *J. Funct. Anal.*, **185**, P. 604–680 (2001).
[17] V. Bonnaillie-Noël, M. Dauge. Asymptotics for the low-lying eigenstates of the Schrödinger operator with magnetic field near corners. *Ann. Henri Poincaré*, **7**, P. 899–931 (2006).
[18] S. Fournais, B. Helffer. Accurate eigenvalue estimates for the magnetic Neumann Laplacian. *Ann. Institut Fourier*, **56**, P. 1–67 (2006).

NANOSYSTEMS: PHYSICS, CHEMISTRY, MATHEMATICS, 2013, 4 (4), P. 484–489

C*-ALGEBRAS IN RECONSTRUCTION OF MANIFOLDS

M. I. Belishev

St. Petersburg Department of the Steklov Mathematical Institute,
St. Petersburg State University, St. Petersburg, Russia
belishev@pdmi.ras.ru

PACS 02.30.Jr, 02.30.Yy

We deal with two dynamical systems associated with a Riemannian manifold with boundary. The first one is a system governed by the scalar wave equation, the second is governed by Maxwells equations. Both of the systems are controlled from the boundary. The inverse problems are to recover the manifold via the relevant measurements at the boundary (inverse data). We show that that the inverse data determine a C*-algebras, whose (topologized) spectra are identical to the manifold. By this, to recover the manifold is to determine a proper algebra from the inverse data, find its spectrum, and provide the spectrum with a Riemannian structure. This paper develops an algebraic version of the boundary control method (M.I.Belishev'1986), which is an approach to inverse problems based on their relations to control theory.

Keywords: inverse problems on manifolds, C*-algebras, boundary control method.

1. Setup

1.1. Acoustics

We deal with a compact C^∞-smooth Riemannian manifold Ω with the boundary Γ, $\dim\Omega = n \geqslant 2$; Δ is the (scalar) Beltrami-Laplace operator on Ω; $\mathcal{H} := L_2(\Omega)$.
Forward problem of acoustics is to find a solution $u = u^f(x,t)$ of the system

$$u_{tt} - \Delta u = 0 \qquad \text{in } (\Omega\backslash\Gamma)\times(0,T) \tag{1.1}$$

$$u|_{t=0} = u_t|_{t=0} = 0 \qquad \text{in } \Omega \tag{1.2}$$

$$u = f \qquad \text{on } \Gamma\times[0,T]\,, \tag{1.3}$$

where $f \in \mathcal{F}^T := L_2\left(\Gamma\times[0,T]\right)$ is a (given) *boundary control*.

With the system one associates a *response operator* $R^T : \mathcal{F}^T \to \mathcal{F}^T$,

$$R^T f := \left.\frac{\partial u^f}{\partial\nu}\right|_{\Gamma\times[0,T]}$$

(for smooth enough f), ν is the outward normal to Γ.
Inverse problem is: *given for a fixed* $T > \operatorname{diam}\Omega$ *the operator* R^{2T}*, to recover* Ω.

1.2. Electrodynamics

Let Ω be *oriented*, $\dim\Omega = 3$. The definitions of the vector analysis operations $\wedge$, curl, div on a manifold see, e.g., in [9].
Forward problem Find a solution $e = e^f(x,t)$, $h = h^f(x,t)$ of the Maxwell system

$$e_t = \operatorname{curl} h,\ h_t = -\operatorname{curl} e \qquad \text{in } \Omega\times(0,T) \tag{1.4}$$

$$e|_{t=0} = 0,\ \ h|_{t=0} = 0 \qquad \text{in } \Omega \tag{1.5}$$

$$\nu\wedge e = f \qquad \text{in } \Gamma\times[0,T]\,, \tag{1.6}$$

$f \in \mathcal{F}^T := L_2([0,T]; T\Gamma)$ is a *boundary control* (time-dependent tangent field on Γ).

With the system, one associates a *response operator* $R^T : \mathcal{F}^T \to \mathcal{F}^T$,

$$R^T f := \nu \wedge h^f \Big|_{\Gamma\times[0,T]}$$

(for smooth enough f).

Inverse problem is: *given for a fixed* $T > \operatorname{diam}\Omega$ *the operator* R^{2T}*, to recover* Ω.

1.3. Nonuiqueness

Let Ω' be such that $\partial\Omega' = \partial\Omega = \Gamma$ and there is an isometry $i : \Omega \to \Omega'$ provided $i|_\Gamma = \mathrm{id}$. Then, for the response operators of the systems (1.1)–(1.3) and (1.4)–(1.6) one has $R'^T = R^T$ for all $T > 0$.

Hence, the map "manifold $\mapsto$ its response operator" in not injective. By this, to determine Ω uniquely is impossible, and we have to clarify the setup of the inverse problems as follows [3]. The only reasonable setup is: *given* R^{2T} *for a fixed* $T > \operatorname{diam}\Omega$*, to construct a Riemannian manifold* $\tilde{\Omega}$ *such that* $\partial\tilde{\Omega} = \partial\Omega = \Gamma$ *and* $\tilde{R}'^{2T} = R^{2T}$.

Philosophical question: From what "material" can such an $\tilde{\Omega}$ be constructed?

Answer in advance: $\tilde{\Omega}$ is a spectrum of a relevant C*-algebra determined by R^{2T}.

2. Eikonal algebra in Acoustics

2.1. Reachable sets

Return to the system (1.1)–(1.3).

Controllability For an open $\sigma \subset \Gamma$, define a *reachable set*

$$\mathcal{U}^s_\sigma := \left\{ u^f(\,\cdot\,, T) \,|\, \operatorname{supp} f \subset \overline{\sigma} \times [T-s, T] \right\} \subset \mathcal{H} \qquad (0 < s \leqslant T)$$

of delayed controls acting from σ. Denote

- $\Omega^s[\sigma] := \{x \in \Omega \,|\, \operatorname{dist}(x,\sigma) < s\}$ (the metric neighborhood of σ)
- $\mathcal{H}\langle\Omega^s[\sigma]\rangle := \{y \in \mathcal{H} \,|\, \operatorname{supp} y \subset \overline{\Omega^s[\sigma]}\}$ (the subspace of functions supported in $\Omega^s[\sigma]$).

A finiteness of the wave propagation speed in Ω implies $\mathcal{U}^s_\sigma \subset \mathcal{H}\langle\Omega^s[\sigma]\rangle$. The Holngren-John-Tataru uniqueness theorem leads to the relation

$$\overline{\mathcal{U}^s_\sigma} = \mathcal{H}\langle\Omega^s[\sigma]\rangle \tag{2.1}$$

(closure in $\mathcal{H}$), which is referred to as a *local approximate boundary controllability* of the system (1.1)–(1.3) [1]. For $T > \operatorname{diam}\Omega$, one has $\overline{\mathcal{U}^T_\sigma} = \mathcal{H}$.

Eikonals Let P^s_σ be the projection in $\mathcal{H}$ onto $\overline{\mathcal{U}^s_\sigma}$. By (2.1) one has

$$P^s_\sigma y = \begin{cases} y & \text{in } \Omega^s[\sigma] \\ 0 & \text{in } \Omega\backslash\Omega^s[\sigma] \end{cases}, \tag{2.2}$$

i.e., P^s_σ cuts off functions on $\Omega^s[\sigma]$. An operator

$$\tau_\sigma := \int_0^T s\, dP^T_\sigma$$

is called an *eikonal*. If $T > \operatorname{diam}\Omega$, then (2.2) implies

$$(\tau_\sigma y)(x) = \operatorname{dist}(x,\sigma)\, y(x), \qquad x \in \Omega,$$

i.e., τ_σ is a multiplication by the distant function. It is a bounded self-adjoint operator in $\mathcal{H}$.

2.2. Algebra $\mathfrak{T}$

Recall that a *spectrum* $\widehat{\mathcal{A}}$ of a commutative Banach algebra $\mathcal{A}$ is the set of its maximal ideals endowed with the Gelfand topology [7], [8]. If $\mathcal{A}$ and $\mathcal{B}$ are two isometrically isomorphic algebras (we write $\mathcal{A} \overset{\text{isom}}{=} \mathcal{B}$), then their spectra are homeomorphic (as topological spaces; we write $\widehat{\mathcal{A}} \overset{\text{hom}}{=} \widehat{\mathcal{B}}$). For the algebra of real continuous functions $C(\Omega)$, one has $\widehat{C(\Omega)} \overset{\text{hom}}{=} \Omega$ [7], [8].

For a set $S \subset \mathcal{A}$, by $\vee S$ we denote the minimal norm-closed subalgebra of $\mathcal{A}$, which contains S. Let $\mathfrak{B}(\mathcal{H})$ be the (normed) algebra of bounded operators in $\mathcal{H}$. By $\mathfrak{T} := \vee\{\tau_\sigma \mid \sigma \subset \Gamma\} \subset \mathfrak{B}(\mathcal{H})$ we denote the (sub)algebra generated by eikonals.

Theorem 1. *If $T > \operatorname{diam}\Omega$ then $\mathfrak{T} \overset{\text{isom}}{=} C(\Omega)$ and hence $\widehat{\mathfrak{T}} \overset{\text{hom}}{=} \widehat{C(\Omega)} \overset{\text{hom}}{=} \Omega$.*

2.3. Solving IP

Connecting operator With the system (1.1)–(1.3) one associates a *connecting operator* $C^T : \mathcal{F}^T \to \mathcal{F}^T$ defined by the relation

$$\left(C^T f, g\right)_{\mathcal{F}^T} = \left(u^f(\,\cdot\,, T), u^g(\,\cdot\,, T)\right)_{\mathcal{H}}\,, \qquad f, g \in \mathcal{F}^T.$$

It is a positive bounded operator. The following is a key fact of our approach (the Boundary Control method).

Proposition 1. *The operator C^T is determined by the response operator R^{2T} via a simple and explicit formula [1], [3].*

Isometry U^T By the definitions, the map

$$U^T : \mathcal{U}_\Gamma^T \ni u^f(\,\cdot\,, T) \mapsto (C^T)^{\frac{1}{2}} f \in \mathcal{F}^T$$

is an isometry. For $T > \operatorname{diam}\Omega$, one has $\overline{\mathcal{U}_\Gamma^T} = \mathcal{H}$, and U^T is a unitary operator from $\mathcal{H}$ onto $\overline{(C^T)^{\frac{1}{2}}\mathcal{F}^T}$.

Let $\tilde{P}_\sigma^s := U^T P_\sigma^s (U^T)^*$ be the projection in $\mathcal{F}^T$ onto the subspace

$$\overline{\left\{(C^T)^{\frac{1}{2}} f \mid \operatorname{supp} f \subset \overline{\sigma} \times [T-s, T]\right\}} = U^T \overline{\mathcal{U}_\sigma^s}\,.$$

By Proposition 1, *$\tilde{P}_\sigma^s$ is determined by the response operator R^{2T}.*

By the latter, the operators

$$\tilde{\tau}_\sigma := U^T \tau_\sigma (U^T)^* = \int_0^T s\, d\left[U^T P_\sigma^s (U^T)^*\right] = \int_0^T s\, d\,\tilde{P}_\sigma^s \tag{2.3}$$

are also determined by R^{2T}. We define an algebra $\tilde{\mathfrak{T}} := U^T \mathfrak{T} (U^T)^* \subset \mathfrak{B}\left(\overline{(C^T)^{\frac{1}{2}}\mathcal{F}^T}\right)$. By the definition, we have

$$\tilde{\mathfrak{T}} = U^T \left[\vee\{\tau_\sigma \mid \sigma \subset \Gamma\}\right] (U^T)^* = \vee\{\tilde{\tau}_\sigma \mid \sigma \subset \Gamma\}\,. \tag{2.4}$$

By the aforesaid, this algebra and its spectrum $\widehat{\tilde{\mathfrak{T}}} =: \tilde{\Omega}$ *are determined by the response operator R^{2T}.* Since $\tilde{\mathfrak{T}} \overset{\text{isom}}{=} \mathfrak{T}$, with regards to Theorem 1 one has

$$\Omega \overset{\text{hom}}{=} \widehat{\mathfrak{T}} \overset{\text{hom}}{=} \widehat{\tilde{\mathfrak{T}}} =: \tilde{\Omega} \tag{2.5}$$

as $T > \operatorname{diam}\Omega$.

Reconstruction The response operator R^{2T} (provided $T > \operatorname{diam}\Omega$) determines the manifold Ω up to a homeomorphism by the following scheme:

$$R^{2T} \overset{\text{Prop}\,1}{\Rightarrow} C^T \Rightarrow \overline{\left\{(C^T)^{\frac{1}{2}} f \mid \operatorname{supp} f \subset \overline{\sigma} \times [T-s,T]\right\}}_{\sigma\subset\Gamma} \Rightarrow$$
$$\Rightarrow \{\tilde{P}^s_\sigma \mid \sigma \subset \Gamma\} \overset{(2.3)}{\Rightarrow} \{\tilde{\tau}_\sigma \mid \sigma \subset \Gamma\} \overset{(2.4)}{\Rightarrow} \tilde{\mathfrak{T}} \Rightarrow$$
$$\Rightarrow \widehat{\tilde{\mathfrak{T}}} \overset{(2.5)}{=} \tilde{\Omega} \overset{\text{hom}}{=} \Omega\,.$$

Then, one can endow $\tilde{\Omega}$ with a proper Riemannian metric and identify $\partial\tilde{\Omega}$ with Γ (see, e.g., [5]).

As a result, we get a Riemannian manifold $\tilde{\Omega}$, which is isometric to the original (unknown) Ω by construction, and $\tilde{R}^{2T} = R^{2T}$ does hold. The inverse problem for the system (1.1)–(1.3) is solved.

3. Eikonal algebra in Electrodynamics

3.1. Maxwell system

Turn to the system (1.4)–(1.6). The Hilbert space $\vec{L}_2(\Omega)$ of the square-summable vector fields (sections of the tangent bundle $T\Omega$) contains the subspace of curls $\mathcal{C} := \left\{\operatorname{curl} h \,\middle|\, h, \operatorname{curl} h \in \vec{L}_2(\Omega)\right\}$.

Electric reachable sets For an open $\sigma \subset \Gamma$, define

$$\mathcal{E}^s_\sigma := \left\{e^f(\,\cdot\,,T) \mid \operatorname{supp} f \subset \overline{\sigma} \times [T-s,T]\right\} \subset \mathcal{C} \qquad (0 < s \leqslant T)\,.$$

We denote $\mathcal{C}\langle\Omega^s[\sigma]\rangle := \{y \in \mathcal{C} \mid \operatorname{supp} y \subset \overline{\Omega^s[\sigma]}\}$. The finiteness of the electromagnetic wave propagation speed in Ω implies $\mathcal{E}^s_\sigma \subset \mathcal{C}\langle\Omega^s[\sigma]\rangle$.

Controllability The Eller-Isakov-Nakamura-Tataru uniqueness theorem leads to

$$\overline{\mathcal{E}^s_\sigma} = \mathcal{C}\langle\Omega^s[\sigma]\rangle \tag{3.1}$$

(the *local boundary controllability*). For $T > \operatorname{diam}\Omega$, one has $\overline{\mathcal{E}^T_\sigma} = \mathcal{C}$.

Projections Let E^s_σ be the projection in $\mathcal{C}$ onto $\overline{\mathcal{E}^s_\sigma}$. This projection acts in more complicated way than its acoustic analog: its action is not reduced to cutting off fields. Moreover, in the general case, for the different σ and σ' the projections E^s_σ and $E^s_{\sigma'}$ *do not commute*.

Eikonals An operator

$$\varepsilon_\sigma := \int_0^T s\, dE^s_\sigma$$

acts in the space $\mathcal{C}$ and is called an *eikonal*. Since $\operatorname{diam}\Omega < \infty$, ε_σ is a bounded positive self-adjoint operator. In the general case, for $\sigma \neq \sigma'$ the eikonals E^T_σ and $E^T_{\sigma'}$ *do not commute*. The following fact plays a key role.

Lemma 1. *(M.N.Demchenko [6]) The representation*

$$(\varepsilon_\sigma y)(x) = \operatorname{dist}(x,\sigma)\, y(x) + \left(K^T y\right)(x), \qquad x \in \Omega$$

holds with a compact operator $K^T : \mathcal{C} \to \vec{L}_2(\Omega)$.

3.2. Algebra $\mathfrak{E}$

Let $\mathfrak{B}(\mathcal{C})$ be the (normed) algebra of bounded operators in $\mathcal{C}$. It contains the two-side ideal $\mathfrak{K}(\mathcal{C})$ of compact operators.

We denote by

$$\mathfrak{E} := \vee\{\varepsilon_\sigma \mid \sigma \subset \Gamma\}$$

the algebra generated by (electric) eikonals. Also, we denote $\mathfrak{K}[\mathfrak{E}] := \mathfrak{E} \cap \mathfrak{K}(\mathcal{C})$ and introduce the factor-algebra

$$\dot{\mathfrak{E}} := \mathfrak{E}/\mathfrak{K}[\mathfrak{E}]$$

Theorem 2. *(M.N.Demchenko [6]) The factor-algebra $\dot{\mathfrak{E}}$ is a commutative Banach algebra. The relation $\dot{\mathfrak{E}} \overset{\text{isom}}{=} C(\Omega)$ holds and implies $\widehat{\dot{\mathfrak{E}}} \overset{\text{hom}}{=} \Omega$.*

3.3. Solving IP

Connecting operator A Maxwell *connecting operator* $C^T : \mathcal{F}^T \to \mathcal{F}^T$ is introduced by the relation

$$\big(C^T f, g\big)_{\mathcal{F}^T} = \big(e^f(\,\cdot\,, T), e^g(\,\cdot\,, T)\big)_{\mathcal{C}}$$

for smooth controls $f, g \in \mathcal{F}^T$ vanishing near $t = 0$ [3]. In contrast to the scalar (acoustic) case, this C^T is an unbounded operator. However, the following principal fact of the BC-method remains valid.

Proposition 2. *The operator C^T is determined by the response operator R^{2T} via a simple and explicit formula [3], [5].*

Isometry U^T By the definitions, the map

$$U^T : \mathcal{E}^T_\Gamma \ni e^f(\,\cdot\,, T) \mapsto (C^T)^{\frac{1}{2}} f \in \mathcal{F}^T$$

is an isometry. For $T > \operatorname{diam} \Omega$, by (3.1) one has $\overline{\mathcal{E}^T_\Gamma} = \mathcal{C}$, and U^T is a unitary operator from $\mathcal{C}$ onto $\overline{(C^T)^{\frac{1}{2}}\mathcal{F}^T} \subset \mathcal{F}^T$.

By Proposition 2, the projection $\tilde{E}^s_\sigma := U^T E^s_\sigma (U^T)^*$ in $\overline{(C^T)^{\frac{1}{2}}\mathcal{F}^T}$ onto the subspace

$$\overline{\Big\{(C^T)^{\frac{1}{2}} f \;\Big|\; \operatorname{supp} f \subset \overline{\sigma} \times [T-s, T]\Big\}} = U^T \overline{\mathcal{E}^s_\sigma}$$

is determined by the response operator R^{2T}.

An operator

$$\tilde{\varepsilon}^T_\sigma := U^T \varepsilon^T_\sigma (U^T)^* = \int_0^T s \, d\left[U^T E^s_\sigma (U^T)^*\right] = \int_0^T s \, d\, \tilde{E}^s_\sigma$$

acts in $\overline{(C^T)^{\frac{1}{2}}\mathcal{F}^T}$ and *is determined by the response operator R^{2T}.*

An algebra

$$\tilde{\mathfrak{E}} := U^T \mathfrak{E} (U^T)^* = U^T \left[\vee\{\varepsilon_\sigma \mid \sigma \subset \Gamma\}\right] (U^T)^* = \vee\{\tilde{\varepsilon}_\sigma \mid \sigma \subset \Gamma\}$$

is a subalgebra of $\mathfrak{B}\left(\overline{(C^T)^{\frac{1}{2}}\mathcal{F}^T}\right)$. By the aforesaid, this algebra, the factor-algebra $\dot{\tilde{\mathfrak{E}}} := \tilde{\mathfrak{E}}/\mathfrak{K}[\tilde{\mathfrak{E}}]$ and its spectrum

$$\widehat{\dot{\tilde{\mathfrak{E}}}} =: \tilde{\Omega}$$

are determined by the response operator R^{2T}.

The isometry $\tilde{\mathfrak{E}} \overset{\text{isom}}{=} \mathfrak{E}$ implies the isometry of the factors $\dot{\tilde{\mathfrak{E}}} \overset{\text{isom}}{=} \dot{\mathfrak{E}}$. Theorem 2 leads to

$$\Omega \overset{\text{hom}}{=} \widehat{\dot{\mathfrak{E}}} \overset{\text{hom}}{=} \widehat{\dot{\tilde{\mathfrak{E}}}} =: \tilde{\Omega}\,.$$

Reconstruction The response operator R^{2T} (provided $T > \operatorname{diam}\Omega$) determines the manifold Ω up to a homeomorphism by the following scheme:

$$\begin{aligned}
&R^{2T} \Rightarrow C^T \Rightarrow \overline{\left\{(C^T)^{\frac{1}{2}} f \;\middle|\; \operatorname{supp} f \subset \overline{\sigma} \times [T-s, T]\right\}}_{\sigma \subset \Gamma} \Rightarrow \\
&\Rightarrow \{\tilde{E}^s_\sigma \mid \sigma \subset \Gamma\} \Rightarrow \{\tilde{\varepsilon}_\sigma \mid \sigma \subset \Gamma\} \Rightarrow \tilde{\mathfrak{E}} \Rightarrow \dot{\tilde{\mathfrak{E}}} \\
&\Rightarrow \widehat{\dot{\tilde{\mathfrak{E}}}} =: \tilde{\Omega} \overset{\text{hom}}{=} \Omega\,.
\end{aligned}$$

Then, one can endow $\tilde{\Omega}$ with a proper Riemannian metric and identify $\partial\tilde{\Omega}$ with Γ (see, e.g., [5]).

As a result, we get a Riemannian manifold $\tilde{\Omega}$, which is isometric to the original (unknown) Ω by construction, and $\tilde{R}^{2T} = R^{2T}$ does hold. The inverse problem for the Maxwell system (1.4)–(1.6) is thus solved.

Acknowledgments

The work is supported by grants RFBR 11-01-00407A and SPbGU 11.38.63.2012, 6.38.670.2013.

References

[1] M.I.Belishev. Boundary control in reconstruction of manifolds and metrics (the BC method). *Inverse Problems*, **13** (5), P. 1–45 (1997).

[2] M.I.Belishev. The Calderon problem for two-dimensional manifolds by the BC-method. *SIAM J.Math.Anal.*, **35** (1), P. 172–182 (2003).

[3] M.I.Belishev. Recent progress in the boundary control method. *Inverse Problems*, **23** (5), R1–R67 (2007).

[4] M.I.Belishev. Geometrization of Rings as a Method for Solving Inverse Problems. *Sobolev Spaces in Mathematics III. Applications in Mathematical Physics, Ed. V.Isakov*, Springer, P. 5–24 (2008).

[5] M.I.Belishev and M.N.Demchenko. Time-optimal reconstruction of Riemannian manifold via boundary electromagnetic measurements. *Journal of Inverse and Ill-Posed Problems*, **19** (2), P. 167–188 (2011).

[6] M.I.Belishev, M.N.Demchenko. C*-algebras and inverse problem of electrodynamics. `http://arXiv:1205.7090`.

[7] G.J.Murphy. *C^*-Algebras and Operator Theory.* Academic Press, San Diego (1990).

[8] M.A.Naimark. *Normed Rings.* WN Publishing, Gronnongen, The Netherlands (1970).

[9] G.Schwarz. Hodge decomposition - a method for solving boundary value problems. *Lecture notes in Math.*, 1607. Springer–Verlag, Berlin (1995).

NANOSYSTEMS: PHYSICS, CHEMISTRY, MATHEMATICS, 2013, 4 (4), P. 490–495

APPLICATION OF GREEN'S FUNCTION APPROACH TO ELECTRONIC STRUCTURE OF CARBON NANOCYLINDERS

J. Smotlacha[1], R. Pincak[2]

[1] Faculty of Nuclear Sciences and Physical Engineering, Czech Technical University, Brehova 7, 110 00 Prague, Czech Republic

[2] Institute of Experimental Physics, Slovak Academy of Sciences, Watsonova 47,043 53 Kosice, Slovak Republic

smota@centrum.cz, pincak@saske.sk

PACS 73.22.Pr; 81.05.ue

The local density of states of the carbon nanostructures can be calculated in different ways. Here, we present the Haydock recursion method which, using the Green's function approach, transforms the given surface into a chain of equivalent sites. Then, using the continued fraction, we apply this procedure on the surface of the nanocylinders.

Keywords: graphene, carbon nanostructures, disclination, Green function, continued fraction.

1. Introduction

The local density density of states ($LDoS$) is one of the most important characteristics describing the electronic properties of the carbon nanostructures. Different methods were used for its calculation: The first exploits the form of the electronic spectra [1], the second deals with the gauge-theory model and the Dirac equation [2, 3], the third works with the Green function which can be calculated using different methods.

In this paper, we first describe the Haydock recursion method and the procedure of the calculation of the Green function. Then we apply this method to the calculation of the Green function and related quantities in the edge sites of the carbon nanocylinder and of the graphene nanoribbon perturbed by two heptagonal defects. Then we investigate the changes of the $LDoS$ for the changing distance of the defects and estimate the minimal and maximal distance of the defects on the perturbed surface of the nanocylinder.

2. Haydock recursion method

The $LDoS$ can be defined as

$$LDoS(E) = \lim_{\delta \to +0} \frac{1}{\pi} \mathrm{Im} G_{00}(E - i\delta), \tag{1}$$

where $G_{00}(E)$ is the Green function. It can be calculated using the recursion procedure which transforms an arbitrary surface into $1-$dimensional chain. This procedure is called the Haydock recursion method [5]. It divides the positions of the investigated surface into the groups of sites, each of them represents the site in the $1-$dimensional chain. Each site is represented by the state vector $|n\rangle$. Then, from the knowledge of the state $|1\rangle$, which corresponds to the usual state of the carbon atom, we can recursively compute the coefficients a_n, b_n corresponding to the particular sites of the chain using

$$|n+1\rangle = (H - a_n)|n\rangle - b_{n-1}|n-1\rangle. \tag{2}$$

The maximal value of n which is n_{max} determines the recursion depth. It is given by the size of the concrete surface, but in the case of infinitely large graphene, nanocone etc., it is up to our choice and it provides the rate of precision. Then we define $G_{00}(E)$ as [4]

$$G_{00}(E) = \frac{1}{E - a_1 - b_1 g_1(E)}, \tag{3}$$

where

$$g_i(E) = \frac{1}{E - a_{i+1} - b_{i+1} g_{i+1}(E)}, \qquad i = 1, ..., n. \tag{4}$$

3. LDoS of nanocylinder

In Fig. 1, we see the surface of armchair and zig-zag nanocylinder together with the labeling of the sites in accordance with the technique described in the previous section. The armchair form should be always metallic, the zig-zag form is mostly semimetallic and rarely metallic. The evidence of the metallicity is given by the peak in the $LDoS$ for the Fermi level [1].

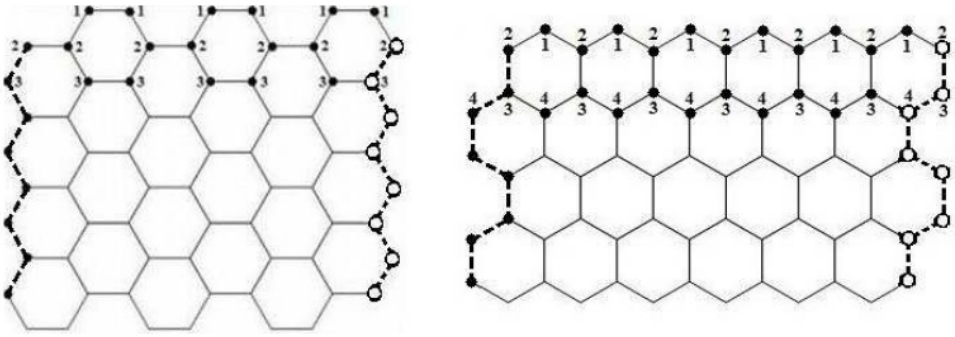

FIG. 1. Surface of two forms of the carbon nanocylinders: armchair (left) and zig-zag (right); the labeling of the sites corresponds to the technique described in the section 2; there are equivalent sites in each line parallel with the edge and that is why we label each line by the same number; the dashed lines consisting of sites denoted by black or white color are identical on the real surface.

To apply the Haydock recursion method, we have to choose the recursion depth n_{max}, which closely corresponds to the length of the nanocylinder. The $LDoS$ for different forms of the nanocylinder is shown in Fig. 2 together with the chosen values of the circumferential and the longitudinal number of atoms. The chosen value of the parameter δ in (1) is 0.1.

3.1. The case of perturbation

Let us investigate the $LDoS$ in the edge sites of a perturbed graphene nanoribbon of the sizes which have the same values as the above mentioned cylindrical surface (see Fig. 3). Because the structure of the surface is different from the previous case (Fig. 1), the placement and labeling of the equivalent sites is changed. For the chosen edge sites, the result is presented in Fig. 4. In this case, the chosen value of the parameter δ is 0.2.

To derive the limiting sizes of the disclinated nanocylinder, we investigate the $LDoS$ in the sites of the defects denoted by number 1 in the disclinated surfaces depicted in Fig.

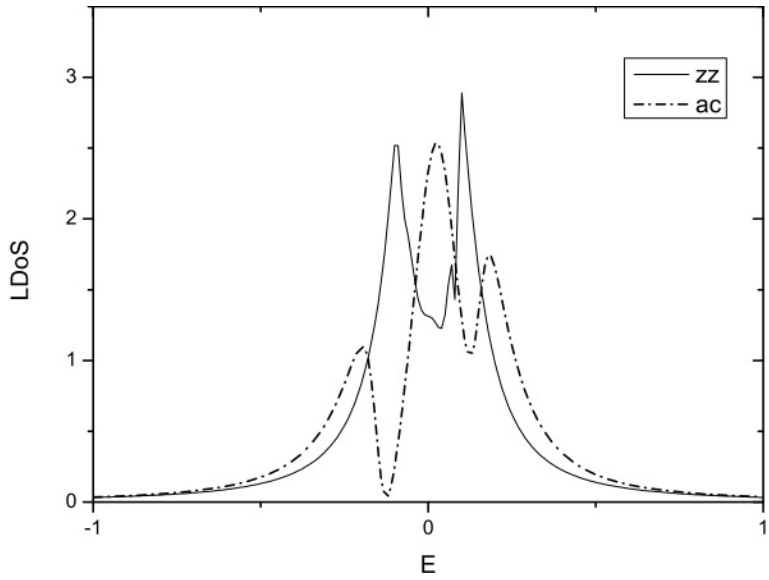

FIG. 2. $LDoS$ for armchair and zig-zag cylinder; longitudinal number of atoms: 12, circumferential number of atoms: 10 for armchair, 20 for zig-zag; here, $\delta = 0.1$.

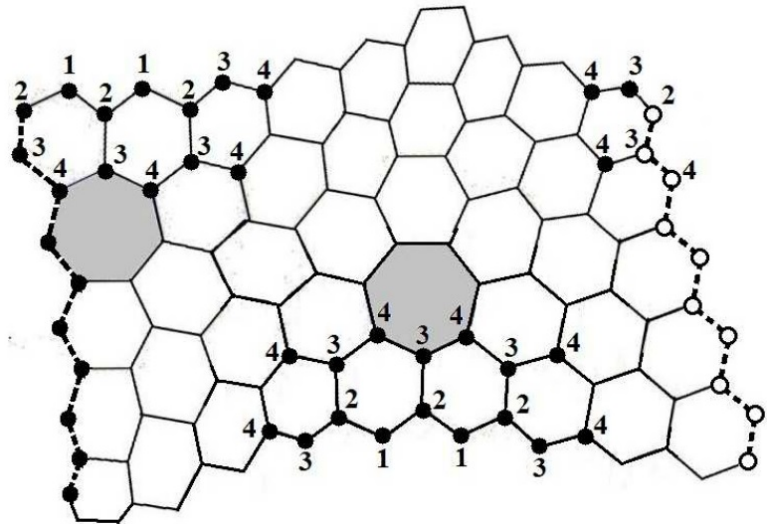

FIG. 3. Surface of the nanoribbon with a small perturbation; due to the mirror symmetry, we have pairs of equivalent sites in each line parallel with the edge, but there is not any line composed of equivalent sites only; so, we distinguish only the sites which are neighboring, next-neighboring etc. with the site 1 for which the $LDoS$ we calculate; the whole number of the sites in the chain is 9; in the case of the semi closed, nanocylindrical structure, the dashed lines consisting of sites denoted by black or white color are identical on the real surface.

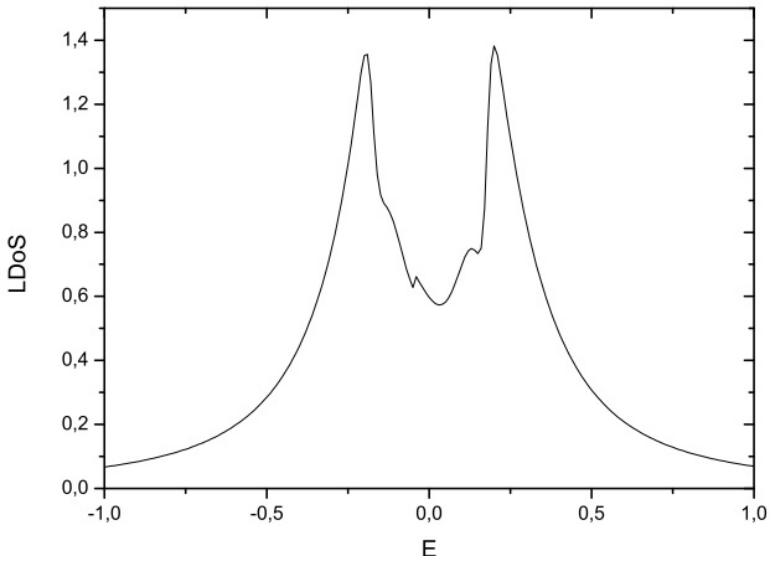

FIG. 4. $LDoS$ of the perturbed cylinder with surface depicted in Fig. 3; here, $\delta = 0.2$.

5 and we compare the results with the results presented in [1], where the $LDoS$ for the simple graphene was presented.

In Fig. 5, we define the distance of the defects in the units of the distance of the neighboring sites. Using the Haydock recursion scheme, we get the plots of the $LDoS$ outlined in Fig. 6. The acquired results should be similar to the $LDoS$ of simple graphene [1]. Then, we suppose the presence of the local minimum for the Fermi level in the corresponding plot.

Let us look through the plots of the $LDoS$ in Fig. 6. From these plots we see that the growing distance of the defects causes decrease of the $LDoS$ for the Fermi energy and violation of the peak. The case (d) in Fig. 6 corresponds to the expected shape of the $LDoS$ [1] and so, it corresponds to the minimal necessary size of the perturbed cylindrical surface.

4. Conclusion

We applied the Haydock recursion method on the calculation of the $LDoS$ of the carbon nanocylinder. We can compare the results presented in Fig. 2 with the calculation in [1], where the form of the electronic spectrum is applied. The results presented in this paper are close to our results. They are also similar to the plots presented in [6]. In both of these papers as well as in Fig. 2, the difference between the armchair and the zig-zag form is given by the peak for the armchair form at the Fermi level. But in Fig. 2, the peak at the Fermi level should be much closer. The inaccuracy is given by the choice of the values of δ and of the parameters a_n, b_n in the Haydock recursion method which does not provide a single solution.

Next, we derived that the minimal size of the disclinated cylindrical surface containing 2 heptagonal defects corresponds to the case (d) in Fig. 5 and that the maximal size corresponds to the surface which is twice longer.

The model of 2 defects can be also applied on a simulation of a dipole or a quadrupole present on a defect-free graphene surface: the dipole can be given by a combination of one pentagonal and one heptagonal defect and the quadrupole by two pentagonal and two

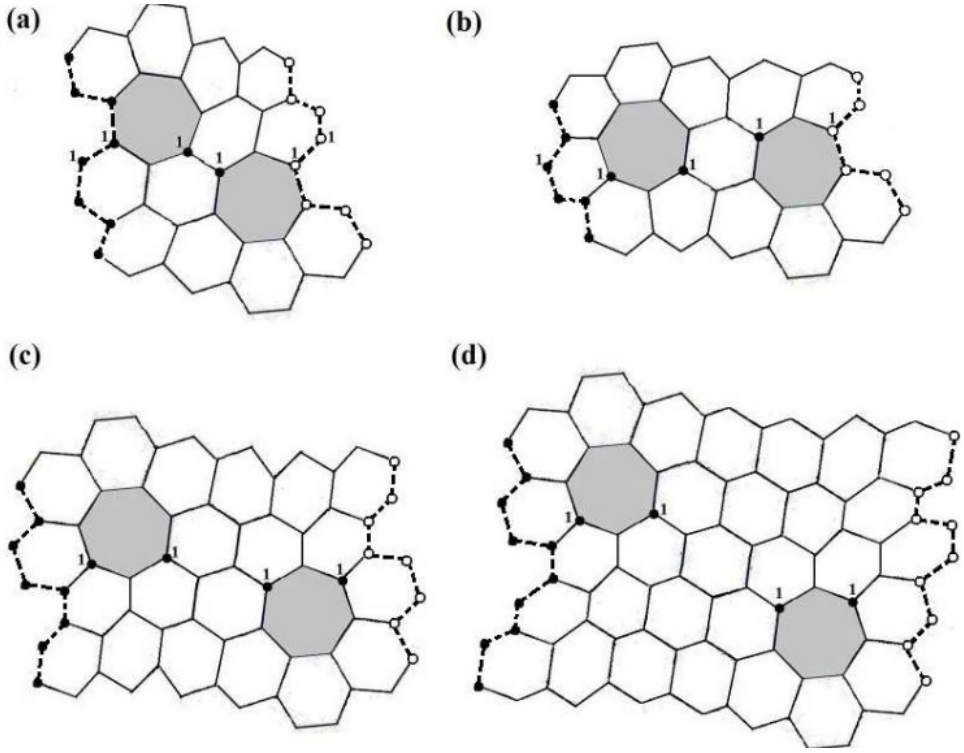

FIG. 5. Perturbed nanostructured surfaces with different distances of the defects. We calculate the *LDoS* for the denoted sites; in the case of the semi closed, nanocylindrical structure, the dashed lines consisting of sites denoted by black or white color are identical on the real surface.

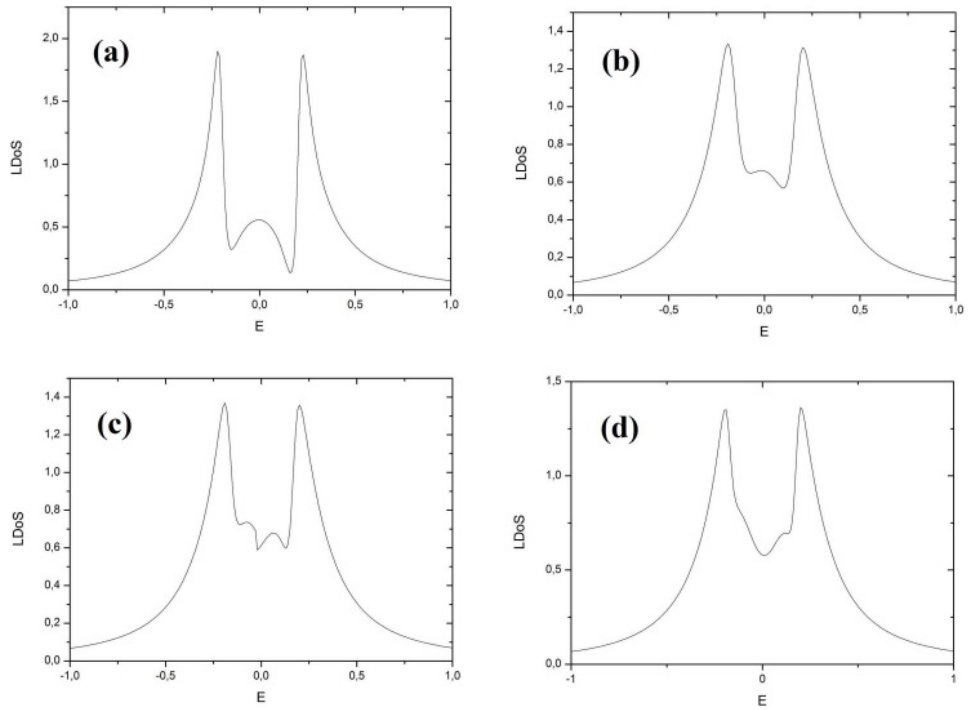

FIG. 6. *LDoS* for the particular cases of the perturbed cylindrical surfaces. The notation (a)-(d) corresponds to Fig. 5. The value of the parameter δ is 0.2.

heptagonal defects. Of course, higher number of defects can give much more possibilities. In the future, the calculations will be focused on these problems.

References

[1] Wakabayashi K., Sasaki K. et. al., Electronic states of graphene nanoribbons and analytical solutions, *Sci. Technol. Adv. Mater.* **11**, 054504 (2010).

[2] Osipov V. A., Kochetov E. A., Pudlak M., Electronic structure of carbon nanoparticles, *JETP* **96**, P. 140-149 (2003).

[3] Kolesnikov D. V., Osipov V. A., Geometry-induced smoothing of van Hove singularities in capped carbon nanotubes, *EPL* **78**, 47002 (2007).

[4] Tamura R., Tsukada M., Disclinations of monolayer graphite and their electronic states, *Phys. Rev. B* **49**, P. 7697-7708 (1994).

[5] Haydock R., Recursive solution of Schrödinger's equation, *Solid State Physics, Academic, New York*, 1980, **35**, 216-294.

[6] Ryndyk D. A., Bundesmann J., Liu M.-H., Richter K., Edge state effects in graphene molecular junctions, arXiv: http://arxiv.org/pdf/1205.3046.pdf (2012).

NANOSYSTEMS: PHYSICS, CHEMISTRY, MATHEMATICS, 2013, 4 (4), P. 496–506

GAUSSIAN CLASSICAL CAPACITY OF GAUSSIAN QUANTUM CHANNELS

E. Karpov[1], J. Schäfer[1], O. V. Pilyavets[1], R. García-Patrón[2,1], N. J. Cerf[1]

[1]QuIC, Ecole Polytechnique de Bruxelles, CP 165, Université Libre de Bruxelles, 1050 Brussels, Belgium
[2] Max-Planck-Institut für Quantenoptik, Hans-Kopfermann-Straße 1, 85748 Garching, Germany

ekarpov@ulb.ac.be

PACS 03.67.Hk, 89.70.Kn

The classical capacity of quantum channels is the tight upper bound for the transmission rate of classical information. This is a quantum counterpart of the foundational notion of the channel capacity introduced by Shannon. Bosonic Gaussian quantum channels provide a good model for optical communications. In order to properly define the classical capacity for these quantum systems, an energy constraint at the channel input is necessary, as in the classical case. A further restriction to Gaussian input ensembles defines the Gaussian (classical) capacity, which can be studied analytically. It also provides a lower bound on the classical capacity and moreover, it is conjectured to coincide with the classical capacity. Therefore, the Gaussian capacity is a useful and important notion in quantum information theory. Recently, we have shown that the study of both the classical and Gaussian capacity of an arbitrary single-mode Gaussian quantum channel can be reduced to the study of a particular *fiducial* channel. In this work we consider the Gaussian capacity of the fiducial channel, discuss its additivity and analyze its dependence on the channel parameters. In addition, we extend previously obtained results on the optimal channel environment to the single-mode fiducial channel. In particular, we show that the optimal channel environment for the lossy, amplification, and phase-conjugating channels is given by a pure quantum state if its energy is constrained.

Keywords: Quantum channels, Information transmission, Quantum Information, Channel Capacity.

1. Introduction

Information transmission and processing are ubiquitous in modern human society. By the end of the XXth century information technologies experienced tremendous growth accompanied by “exponential” downscaling of the hardware elements. Simple extrapolation shows that the element size will soon achieve the level where quantum effects cannot be neglected. This is one of the reasons why the interdisciplinary field known as quantum information theory appeared. Another reason comes from a possibility to apply particular properties of quantum systems in order to solve those problems which are intractable using only classical means. Information theory provides a quantitative measure of information and the tools for studying the information transmission through communication channels. A fundamental quantity characterizing their performance is the maximal achievable rate at which the information can be reliably transmitted. This tight upper bound is called *capacity* of the communication channel. If the quantum nature of information carriers is taken into account one has to describe communication channels as transformations of quantum states. One of the most general transformations allowed by quantum mechanics is a completely positive trace-preserving map which is identified with a quantum channel.

In addition to the information in a usual sense, which can be measured in bits, in quantum information theory one introduces also other types of information related to the non-classical properties of quantum states, e.g., entanglement. In our paper we discuss the classical capacity of quantum channels focussing on bosonic Gaussian quantum channels. They provide a realistic model for the information transmission via optical communication lines.

The paper is organized as follows. In Section 2 we define the classical capacity of quantum channels. In Section 3 we describe Gaussian quantum channels. In Section 4 we introduce the Gaussian capacity and the type of Gaussian ensembles that achieve this capacity. In Section 5 we present our recently proposed decomposition of Gaussian channels in terms of a particular *fiducial* channel, find the Gaussian capacity of the fiducial channel and discuss its additivity. In Section 6 we apply this decomposition to maximize the Gaussian capacity of the fiducial channel over the set of states of the environment mode which respect an energy constraint. In Section 7 we present our conclusion.

2. Classical capacity of quantum channels

Quantum channels are completely positive trace-preserving (CPTP) maps Φ that act on density operators $\hat{\rho}$ defined on a Hilbert space $\mathcal{H}$ [1]. The transmission of classical information by quantum channels involves an encoding of classical symbols (alphabet) into a set of quantum input states $\hat{\rho}_i$. The input state transmitted via a quantum channel Φ is transformed to the output state $\hat{\rho}_{\mathrm{out},i} = \Phi[\hat{\rho}_{\mathrm{in},i}]$. Depending on the coding scheme each individual symbol state $\hat{\rho}_{\mathrm{in},i}$ is used for the information transmission with some probability p_i, therefore, the average input state sent through the channel is $\hat{\bar{\rho}}_{\mathrm{in}} = \sum_i p_i \hat{\rho}_{\mathrm{in},i}$. Since the CPTP map is linear the average output state is $\hat{\bar{\rho}}_{\mathrm{out}} = \Phi[\hat{\bar{\rho}}_{\mathrm{in}}] = \sum_i p_i \Phi[\hat{\rho}_{\mathrm{in},i}] = \sum_i p_i \hat{\rho}_{\mathrm{out},i}$. In other words, the channel outputs the state $\hat{\rho}_{\mathrm{out},i}$ with probability p_i. The so-called "Holevo χ-quantity" given by following equation [1]

$$\chi[\Phi, \{\hat{\rho}_i, p_i\}] = S\left(\hat{\bar{\rho}}_{\mathrm{out}}\right) - \sum_i p_i S\left(\hat{\rho}_{\mathrm{out},i}\right) \tag{1}$$

provides a tight upper bound for the maximal amount of information that one can extract from the output ensemble $\{\Phi[\hat{\rho}_i], p_i\}$ by using all possible measurements. Then, the supremum of the Holevo χ-quantity over the whole set of input ensembles

$$C_\chi(\Phi) = \sup_{\{\hat{\rho}_i, p_i\}} \chi[\Phi, \{\hat{\rho}_i, p_i\}] \tag{2}$$

gives the tight upper bound on the amount of information that can be transmitted on average by one invocation of quantum channel Φ provided that the input symbol states are not entangled over different channel uses [2], [3]. This quantity is called the *one-shot capacity*. However, one may increase the amount of information transmitted per channel use by entangling the input states over a sequence of channel uses. Therefore, the *classical capacity* is defined by the limit [2], [3]

$$C(\Phi) = \lim_{m\to\infty} \frac{1}{m} C_\chi(\Phi^{\otimes m}) \geq C_\chi(\Phi). \tag{3}$$

If the equality $C(\Phi) = C_\chi(\Phi)$ holds then the classical capacity is *additive*. The additivity of the classical capacity of quantum channels has long been an open problem until Hastings has shown an example of a channel whose capacity is non-additive [4]. Hence, the additivity has to be studied for each particular channel individually. We focus our study

on bosonic Gaussian channels which constitute an important part of "Gaussian quantum information" [5].

3. Gaussian channels

Bosonic systems are so-called *continuous variables* systems described by observables with continuous spectra acting on states defined in an infinite-dimensional Hilbert space. The typical example of bosonic systems is the quantized electromagnetic field seen as a collection of quantum harmonic oscillators (bosonic modes). The infinite-dimensional Hilbert space of each mode is spanned by a countable basis of Fock states (number stats), which are the eigenstates of the number operator $\hat{N}|n\rangle = n|n\rangle$, where n is a non-negative integer number and the number operator $\hat{N} = \hat{a}^\dagger \hat{a}$ is defined via bosonic creation and annihilation operators that act as follows:

$$\begin{aligned} \hat{a}|0\rangle = 0, \quad \hat{a}|n\rangle = \sqrt{n}|n-1\rangle \qquad \text{if } n \geq 1, \\ \hat{a}^\dagger|n\rangle = \sqrt{n+1}|n+1\rangle. \end{aligned} \tag{4}$$

These operators satisfy the bosonic commutation relation $[\hat{a}, \hat{a}^\dagger] = 1$ (throughout the paper we are using natural units $\hbar = \omega = 1$).

A convenient representation of these infinite-dimensional systems is the *phase-space* representation based on the use of quadrature operators

$$\hat{q} = \frac{1}{\sqrt{2}}\left(\hat{a} + \hat{a}^\dagger\right), \qquad \hat{p} = \frac{i}{\sqrt{2}}\left(\hat{a} - \hat{a}^\dagger\right). \tag{5}$$

These operators have a continuous spectrum and satisfy the same canonical commutation relations as position and momentum operators. For m bosonic modes one defines a vector of quadrature operators

$$\hat{\boldsymbol{x}} = (\hat{x}_1, \hat{x}_2, \ldots, \hat{x}_{2m})^{\mathrm{T}} = (\hat{q}_1, \hat{p}_1, \ldots, \hat{q}_m, \hat{p}_m)^{\mathrm{T}}. \tag{6}$$

Then the canonical commutation relation is expressed as $\{\hat{x}_i, \hat{x}_j\} = i\Omega_{ij}$, where Ω_{ij} is the matrix element of *symplectic* matrix

$$\boldsymbol{\Omega} = \bigoplus_{n=1}^{m} \begin{pmatrix} 0 & 1 \\ -1 & 0 \end{pmatrix}. \tag{7}$$

In this representation quantum state $\hat{\rho}$ of m modes is described by its Wigner function:

$$W(\boldsymbol{x}) = \int_{\mathbb{R}^{2m}} \frac{d^{2m}\boldsymbol{\xi}}{(2\pi)^m} \langle \boldsymbol{q} + \boldsymbol{\xi}/2|\hat{\rho}|\boldsymbol{q} - \boldsymbol{\xi}/2\rangle e^{-i\boldsymbol{p}\boldsymbol{\xi}} \tag{8}$$

where $|\boldsymbol{q}\rangle$ is an eigenstate of operator $\hat{\boldsymbol{q}} = (\hat{q}_1, \hat{q}_2, \ldots, \hat{q}_m)^{\mathrm{T}}$. The Wigner function is commonly called *quasiprobability* distribution because, on one hand, its marginals provide valid probability distributions for both quadratures q and p. On the other hand, it may take negative values and, in any case, it cannot be a joint probability distribution of the values of observables $\hat{q}$ and $\hat{p}$ because if such distribution existed it would violate the Heisenberg uncertainty relation. In order to define the Wigner function one has to know, in general, its values in all points of the $2m$-dimensional phase-space. However, the amount of parameters, which determine the Wigner function of a Gaussian state, can be essentially reduced.

Given a density operator $\hat{\rho}$ one defines the *displacement vector* of the first moments

$$\boldsymbol{d} = \mathrm{Tr}[\hat{\boldsymbol{x}}\hat{\rho}] \tag{9}$$

and the *covariance matrix* (CM) $\boldsymbol{V}$ of the second "centered" moments of the quadratures

$$V_{ij} = \frac{1}{2}\mathrm{Tr}[\{\hat{x}_i - d_i, \hat{x}_j - d_j\}\hat{\rho}], \tag{10}$$

where $\{\,,\,\}$ is the anticommutator. Then the Wigner function of a Gaussian state is completely determined by the displacement vector $\boldsymbol{d}$ and the covariance matrix $\boldsymbol{V}$:

$$W(\boldsymbol{x}) = \frac{1}{(2\pi)^m\sqrt{\det \boldsymbol{V}}} e^{-\frac{1}{2}(\boldsymbol{x}-\boldsymbol{d})^{\mathrm{T}}\boldsymbol{V}^{-1}(\boldsymbol{x}-\boldsymbol{d})}. \tag{11}$$

Quantum channels which preserve the "Gaussian" property of quantum states are called *Gaussian channels*. They are CPTP maps which are closed on the set of Gaussian states. Any such transformation of m-mode Gaussian input states to m-mode Gaussian output states is given by its action on the parameters determining the state

$$\boldsymbol{d}_{\mathrm{out}} = \boldsymbol{X}\boldsymbol{d}_{\mathrm{in}} + \boldsymbol{d}_{\mathrm{ch}}, \tag{12}$$

$$\boldsymbol{V}_{\mathrm{out}} = \boldsymbol{X}\boldsymbol{V}_{\mathrm{in}}\boldsymbol{X}^{\mathrm{T}} + \boldsymbol{Y}, \tag{13}$$

where $\boldsymbol{d}_{\mathrm{ch}}$ is the displacement introduced by the channel, $\boldsymbol{X}$ is a real $2m \times 2m$ matrix, and $\boldsymbol{Y}$ is a real, symmetric and positive-semidefinite $2m \times 2m$ matrix fulfilling the following condition:

$$\boldsymbol{Y} + \frac{i}{2}\left(\boldsymbol{\Omega} - \boldsymbol{X}\boldsymbol{\Omega}\boldsymbol{X}^{\mathrm{T}}\right) \geq 0. \tag{14}$$

Matrices $\boldsymbol{X}$, $\boldsymbol{Y}$, and vector $\boldsymbol{d}_{\mathrm{ch}}$ completely define a Gaussian channel $\Phi(\boldsymbol{X}, \boldsymbol{Y}, \boldsymbol{d}_{\mathrm{ch}})$.

4. Gaussian capacity

The classical capacity as defined by Eqs. (1)–(3) may be infinite for bosonic channels. We can demonstrate it for the example of a Gaussian channel with $\det\boldsymbol{X} > 0$. Let us consider a sequence of input ensembles $\{\rho_i, p_i^{(m)}\}$ belonging to the same set of symbol states ρ_i but taken with different probability distributions $p_i^{(m)}$ in such a way that the energy of the average state is increasing up to infinity if $m \to \infty$. In this case the entropy of the average output state in the first term in Eq. (1) can be increasing up to infinity while the second term remains the same. A similar problem appears for Gaussian channels in standard ("classical") information theory, where the meaningful definition of the capacity is given by imposing an "input power" constraint. With this constraint, the capacity is a function of the input power. A similar constraint exists in the quantum case. Namely, the mean number of photons of the average input state is upper bounded. Therefore, for one bosonic mode we have

$$\mathrm{Tr}\left[\hat{\bar{\rho}}_{\mathrm{in}}\hat{a}^{\dagger}\hat{a}\right] \leq \bar{N}, \qquad \hat{\bar{\rho}}_{\mathrm{in}} = \int \mu(d\boldsymbol{w})\hat{\rho}_{\boldsymbol{w}}, \tag{15}$$

where $\bar{N}$ is the mean number of photons per quadrature and $\mu(d\boldsymbol{w})$ is a probability measure on the whole set of quantum states parametrized by $\boldsymbol{w}$ (the probability measure plays a role of p_i for the continuous variables case). For simplicity we will call this bound "input

energy constraint". Then the classical one-shot capacity of a bosonic channel Φ is defined as:

$$C_\chi(\Phi, \bar{N}) = \max_{\mu:\hat{\bar{\rho}}_{\rm in}\in\mathcal{E}_{\bar{N}}} \chi(\Phi, \mu), \tag{16}$$

$$\chi(\Phi, \mu) = S(\Phi[\hat{\bar{\rho}}_{\rm in}]) - \int \mu(d\boldsymbol{w}) S(\Phi[\hat{\rho}_{\boldsymbol{w}}]), \tag{17}$$

where the average input state $\hat{\bar{\rho}}_{\rm in}$ is given by Eq. (15) and $\mathcal{E}_{\bar{N}}$ denotes the set of states satisfying the input energy constraint (15). The classical capacity constrained on a set $\mathcal{E}$ of average input states was considered in [6, 7]. The definition of the classical capacity given by Eq. (3) requires the generalization of the constraint (15) to an arbitrary number of modes $\mathrm{Tr}[\hat{\bar{\rho}}^{(m)}\hat{N}^{\otimes m}] \leq 2m(\bar{N} + 1/2)$. This constraint leads to another possible type of non-additivity, which is not related to the entanglement of the input states. Indeed, this constraint specifies the amount of input photons per channel use only on average. Even if the one-shot capacity $C_\chi(\Phi)$ constrained on a given number of input photons is additive, by distributing the available amount of input photons between the channel uses in a proper way, one may expect to achieve a higher $C_\chi(\Phi^{\otimes m})$ compared to $\chi(\Phi^{\otimes m}, \bar{\mu})$, where $\bar{\mu}$ corresponds to the uniform distribution of the amount of input photons between the uses of the channel. Nevertheless, as proven in [7], this scenario does not take place due to the concavity of $\chi(\Phi, \bar{\mu})$ as a function of μ. In particular, it is proven that the uniform distribution of the amount of input photons between the channel uses achieves the classical capacity of Gaussian channels if the one-shot capacity is additive for a fixed (though possibly different) amount of input photons at each channel use [7]. This is the case, indeed, for *entanglement breaking* channels, whose classical capacity was proven to be additive [8, 9].

Thus, the additivity problem for the classical capacity of Gaussian channels is resolved for the class of the entanglement breaking channels. Hence, in order to evaluate their capacity it is sufficient to find only the one-shot capacity. However, this simplified problem is still a highly non-trivial task. At the moment the classical capacity is known only for the lossy channel provided that its environment is pure (i.e., in a squeezed vacuum state) and its energy is above some threshold [10, 11] (the lossy channel can be realized by a beamsplitter mixing the input signal mode with the environment mode). Therefore, the evaluation of different bounds on the capacity is a valuable alternative.

A natural lower bound is the *Gaussian capacity* defined as the classical capacity with an additional restriction on the set of admissible input states. In [12] we defined this quantity by requiring that all individual symbol states and the modulated average state are Gaussian. We have shown there that the optimal ensemble achieving the Gaussian capacity, as we define it, is the same input ensemble as the one that was imposed by a previous more restrictive definition (see, for example, [13]). This optimal input ensemble is generated by phase space translates of a single Gaussian pure state modulated according to a Gaussian distribution with CM $\boldsymbol{V}_{\rm m}$. For such an ensemble, the covariance matrices of the individual symbol states are the same. Thus, the CM of the average input state $\bar{\boldsymbol{V}}_{\rm in}$ is equal to $\boldsymbol{V}_{\rm in} + \boldsymbol{V}_{\rm m}$ and the input energy constraint therefore reads

$$\mathrm{Tr}\,[\boldsymbol{V}_{\rm in} + \boldsymbol{V}_{\rm m}] \leq 2\bar{N} + 1. \tag{18}$$

Recall that the von Neumann entropy of a Gaussian state depends only on its covariance matrix. Moreover, the action of a Gaussian channel on the covariance matrix does not depend on displacements $\boldsymbol{d}_{\rm in}$ and $\boldsymbol{d}_{\rm ch}$. Hence, all output entropies in the second term of

Eq. (1) are equal. Therefore, the Holevo χ-quantity is the difference of the von Neumann entropies of the average output state and output symbol state:

$$\chi[\Phi, \bar{\boldsymbol{V}}_{\rm in}, \boldsymbol{V}_{\rm in}] = S(\Phi[\bar{\boldsymbol{V}}_{\rm in}]) - S(\Phi[\boldsymbol{V}_{\rm in}]) = g\left(\bar{\nu} - \frac{1}{2}\right) - g\left(\nu - \frac{1}{2}\right), \tag{19}$$

$$g(x) = (x+1)\log_2(x+1) - x\log_2(x), \tag{20}$$

where $\bar{\nu}$ and ν are symplectic eigenvalues of the C*M* of the average output state $\Phi[\bar{\boldsymbol{V}}_{\rm in}]$ and an individual output symbol state $\Phi[\boldsymbol{V}_{\rm in}]$, respectively. The new form of the Holevo χ-quantity given by Eq. (19) reduces the problem of calculating the one-shot Gaussian capacity to the maximization of the difference of two entropies under the constraint (18). This maximization can be done using the method of Lagrange multipliers. The evaluation of the Gaussian capacity is relatively simple due the restriction to Gaussian states. Below we will show that it can be expressed in a closed form in a certain domain of parameters. The importance of this bound is also highlighted by the fact that in all cases where the classical capacity is known, the Gaussian capacity coincides with it. In addition, Gaussian states maximize the von Neumann entropy on the set of all states with the same energy. This leads to a natural conjecture that the Gaussian capacity always coincides with the classical capacity.

5. Single-mode Gaussian channels

One can try to further simplify the calculation of the Gaussian capacity using an equivalence of any single-mode Gaussian channel Φ to one of seven *canonical channels* $\Phi^{\rm C}$ [9, 14, 15] preceded and followed by unitary operations:

$$\Phi = U_2 \circ \Phi^{\rm C} \circ U_1. \tag{21}$$

Since unitary transformations do not change the entropy the Holevo χ-quantity of any Gaussian channel Φ is equal to the one of the corresponding canonical channel $\Phi^{\rm C}$. However, if the unitary transformation U_1 which precedes the canonical channel in the decomposition (21) involves a squeezing operation then the energy of the state at the input of Φ and Φ, respectively, is different.

In order to find the Gaussian capacity of Φ one has to consider both the canonical channel and preceding squeezing operation. Actually, in this case, the expressions for the Gaussian capacity can be obtained in a closed form for five of the seven canonical channels preceded by squeezing operations. However, this is possible only if the input energy $\bar{N}$ exceeds a certain energy threshold. The latter depends on the parameters of the corresponding canonical channel and the squeezing parameter [16]. These five canonical channels have the same matrix $\boldsymbol{Y}$ which is proportional to identity: $\boldsymbol{Y} = y\,\mathbb{I}$. Moreover, all of them transform thermal input states to thermal output states. Therefore, we call them *thermal* channels $\Phi^{\rm TH}$. They include lossy, amplification, classical additive-noise, phase-conjugating and zero-transmission channels [14].

In order to go beyond the aforementioned results, we proposed another decomposition in terms of a *fiducial* channel $\Phi^{\rm F}$ [12]

$$\Phi = U_2 \circ \Phi^{\rm F} \circ \Theta_1, \tag{22}$$

where Θ_1 is a passive unitary operation which corresponds to a rotation in the phase space. If a Gaussian channel $\Phi(\boldsymbol{X}, \boldsymbol{Y}, \boldsymbol{d})$ is canonically equivalent to one of the thermal channels

$\Phi^{\rm TH}$, then the fiducial channel $\Phi^{\rm F}(\boldsymbol{X}^{\rm F}, \boldsymbol{Y}^{\rm F}, 0)$ in Eq. (22) is given by two matrices [see Eqs. (12)-(14)]

$$\boldsymbol{X}^{\rm F} = \boldsymbol{X}^{\rm TH} = \sqrt{|\tau|}\begin{pmatrix} 1 & 0 \\ 0 & \mathrm{sgn}(\tau) \end{pmatrix}, \quad \boldsymbol{Y}^{\rm F} = y\begin{pmatrix} e^{2s} & 0 \\ 0 & e^{-2s} \end{pmatrix}, \qquad \tau = \det \boldsymbol{X}, \quad y = \det \boldsymbol{Y}. \tag{23}$$

The dependence of the squeezing parameter s on the matrices $\boldsymbol{X}, \boldsymbol{Y}$ that define Φ is presented in [12]. The fiducial channel is defined by three scalar parameters (τ, y, s). The decomposition (22) is important for the following reason. Rotations change neither the entropy nor the energy of quantum states; therefore, the state having passed through Θ_1 and entering $\Phi^{\rm F}$ has the same energy as the input state entering Φ. This allows us to conclude that both the classical capacity and the Gaussian capacity of $\Phi(\boldsymbol{X}, \boldsymbol{Y}, \boldsymbol{d})$ are equal to those of the corresponding $\Phi^{\rm F}_{(\tau,y,s)}$ [12]. This statement can be extended to Gaussian channels canonically equivalent to "non-thermal" (or so-called "pathological") channels. These canonical channels may be considered as limiting cases of the fiducial channel with properly chosen preceding squeezing operations. Thus, we have reduced the classical capacity (and Gaussian capacity) of any Gaussian channel to the one of the corresponding fiducial channel. For this reason it is sufficient to study the Gaussian capacity of the fiducial channel in the full range of its parameters in order to obtain the Gaussian capacity of any single mode Gaussian channel. This can be done using the method of Lagrange multipliers. It leads to a general formula for the Gaussian capacity of all Gaussian channels canonically equivalent to thermal channels [12]:

$$C^{\rm G}\left(\Phi_{(\tau,y,s)}, \bar{N}\right) = g\left(|\tau|\bar{N} + y\,\cosh(2s) + \frac{|\tau|-1}{2}\right) - g\left(y + \frac{|\tau|-1}{2}\right), \tag{24}$$

$$\bar{N} \geq \bar{N}_{\rm thr} = \frac{1}{2}\left(e^{2|s|} + \frac{2y}{|\tau|}\sinh(2|s|) - 1\right). \tag{25}$$

It holds for input energies, which are higher than the threshold $\bar{N}_{\rm thr}$. This corresponds to the so-called *quantum water-filling* solution [17–20]. It implies that the overall modulated output state is a thermal state. The optimal ensemble is composed of individual symbol states, which are displaced squeezed vacuum states determined by the same squeezing parameter s that enters the matrix $\boldsymbol{Y}^{\rm F}$ [see (23)], where the latter represents the effect of the environment in the fiducial channel

$$\Phi^{\rm F}[\bar{\boldsymbol{V}}_{\rm in}] \propto \mathbb{I}, \quad \boldsymbol{V}_{\rm in} = \frac{1}{2}\mathrm{diag}(e^{2s}, e^{-2s}). \tag{26}$$

Notice that the squeezing of the individual input symbol state requires energy. Nevertheless, the condition (25) guarantees that the amount of input energy is sufficient to allow such optimal input states. It is known that these optimal symbol states minimize the entropy at the output of the channel on the set of all Gaussian states. Furthermore, the Gaussian capacity is additive above the input energy threshold [12, 21].

For both types of non-thermal canonical channels the formula (24) is never applicable. However, we go a step further and find the Gaussian capacity of the fiducial channel below the threshold and we find a solution which is also valid for non-thermal channels. In this case the solution of the optimization problem was already found for the lossy [17] and classical additive-noise channel [18–20] with squeezed environment. An optimal input ensemble is given by CMs $\boldsymbol{V}_{\rm in}$ and $\bar{\boldsymbol{V}}_{\rm in}$ which commute with $\boldsymbol{Y}^{\rm F}$. The optimal value of the squeezing of the individual symbol state is determined by a solution of a transcendental

equation. This solution allows us to study the properties of the Gaussian capacity as a function of the parameters of the additive noise or lossy channels. Here, we generalize this result by extending the solution to the fiducial channel. In our notations the corresponding transcendental equation can be written in two equivalent forms:

$$\begin{aligned} g'\left(\bar{\nu}-\frac{1}{2}\right)\sinh(2\bar{s})-g'\left(\nu-\frac{1}{2}\right)\sinh\left[2(s-r)\right]e^{-2r}\frac{y}{\nu}=0,\\ g'\left(\bar{\nu}-\frac{1}{2}\right)\sinh(2\bar{s})-g'\left(\nu-\frac{1}{2}\right)\sinh\left[2(s_\nu-r)\right]e^{-2r}=0, \end{aligned} \tag{27}$$

where

$$\Phi^{\mathrm{F}}[\bar{\boldsymbol{V}}_{\mathrm{in}}]=\bar{\nu}\,\mathrm{diag}(e^{2\bar{s}},e^{-2\bar{s}}),\quad \Phi^{\mathrm{F}}[\boldsymbol{V}_{\mathrm{in}}]=\nu\,\mathrm{diag}(e^{2s_\nu},e^{-2s_\nu}), \tag{28}$$

function $g'(x)$ is the derivative of $g(x)$, variables y and s are the parameters of the fiducial channel (23), and r is the squeezing parameter which enters the CM of the individual input symbol state $\boldsymbol{V}_{\mathrm{in}}=(1/2)\mathrm{diag}(e^{2r},e^{-2r})$. The squeezing parameter r plays a role of the unknown variable in the equation. By analyzing this equation we have found that the signs of the solution r and s coincide.

6. Optimal environment

By studying how the Gaussian capacity depends on the channel parameters [19, 22] we arrived to a new problem, which was formulated first for the lossy channel [17]. Here we consider this problem for the fiducial channel Φ^{F}. In order to formulate it we use the Stinespring dilation which allows us to realize the channel by a joint unitary transformation of a two-mode (product) state. The latter consists of the input and environment modes. If $\tau\neq 1$ then the CM of the environment mode $\boldsymbol{V_e}$ is proportional to $\boldsymbol{Y}^{\mathrm{F}}$, i.e. $|1-\tau|\boldsymbol{V_e}=\boldsymbol{Y}^{\mathrm{F}}$. If $\tau=1$ then there is no Stinespring dilation with a single environment mode however, in this case, $\boldsymbol{Y}^{\mathrm{F}}$ represents a classical Gaussian noise "added" to the input state by the channel. The CM of the classical noise $\boldsymbol{V_e}=\boldsymbol{Y}^{\mathrm{F}}$. In both cases, the trace of $\boldsymbol{V_e}$ has the same meaning. It determines the energy contained in the environment mode or the energy of the noise.

Recall that the definition of the Gaussian capacity includes a maximization of χ^{G} [see (19)] over $\bar{\boldsymbol{V}}_{\mathrm{in}}$ and $\boldsymbol{V}_{\mathrm{in}}$ under the energy constraint (18). In this work we impose a similar energy constraint also on the environment mode (or added noise) and look for the optimal CM $\boldsymbol{V_e}$ which maximizes the Gaussian capacity. Since in all cases the CM $\boldsymbol{V_e}$ is proportional to $\boldsymbol{Y}^{\mathrm{F}}$, the constraint on its trace is equivalent to the corresponding constraint on the trace of $\boldsymbol{Y}^{\mathrm{F}}$:

$$M_e=\mathrm{Tr}[\boldsymbol{Y}^{\mathrm{F}}]=2y\cosh(2s). \tag{29}$$

At first, we consider the simplest case which corresponds to the input energy being above the threshold $\bar{N}_{\mathrm{thr}}$. In this case, we can use our expression for the Gaussian capacity (24). Due to the constraint (29) parameter y is a function of s. According to the waterfilling solution, if both $\bar{N}$ and M_e are constant the argument of the first term in (24) remains also constant, even if s is varied. Then the first derivative of $C^{\mathrm{G}}\left(\Phi^{\mathrm{F}},\bar{N}\right)$ with respect to s is obtained from the second term in (24) in the form

$$\frac{d}{ds}C^{\mathrm{G}}\left(\Phi^{\mathrm{F}},\bar{N}\right)=M_e\,g'\left(y+\frac{|\tau|-1}{2}\right)\frac{\sinh(2s)}{\cosh^2(2s)}. \tag{30}$$

The sign of this derivative is the same as the sign of s because $g'(x)$ is a positive function and M_e is a positive constant. This means that $C^{\mathrm{G}}\left(\Phi^{\mathrm{F}}, \bar{N}\right)$ is a monotonically increasing function of the absolute value of s. Therefore, its maximum lays at the boundaries of the allowed interval for s. There are two reasons for the existence of such boundaries in this problem.

One is due to the condition $\bar{N} > \bar{N}_{\mathrm{thr}}$ which provides that Eq. (30) is valid. This condition together with the constraint (29) upperbounds by some threshold value $s_{\mathrm{thr}} > 0$ the interval of the absolute values of $|s|$, where Eq. (30) is applicable. As a consequence for $|s| > s_{\mathrm{thr}}$ the condition (24) is violated. The particular case $\tau = 0$ corresponds to the so-called zero-transmission channel where Eq. (30) is not valid. However, this case is trivial because here the classical capacity is always equal to zero; therefore, the bound s_{thr} does not exist.

The second reason follows from the condition that the symbol state at the output of the channel must be a valid quantum state. This is provided by the condition (14), which is equivalent to $\boldsymbol{Y}^{\mathrm{F}} + \frac{i}{2}(1-\tau)\Omega \geq 0$ for the fiducial channel (actually, it is also equivalent to a simle inequality for channel parameters $y \geq |1-\tau|/2$ [12]). If $\tau \neq 1$ then this condition can be rewritten in the form $\boldsymbol{V_e} + \frac{i}{2}\Omega \geq 0$ (or simply $y \geq 0$). This is equivalent to the requirement that the environment mode must be in a valid quantum state. Due to the constraint (29) it upperbounds the absolute values of $|s|$ by the value s^*, which corresponds to the environment mode being in a pure state with $\det(\boldsymbol{V_e}) = 1/4$. If $\tau = 1$ then the condition (14) for the fiducial channel is equivalent to $\boldsymbol{Y}^{\mathrm{F}} \geq 0$. Since it is satisfied for all real values of s no finite upper bound s^* exists.

If $s^* < s_{\mathrm{thr}}$ then for all $|s| \leq s^*$ Eq. (30) is valid. Using Eq. (30) we conclude that the maximum of the Gaussian capacity is achieved by the environment mode being in a pure quantum state defined by $|s| = s^*$.

If $s^* > s_{\mathrm{thr}}$ (or s^* does not exist) Eq. (24) is not applicable in the interval $s_{\mathrm{thr}} < |s| \leq s^*$ and, therefore, we cannot apply our conclusions based on Eq. (30) to this interval of $|s|$. Nevertheless, in this case, we can also study the derivative of the Gaussian capacity over s using Eq. (27). Notice, that Eq. (27) is equivalent to $(\partial/\partial r)\chi^{\mathrm{G}}[\Phi, \bar{\boldsymbol{V}}_{\mathrm{in}}, \boldsymbol{V}_{\mathrm{in}})] = 0$. Let us take the input states with CMs $\boldsymbol{V}_{\mathrm{in}}$ and $\bar{\boldsymbol{V}}_{\mathrm{in}}$ that satisfy Eq. (27). Using the constraint (29) we deduce

$$\frac{d}{ds} y(s) e^{\pm 2s} = \pm \frac{M_e}{\cosh^2(2s)}. \tag{31}$$

Then we have

$$\begin{aligned} \frac{d}{ds} C^{\mathrm{G}}\left(\Phi, \bar{N}\right) &= \frac{\partial}{\partial s} \chi^{\mathrm{G}}[\Phi, \bar{\boldsymbol{V}}_{\mathrm{in}}, \boldsymbol{V}_{\mathrm{in}}] \\ &= \frac{M_e}{\cosh^2(2s)} \left[g'(\nu - 1/2) \sinh(2s_\nu) - g'(\bar{\nu} - 1/2) \sinh(2\bar{s}) \right]. \end{aligned} \tag{32}$$

Using (27) again we can rewrite it in the form

$$\frac{d}{ds} C^{\mathrm{G}}\left(\Phi, \bar{N}\right) = \frac{M_e}{\cosh^2(2s)} g'(\nu - 1/2) e^{2s_\nu} \left(1 - e^{-4r}\right), \tag{33}$$

where r satisfies (27). Since the sign of r is the same as the sign of s, the sign of the first derivative of $C^{\mathrm{G}}\left(\Phi, \bar{N}\right)$ coincides with the sign of s. It means that $C^{\mathrm{G}}\left(\Phi^{\mathrm{F}}, \bar{N}\right)$ is a monotonically increasing function of the absolute values of s regardless if $|s|$ is higher or lower than s_{thr}. As a result, the only bound on $|s|$ is s^* (if it exists for the considered parameters of the channel).

Let us summarize our results for different values of τ determining the type of the fiducial channel:

- If $\tau \neq 0$ and $\tau \neq 1$ then the allowed interval of s is finite. Its boundaries, where the maximum of the Gaussian capacity is achieved, correspond to the environment mode being in a pure state. For the lossy channel, this result was formulated as "environment purity theorem" and proved in [17].
- If $\tau = 0$ then the classical capacity is equal to zero for all s in the allowed interval, which is finite, i.e. $|s| \leq s^*$. The environment mode should be in a proper quantum state, but not necessarily pure.
- If $\tau = 1$ then the constraint (14) reduces to $\boldsymbol{Y}^{\mathrm{F}} \geq 0$ which corresponds to the classical additive-noise channel. Since the allowed interval of s, in this case, is the whole real axis, the optimal $\boldsymbol{V_e}$ is obtained in the limit $|s| \to \infty$ under the condition $2y\cosh(2s) = M_e = \mathrm{const}$. This gives $\boldsymbol{V}_e = \mathrm{diag}(M_e, 0)$ (for positive s) which corresponds to the single-quadrature classical noise channel [9]. This inspires a further study of optimal environment for Gaussian quantum channels. For instance, the generalization of out results to the case of multimode environments (broadband channels) that was discussed in [17] would be an interesting task.

7. Conclusion

We studied the classical information transmission through Gaussian quantum channels by analyzing the Gaussian capacity which, as we argue, is of great importance for the field of quantum information theory. We have used a recently found decomposition of an arbitrary single-mode Gaussian channel which allows us to reduce the problem of calculating its Gaussian capacity to the one of a particular fiducial channel. For the latter, we have developed a method of evaluating its Gaussian capacity and discussed its additivity. Finally, we have applied our results to a new problem of maximizing the Gaussian capacity under the environment energy constraint. We have shown that for a single mode the optimal environment almost in all cases is in a pure state. In a particular case, the environment is classical (noise) and all the noise energy is concentrated in one quadrature of the optimal noise CM. We expect that the decomposition in terms of the fiducial channel will be useful in further research on the Gaussian capacity, in particular, for finding the optimal state of the environment of multimode Gaussian channels.

Acknowledgements

The authors acknowledge financial support from the F.R.S.-FNRS under the Eranet project HIPERCOM, from the Interuniversity Attraction Poles program of the Belgian Science Policy Office under grant IAP P7-35 "photonics@be", from the Belgian FRIA foundation, from the Brussels Capital Region under the project CRYPTASC, from the ULB under the program "Ouvertures internationales", and from the Alexander von Humboldt foundation.

References

[1] Holevo A. S. Some estimations of the amount of information transmitted by quantum communication channel. *Probl. Peredachi Inf.* **9** (3), P. 3–11 (1973).

[2] Schumacher B., Westmoreland M. D. Sending classical information via noisy quantum channel. *Phys. Rev.* A **56**, P. 131–138 (1997).

[3] Holevo A. S. The capacity of quantum communication channel with general signal states. *IEEE Trans. Inf. Theory*, **44**, P. 269–272 (1998).

[4] Hastings M. B. Superadditivity of communication capacity using entangled inputs. *Nature Phys.* **5**, P. 255–257 (2009).
[5] Weedbrook C., Pirandola S., García-Patrón R., Cerf N. J., Ralph T. C., Shapiro J. H., Lloyd S. Gaussian Quantum Information. *Rev. Mod. Phys.* **84**, P. 621–669 (2012).
[6] Holevo A. S. Quantum systems, channels, information: a mathematical introduction. De Gruyter studies in mathematical physics. Walter de Gruyter GmbH & Co. KG, Berlin. **16**, P. 11–349 (2012).
[7] Holevo A. S., Shirokov M. E. On Shor's channel extension and constrained channels. *Comm. Math. Phys.* **249**, P. 417–430 (2004).
[8] Shirokov M. E. The Holevo capacity of infinite dimensional channels and the addititivity problem. *Comm. Math. Phys.* **262**, P. 131–159 (2006).
[9] Holevo A. S. Entanglement breaking channels in infinite dimensions. *Probl. Inf. Transmiss.* **44** (3), P. 3–18 (2008).
[10] Giovannetti V., Guha S., Lloyd S., Maccone L., Shapiro J. H., Yuen H. P. Classical capacity of the lossy bosonic channel: the exact solution. *Phys. Rev. Lett.* **92** (2), P. 027902-1–027902-4 (2009).
[11] Lupo C., Pilyavets O. V., Mancini S. Capacities of lossy bosonic channel with correlated noise. *New J. Phys.* **11**, P. 063023-1–063023-18 (2009).
[12] Schäfer J., Karpov E., García-Patrón R., Pilyavets O. V., Cerf N. J. Equivalence relations for the classical capacity of single-mode Gaussian quantum channels. *Phys. Rev. Lett.* **111**, P. 030503-1–030503-5 (2013).
[13] Eisert J., Wolf M. M. Gaussian quantum channels. In: *Quantum information with continuous variables of atoms and light*, edited by Cerf N. J., Leuchs G., Polzik E. S. Imperial College Press, London. **1**, P. 23–42 (2007).
[14] Caruso F., Giovannetti V., Holevo A. S. One-mode bosonic Gaussian channels: a full weak-degradability classification. *New J. Phys.* **8** P. 310-1–310-18 (2006).
[15] Holevo A. S. One-mode quantum Gaussian channels: structure and quantum capacity. *Probl. Inf. Transmiss.* **43** (1), P. 1–11 (2007).
[16] Lupo C., Pirandola S., Aniello P., Mancini S. On the classical capacity of quantum Gaussian channels. *Phys. Scr.* **T143**, P. 014016-1–014016-6 (2011).
[17] Pilyavets O. V., Lupo C., Mancini S. Methods for Estimating Capacities and Rates of Gaussian Quantum Channels. *IEEE Trans. Inf. Theory.* **58**, P. 6126–6164 (2012).
[18] Schäfer J., Karpov E., Cerf N. J. Gaussian capacity of the quantum bosonic memory channel with additive correlated Gaussian noise. *Phys. Rev.* A **84**, P. 032318-1–032318-16 (2011).
[19] Schäfer J., Karpov E., Cerf N. J. Quantum water-filling solution for the capacity of Gaussian information channels. *Proceedings of SPIE.* **7727**, P. 77270J-1–77270J-12 (2010).
[20] Schäfer J., Karpov E., Cerf N. J. Capacity of a bosonic memory channel with Gauss-Markov noise. *Phys. Rev.* A **80**, P. 062313-1–062313-11 (2009).
[21] Hiroshima T. Additivity and multiplicativity properties of some Gaussian channels for Gaussian Inputs. *Phys. Rev.* A **73**, P. 012330-1–012330-9 (2006).
[22] Pilyavets O. V., Zborovskii V. G., Mancini S. Lossy bosonic quantum channel with non-Markovian memory. *Phys. Rev.* A **77**, P. 052324-1–052324-8 (2008).

NANOSYSTEMS: PHYSICS, CHEMISTRY, MATHEMATICS, 2013, 4 (4), P. 507–511

EXPERIMENTAL AND THEORETICAL CHARACTERISATION OF JOSEPHSON SELF-COUPLING IN SUB-TERAHERTZ FLUX-FLOW OSCILLATOR

D. R. Gulevich[1], P. N. Dmitriev[2], V. P. Koshelets[2], F. V. Kusmartsev[1]

[1]Department of Physics, Loughborough University, United Kingdom
[2]Kotel'nikov Institute of Radio Engineering and Electronics, RAS, Moscow, 125009, Russia

PACS 85.25.Cp, 74.50.+r, 07.57.Hm

We present experimental and numerical results for a flux flow oscillator based on superconducting Josephson junctions. Our computationally efficient theoretical model takes into account Josephson self-coupling of the flux flow oscillator and is in a good agreement with our experimental results and previous studies.

Keywords: flux flow oscillator, superconducting Josephson junctions, fluxons, Terahertz radiation.

1. Introduction

Flux-flow oscillator (FFO) [1] is a long Josephson junction where the flux of Josephson vortices (fluxons) excite linear modes of electromagnetic waves. Typically, a length of a FFO is made considerably longer than the Josephson penetration length in order to accommodate a chain of fluxons. Because of its potential to be used as source of Terahertz and sub-Terahertz waves [2], it has attracted considerable attention from the scientific community. Investigation of FFO under the influence of different conditions such as noise and inhomogeneous bias has been done in a range of experimental [2–4] and theoretical [5–8] studies. It has been shown that fluxons in the long Josephson junction exhibit a rich behavior which is not limited to a one-dimensional fluxon motion, but involves a range of essentially two-dimensional effects [9], including excitation of the transverse modes [10]. In order to investigate the influence of two-dimensional modes on the dynamics of fluxons in a FFO, a reliable theoretical model is needed which would take into account the Josephson self-coupling effect [11] and would be efficient enough to be generalized to a model of a two-dimensional FFO which requires substantial computational resources. Here, we present our studies of the conventional FFO before proceeding to the investigation of two-dimensional effects.

2. Experimental results

Design of the harmonic mixer and all matching circuits was similar to the traditional one that was successfully used for FFO linewidth measurements (see for details [2, 3] and [4]). Current-voltage characteristics (IVCs) of the FFO measured at different magnetic fields are presented in Figure 1a. The level of the microwave power delivered to SIS matched to FFO is presented by color palette (blue corresponds to no power, red marks regions where induces by FFO SIS current exceeds 25 per cent of the quasi-particle SIS jump, see Fig. 1b). Note that the frequency of the FFO is determined by its voltage according to the Josephson relation. One can see that both SIS and FFO demonstrate perfect tunnel junction behavior with small leakage current and "0" return current of the FFO at large magnetic fields. The FFO provides enough

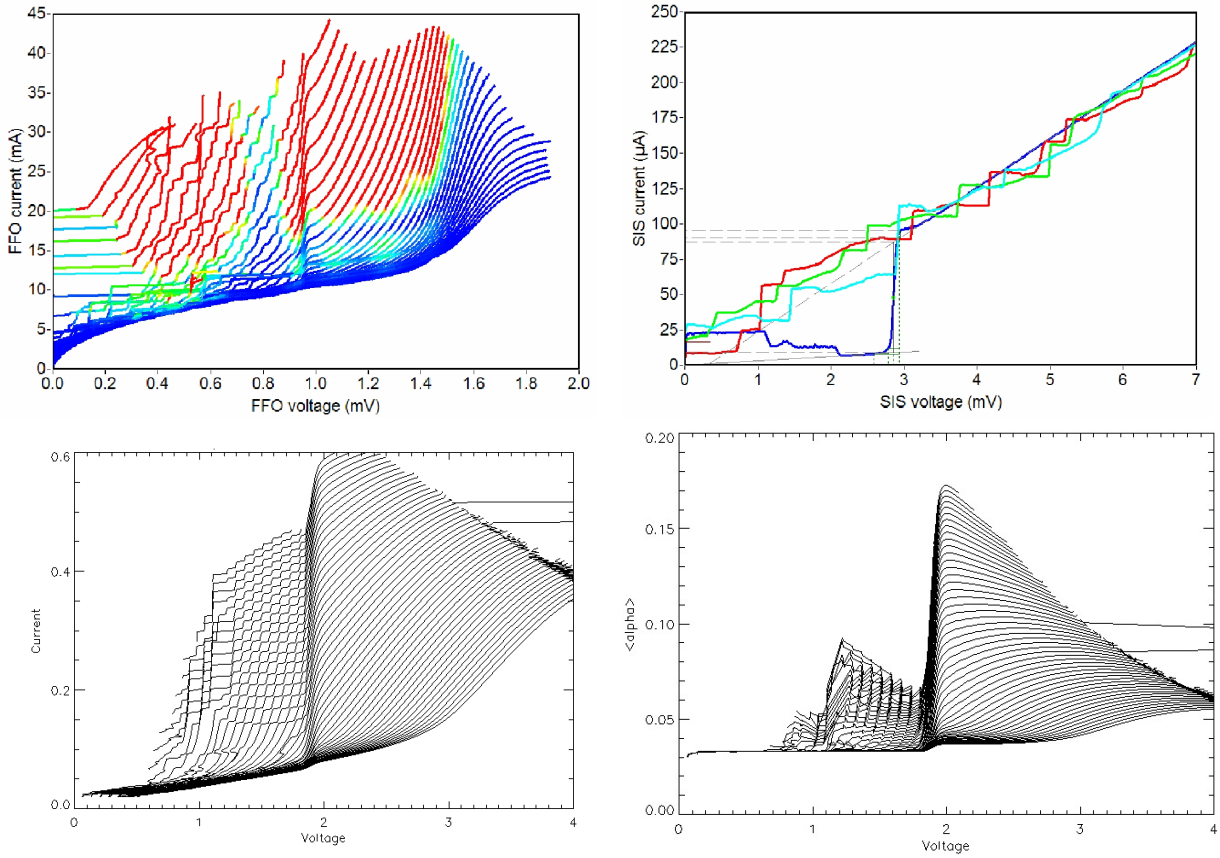

FIG. 1. (a) Experimental IVCs of the FFO measured at different magnetic fields created by current applied to integrated control line. (b) IVC of the SIS mixer: Blue – autonomous; Red, green and cyan – pumped by the FFO at frequencies 500, 600 and 700 GHz correspondingly. Note that the Josephson steps are very sharp and prominent. Positions of the steps exactly correspond to the FFO frequency. (c) Numerical IVC for FFO according to the model described in the text. The axes are normalized voltage v_{dc} and bias current γ. Different lines correspond to different values of the magnetic field h starting from 1.4 (top) to 4.0 (bottom) with the step 0.05. (d) Dependence of average damping $\langle\alpha\rangle$ versus voltage in our numerical model. Different lines correspond to different values of the magnetic field h starting from 1.4 (top) to 4.0 (bottom) with the step 0.05. Steps corresponding to one- two- and three-quanta transitions occurring at $v_g/3 = 1.9$, $v_g/5 = 1.14$ and $v_g/7 \approx 0.81$ are clearly visible. Four-quanta transition step at $v_g/9 \approx 0.63$ may also be identified for some values of magnetic field.

power to pump SIS in the design frequency range 400-750 GHz (0.8-1.5 mV). Furthermore, narrowband radiation has been measured, as in the previous experimental studies [3].

3. Numerical model

To describe FFO, we use a model of a long Josephson junction [12] with x-dependent damping parameter $\alpha(x)$,

$$\varphi_{tt} + \alpha(x)\,\varphi_t - \varphi_{xx} - \beta\,\varphi_{xxt} + \sin\varphi - \gamma = 0 \qquad (1)$$

with the boundary conditions $\varphi_x(0,t) = \varphi_x(L,t) = h$ and homogeneous bias current γ. In a general case, the dependence of the bias current on x would be defined by the experimental implementation of the system. Our choice of neglecting the x-dependence is justified by our interest in universal phenomena, in a FFO rather than those related to a specific implementation. Nevertheless, the generalization to the x-dependent bias current $\gamma = \gamma(x)$ is straightforward and will not affect the computation time of the numerical scheme implemented here. The damping parameter $\alpha(x)$ in eq. (1) is subjected to Josephson self-coupling (JSC) [11]. JSC arises as a result of assisted quantum tunneling of quasiparticles in the presence of an AC field. We take this effect into account by using a damping parameter which is related to the amplitude of the AC field at a each point of the junction, $\alpha(x) = \gamma_{qp}/v_{dc}$ with [13]

$$\gamma_{qp} = \sum_{n=-\infty}^{n=\infty} J_n^2\left(\frac{v_{ac}}{2\omega}\right)\ \gamma_{dc}\left(v_{dc} + 2n\omega\right), \tag{2}$$

where v_{dc} and v_{ac} are normalized DC and AC voltages: $v_{dc} = 2eV_{dc}/\hbar\omega_p$, $v_{ac} = 2eV_{ac}/\hbar\omega_p$, ω is normalized to the plasma frequency ω_p, J_n are Bessel functions and $\gamma_{dc}(v)$ is modelled by

$$\gamma_{dc}(v) = \alpha_0\, v\, \left(1 + b\,\frac{(v/v_g)^p}{1 + (v/v_g)^p}\right).$$

We took values of the parameters $b = 35$, power index $p = 80$, and gap voltage $v_g = 5.7$ to be consistent with the model used in [8]. Also, for the sake of consistency with the previous study [8], the length of the FFO was taken to be $L = 40$ Josephson penetration lengths, damping parameters $\alpha_0 = 0.033$ and $\beta = 0.035$. As it is reasonable to assume that self-coupling of FFO is dominated by a single harmonic the DC and AC components can be found by approximations

$$v_{dc} = \langle\dot{\varphi}\rangle \qquad \text{and} \qquad v_{ac} = \frac{1}{2}\left(\max\dot{\varphi} - \min\dot{\varphi}\right),$$

which save much of the computational time as compared to finding of the amplitudes with the fast Fourier transform. Equation (1) was solved numerically by the explicit finite difference scheme at fixed function $\alpha(x)$. The self-consistent $\alpha(x)$ has been found by an iterative procedure until the desired accuracy in $\alpha(x)$ is reached. The number of discrete points along X was 200, the time step and the integration time were varied in accordance with the specific choice of parameters. The code has been written in IDL programming language widely used in astronomy applications [14]. The results of our numerical simulations are presented on Fig. 1c and are in qualitative agreement with our experimental results on Fig. 1a and earlier numerical studies [6–8].

The slopes of the IVC curves differ slightly from the experimental results at high values of the bias current. This can possibly be attributed to the fact that we have used ideal, non-radiative boundary conditions, while in the experimental system, a certain amount of the radiation power may escape through the boundary, causing the IVC curves to bend up as seen on the experimental graph 1a. Fig. 1d shows our numerical results for the dependence on voltage of the average damping parameter defined as:

$$\langle\alpha\rangle = \frac{1}{L}\int_0^L \alpha(x)dx$$

Distribution of the AC amplitude v_{ac} and the distribution of the damping parameter α along the FFO is shown on Fig. 2a,c and 2b,d for two different sets of values for magnetic field and bias current. The spectrum of frequencies at the FFO's left boundary is shown on Fig. 2e and f. At certain regimes the spectrum becomes sophisticated with more harmonics turning up like on Fig. 2f. In this case, although the dependence of the spectrum on the choice of the

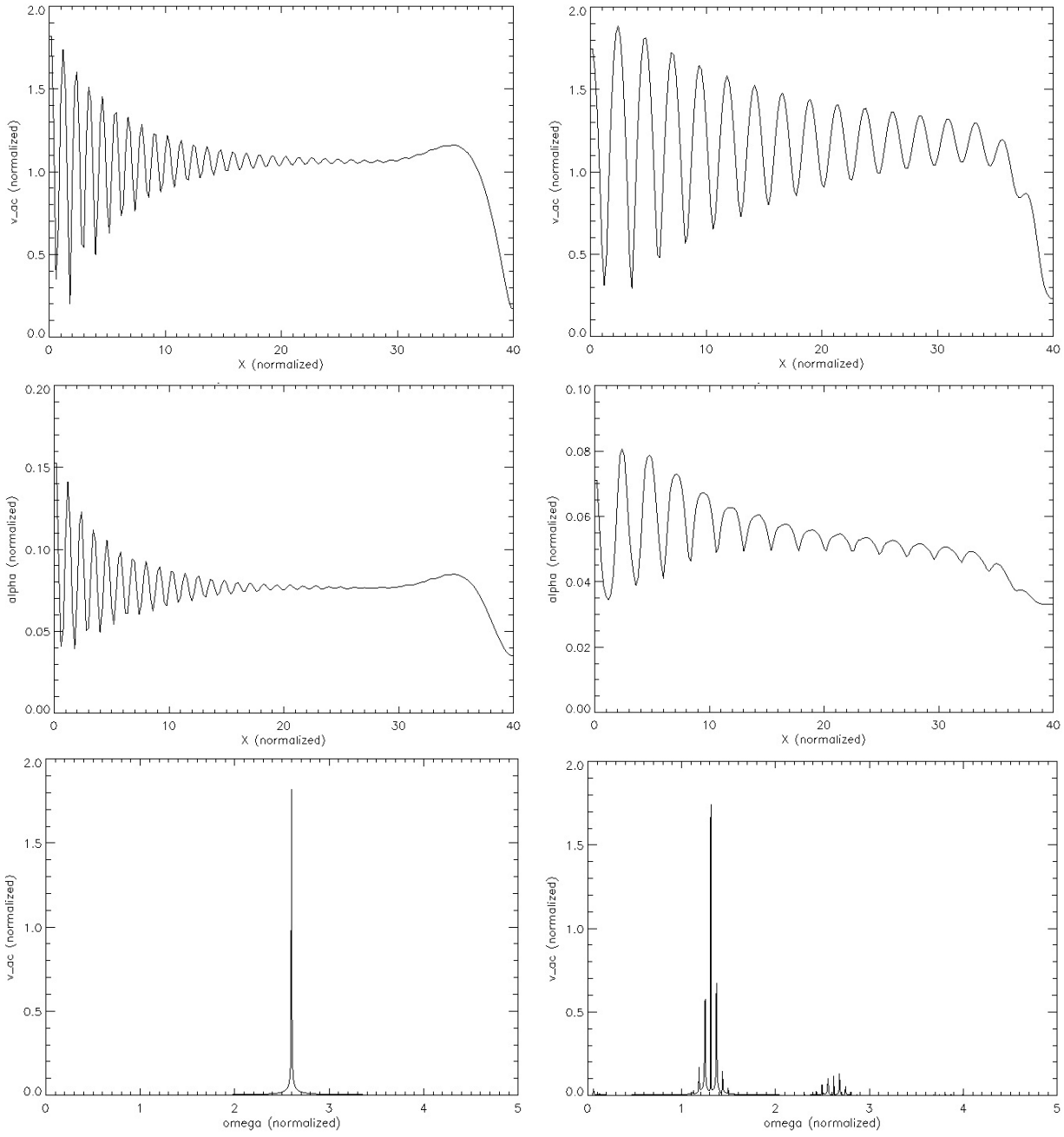

FIG. 2. (a), (b) - distribution of the amplitude of AC drive v_{ac} on the main harmonics $\omega = v_{dc}$ along the FFO; (c), (d) - distribution of damping parameter in the FFO; (e), (f) - frequency spectrum at the FFO's left boundary; X axis is normalized frequency and Y axis shows v_{ac}. Calculations were performed for two set of parameters: $h = 3.0$, $\gamma = 0.3$ (a,c,e) and $h = 2.0$, $\gamma = 0.2$ (b,d,f), correspondingly.

calculation parameters, such as time step and maximum integration time, has not been observed, the influence of a numerical artifact may not be completely excluded.

4. Conclusion

To summarize, we have presented a theoretical model which is consistent with our experimental results and previous theoretical studies. The model is numerically efficient, and therefore, has the potential to be generalized for the study of the rich two-dimensional dynamics of magnetic flux in two-dimensional FFOs.

Acknowledgements

The work was supported by the RFBR and the Ministry of Education and Science of the Russian Federation.

References

[1] T. Nagatsuma et al. *J. Appl. Phys.*, **54**, 3302 (1983); *ibid* **56**, 3284 (1984); *ibid* **58**, 441 (1985); *ibid* **63**, 1130 (1988).
[2] V. P. Koshelets and S. V. Shitov. *Supercond. Sci. Technol.*, **13**, R53 (2000).
[3] V. P. Koshelets et al. Supercond. *Sci. Technol.*, **17**, S127 (2004); V. P. Koshelets et al. *IEEE Trans. Appl. Supercond.*, **17**, 336 (2007); M. Yu. Torgashin et al. *IEEE Trans. Appl. Supercond.*, **17**, 339 (2007).
[4] IRE RAS Lab. of Supercond. Devices web page, `http://www.cplire.ru/html/lab234/publications.htm`.
[5] E. A. Matrozova, A. L. Pankratov and L. S. Revin. *J. Appl. Phys.*, **112**, 053905 (2012); L. S. Revin and A. L. Pankratov. *Phys. Rev. B*, **86**, 054501 (2012); E. A. Matrozova et al. *J. Appl. Phys.*, **110**, 053922 (2011); A. L. Pankratov. *Phys. Rev. B*, **78**, 024515 (2008); A. L. Pankratov et. al. *J. Phys.: Conf. Ser.*, **97**, 012303 (2008); A. L. Pankratov, V. L. Vaks and V. P. Koshelets. *J. Appl. Phys.*, **102**, 063912 (2007).
[6] A. S. Sobolev, A. L. Pankratov, and J. Mygind. *Physica C*, 435, 112 (2006).
[7] M. Jaworski. *Phys. Rev. B*, **81**, 224517 (2010).
[8] A. L. Pankratov, A. S. Sobolev, V. P. Koshelets, and J. Mygind. *Phys. Rev. B*, **75**, 184516 (2007).
[9] K. Nakajima et al. *J. Appl. Phys.*, **47**, 1620 (1976); D. R. Gulevich and F. V. Kusmartsev. *Phys. Rev. Lett.*, **97**, 017004 (2006); D. R. Gulevich and F. V. Kusmartsev. *Supercond. Sci. Tech.*, **20**, S60 (2007); D. R. Gulevich and F. V. Kusmartsev. *New J. Phys.*, **9**, 59 (2007); D.R. Gulevich et al. *Physica C*, **468**, 1903 (2008); D. R. Gulevich et al. *J. Appl. Phys.*, **104**, 064507 (2008); H. Farhan-Hassan et al. Flux-Flow Oscillator (FFO) Made with the Fluxon Cloning Circuits. *Terahertz and Mid Infrared Radiation*, p. 29, Springer (2011).
[10] D. R. Gulevich et al. *Phys. Rev. Lett.*, **101**, 127002 (2008); D. R. Gulevich et al. *Phys. Rev. B*, **80**, 094509 (2009).
[11] N.R. Werthamer. *Phys. Rev.*, **147**, 255 (1966); L.-E. Hasselberg, M.T. Levinsen, and M.R. Samuelsen. *Phys. Rev. B*, **9**, 3757 (1974); V.P. Koshelets, et al. *Phys. Rev. B*, **56**, 5572 (1997).
[12] K. K. Likharev. *Dynamics of Josephson Junctions and Circuits*. Gordon and Breach, New York, 1986. A. Barone and G. Paterno. *Physics and Applications of the Josephson Effect*, Wiley, New York, 1982.
[13] J. R. Tucker. *IEEE Journal of Quantum Electronics*, **15**, 1234 (1979); J. R. Tucker and M. J. Feldman. *Rev. Mod. Phys.*, **57**, 1055 (1985).
[14] Interactive Data Language (IDL): `http://www.ittvis.com` and `http://idlastro.gsfc.nasa.gov`.

NANOSYSTEMS: PHYSICS, CHEMISTRY, MATHEMATICS, 2013, 4 (4), P. 512–523

GENETIC ALGORITHM FOR CONSTRUCTING GRAPHENE NANORIBBON WITH GIVEN ELECTRONIC TRANSPORT PROPERTIES

I. S. Lobanov, A. I. Trifanov, E. S. Trifanova

St. Petersburg National Research University of Information Technologies, Mechanics and Optics, St. Petersburg, Russia

lobanov.igor@gmail.com, alextrifanov@gmail.com, etrifanova@gmail.com

PACS 72.80.Vp, 73.21.Hb, 73.22.Dj, 73.22.Pr, 73.63.Nm

Electronic transport in carbon nanoribbon is studied in a quantum graph model. A numerical method for current-voltage curve calculation is proposed. Various optimizations of a parallelization scheme are discussed. A parallel genetic algorithm to solve an inverse transport problem is invented.

Keywords: quantum graph, electronic properties, genetic algorithm, graphene nanoribbon.

1. Introduction

In last decade, carbon nanoribbons have proven to be one of the most promising nanosystems for microelectronics [10]. There is a huge number of works devoted to the construction of diodes, transistors, antennas and other devices based on nanoribbons, see e.g. recent publications [7–9]. Unfortunately, the theoretical prediction of properties of non-trivial geometry nanoribbons a is very complicated task, which will probably not be solved for decades. For that reason, nanoribbons are commonly simulated numerically. The most precise methods belong to the family of ab-initio methods and are applicable to the simulation of systems with dozens of atoms. Methods more appropriate for practical usage are based on density functional theory, which give results quite satisfactorily with experimental data, and are appropriate for use with systems not larger than few hundreds of atoms [6]. The only method suitable for the simulation of systems with many thousands of atoms is based on the tight-binding model [12]. However, even the tight-binding model requires sophisticated implementation to simulate millions atoms [11, 13].

In the present work, we describe a high-performance simulator of carbon nanoribbons based on a quantum graph model, which is a more precise model than the tight-binding approximation. We describe the parallelization of the proposed algorithm, which is capable of analyzing systems of millions atoms using existing supercomputers. A variant of genetic algorithm for solution of inverse transport problem is provided. Crossover and mutation operations are modified to fit the underlying physical problem.

2. Theoretical background

For convenience, we recall the basics of the quantum graph model, see for details [1–5]. By definition, a quantum graph is a collection of line segments glued at the ends together with Schrödinger operator on them. Almost everywhere, the quantum graph is a one dimensional manifold with the exception of gluing points. Hence, the motion of a

spinless nonrelativistic particle is described by the convenient one-dimensional Schrödinger operator on every edge:

$$-\phi_e'' + q_e\phi_e = E\phi_e, \tag{1}$$

where ϕ_e and q_e are restrictions of the wave function ϕ and the scalar potential q to the edge e, and E is energy. At the gluing point, the behavior of the wave function ϕ is determined by boundary conditions, which are in most cases chosen to be Kirchhoff conditions:

$$\phi_{e_1}(v) = \ldots = \phi_{e_k}(v), \quad \sum_{n=1}^{k} \phi'_{e_n}(v) = 0,$$

where $e_1, \ldots, e_k$ are all edges having common end v, $\phi_e(v)$ is the value of the wave function at the vertex v, and $\phi'_e(v)$ is the derivative of the wave function ϕ at the vertex v along external normal to the edge e.

Due to the existence and uniqueness theorem for the solution of ordinary differential equations. Equation (1) can be written as system of two algebraic energy dependent equations:

$$D_e(E)\begin{pmatrix}\phi_e(0)\\ \phi_e(l)\end{pmatrix} = N_e(E)\begin{pmatrix}-\phi'_e(0)\\ \phi'_e(l)\end{pmatrix},$$

where 0 and l denote the ends of the edge e, and the square matrices D_e and N_e define Dirichlet-to-Neumann (DN) mapping (also called Weyl function or Krein Q-function). As proven in the theory of boundary triples, the DN mapping can be chosen satisfying the following conditions:

(1) D_e and N_e are entire functions of the variable E;
(2) $N_e^{-1}D_e$ and $D_e^{-1}N_e$ are meromorphic functions of E with simple poles at the Neumann and Dirichlet spectra, respectively;
(3) eigenvalues of $N_e^{-1}D_e$ and $D_e^{-1}N_e$ are monotonic functions of E on every real interval of continuity.

For a vanishing scalar potential, the DN mapping is known explicitly:

$$D(E) = \sqrt{-E}\begin{pmatrix}\alpha & -\frac{1}{\alpha}\\ -\frac{1}{\alpha} & \alpha\end{pmatrix}, \quad N(E) = \begin{pmatrix}\alpha & \frac{1}{\alpha}\\ \frac{1}{\alpha} & \alpha\end{pmatrix}, \quad \alpha = \exp\left(\frac{i}{2}\sqrt{-E}\right).$$

We denote by F vector of values of wave function ϕ at all ends of all segments of the quantum graph, and denote by F' the vector of the external derivatives. Then, in terms of DN mapping, the Schrödinger equation can be written as

$$D(E)F = N(E)F', \tag{2}$$

and boundary conditions can be written as

$$BF = CF'. \tag{3}$$

It is worth noting that all matrices B and C satisfying $BC^* = CB^*$, such that the matrix $(B|C)$ has maximal rank, define self-adjoint boundary conditions, and all self-adjoint boundary conditions can be written in the form (3). Moreover, without loss of generality, B and C can be chosen to be self-adjoint and B can be non-negatively defined. To solve the Schrödinger equation for the energy E, it is convenient to consider matrix

$$R(E) = CN^{-1}(E)D(E) - B,$$

since E is an eigenvalue of the quantum graph, if and only if $R(E)$ is degenerate or E belongs to the Dirichlet spectrum. The eigenvalues of R are real and monotonous functions of E on every segment not containing points of Dirichlet spectrum, hence computation

of zeros of the eigenvalues as functions of E is a relatively simple problem. However, computation of the eigenvalues of $R(E)$ is a slow operation of complexity $O(n^3)$, where n is the number of edges in the quantum graph. The complexity can be significantly reduced in some cases, since matrices $D(E), N(E)$ and often B and C are sparse; the corresponding divide-and-conquer algorithm is outlined below.

Consider a subgraph of the quantum graph. We call a lead every end of a segment glued to an edge not belonging to the subgraph. Restriction of a solution of the stationary Schrödinger equation on the quantum graph to the subgraph should satisfy Equations (2) and (3) for the appropriate matrices B and C, but in this case, the matrices are not of the maximal rank, since we have no boundary conditions at leads [1]. Solving the system of equations with respect to the values of the wave function and derivatives of the wave function at vertices having attached boundary conditions, we obtain smaller system again of the form (2), but vectors F and F' contain in this case only values at leads. The functions D and N in the newly obtained system define Dirichlet-to-Neumann mapping for the subgraph and have all mentioned above properties of DN mappings. The complexity of the DN mapping calculation by Gaussian elimination is $O(m^2(m-n))$, where m is the number of all ends of all edges in the subgraph, and n is the number of leads.

The proposed divide-and-conquer algorithm for the DN mapping calculation for a subgraph is based on splitting the large subgraph graph into smaller subgraphs, which are then divided into even smaller subgraphs and so on; the DN mapping for smallest subgraphs (edges and vertices) are known exactly, the DN mappings for larger subgraphs are calculated using the above-mentioned elimination process using the DN mappings for smaller subgraphs. Clearly, the complexity of the algorithm depends on the way the splitting is done. We denote by δ the supremum of logarithm of ratio of the number of ends lying on a sphere in the quantum graph to the number of ends lying in the ball bounded by the sphere. Assuming that we divide every subgraph into two parts with halved diameter, the complexity of the algorithm is estimated as $O(m^{3\delta}) + O(m \ln m)$, where m is the number of edges in the largest subgraph [1]. For example, a $\mathbb{Z}$-periodic graph with afinite fundamental domain, the complexity is $O(m \ln m)$, for a $\mathbb{Z}^2$-periodic graph with finite fundamental domain, the complexity is $O(m^{3/2})$.

Now, we consider a transport problem for a quantum graph consisting of a compact part and attached semi-infinite segments with constant potentials. As is well-known, the scattering matrix of the system is given by [1]

$$S(E) = (D(E) - T(E)N(E))^{-1}(D(E) + T(E)N(E)), \quad T(E) = \mathrm{diag}\sqrt{V - E}, \qquad (4)$$

where V is the vector of scalar potentials on semi-infinite segments, $\mathrm{diag}V$ denotes the diagonal matrix with the diagonal V. Provided $D(E)$ and $N(E)$ are already calculated, the complexity of the scattering matrix calculation is equal to sum of complexities of matrix inversion and multiplication, which are less than $O(n^3)$, where n is the number of all leads.

3. Quantum graph model of graphene nanoribbon in elecric field

The calculation of transport properties for a quantum mechanical system is generally a complex theoretical and numerical problem, therefore, simplified models are generally used. Current state of artdensity functional theory is used to model systems with hundreds of atoms, while the tight binding approximation is used to model systems with millions of atoms. In the present work, we use the quantum graph model, which is slightly slower, but it takes into account the continuous character of electron motion. The tight binding approximation can be considered as a special case of the quantum graph model.

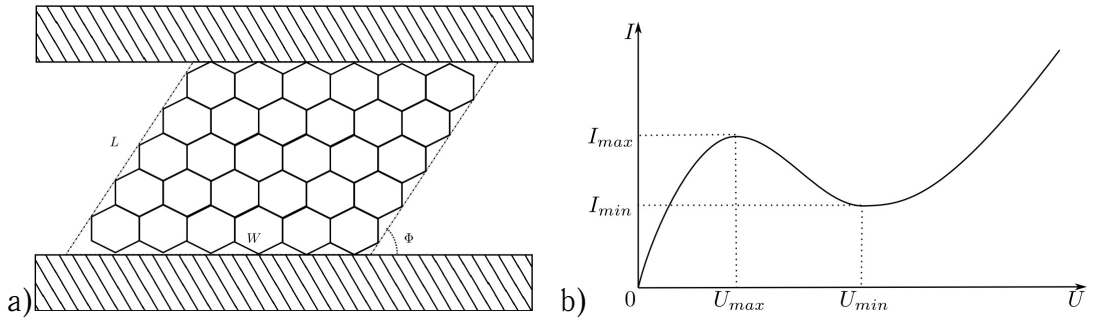

FIG. 1. (a) Graphene nanoribbon. (b) Typical current-voltage characteristics of parallelogram shaped nanoribbon.

One of the most challenging transport problems is transport in the presence of an external electric field, which often breaks the symmetry of the problem. Howeve,r for the quantum graph model, consideration of the electric field is relatively simple, since:

(1) The electric field is an explicit parameter of the model. Variation of the field does not imply recalculation of auxiliary parameters, introducing additional assumptions and so on.
(2) Calculation of the scattering matrix does not require one to solve the spectral problem. In fact, the transport problem is easier to solve than the spectral problem.

Since all transport properties can be expressed in terms of the scattering matrix, we focus on the calculation of the scattering matrix, and as an example, we consider computation of current-voltage characteristics.

Consider a parallelogram shaped graphene nanoribbon with zigzag sides attached to two electrodes, see Figure 1 (a). We denote by W the number of benzene rings lying on one electrode, by L the distance between electrodes in benzene rings and by Φ the cutting angle; let $T = \tan\Phi$. In the quantum graph model, the electron moves along segments representing chemical bonds, and the segments are glued at the carbon atoms. Boundary conditions are assumed to be Kirchhoff conditions. We model the electrodes by semi-infinite segments. To avoid unrealistic interface states, we attach separate semi-infinite segments to every atom lying on an electrode.

Typical behavior of the current-voltage characteristics (IV curve) is shown in Figure 1 (b). In applications, only key features of IV curve are of importance, e.g. in the considered case the first local maximum (U_{max}, I_{max}) and the first local minimum (U_{min}, I_{min}) should be taken into account.

For the quantum graph model we use the convenient Landauer formula to calculate conductance:

$$\frac{e^2}{\pi\hbar}\sum_{s,d}|S_{ds}|^2 - |S_{sd}|^2,$$

where s runs over all indices of the semi-infinite segments corresponding to one electrode, and d, to another. The crucial part of the computation is calculation of the scattering matrix by the formula (4), which requires one to compute the Dirichlet-to-Neumann mapping. As mentioned before, the complexity of the DN mapping computation highly depends on how the quantum graph is split into subgraphs. Below, we provide explicit splitting which is best suited for long narrow ribbons.

The considered nanoribbon can be divided into primitive parts as shown in Figures 2 and 3. The nanoribbon is divided to collection of chains, where all the elements of every

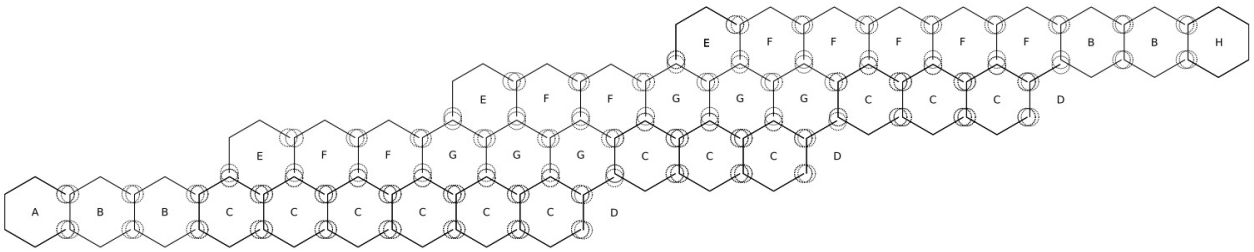

FIG. 2. Splitting of the nanoribbon to primitive pieces.

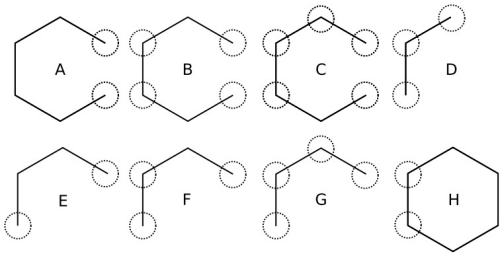

FIG. 3. List of primitive pieces of graphene nanoribbon.

chain are located a fixed distance from electrodes and therefore, have the same potential. To calculate the DN mapping for one chain, we first calculate the DN mapping for two segments having distinct angles with electric field, then compute the DN mappings for all primitive pieces, compute the DN mappings for the chains containing pieces of one type, and finally compute the DN mapping for the whole chain. The computation of the DN mapping for the chain of equal elements has a complexity $O(\ln m)$, where m is the length of the chain, since all subchains of equal length have equal DN mappings. Since the number of leads of the primitive pieces and the number of the primitive pieces are fixed, the overall complexity of computing the DN mapping for one chain is $O(\ln W)$. Every chain has more than W ends, and no more than W ends are leads (more precisely $2(W - [T])$), hence the complexity of gluing two chains together is less than $O(W^3)$. Since the total number of chains is L, the complexity of the calculation of the DN mapping for the whole nanoribbon is $O(LW^3)$. It is worth noting that the proposed splitting gives linear complexity with respect to length L of the ribbon, which is better than the above-given theoretical estimate $O(L^{3/2}W^{3/2})$. Hence, the provided splitting is best suited for very long ribbons.

For the case of a short and wide nanoribbon, one can split the quantum graph into narrow chains of length L and then glue them. Such splitting gives us complexity $O(WL^3)$. The worst case is a ribbon with equal W and L, where two provided partitions leads to the algorithm of complexity $O(L^4)$.

The computation time of current for a given voltage for the nanoribbon using the method described in the previous section is several hours for nanoribbon with W ca. 100 and L ca. 1000. Hence, for the simulation of large graphs and the use of genetic algorithms, one should speed up computations, which can be done using both sophisticated algorithms for matrix operations and parallel computations. Optimization of matrix operations is a well-studied subject, see e.g. [14], documentation on LAPACK and so on. Here, we discuss opportunities for parallelization. The main observation is the independence of the Dirichlet-to-Nuemann mapping calculations for distinct subgraphs, hence computations for such subgraphs can be performed concurrently. But, one should take into account that to

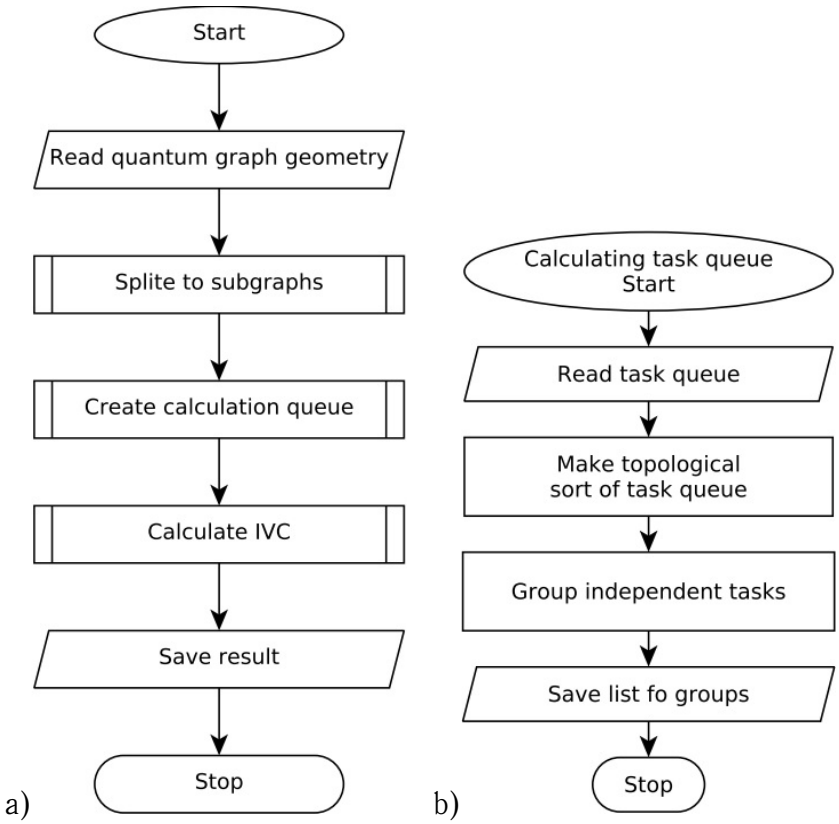

FIG. 4. (a) Flowchart for the I-V curve calculation. (b) Flowchart for the queue generation

compute the DN mapping for a subgraph, one should preliminarily compute the mappings for all parts of the subgraph, hence subgraphs form an hierarchy, where computations on lower levels must be done prior to higher ones. Finally, to perform parallel a computation of the DN mapping for the whole quantum graph, one should divide the graph into subgraphs, calculate the dependence of the graphs, collect subgraphs to groups which can be analyzed simultaneously and execute all groups in correct order. It is worth noting that the memory requirement should be taken into consideration while forming computation groups, since the storage of all temporary buffers in memory simultaneously requires much more resources than available on modern computers. That means that some kind of dynamic memory allocation should be done. Unfortunately, contemporary parallel memory managers are to slow for such tasks. To overcome this difficulty, we have implemented a memory manager that preallocates all the memory by using overlapping regions, which however will never be accessed simultaneously under the given order of DN mappings calculation. Further opportunities for parallelization are the parallel matrix operations and parallel calculation for different energy and electric field values. Flowcharts for the parallel calculation of I-V curve for the nanoribbon are shown on Figures 4-8.

4. Inverse transport problem

The inverse transport problem is to recover system geometry based on given transport properties. We are going to consider the current-voltage curve, which is one of the most important transport properties. Solution of the inverse problem is extremely complex

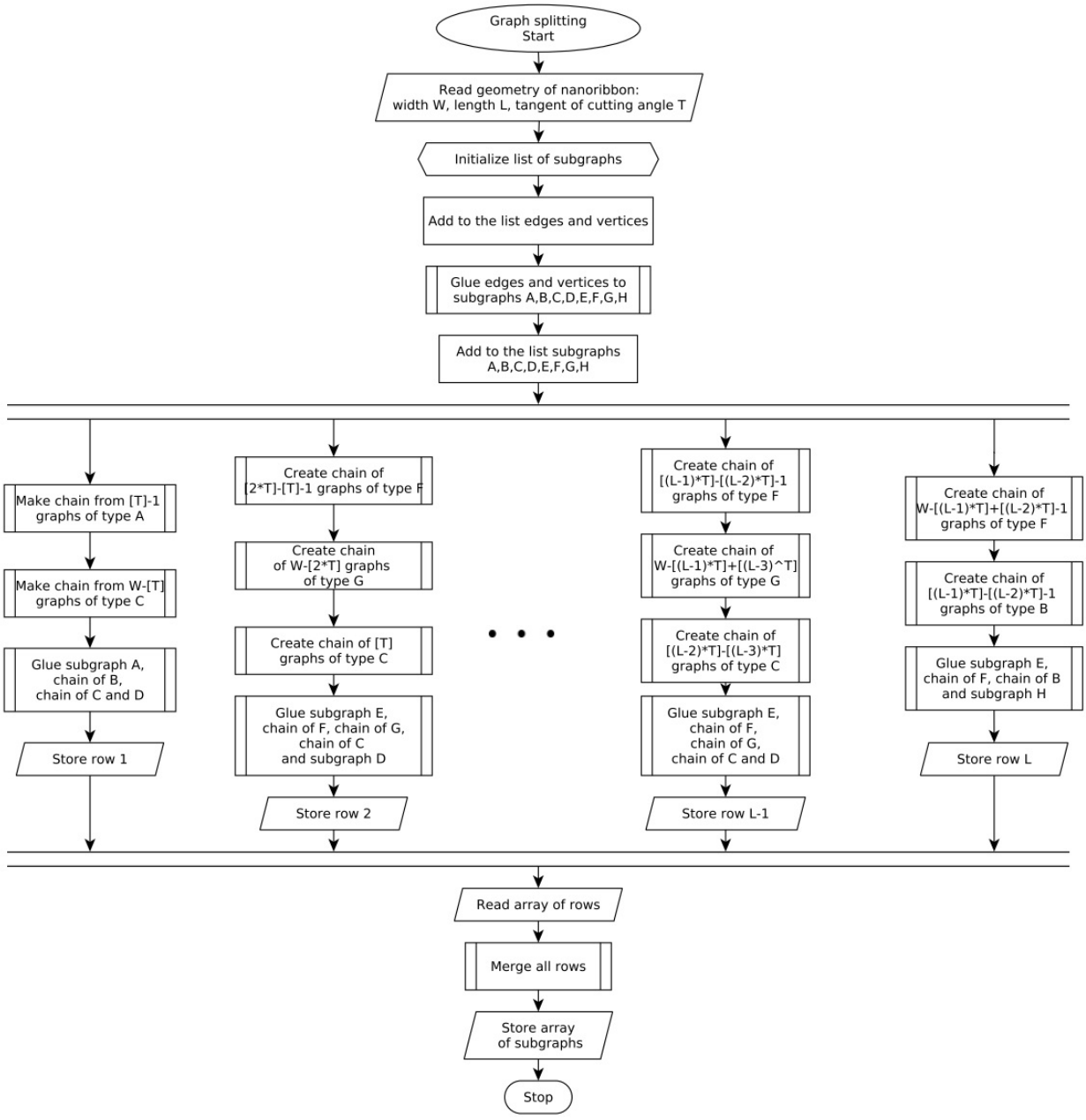

FIG. 5. Flowchart for the nanoribbon splitting

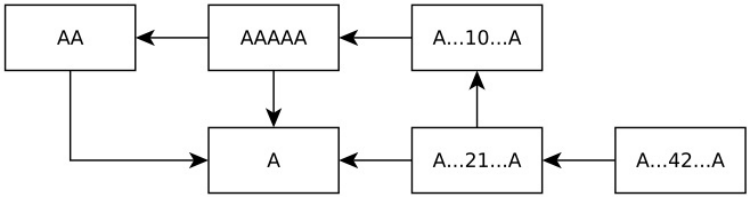

FIG. 6. Demonstration of optimal splitting of chain of 42 graphs of type A to subgraphs

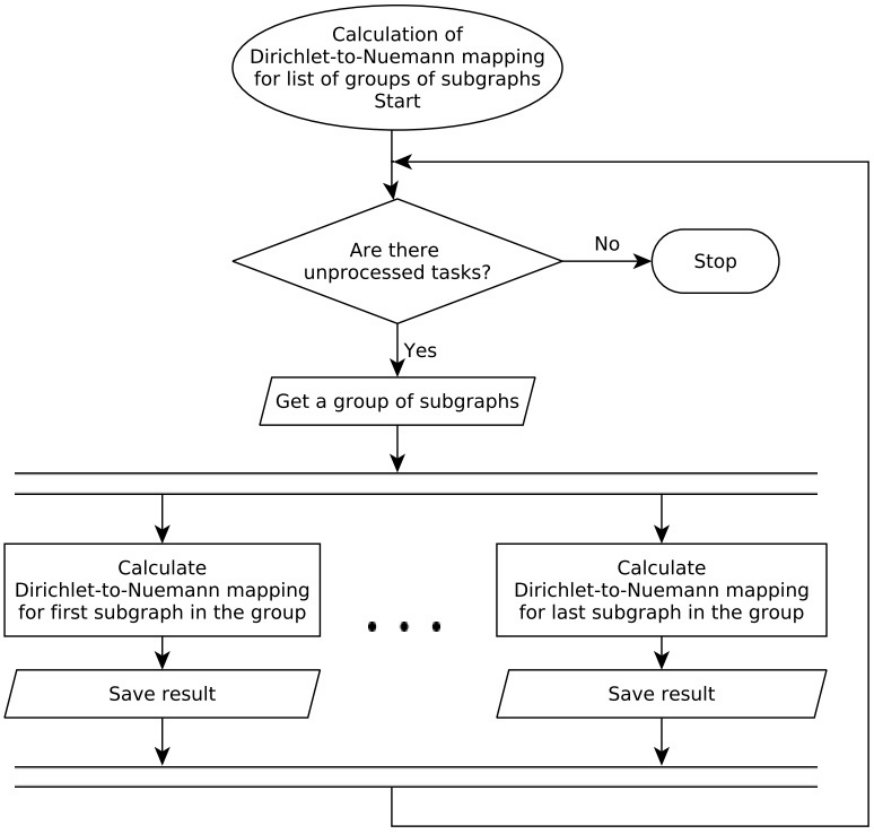

FIG. 7. Flowchart for the execution of enqueued calculations

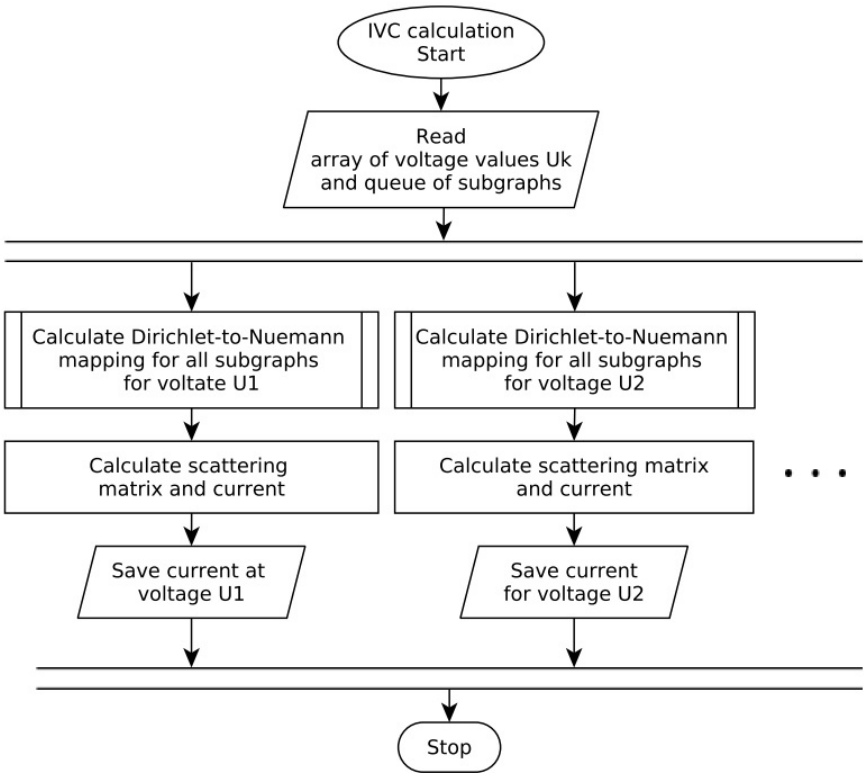

FIG. 8. Flowchart for the current-voltage characteristics calculation

and has no general solution at the moment. However, in the present work we propose a genetic algorithm to construct a nanoribbon with properties close to the given I-V curve.

Due to the high complexity of calculating the fitness function in the problem, only parallel algorithms deserve consideration. At the moment, there are four main classes of parallel genetic algorithms: global master-slave, global fine-grained, coarse grained and hierarchical. The fine-grained algorithm was implemented, since it has good scalability as we show below. We divide the whole population to subpopulations, which are processed concurrently on different processing nodes. To avoid degeneracy and to balance the load, individuals are exchanged between subpopulations. Depending on the timing of when individuals are exchanged, the algorithm can be synchronous or asynchronous. The island model was chosen for implementation, since it can be adapted to arbitrary topology.

We use processes of two types: the first type computes mutation, crossover and selection, while the second type assists ones of the first type by computing the fitness function (the I-V curve). Clearly, the number of processes in an ideal situation should coincide with the number of individuals. One ”master” process is selected, which should send stop signal to other nodes as soon as the desired fitness is achieved.

Every assisting node waits until the ribbon geometry is received. Upon receipt of the gometry, the I-V curve is computed as described in the previous section, then the fitness is calculated as the distance between the obtained curve and the desired one. The fitness and the I-V curve are sent back to the evolution computing nodes. If the stop signal is received, then the process terminates, otherwise the process again waits for input.

The stop conditions are only checked by the designated node. If desired fitness value is achieved or the maximum number of iterations is done, the designated node sends a stop signal to all nodes and prints the individual that has the geometry closest to the desired current-voltage curve displayed.

The input parameters of the algorithm are positions of the first local maximum (V_{max}, I_{max}) and the first local minimum (V_{min}, I_{min}) of the I-V curve. The results of the computation are the width W, the length L and the cutting angle Φ of the nanoribbon. The set of the parameters can be extended to a wider class of geometries, e.g. one can append intrusions.

The genetic algorithm starts with the generation of a subpopulation on every island. Every individual is a nanoribbon geometry, which in our case is described by the values W, L and Φ. On initialization, the geometric parameters are generated randomly using a uniform distribution, where the maximum values of W and L are bounded by available processing power and physical motivations.

Further randomly chosen individuals mutate. The number of mutating individuals has a constant ratio to the size of subpopulation; the ratio is a parameter of the algorithm. The mutation operation has the following steps: geometric parameters subjected to mutation are chosen randomly; a value is appended to each of the parameters normally distributed; the obtained parameters are checked for correctness; if the geometry is invalid, the individual is eliminated.

In the island model, crossover is done only inside subpopulations. To improve algorithm convergence, the crossover (inside) population makes use of a simplified model. Roughly speaking, the nanoribbon can be considered as an electrical circuit. The I-V curves for parallel and series circuits are well known and can be used for a fast, rough estimate of the results for gluing nanoribbons together. Hence, during crossover, the inside subpopulation I-V curves for all individual pairs in the subpopulation are estimated

using classical methods, and from these, the most promising pairs are chosen to produce offspring.

As well known genetic algorithms for small populations tend to converge to a local maximum of the fitness function, which for complex fitness functions, is most likely not the global maximum. To avoid this trap, the population size must be increased, or in the island model, individuals must be exchanged between islands. Experiments show that the best convergence is obtained When the best individuals exchange islands. Since the fitness computation time varies from several seconds to several hours, depending on the geometry of the nanoribbon, an iteration of genetic algorithm on one island may be several times slower than the iteration on another island. Therefore, the individual exchange must be asynchronous. Every island, after the fitness calculation, sends a fixed number of its best individuals to a different, randomly chosen island. Before the crossover, every island checks, if there are migrants waiting, which are appended to the subpopulation.

Finally, if the size of a subpopulation becomes larger than the predefined value, the worst individuals are eliminated to decrease the subpopulation size. Hence, the size of every subpopulation varies, but cannot become larger than the fixed value determined by the available computation power.

5. Parallel genetic logarithm convergence

The inverse transport problem is one of complex optimization, with lots of local optima. Separation of the population into subpopulations improves the convergence to an optimum, but the obtained solution may be far from a global optimum. If a subpopulation comes close to a local optimum, the subpopulation starts to degenerate, which leads to a waste of computational resources. To eliminate such a situation, we mix the population by exchanging the best individuals between islands. In the present section, we estimate the convergence rate of such an algorithm.

Individuals exchanged in a real situation depends on topology, but for simplicity, we assume that the connection graph is complete.

Let f^0 be the mean value of the fitness function in the initial population. We assume that after one iteration, the mean value of the fitness function is improved p times, that is

$$f^{k+1} = p \cdot f^k = p^k \cdot f^0.$$

Hence, to obtain the desired value F for the fitness function, we should make $n = \log_p \frac{F}{f^0}$ iterations.

Now, we consider several populations exchanged by individuals. We assume that for every subpopulation the estimate above is valid, Hence, without exchange, an increase in the population size gives no speed up in the convergence. We now consider the improvement of the fitness function after the exchange. We denote by f_j^k the mean value of the fitness function in a subpopulation j on an iteration k. We estimate the convergence by a geometric progression, that is, we assume $f_j^{k+1} = s_j f^k$ for some parameter $s_j = p \cdot q_j$. Let M be the number of all possible distinct individuals, N be the number of individuals in every subpopulation. Taking into account the quality of individuals to exchange, we get the estimate $q_k = p^\beta$, $0 < \beta < 1$, for non overlapping populations. Taking into account the existence of identical species in distinct subpopulations, we get estimate

$$s_k = p^{\beta \sum_{j=1}^m P_j}, \quad P_j = \prod_{i=1}^{J} \prod_{j=0}^{N-1} \frac{M - i \cdot N - j}{M}.$$

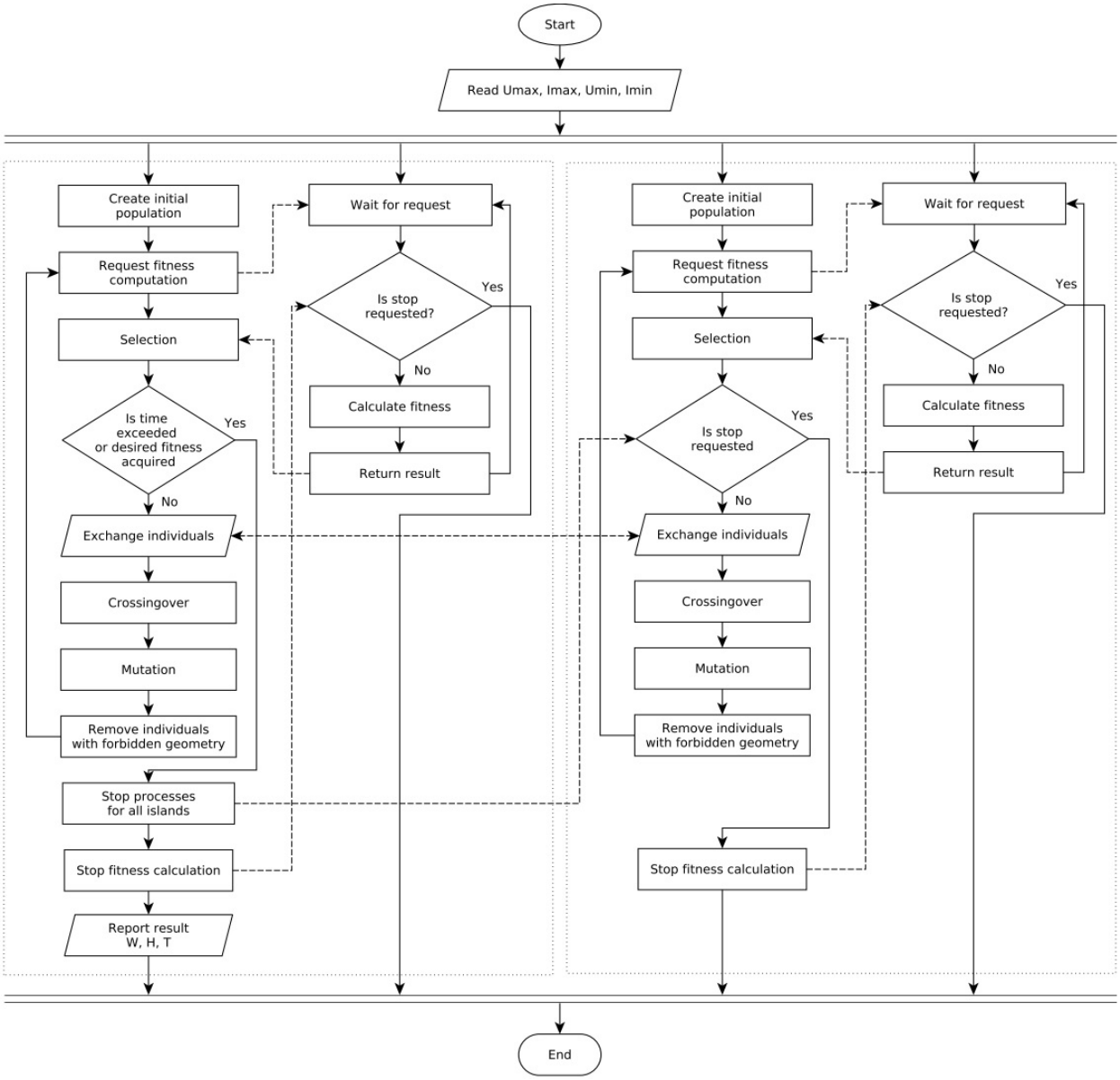

FIG. 9. Flowchart of parallel genetic algorithm

Using latter estimate, we obtain the number of steps required to achieve the desired fitness F using k subpopulations:

$$n_j = \frac{\log_p \frac{F}{f_j^0}}{\beta \cdot \sum_{k=1}^{m} P_k}.$$

Hence, the parallel algorithm gives the following for rate enhancement:

$$S(m) = \frac{\min n_j}{n}.$$

Estimates of the rate enhancement are shown on Figure 10 for parameters $N = 1000$, $\frac{F}{f_j^0} = 10^3$, $p = 1.1$, $\beta = 0.058$.

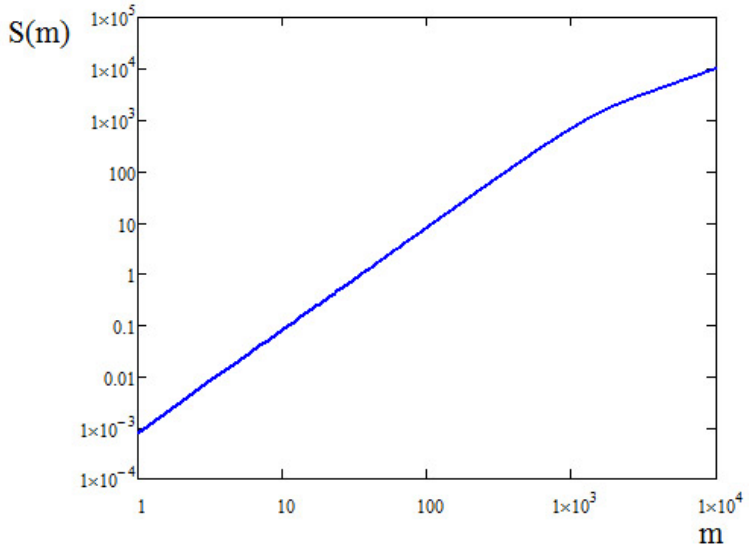

FIG. 10. Speed up of parallel genetic algorithm as function of number of processors

Acknowledment

The work is supported by state contract 07.514.11.4146.

References

[1] I.S. Lobanov, E.S. Trifanova. Direct and inverse problems for quantum graph model. *Nanosystems: Physics, Chemistry, Mathematics*, **3** (5), P. 6–32 (2012).
[2] P. Kuchment. Graph models of wave propagation in thin structures. *Waves in Random Media*, **12**, (4), P. R1–R24 (2002).
[3] U. Smilansky. Discrete graphs — a paradigm model for quantum chaos. *Seminaire Poincare XIV*, P. 89–114 (2010).
[4] *Analysis on Graphs and its Applications*, Ed by. Exner P. et al. Proc. Symp. Pure Math., AMS, 2008.
[5] *Quantum Graphs and Their Applications*, Ed. By Berkolaiko G. et al. Contemp. Math., 2006, V. 415.
[6] P. Jadaun, B.R. Sahu, L.F. Register, S.K. Banerjee. Density functional theory studies of interactions of graphene with its environment: Substrate, gate dielectric and edge effects. *Solid State Communications*, **152** (15), P. 1497–1502 (2012).
[7] G. Deligeorgis, F. Coccetti, G. Konstantinidis, R. Plana. Radio frequency signal detection by ballistic transport in Y-shaped graphene nanoribbons. *Appl. Phys. Lett.*, **101**, P. 013502 (2012).
[8] C. Cocchi, D. Prezzi, et al. Optical Excitations and Field Enhancement in Short Graphene Nanoribbons. *The Journal of Physical Chemistry Letters*, **3** (7), P. 924–929 (2012).
[9] W.S. Hwang, K. Tahy, et al. Transport properties of graphene nanoribbon transistors on chemical-vapor-deposition grown wafer-scale graphene. *Appl. Phys. Lett.*, **100**, P. 203107 (2012).
[10] O.V. Yazyev. A Guide to the Design of Electronic Properties of Graphene Nanoribbons. *Acc. Chem. Res.*, Article ASAP (2013).
[11] Miao Gao, Gui-Ping Zhang, Zhong-Yi Lu. Electronic transport of a large scale system studied by renormalized transfer matrix method: application to armchair graphene nanoribbons between quantum wires. `arXiv:1305.6682`.
[12] Y. Wu, P.A. Childs. Conductance of Graphene Nanoribbon Junctions and the Tight Binding Model. *Nanoscale Res. Lett.*, **6**, P. 62 (2011).
[13] S. Ihnatsenka. Computation of electron quantum transport in graphene nanoribbons using GPU. *Computer Physics Communications*, **183** (3), P. 543–546 (2012).
[14] W.H. Press, S.A. Teukolsky et.al., *Numerical Recipes 3rd Edition: The Art of Scientific Computing*. Cambridge university press, 2007, 1235 p.

NANOSYSTEMS: PHYSICS, CHEMISTRY, MATHEMATICS, 2013, 4 (4), P. 524–528

HYSTERESIS OF CONDUCTIVITY IN THE GRANULAR SILVER FILMS

I. A. Gladskikh, N. B. Leonov, S. G. Przhibel'skii, T. A. Vartanyan

Saint Petersburg National Research University of Information Technologies, Mechanics and Optics, 49 Kronverkskiy, Saint Petersburg, 197101, Russia

138020@mail.ru

PACS 73.61.At

The electrical properties of the granular silver films located on a surface of sapphire substrates are experimentally investigated during deposition and thermal annealing. The strong influence of surface-based silver atom diffusion on film formation is revealed, both during and after deposition. The effect of resistance switching in the films of the various thicknesses close to the percolation threshold, depending on the applied voltage is found and investigated. These sharp changes of resistance of 5–7 orders can be reversible or irreversible, depending on film thickness.

Keywords: granular metal films, metal nanoparticles, resistance switching.

1. Introduction

Thin metal films are widely used in various applications as electric current conductor, chemical sensors, optical filters, etc. Their electrical properties depend on the nature of the metal and, to an even greater extent, on their morphology. Continuous films have metallic conductivities, characterized by low resistance and positive temperature coefficients. The resistance of metal films consisting of separate granules is much greater than the resistance of the bulk metal and depends on the substrate material and the distance between the granules. The conductivity of such a system is characterized by a negative temperature coefficient of resistance. The energy of activation is estimated to be about several tenths of an eV. The charge transfer can be carried out either by the hopping mechanism via traps in the subsurface layer of the substrate, or by a process of thermally activated tunneling [1–4].

The granular film that is formed on a dielectric substrate at the beginning of the vacuum deposition process transforms into a continuous film during material accumulation. The appearance of a continuous metal path between the electrodes, spaced from each other on a macroscopic distance, occurs long before the formation of a continuous film, and is called the percolation transition. After the percolation threshold, the electrical properties of the film become similar to properties of the bulk metal.

The electrical properties of metal films at the percolation threshold are most interesting, because when the distance between granules is very small, then small changes in the amount and distribution of the metal cause relatively large changes in the conductivities of the films. Such structure can be obtained by heating of the films having low resistances. Indeed, due to the diffusion of the metal allows, the separated granules are formed [5, 6].

2. Experimental

In this study we investigated granular silver films on the surface of sapphire substrates at the percolation threshold. The granular films were produced by the thermal evaporation of silver onto the surface of the sapphire substrate in the gap (3 mm $\times$ 2 cm) between the silver electrodes inside the vacuum chamber PVD 75 (Kurt J. Lesker) at a residual gas pressure less

than 5×10-7 Torr. During the deposition, the electrical properties of the films were controlled by a picoammeter (Keithley – 6487). We investigated films with thicknesses from 50 to 150 Å, deposited at the rates of 0.1–1 Å/sec.

During deposition, the film resistance decreases exponentially (Fig. 1a). For the films of the same thickness the resistance was lower provided they were obtained at a larger rate of deposition. Immediately after the deposition, the film resistance continues to change rapidly (Fig. 1b) and after an hour, the resistance can vary by 3–4 orders of magnitude. A day after the deposition, the resistance of the films obtained at the low deposition rate (0.1 Å/sec) was $1.3 \cdot 10^{12}$ ohms, while the resistance of the films obtained at the deposition rate of 0.6 Å/sec was 1 kohm.

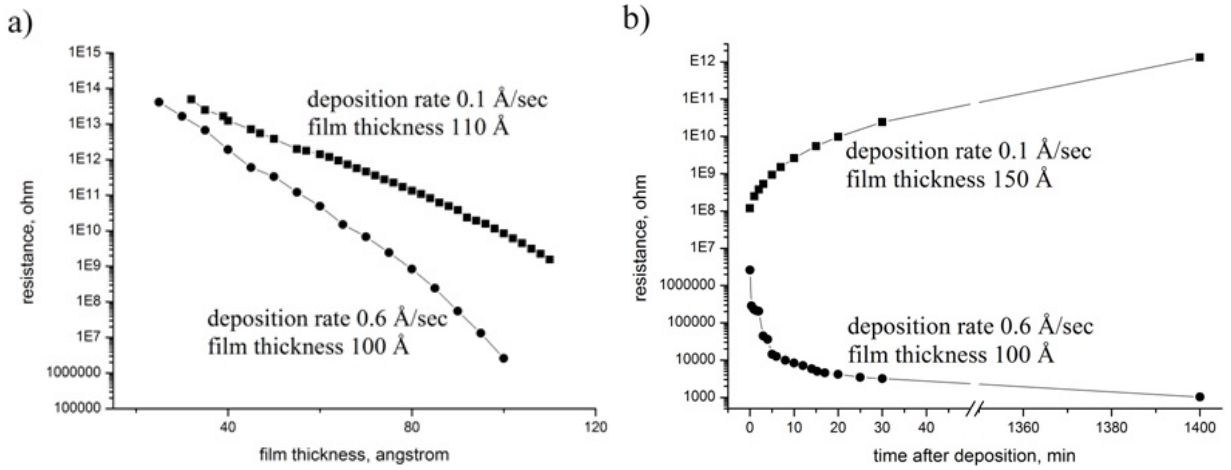

FIG. 1. a) The dependence of the resistance of the films on their thicknesses and rates of deposition; b) the change of resistance of the films during the time after deposition (resistance was measured at a voltage of 5 V)

These results indicate the strong influence that silver atom diffusion has on film formation both during and after deposition. At the low deposition rate separate large particles with irregular shapes and sizes of about 200–300 nm are formed (Fig. 2a). After deposition, small particles and adsorbed atoms diffuse over the surface and stick to the larger particles. Thus, the distance between particles increases and, as a result, the conductivity of the film diminishes. At deposition rates of 0.5 Å/sec or more, films with the thickness of more than 50 Å are formed. They represent the endless conductive labyrinth structure consisting of a network of irregularly-shaped particles. These wires have cross sections of about 30 nm at a film thickness of 10 nm. Such films have resistance typical for bulk metals, namely from several tens ohms to several kohms.

So, it is possible to differentiate two typical cases: the film consisting of separate granules, having a complex shape, and the conductive film having a labyrinth structure. Henceforth, we will consider only the second option.

After deposition, the granular silver films were subjected to heating. During annealing, the material is redistributed to form separate particles. In this case, a nonlinear increase of the resistance over time (Fig. 3) and a sharp step of the resistance after 60 minutes of heat treatment were observed. The sharp increase in the resistance points to a breaking of the conductive metal structure between electrodes.

The inset in Fig. 3 shows a SEM image of a 100 Å granular film deposited at a rate of 0.6 Å/sec after heating. Particles became larger in comparison with the just deposited film.

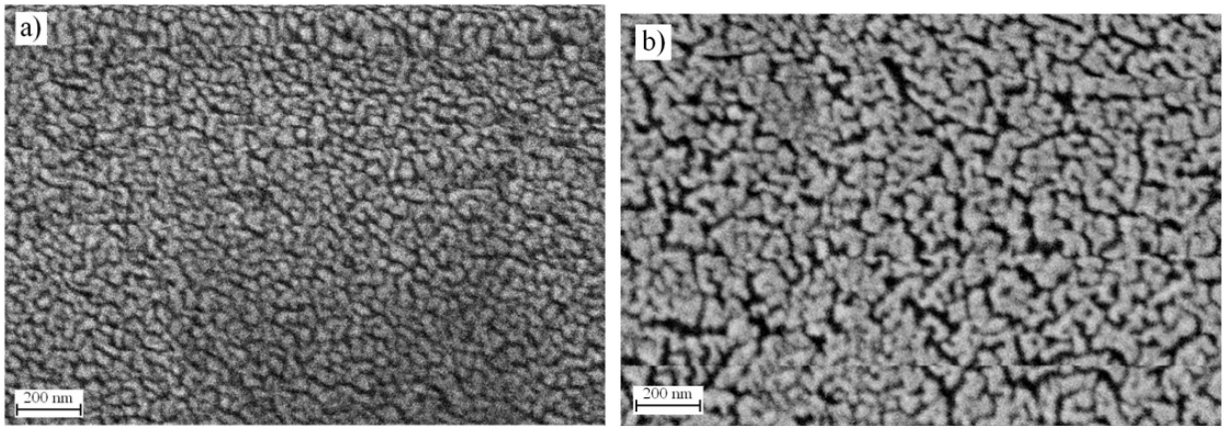

FIG. 2. SEM image of the granular silver films on the surface of the sapphire substrate with thickness of 100 Å deposited at the rate of 0.1 Å /sec (a) and 0.6 Å/sec (b)

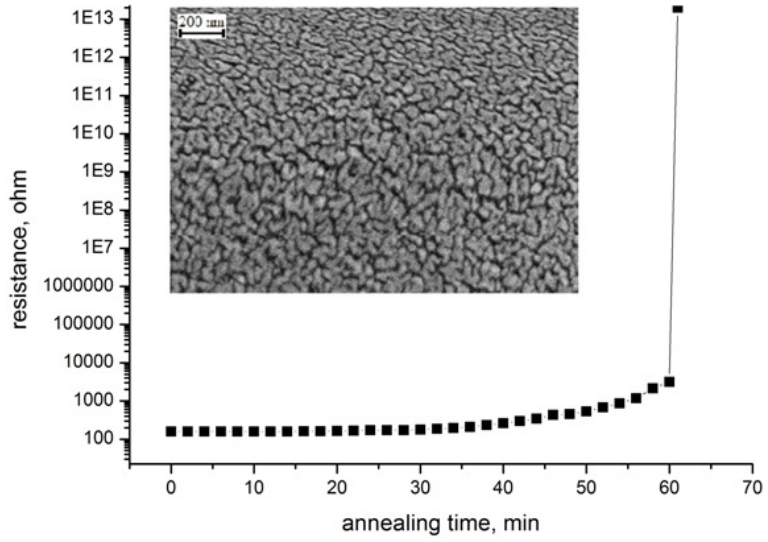

FIG. 3. Resistance of the granular silver film with thickness of 100 Å annealed at 120°C as a function of annealing time. On the insert the SEM image of the silver film after heating is presented

Distances between the particles are still very small, nevertheless, this film consists of individual separated particles as confirmed by its very high resistance. After the jump of the resistance, heating of the film was stopped.

3. Results and Discussion

After heating, the morphology of the films and their optical properties did not change appreciably, however, the resistance of the films increased by 10–12 orders and the films acquired the ability to switch their resistance under the influence of applied voltage. Fig. 4a shows the current-voltage characteristics of the silver film after heating. The 50 Å thick film was deposited at a rate of 1 Å/sec. As can be seen, at an applied voltage of less than 7 V (region I), the film has low conductivity with resistance of $1.5 \cdot 10^{12}$ ohms. In this region the current increases almost linearly with the applied voltage. The film switches to the high conductivity state at the threshold field strength of 7 volts (II). Further increase of the voltage reduces the

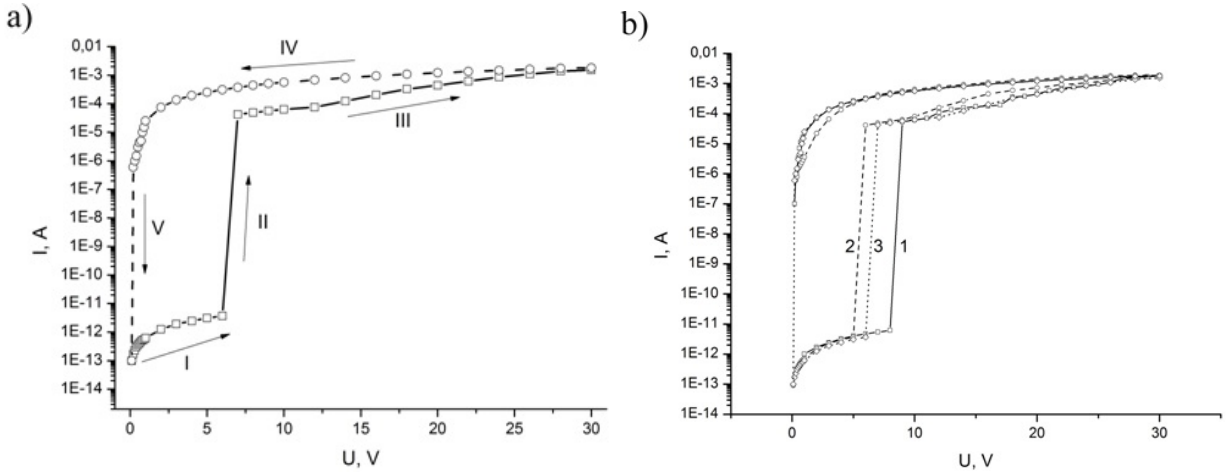

FIG. 4. a) I–V characteristics of the granular silver film on the surface of the sapphire substrate with the thickness of 50 Å after heat treatment at 90 °C for 60 minutes with increasing (solid line) and decreasing (dashed line) voltage; b) series of cycles of I–V characteristics measured with an interval of 3 minutes

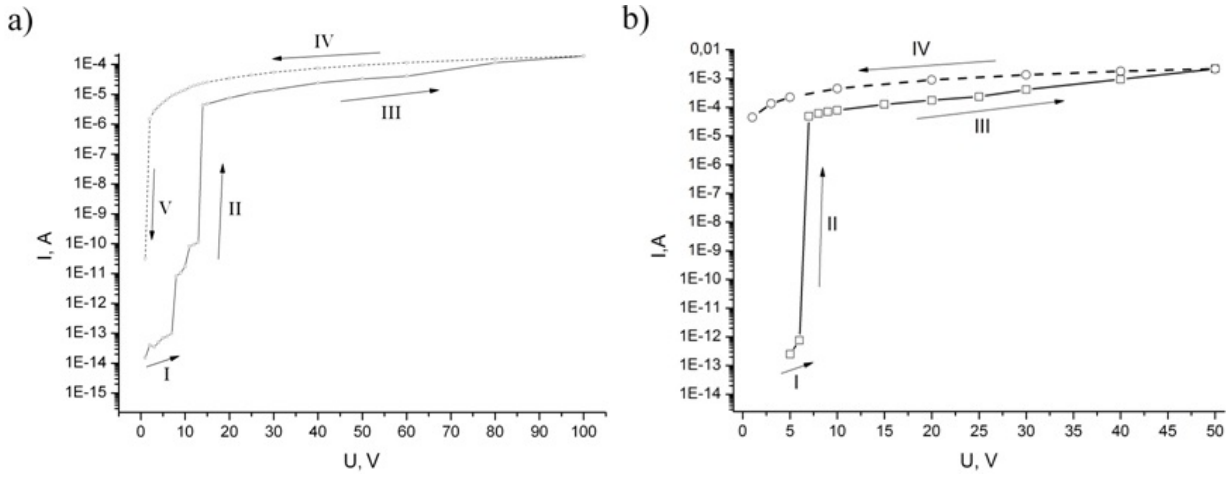

FIG. 5. I–V characteristics of the granular silver films on the surface of the sapphire substrate with the thickness of 85 Å (a) and 115 Å (b) after heat treatment at 120 °C for 60 minutes with increasing (solid line) and decreasing (dashed line) voltage

resistance to 16 ohms (III). The current-voltage characteristic has an ohmic character, then the voltage is reduced (IV), but at a voltage of 0.1 V film passes to the initial high-resistance state (V).

During subsequent voltage increase/decrease cycles the current-voltage characteristics of the film were very stable (Fig. 4b), with slight fluctuations in the voltage required to switch the film into its low-resistance state.

The situation is different for thicker films. Fig. 5 shows the current-voltage characteristics of heated 85 and 115 Å films , deposited at 0.6 Å/s. For these films, a nonlinear increase of the current was observed in region I , wherein, noticeable fluctuations of the resistance were observed. In repeated measurements for the 85 Å film, the switching voltage was greatly decreased, and after the third cycle, the film remained in the low-resistance state after

removing the applied voltage. The 115 Å film remained in the low-resistance state after the first switching of the resistance, but it could be switched into the low-conductivity state after short-term heating.

Similar resistance switching has been described in previous literature for different thin-film materials. They can be divided into two general categories: threshold switching, in which electrical power is required to maintain the ON state (state with low resistance) and memory switching, in which both states (ON and OFF) can be maintained without electrical power [7–9]. Changes in conductivity can be either structural, involving nanoparticle deformation or diffusion of the material under an applied voltage, or electronic, i.e. caused by the injection of electrons under the influence of high electric fields arising between nanoparticles at film discontinuities. However, the fact that granular silver films with thickness greater than 85 Å do not switch to low conductivity states indicate that the transfer of material plays an important role in creation of the conducting channels.

4. Conclusion

The paper presents the results of conductivity studies for silver granular films with different thicknesses deposited on the surface of a sapphire substrate. The films were produced by the standard method of thermal deposition of an atomic beam on the cold substrate. The resistance changes during and immediately after deposition were measured. After thermal treatment of the films, a resistance switching effect was observed, while the film structure and its optical properties were not substantially changed. The value of the resistance switching can be up to 10^7 ohms, and the voltage required to switch ON the structure (to the low-resistance state) may vary within a wide range depending on the duration of the annealing.

References

[1] D.S. Herman, T.N. Rodin. Electrical conduction between metallic microparticles. *J. Appl. Phys.*, **37**, P. 1594–1601 (1966).
[2] E.V. Vashchenko, I.A. Gladskikh, et al. Conductivity and photoconductivity of granular silver films on sapphire substrates. *J. Optical Technology*, **80** (5), P. 3–10 (2013).
[3] C.A. Neugebauer, M.N Web. Electrical conduction mechanism in ultrathin, evaporated metal films. *J. of Appl. Phys.*, **33**, P. 74–82 (1962).
[4] R.M. Hill. Electrical conduction in discontinuous metal films. *Contemp. Phys.*, **10** (3), P. 221–240 (1969).
[5] N.J. Simrick, J.A. Kilner, A. Atkinson. Thermal stability of silver thin films on zirconia substrates. *Thin Solid Films*, **520**, P. 2855–2867 (2012).
[6] J. Dufourcq, P. Mur, et al. Metallic nano-crystals for flash memories. *Materials Science and Engineering C*, **27**, P. 1496–1499 (2007).
[7] A. Kiesow, J.E. Morris, C. Radehaus, A. Heilmann. Switching behavior of plasma polymer films containing silver nanoparticles. *J. Appl. Phys.*, **94** (10), P. 6988–6990 (2003).
[8] O. Baker, B. Shedd, et al. Size Control of Gold Nanoparticles Grown on Polyaniline Nanofibers for Bistable Memory Devices. *ACS NANO*, **5** (5), P. 3469–3474 (2011).
[9] K. Fujiwara, T. Nemoto, et al. Resistance Switching and Formation of a Conductive Bridge in Metal/Binary Oxide/Metal Structure for Memory Devices. *Jpn. J. Appl. Phys.*, **47** (8), P. 6266–6271 (2008).

NANOSYSTEMS: PHYSICS, CHEMISTRY, MATHEMATICS, 2013, 4 (4), P. 529–537

EFIMOV'S EFFECT FOR PARTIAL INTEGRAL OPERATORS OF FREDHOLM TYPE

Yu. Kh. Eshkabilov, R. R. Kucharov

Department of Mechanics and Mathematics, National University of Uzbekistan, Tashkent, Uzbekistan

yusup62@mail.ru, ramz3364647@yahoo.com

PACS 02.30.Tb

We study the existence of an infinite number of eigenvalues (the existence of Efimov's effect) for a self-adjoint partial integral operators. We prove a theorem on the necessary and sufficient conditions for the existence of Efimov's effect for the Fredholm type partial integral operators.

Keywords: essential spectrum, discrete spectrum, Efimov's effect, partial integral operator..

1. Introduction

Linear equations and operators involving partial integrals appear in elasticity theory [1–3], continuum mechanics [2, 4–6], aerodynamics [7] and in PDE theory [8, 9]. Self-adjoint partial integral operators arise in the theory of Schrodinger operators [10–13]. Spectral properties of a discrete Schrodinger operator H are tightly connected (see [13,14]) with those of the partial integral operators which participate in the presentation of operator H.

Let Ω_1 and Ω_2 be closed boundary subsets in $\mathbb{R}^{\nu_1}$ and $\mathbb{R}^{\nu_2}$, respectively. The partial integral operator (PIO) of Fredholm type in the space $L_p(\Omega_1 \times \Omega_2)$, $p \geq 1$ is an operator of the following form [15]

$$T = T_0 + T_1 + T_2 + K, \tag{1}$$

where operators T_0, T_1, T_2 and K are defined by the following formulas:

$$T_0 f(x,y) = k_0(x,y) f(x,y),$$
$$T_1 f(x,y) = \int_{\Omega_1} k_1(x,s,y) f(s,y) ds,$$
$$T_2 f(x,y) = \int_{\Omega_2} k_2(x,t,y) f(x,t) dt,$$
$$K f(x,y) = \int_{\Omega_1} \int_{\Omega_2} k(x,y;s,t) f(s,t) ds dt.$$

Here k_0, k_1, k_2 and k are given measurable functions on $\Omega_1 \times \Omega_2$, $\Omega_1^2 \times \Omega_2^2$, $\Omega_1 \times \Omega_2$ and $(\Omega_1 \times \Omega_2)^2$, respectively. All integrals have to be understood in the Lebesgue sense.

In 1975, Likhtarnikov and Vitova [16] studied spectral properties of partial integral operators. In [16], the following restrictions were imposed: $k_1(x,s) \in L_2(\Omega_1 \times \Omega_1)$, $k_2(y,t) \in L_2(\Omega_2 \times \Omega_2)$ and $T_0 = K = 0$. In [17] spectral properties of PIO with positive kernels were studied (under the restriction $T_0 = K = 0$). Kalitvin and Zabrejko [18] studied the spectral properties of PIO in the space $L_p, p \geq 1$. Kernels of PIO in all mentioned articles are functions of two variables and $T_0 = 0$. In [19], a full spectral description of self-adjoint

PIO in the space $C([a,b]\times[c,d])$ with continuous kernels was given. Self-adjoint PIO with $T_0 \neq 0$ were first studied in [10], where theorem about essential spectrum was proved. The finiteness and infiniteness of a discrete spectrum of self-adjoint PIO arising in the theory of Schrodinger operators was investigated in [11–13].

In [20], PIOs in some functional spaces were investigated and a number of applications were considered. Some important spectral properties of PIO in the space L_2 are still open. The present paper is dedicated to the mentioned problem.

We study the existence of an infinite number of eigenvalues (the existence Efimov's effect) for a self-adjoint partial integral operators.

2. The notations and necessary information

Let A be a linear self-adjoint operator in the Hilbert space $\mathcal{H}$. Resolvent set, spectrum, essential spectrum and discrete spectrum of the operator A are denoted by ρ, σ, σ_{ess} and σ_{disc}, respectively (see [21]).

We define the numbers

$$\mathcal{E}_{\min}(A) = \inf\{\lambda : \lambda \in \sigma_{ess}(A)\},$$

$$\mathcal{E}_{\max}(A) = \sup\{\lambda : \lambda \in \sigma_{ess}(A)\}.$$

We call the number $\mathcal{E}_{\min}(A)$ ($\mathcal{E}_{\max}(A)$) the lower (the higher) boundary of the essential spectrum of A.

Let $\Omega_1 = [a,b]^{\nu_1}$, $\Omega_2 = [c,d]^{\nu_2}$ and k_0, k_1, k_2 are continuous functions on $\Omega_1\times\Omega_2$, $\Omega_1^2\times\Omega_2$, $\Omega_1\times\Omega_2^2$ respectively, k_0 is real function, $k_1(x,s,y) = \overline{k_1(s,x,y)}$, $k_2(x,t,y) = \overline{k_2(x,y,t)}$. We define the linear self-adjoint bounded operator H in the Hilbert space $L_2(\Omega_1\times\Omega_2)$ by rule

$$H = T_0 - (T_1 + T_2). \tag{2}$$

We set

$$T = T_1 + T_2.$$

For the essential spectrum of the operators H and T the equalities

$$\sigma_{ess}(T) = \sigma(T_1)\cup\sigma(T_2),$$

$$\sigma_{ess}(H) = \sigma(T_0 - T_1)\cup\sigma(T_0 - T_2) \tag{3}$$

are held (see [22],[10]).

Let $k_1(x,s,y) = \alpha = const > 0, k_2(x,t,y) = \beta = const > 0$ in the model (2). Then at the $\mathcal{E}_{\min}(H) = 0$ the Efimov's effect (the existence infinite numbers of eigenvalues below the lower boundary $\mathcal{E}_{\min}(H)$ of the essential spectrum) in the model (2) was demonstrated by S. Albeverio, S.N.Lakaev, Z.I. Muminov [11] and Rasulov T.Kh. [12].

We study the existence Efimov's effect in the model (2) in the case $\mathcal{E}_{\min}(H) \neq 0$. Consider this problem for the function $k_0(x,y)$ of the form $k_0(x,y) = u(x)u(y)$ and $k_0(x,y) = u(x) + u(y)$.

Let $u(x)$ and $v(y)$ be a continuous nonnegative function on Ω_1 and Ω_2, respectively and suppose $k_1(x,s,y) = k_1(x,s)$, $k_2(x,t,y) = k_2(y,t)$. We define the self-adjoint compact integral operators $Q_1 : L_2(\Omega_1) \to L_2(\Omega_1)$ and $Q_2 : L_2(\Omega_2) \to L_2(\Omega_2)$ by the following equalities

$$Q_1\varphi(x)=\int_{\Omega_1}k_1(x,s)\varphi(s)ds,\quad Q_2\psi(y)=\int_{\Omega_2}k_2(y,t)\psi(t)dt$$

and suppose that $Q_1\geq\theta,\ \ Q_2\geq\theta$.

We define by V_1 and V_2 multiplication on the space $L_2(\Omega_1)$ and $L_2(\Omega_2)$ are acting by the following formulas

$$V_1\varphi(x)=u(x)\varphi(x),\quad V_2\psi(y)=v(y)\psi(y).$$

We consider the operators $H_k, k=1,2$ in the Friedrichs model:

$$H_1=V_1-Q_1, \tag{4}$$

$$H_2=V_2-Q_2. \tag{5}$$

3. Efimov's effect for PIO

Let $u(x)\geq 0,\ \ x\in\Omega_1, v(y)\geq 0,\ \ y\in\Omega_2$ and $u^{-1}(\{0\})\neq\emptyset,\ \ v^{-1}(\{0\})\neq\emptyset$.

Theorem 3.1. *Let $k_0(x,y)=u(x)+v(y)$, $u(x)\geq 0$, $v(y)\geq 0$ and $Q_1\geq\theta,\ \ Q_2\geq\theta$.*
(a) the $\sigma_{ess}(H)=\sigma(H_0)$ iff the $\sigma_{disc}(H)=\emptyset$;
(b) if $\sigma_{disc}(H)\neq\emptyset$, then $\sigma_{disc}(H_1)\neq\emptyset$ and $\sigma_{disc}(H_2)\neq\emptyset$;
(c) if $\sigma_{disc}(H)\neq\emptyset$, then $\mathcal{E}_{\min}(H)=\inf\{\lambda:\lambda\in\sigma_{disc}(H_1)\cup\sigma_{disc}(H_2)\}$;
(d) Efimov's effect exists in the model (2) iff Efimov's effect exists in Friedrich's model (4) and $\sigma_{disc}(H_2)\neq\emptyset$ or Efimov's effect exists in Friedrich's model (5) and $\sigma_{disc}(H_1)\neq\emptyset$.

Proof. We define the operator $W=H_1\otimes E+E\otimes H_2$ on the space $L_2(\Omega_1)\otimes L_2(\Omega_2)$. For the spectrum of the operator W we have [18]

$$\sigma(W)=\sigma(H_1)+\sigma(H_2).$$

But, the operators W and H is unitary equivalent (see [10]), i.e. $W\cong H$. Consequently, that

$$\sigma(H)=\sigma(H_1)+\sigma(H_2). \tag{6}$$

Also, if we define the operators A_1 and A_2 by

$$A_1=H_1\otimes E+E\otimes V_2,\quad A_2=V_1\otimes E+E\otimes H_2$$

we see $A_1\cong T_0-T_1,\quad A_2\cong T_0-T_2$. Thus we have

$$\sigma(T_0-T_1)=\sigma(H_1)+\sigma(V_2),$$
$$\sigma(T_0-T_2)=\sigma(V_1)+\sigma(H_2).$$

Then, by the equality (6) for the essential spectrum of the operator H we obtain

$$\sigma_{ess}(H)=(\sigma(H_1)+\sigma(V_2))\cup(\sigma(V_1)+\sigma(H_2)). \tag{7}$$

On the other hand

$$\sigma_{ess}(H_k)=\sigma(V_k),\ \ k=1,2. \tag{8}$$

Now, from the equalities (6), (7) and (8) it follows proof of theorem 1. □

Corollary 3.1. *Let be $k_0(x,y)=u(x)+v(y)$ and $k_1(x,s,y)=k_1(x,s)$, $k_2(x,t,y)=k_2(y,t)$.*

a) for the existence of Efimov's effect in model (2) *it is necessary, that* $\dim(Ran(Q_1)) = \infty$ *or* $\dim(Ran(Q_2)) = \infty$*;*

b) if $\dim(Ran(Q_1)) < \infty$ *and* $\dim(Ran(Q_2)) < \infty$*, then Efimov's effect is absent in model* (2).

Suppose, that $k_0(x,y) \geq 0, 0 \in Ran(k_0)$ and $T_k \geq \theta, k = 1,2$. Let $N_0(H)$ be the number of all eigenvalues (with account multiplicity) below the lower boundary of the essential spectrum in model (2), i.e.

$$N_0(H) = \sum_{\lambda \in \sigma_{disc}(H),\ \lambda < \mathcal{E}_{\min}(H)} n_H(\lambda),$$

where $n_H(\lambda)$ – the multiplicity of the eigenvalue λ of the operator H and $N(T)$ is the number of all eigenvalues(with account multiplicity) of the discrete spectrum of operator T, i.e.

$$N(T) = \sum_{\lambda \in \sigma_{disc}(T)} n_T(\lambda).$$

Theorem 3.2. *Let the relation*

$$T_0 \geq (\mathcal{E}_{\min}(H) + \mathcal{E}_{\max}(T)) \cdot E$$

is hold, where E *- identical operator. Then*

$$N_0(H) \leq N(T).$$

Proof. We have

$$\sigma_{ess}(\mathcal{E}_{\max}(T) \cdot E - T) = \{\xi :\ \ \xi = \mathcal{E}_{\max}(T) - \lambda,\ \ \lambda \in \sigma_{ess}(T)\}.$$

Then

$$\sigma_{ess}(\mathcal{E}_{\max}(T) \cdot E - T) \subset [0, \infty)$$

and

$$0 \in \sigma_{ess}(\mathcal{E}_{\max}(T) - T),\ \ N(\mathcal{E}_{\max}(T) \cdot E - T) = N(T).$$

Hence it follows

$$\mathcal{E}_{\min}(T) = \mathcal{E}_{\min}(\mathcal{E}_{\max}(T) \cdot E - T) = 0.$$

Let the inequality

$$T_0 \geq (\mathcal{E}_{\min}(H) + \mathcal{E}_{\max}(T)) \cdot E$$

hold. Consequently, we obtain

$$\mathcal{E}_{\max}(T) \cdot E - T \leq H - \mathcal{E}_{\min}(H) \cdot E$$

Then by lemma 2.1 [23] we have

$$\mu_k(\mathcal{E}_{\max}(T) \cdot E - T) \leq \mu_k(H - \mathcal{E}_{\min}(H) \cdot E),\ \ k \in \{1, 2,\ \ ...,\ \ N(T) + 1\}. \qquad (10)$$

where $\{\mu_k(A)\}$ – the set of all eigenvalues of operator A below the lower boundary of the essential spectrum, which was constructed by the mini-max principle. By theorem 2.1 [23] we have

$$\mu_{N(T)+1}(\mathcal{E}_{\max}(T)\cdot E - T) = 0.$$

Therefore, from inequality (10)

$$\mu_{N(T)+k}(H - \mathcal{E}_{\min}(H)\cdot E) = 0, \;\; k \in \mathbb{N}\cup\{0\},$$

i.e. the number of negative eigenvalues of operator $H - \mathcal{E}_{\min}(H)\cdot E$ taking into account multiplicity, is no more than $N(T)$. Consequently, the number of eigenvalues of the operator H below the lower boundary $\mathcal{E}_{\min}(H)$ of the essential spectrum, also will be no more than $N(T)$, i.e.

$$N_0(H) \le N(T). \qquad \square$$

Corollary 3.2. *Let be* $N(T) < \infty$. *If*

$$\mathcal{E}_{\min}(H) + \mathcal{E}_{\max}(T) \le 0,$$

then Efimov's effect is absent in model (2).

Let $u(x)$ and $v(y)$ be nonnegative continuous functions on Ω_1 and Ω_2, respectively. Suppose, that $u^{-1}(\{0\}) = \{x^{min}\}, v^{-1}(\{0\}) = \{y^{min}\}$.

Theorem 3.3. *Let be* $k_0(x,y) = u(x)v(y)$. *Then*
(a) the equality $\mathcal{E}_{\min}(H) = -\max\{\|Q_1\|, \|Q_2\|\}$ *holds;*
(b) if $\dim(Ran(Q_1)) < \infty$ *and* $\dim(Ran(Q_2)) < \infty$, *then Efimov's effect is absent in model* (2).

Proof. (a) We define the family $\{W_1(\alpha)\}_{\alpha\in\Omega_2}$ of self-adjoint operators in Fredrich's model on the space $L_2(\Omega_1)$:

$$W_1(\alpha)\varphi(x) = u(x)v(x)\varphi(x) - Q_1\varphi(x).$$

We set

$$\sigma_1 = \{\lambda \in (-\infty, 0) : \;\; \textit{for some } \alpha_0 \in \Omega_2 \;\; \textit{the number}$$
$$\lambda \;\; \textit{is eigenvalue of the operator } W_1(\alpha_0)\}.$$

Then by the theorem 6 from [24] we have

$$\sigma(T_0 - T_1) = \sigma_0 \cup \sigma_1,$$

where $\sigma_0 = \sigma(T_0)$. However,

$$((T_0 - T_1)f, f) \ge -(T_1 f, f) \ge -\|Q_1\|, \quad f \in L_2(\Omega_1\times\Omega_2),$$

because $\|T_1\| = \|Q_1\|$. Conversely, $W_1(y_{\min}) = -Q_1$, i.e. the number $-\|Q_1\|$ is eigenvalue of the operator $W_1(y_{\min})$. Consequently, $-\|Q_1\| \in \sigma_1$, i.e. $-\|Q_1\| \in \sigma(T_0 - T_1)$. Then we have $\mathcal{E}_{\min}(T_0 - T_1) = \|Q_1\|$. Analogously, for the operator $T_0 - T_2$ we obtain, that $\mathcal{E}_{\min}(T_0 - T_2) = -\|Q_2\|$. Finally, from (3) follows, that $\mathcal{E}_{\min}(H) = -\max\{\|Q_1\|, \|Q_2\|\}$.

(b) By statement (a) of theorem 3.3 we have $\mathcal{E}_{\min}(H) = -\max\{\|Q_1\|, \|Q_2\|\}$. However, $\mathcal{E}_{\max}(T) = \max\{\|Q_1\|, \|Q_2\|\}$ (see [25]) Consequently, the condition of theorem 2 is satisfied. Still, by theorem 3.1 from [25] (also see [18]) we have

$$N(T) = \sum_{\substack{p+q\notin\sigma_{ess}(T),\\ p\in\sigma_{disc}(Q_1),\\ q\in\sigma_{disc}(Q_2)}} n_{Q_1}(p)\cdot n_{Q_2}(q),$$

where $\sigma_{ess}(T) = \sigma(Q_1)\cup\sigma(Q_2)$. Then, from the inequality $\dim(Ran(Q_1)) < \infty$ and $\dim(Ran(Q_2)) < \infty$, we obtain $N(T) < \infty$. Consequently, by theorem 3.2 Efimov's effect is absint in model (2). □

Remark 3.1. *The author's previous work [14] showed the existence of Efimov's effect in the case* $\dim(Ran(Q_1)) = 1$ *and* $\dim(Ran(Q_2)) = \infty$ *in the model* (2) *for the* $\mathcal{E}_{\min}(H) \neq 0$.

4. The examples

Example 4.1. On $\Omega = [0,1]^\nu$, we consider the functions

$$u(x) = {x_1}^{\alpha_1}\cdot ... \cdot {x_\nu}^{\alpha_\nu},\ \ v(y) = {y_1}^{\beta_1}\cdot ... \cdot {y_\nu}^{\beta_\nu},$$

where $\alpha_k \geq 0, \beta_j \geq 0, k, j \in \{1, .., \nu\}$.
In the space $L_2(\Omega^2)$, we define the operators

$$T_0 f(x,y) = (u(x)+v(y))f(x,y),$$
$$T_1 f(x,y) = \int_\Omega exp(|x-s|)f(s,y)ds,$$
$$T_2 f(x,y) = \int_\Omega exp(|y-t|)f(x,t)dt,$$

where

$$|x| = \sqrt{{x_1}^2 + ... + {x_\nu}^2}.$$

If $\alpha_1 + ... + \alpha_\nu > 2\nu$ and $\beta_1 + ... + \beta_\nu > 2\nu$, then Efimov's effect exist for operator (2).

We define subsets $A_n (n \in \mathbb{N})$ and $B_n (n \in \mathbb{N})$ by the following way

$$A_n = \{t \in \Omega :\ \ 0 \leq t_i < \frac{1}{n},\ \ i = 1, ..., \nu\},\ \ n \in \mathbb{N},$$

$$B_n = \{t \in \Omega :\ \ 0 \leq t_i < \frac{1}{n+1},\ \ i = 1, ..., \nu\},\ \ n \in \mathbb{N}.$$

We have $B_n \subset A_n,\ \ n \in \mathbb{N}$. We set

$$G_n = A_n \backslash B_n,\ \ n \in \mathbb{N}.$$

Then $G_n \cap G_m = \emptyset$ at $n \neq m$ and $G_n \subset O_{\frac{1}{n}}(\theta) \cap \Omega$, where $O_r(\theta)$ – the open ball with radius r in center $\theta \in \mathbb{R}^\nu$($\theta$ – the zero element of the space $\mathbb{R}^\nu$). For the Lebesque measure $\mu(G_n)$ of the set G_n we obtain

$$\mu(G_n) = \mu(A_n) - \mu(B_n) = \frac{1}{n^\nu} - \frac{1}{(n+1)^\nu} > \frac{1}{n^\nu} - \frac{1}{n^\nu + 1} = \frac{1}{n^\nu(n^\nu+1)} > \frac{1}{2n^{2\nu}}$$

for all $n \in \mathbb{N},\ n \geq 2$. On the other hand

$$\sup_{t \in G_n} u(t) = \left(\frac{1}{n}\right)^{\alpha_1 + \ \ldots \ + \alpha_\nu}, \ \ n \in \mathbb{N}.$$

Consequently, if $\alpha_1 + \ \ldots \ + \alpha_\nu > 2\nu$, then the following inequality

$$\sup_{t \in G_n} u(t) < \mu(G_n) \inf_{t,u \in G_n} k_1(t,u), \ \ n \in \mathbb{N} \backslash \{1\}.$$

holds, i.e. the condition of theorem 4.1 from [26] is satisfied. So, by theorem 4.1 operator $H_1 = V_1 - Q_1$ has an infinite number of negative eigenvalues.

Analogously, we show that, at the $\beta_1 + \ \ldots \ + \beta_\nu > 2\nu$ the operator $H_2 = V_2 - Q_2$ has infinite number of negative eigenvalues.

Therefore, by the theorem 3.1 $\mathcal{E}_{\min}(H) \neq 0$ and Efimov's effect exists for the PIO H.

Remark 4.1. The statement of theorem 4.1 from [26] holds for the set $\Omega = [0,1]^\nu$ for arbitrary $\nu \in \mathbb{N}$. In work [26] proof was given for the simple case $\nu = 1$. The proof of theorem 4.1 [26] for the case $\nu \geq 2$ is analogous to the case $\nu = 1$.

Example 4.2. We consider the sequence $p_0 = 0,\ \ p_1 = 1/2,\ \ p_n = p_{n-1} + 1/2^n,\ \ n \in \mathbb{N}$. We set

$$q_n = \frac{p_n - p_{n-1}}{2}, \ \ n \in \mathbb{N}.$$

On $[0,1]$, we define the function

$$u(x) = \begin{cases} 0, & \text{if } \ x \in [0, 1/2], \\ u_0(x), & \text{if } \ x \notin [0, 1/2], \end{cases}$$

where $u_0(x) = \sum\limits_{n \in \mathbb{N}} \delta_n r_n(x)$,

$$r_\kappa(x) = \begin{cases} \dfrac{p_\kappa - x}{p_\kappa - q_{\kappa+1}}, & \text{if } \ x \in [p_\kappa, q_{\kappa+1}], \\ \dfrac{p_{\kappa+1} - x}{p_{\kappa+1} - q_{\kappa+1}}, & \text{if } \ x \in [q_{\kappa+1}, p_{\kappa+1}], \\ 0, & \text{if } \ x \notin [p_\kappa, p_{\kappa+1}], \end{cases}$$

$$\delta_1 = 1, \quad \delta_n \leq \left(\frac{\sqrt{2}}{3}\right)^n, \quad n \geq 2.$$

In the space $L_2[0,1]$, we consider the sequence of orthonormal functions

$$\varphi_n(y) = 2^{(n+1)/2} \sin \xi_n(y), \ \ n \in \mathbb{N},$$

where

$$\xi_\kappa(y) = \begin{cases} \dfrac{\pi}{p_\kappa - p_{\kappa-1}}(y - p_{\kappa-1}), & \text{if } y \in [p_{\kappa-1}, p_\kappa], \\ 0, & \text{if } y \notin [p_{\kappa-1}, p_\kappa]. \end{cases}$$

We define the kernel

$$k_2(y,t) = \sum_{n\in\mathbb{N}} \left(\frac{2}{3}\right)^n \varphi_n(y)\varphi_n(t). \tag{11}$$

Series (11) converges uniformly in the square $[0,1]^2$. Hence, the integral operator Q_2, defined by its kernel $k_2(y,t)$, is self-adjoint and positive in $L_2[0,1]$. It is clear, that $\dim(Ran(Q_1)) = 1$ and $\dim(Ran(Q_2)) = \infty$.

In the space $L_2([0,1]^2)$, we consider the model

$$H = H_0 - (\gamma T_1 + T_2), \ \ \gamma \geq \frac{2}{3}, \tag{12}$$

where

$$T_0 f(x,,y) = u(x)u(y)f(x,y),$$
$$T_1 f(x,y) = \int_0^1 f(s,y)ds,$$
$$T_2 f(x,y) = \int_0^1 k_2(y,t)f(x,t)dt.$$

Then

$$\mathcal{E}_{\min}(H) = \mathcal{E}_{\min}(H_0 - (\gamma T_1 + T_2))$$

and there exists Efimov's effect for operator (12) below the lower boundary $\mathcal{E}_{\min}(H) = -\gamma$ of the essential spectrum [14].

References

[1] Kalitvin A. S. On partial integral operators in contact problems of elasticity. (in Russian) *Proc. 26 Voronezh Winter School*, **54**, (1994).

[2] Kovalenko E. V. On the approximate solution of one type of integral equations arising in elasticity type mathematical physics (in Russian). *Izv. Akad. Nauk Arm. SSR*, **34**, No 5, P. 14–26 (1981).

[3] Vekua I. N. New Methods of Solving Elliptic Equations (in Russian). Gostekhizdat, Moscow-Leningrad (1948).

[4] Aleksandrov V. M., Kovalenko E. V. On some class of integral equations arising in mixed boundary value problems of continuum mechanics. *Sov. Phys. Dokl.* **25**, No 2, P. 354–356 (1980).

[5] Aleksandrov V. M., Kovalenko E. V. On the contact interaction of bodies with coatings and abrasion. *Sov. Phys. Dokl.* **29**, No 4, P. 340–342 (1984).

[6] Aleksandrov V. M., Kovalenko E. V. Problems of Continuum Mechanics with Mixed Boundary Conditions (in Russian). Nauka, Moscow (1986).

[7] Kalitvin A. S. On some class of partial integral equations in aerodynamics, (in Russian). *Sost. Persp. Razv. Nauch. – Tekhn. Pod. Lipetsk. Obl(Lipetsk)*. P. 210–212 (1994).

[8] Goursat E. Cours d'Analyse Mathematique. Gautheir-Villars, Paris (1943).

[9] Muntz C. H. Zum dynamischen Warmeleitungs problem. *Math. Z.* **38**, P. 323–337 (1934).

[10] Eshkabilov Yu. Kh. On a discrete "three-particle" Schrödinger operator in the Hubbard model. *Theor. Math. Phys.*, **149** (2), P. 1497–1511 (2006).
[11] Albeverio S., Lakaev S. N., Muminov Z. I. On the number of eigenvalues of a model operator associated to a system of three-particles on lattices *Russ. J. Math. Phys.* **14** (4), P. 377-387 (2007).
[12] Rasulov T. Kh. Asymptotics of the discrete spectrum of a model operator assotiated with a system of three particles on a lattice. *Theor. Math.Phys.* **163** (1), P.429–437 (2010).
[13] Eshkabilov Yu. Kh., Kucharov R. R. Essential and discrete spectra of the three-particle Schrödinger operator on a lattice. *Theor. Math. Phys.,* **170** (3), P.341-353 (2012).
[14] Eshkabilov Yu. Kh. Efimov's effect for a 3-particle model discrete Schrödinger operator. *Theor. Math. Phys.*, **164** (1), P. 896-904 (2010).
[15] Appell J., Frolova E. V., Kalitvin A. S., Zabrejko P. P. Partial integral operators on $C([a,b]\times[c,d])$. *Integral Equ. Oper. Theory*, **27**, P. 125–140 (1997).
[16] Likhtarnikov L. M., Vitova L. Z. On the spectrum of an integral operator with partial integrals (in Russian). *Litov. Mat. Sbornik*, **15**, No 2, P.41–47 (1975).
[17] Kalitvin A. S. On the spectrum of a linear operators with partial integrals and positive kernels (in Russian). In *Pribl. Funk. Spektr. Theor.*, Leningrad, P. 43–50 (1988).
[18] Kalitvin A. S., Zabrejko P. P. On the theory of partial integral operators. *J. Integral Eq. Appl.*, **3** (3), P. 351–382 (1991).
[19] Eshkabilov Yu. Kh. Spectra of partial integral operators with a kernel of three variables. *Central Eur. J. Math.*, **6** (1), P. 149–157 (2008).
[20] Appell J., Kalitvin A. S., Zabrejko P. P. Partial Integral operators and Integro-differential Equations. (Pure and Applied Mathematics: A Series of Monographs and Textbooks, 230), Marcel Dekker, Inc., New York (2000).
[21] Reed M., Simon B. Methods of Modern Mathematical Physics, Vol.1, Functional Analysis. Acad. Press, New York (1972).
[22] Eshkabilov Yu. Kh. Essential and discrete spectre of partially integral operators. *Siberian Advances in Mathematics*, **19** (4), P. 233–244 (2009).
[23] Eshkabilov Yu. Kh. On infinity of the discrete spectrum of operators in the Friedrichs model. *Siberian Advances in Mathematics*, **22** (1), P. 1-12 (2012).
[24] Eshkabilov Yu. Kh. Perturbation spectra of multiplication with a partial integral operator (in Russian). *Acta NUUz*, No 2, P. 17–21 (2006).
[25] Eshkabilov Yu. Kh. On the spectra of the tensor sum of compact operators (in Russian). *Uzbek. Mat. J.*, No 3, P. 104–112 (2005).
[26] Eshkabilov Yu. Kh. On infinite number of negative eigenvalues of the Friedrichs model (in Russian). *Nanosystems: Physics, Chemistry, Mathematics*, **3** (6), P. 16–24 (2012).

NANOSYSTEMS: PHYSICS, CHEMISTRY, MATHEMATICS, 2013, 4 (4), P. 538–544

THE CONUCTIVITY LOW ENERGY ASYMPTOTICS FOR MONOLAYER GRAPHENE

N. E. Firsova

Institut for Problems of Mechanical Engineering RAS, St. Petersburg, Russia

nef2@mail.ru

PACS 02.73

The electron scattering problem in the monolayer graphene with short range impurities is considered. The main novel element in the suggested model is the band asymmetry of the defect potential in the 2+1-dimensional Dirac equation. This asymmetry appears naturally if the defect violates the symmetry between sublattices. Our goal in the present paper is to take into account a local band asymmetry violation arising due to the defect presence. We analyze the effect of the electron scattering on the electronic transport parameters in monolayer graphene. The explicit exact formulae obtained for S-matrix for $\delta-$shell potential allowed us to study the asymptotic behavior of such scattering data as scattering phases, transport cross section, the transport relaxation time and the conductivity for small values of the Fermi energy. The obtained results are in good agreement with experimental curves which show that the considered model is reasonable.

Keywords: monolayer graphene, conductivity, low energy asymptotics, Dirac equation.

1. Introduction

Recently, much attention has been paid to the problem of the electronic spectrum of graphene (see the review [1]). Its 2D-structure and the presence of the cone points in the electronic spectrum make actual a comprehensive study of the external field effect on the spectrum and other characteristics of the electronic states described by the Dirac equation in the 2+1 space-time. We consider in the present paper the transport phenomena in the 2+1 Dirac equation model of the monolayer graphene due to the short-range perturbation. We do not take into account the inter-valley transitions. Particular attention to this case stems from the effectiveness of short-range scatterers in contrast to the long-range ones: an effect of the latter is suppressed by the Klein paradox [2]. Short-range potential impurities in graphene were considered in papers [3–6]. In [6], for instance, electrons were assumed to be confined in a quantum dot where the dot was represented by a $\delta^{(2)}(\vec{r})$-potential well. Artificially representing the quantum dot by such a strongly singular potential leads to divergences in the Lippmann-Schwinger equation. To overcome the problem in [7] the δ-shell model was suggested which removed the singularity. The Dirac equation for the δ-shell potential is free of such divergences. In [7] a new model of the short-range impurities in graphene was considered where the shell delta function potential form was suggested taking into account for the first time the obvious fact that the Kohn-Luttinger matrix elements of the short-range perturbations calculated on the upper and lower band wave functions are not equal in a general case. This means that the perturbation must be generically described by a Hermitian matrix. In [7] the diagonal matrix case corresponding to a presence of the chemical potential and the mass perturbation was studied taking firstly into account a local band symmetry violation arising due to the defect presence. In [7] for the model the characteristic equation for eigenvalues and resonances was obtained describing their dependence on the perturbation parameters. In [8] in the framework of the

model suggested in [7] the electron scattering was studied and the exact analytical formula for S-matrix was found.

In the present paper we analyze the effect of the electron scattering studied in [8] on the electronic transport in the monolayer graphene. We compare our theoretical results with the available experimental data.

2. The main results

The Dirac equation describing electronic states in monolayer graphene in the framework of the model described above (see [6, 7]) reads:

$$\left[-i\hbar v_F \sum_{\mu=1}^{2} \gamma_\mu \partial_\mu - \gamma_0 \left(m + \delta m\right) v_F^2\right] \psi = \left(E - V\right) \psi, \tag{1}$$

where v_F is the Fermi velocity of the band electron, γ_μ are the Dirac matrices,

$$\gamma_0 = \sigma_3, \quad \gamma_1 = \sigma_1, \quad \gamma_2 = i\sigma_2,$$

σ_j are the Pauli matrices, $2m_d v_F^2 = E_g$ is the electronic bandgap, and $\psi\left(\overrightarrow{r}\right)$ is the two-component spinor. The spinor structure takes into account the two-sublattice structure of the graphene.

We consider firstly the gapless case $m = 0$. Then we have

$$\left[-i\hbar v_F \sum_{\mu=1}^{2} \gamma_\mu \partial_\mu - \gamma_0 \delta m \; v_F^2\right] \psi = \left(E - V\right) \psi. \tag{2}$$

To treat this equation mathematically, we make (2) dimensionless dividing it by $\hbar v_F k_F$. We get

$$\left[-i \sum_{\mu=1}^{2} \gamma_\mu \partial_\mu - \gamma_0 \delta \tilde{m}\right] \psi = \left(\tilde{E} - \tilde{V}\right) \psi. \tag{3}$$

Here $\delta\tilde{m} = \delta m v_F (\hbar k_F)^{-1}$, $\tilde{E} = E(\hbar v_F k_F)^{-1}$, $\tilde{V} = V(\hbar v_F k_F)^{-1}$. $\tilde{V}\left(\overrightarrow{\tilde{r}}\right)$ is the local perturbation of the chemical potential. A local mass (gap) perturbation, $\delta\tilde{m}$, related to the local sublattices symmetry violation, can be induced for instance by defects in the graphene film or in the substrate (see [8]). We consider here the shell delta function model of the perturbation

$$\delta\tilde{m}\left(\tilde{r}\right) = -b\delta\left(\tilde{r} - \tilde{r}_0\right), \quad \tilde{V}\left(\tilde{r}\right) = -a\delta\left(\tilde{r} - \tilde{r}_0\right), \tag{4}$$

where $\tilde{r} = rk_F$ and $\tilde{r}_0 = r_0 k_F$ are respectively the polar coordinate radius and the perturbation radius. The finite radius r_0 plays a role of the regulator and is necessary in order to exclude deep states of the atomic energy scale. The finite perturbation radius r_0 leads to the quasi-momentum space form-factor proportional to the Bessel function that justifies our neglect of transitions between the Brillouin band points K and K', [9] .The perturbation matrix elements

$$\mathrm{diag}\left(\tilde{V}_1, \tilde{V}_2\right) \delta\left(\tilde{r} - \tilde{r}_0\right),$$

are related to the a, b parameters as follows:

$$-\tilde{V}_1 = a + b, \quad -\tilde{V}_2 = a - b.$$

Solving the Dirac equation (3) in the regions $0 \leq \tilde{r} < \tilde{r}_0$, $\tilde{r}_0 < \tilde{r} < \infty$ and matching these solutions at the circumference of the circle of the radius $\tilde{r} = \tilde{r}_0$, the characteristic equation was obtained for eigenvalues and resonances, [7]. Calculating the ratio of the outgoing and

ingoing waves, the formulae for S-matrix components were found in the angular momentum representation, [8]:

$$S_j(kr_0) = -\frac{F_j^{(2)}(k\tilde{r}_0)}{F_j^{(1)}(k\tilde{r}_0)}, \quad j = \pm\frac{1}{2}, \pm\frac{3}{2}, \ldots, \quad k = E, \tag{5}$$

where $F_j^{(\alpha)}(k\tilde{r}_0)$, $\alpha = 1, 2$, is given by the formula:

$$F_j^{(\alpha)}(k\tilde{r}_0) = \left[I_{j-1/2}(k\tilde{r}_0) H_{j+1/2}^{(\alpha-)}(k\tilde{r}_0) - I_{j+1/2}(k\tilde{r}_0) H_{j-1/2}^{(\alpha)}(k\tilde{r}_0)\right]$$
$$T(a,b)\left[(a-b) I_{j+1/2}(k\tilde{r}_0) H_{j+1/2}^{(\alpha)}(k\tilde{r}_0) + (a+b) I_{j-1/2}(k\tilde{r}_0) H_{j-1/2}^{(\alpha)}(k\tilde{r}_0)\right],$$
$$\alpha = 1, 2, \quad j = \pm\frac{1}{2}, \pm\frac{3}{2}, \ldots. \tag{6}$$

Here,

$$T(a,b) = \begin{cases} \tan\sqrt{a^2-b^2}\,/\sqrt{a^2-b^2} & \text{if } a^2 > b^2, \\ \tanh\sqrt{b^2-a^2}\,/\sqrt{b^2-a^2} & \text{if } b^2 > a^2, \end{cases} \tag{7}$$

where we choose the principal value of the roots. Since for Hankel functions we have for real variables $\overline{H_n^{(2)}(x)} = H_n^{(1)}(x)$ the scattering matrix (5), (6) is unitary on the continuum spectrum $\Im\tilde{E} = 0$. Using the relation [11],

$$I_{j-1/2}(k\tilde{r}_0) N_{j+1/2}(k\tilde{r}_0) - I_{j+1/2}(k\tilde{r}_0) N_{j-1/2}(k\tilde{r}_0) = -\frac{2}{\pi(k\tilde{r}_0)}, \tag{8}$$

we can rewrite (6) in the form

$$F_j^{(\alpha)}(k\tilde{r}_0) =$$
$$-(-1)^\alpha \frac{2i}{\pi(k\tilde{r}_0)} - T(a,b)\left[(a-b) I_{j+1/2}(k\tilde{r}_0) H_{j+1/2}^{(\alpha)}(k\tilde{r}_0) + (a+b) I(k\tilde{r}_0)_{j-1/2} H_{j-1/2}^{(\alpha)}(k\tilde{r}_0)\right],$$
$$\alpha = 1, 2, \quad j = \pm\frac{1}{2}, \pm\frac{3}{2}, \ldots. \tag{9}$$

So the poles of the scattering matrix (5), i.e. the eigenvalues and resonances, are determined as solutions of the characteristic equation

$$F_j^{(1)}(k\tilde{r}_0) = 0, \quad j = \pm\frac{1}{2}, \pm\frac{3}{2}, \ldots \tag{10}$$

or

$$T(a,b)\left[(a-b) I_{j+1/2}(k\tilde{r}_0) H_{j+1/2}^{(1)}(k\tilde{r}_0) + (a+b) I_{j-1/2}(k\tilde{r}_0) H_{j-1/2}^{(1)}(k\tilde{r}_0)\right]$$
$$= \frac{2i}{\pi(k\tilde{r}_0)}, \quad j = \pm\frac{1}{2}, \pm\frac{3}{2}, \ldots. \tag{11}$$

Using the relations $H_n^{(1)}(x) = I_n(x) + iN_n(x)$, $H_n^{(2)}(x) = I_n(x) - iN_n(x)$, we can write S-matrix (5) as follows:

$$S_j(k\tilde{r}_0) = -\frac{A_j(k\tilde{r}_0) - iB_j(k\tilde{r}_0)}{A_j(k\tilde{r}_0) + iB_j(k\tilde{r}_0)} = \frac{B_j(k\tilde{r}_0) + iA_j(k\tilde{r}_0)}{B_j(k\tilde{r}_0) - iA_j(k\tilde{r}_0)}, \quad j = \pm\frac{1}{2}, \pm\frac{3}{2}, \ldots. \tag{12}$$

Therefore, it can be presented in the standard form:

$$S_j\left(k\tilde{r}_0\right)=\exp\left(2i\delta_j\left(k\tilde{r}_0\right)\right),\quad j=\pm\frac{1}{2},\pm\frac{3}{2},\ldots, \tag{13}$$

where for the scattering phases we have

$$\delta_j\left(k\tilde{r}_0\right)=\tan^{-1}\frac{A_j\left(k\tilde{r}_0\right)}{B_j\left(k\tilde{r}_0\right)},\quad j=\pm\frac{1}{2},\pm\frac{3}{2},\ldots. \tag{14}$$

The functions $A_j\left(k\tilde{r}_0\right)$, $B_j\left(k\tilde{r}_0\right)$, $j=\pm\frac{1}{2},\pm\frac{3}{2},\ldots$ are determined (see (9)) as follows:

$$A_j\left(k\tilde{r}_0\right)=-T\left(a,b\right)\left[\left(a-b\right)I^2_{j+1/2}\left(k\tilde{r}_0\right)+\left(a+b\right)I^2_{j-1/2}\left(k\tilde{r}_0\right)\right], \tag{15}$$

$$B_j\left(k\tilde{r}_0\right)=\frac{2}{\pi\left(k\tilde{r}_0\right)}-T\left(a,b\right)\left[\left(a-b\right)I_{j+1/2}\left(k\tilde{r}_0\right)N_{j+1/2}\left(k\tilde{r}_0\right)+\left(a+b\right)I_{j-1/2}\left(k\tilde{r}_0\right)N_{j-1/2}\left(k\tilde{r}_0\right)\right],$$
$$j=\pm\frac{1}{2},\pm\frac{3}{2},\ldots. \tag{16}$$

Lemma1. Scattering phases $\delta_j\left(k\tilde{r}_0\right)$, $j=\pm\frac{1}{2},\pm\frac{3}{2},\ldots$, of the $S_j\left(k\tilde{r}_0\right)$-matrix of the Dirac equation (3) near the Dirac point $k=0$, is for low energies (small momentum) i.e. for $\left(k\tilde{r}_0\right)\to 0$ have asymptotics uniformly on a set of j

$$\delta_{\pm j}\left(k\tilde{r}_0\right)=-\frac{\pi T\left(a,b\right)\left(a\pm b\right)}{\left[\left(j-\frac{1}{2}\right)!\right]^2}\left(\frac{k\tilde{r}_0}{2}\right)^{2j}\left[1+o(1)\right],\quad k\tilde{r}_0\to 0,\quad j=\frac{1}{2},\frac{3}{2}\ldots. \tag{17}$$

Proof. From (14)–(16) we see

$$\tan\delta_j\left(k\tilde{r}_0\right)=\frac{\pi\left(k\tilde{r}_0\right)}{2}T\left(a,b\right)\left[\left(a-b\right)I^2_{j+1/2}\left(k\tilde{r}_0\right)+\left(a+b\right)I^2_{j-1/2}\left(k\tilde{r}_0\right)\right]$$
$$\times\left[1+\frac{\pi k\tilde{r}_0}{2}T\left(a,b\right)\left[\left(a-b\right)I_{j+1/2}\left(k\tilde{r}_0\right)N_{j+1/2}\left(k\tilde{r}_0\right)+\left(a+b\right)I_{j-1/2}\left(k\tilde{r}_0\right)N_{j-1/2}\left(k\tilde{r}_0\right)\right]\right]^{-1},$$
$$j=\pm\frac{1}{2},\pm\frac{3}{2},\ldots. \tag{18}$$

Asymptotic behavior of the scattering phases $\delta_j\left(k\tilde{r}_0\right)$ at $k\tilde{r}_0\to 0$ can be obtained expanding the cylinder functions for small arguments (see [11])

$$I_n\left(x\right)\sim\left(1/n!\right)\left(x/2\right)^n,\quad n=0,1,2\ldots, \tag{19}$$

$$N_n\left(x\right)\sim\begin{cases}-\left(\Gamma\left(n\right)/\pi\right)\left(2/x\right)^n & \text{for } n>0,\\ \left(2/\pi\right)\log\left(\gamma_{\in}x/2\right) & \text{for } n=0,\end{cases} \tag{20}$$

where $\gamma_E\approx 0,577$ is the Euler –Mascerone constant and $\Gamma\left(n\right)$is the $gamma$-function. From (18)–(20), we obtain asymptotic uniform on the set of j

$$\tan\delta_{\pm j}\left(k\tilde{r}_0\right)=\frac{\pi T\left(a,b\right)\left(a\pm b\right)}{\left[\left(j-\frac{1}{2}\right)!\right]^2}\left(\frac{k\tilde{r}_0}{2}\right)^{2j}\left[1+o(1)\right],\quad k\tilde{r}_0\to 0,\quad j=\frac{1}{2},\frac{3}{2}\ldots. \tag{21}$$

Expanding the function $\tan^{-1}(\tan\delta_{\pm j}(k\tilde{r}_0)\,)$, $k\tilde{r}_0\to 0$, we find

$$\delta_{\pm j}(k\tilde{r}_0)=\frac{\pi T(a,b)(a\pm b)}{\left[\left(j-\frac{1}{2}\right)!\right]^2}\left(\frac{k\tilde{r}_0}{2}\right)^{2j}[1+o(1)]\left[1+O\left(\left(\frac{(k\tilde{r}_0)}{2}\right)^{4j}\right)\right],$$
$$k\tilde{r}_0\to 0,\quad j=\frac{1}{2},\frac{3}{2},\dots.$$

Hence we come to (17).■

Let us now define $\delta_{\pm j}(k_Fr_0)=\delta_{\pm j}(k\tilde{r}_0)$, $S_j(k_Fr_0)=S_j(k\tilde{r}_0)$, $j=\pm\frac{1}{2},\pm\frac{3}{2},\dots$. Then the transport cross section can be written in terms of the scattering phases

$$\sum\nolimits_{tr}(k_F,r_0)=\frac{2}{k_F}\ \left(\sum\nolimits_1\right)_{tr}(k_Fr_0)\,, \tag{22}$$

where

$$\left(\sum\nolimits_1\right)_{tr}(k_Fr_0)=\left(\sum\nolimits_1\right)_{tr}(k\tilde{r}_0)=\sum_{j=\pm\frac{1}{2},\pm\frac{3}{2},\dots}[\sin(\delta_{j+1}(k\tilde{r}_0)-\delta_j(k\tilde{r}_0))]^2. \tag{23}$$

The transport relaxation time τ_{tr} can be calculated using the following relation:

$$1/\tau_{tr}\ (k_Fr_0)=N_iv_F\sum\nolimits_{tr}(k_F,r_0)\,. \tag{24}$$

The Boltzmannian conductivity is determined by the formula

$$\sigma\left(E_F,r_0\right)=\frac{e^2}{h}\left(E_F\tau_{tr}(k_F,r_0)/\hbar\right). \tag{25}$$

Theorem 1. We have for the transport cross section of the problem (2)

$$\sum\nolimits_{tr}(k_F,r_0)=\pi^2T(a,b)^2\left(a^2+3b^2\right)k_Fr_0^2\ [1+o(1)]\,,\quad k_Fr_0\ll 1. \tag{26}$$

The conductivity for problem (2) for low energies has asymptotics

$$\sigma=\sigma_0[1+o(1)]\,,\quad k_Fr_0\ll 1, \tag{27}$$

where

$$\sigma_0=\frac{e^2}{h}\left[\pi^2T(a,b)^2\left(a^2+3b^2\right)N_ir_0^2\ \right]^{-1}. \tag{28}$$

Proof. From Lemma 1, we see that $\delta_{\pm j}(k\tilde{r}_0)\to 0$, when $(k\tilde{r}_0)\to 0$, $j=\frac{1}{2},\frac{3}{2}\dots$. It means that expanding, we obtain

$$\sin(\delta_{j+1}(k\tilde{r}_0)-\delta_j(k\tilde{r}_0))=\ (\delta_{j+1}(k\tilde{r}_0)-\delta_j(k\tilde{r}_0))\left(1+O\left(\delta_{j+1}(k\tilde{r}_0)-\delta_j(k\tilde{r}_0)\right)^2\right),$$
$$k\tilde{r}_0\to 0,\quad j=\pm\frac{1}{2},\pm\frac{3}{2},\dots$$

or

$$\sin(\delta_{j+1}(k\tilde{r}_0)-\delta_j(k\tilde{r}_0))=\ (\delta_{j+1}(k\tilde{r}_0)-\delta_j(k\tilde{r}_0))(1+o(1)),\quad k\tilde{r}_0\to 0,\quad j=\pm\frac{1}{2},\pm\frac{3}{2},\dots.$$

So we find that (see (23))

$$\left(\sum\nolimits_1\right)_{tr}(k\tilde{r}_0)=\left(\sum\nolimits_2\right)_{tr}(k\tilde{r}_0)\left[1+o(1)\right],\quad k\tilde{r}_0\to 0,\quad j=\pm\frac{1}{2},\pm\frac{3}{2},\ldots, \tag{29}$$

where

$$\left(\sum\nolimits_2\right)_{tr}(k\tilde{r}_0)=\sum_{j=\pm\frac{1}{2},\pm\frac{3}{2},\ldots}\left(\delta_{j+1}(k\tilde{r}_0)-\delta_j(k\tilde{r}_0)\right)^2. \tag{30}$$

Transforming (30), we get

$$\left(\sum\nolimits_2\right)_{tr}=2\left\{\delta_{1/2}^2+\delta_{-1/2}^2-\delta_{1/2}\delta_{-1/2}-\sum_{j=\frac{1}{2},\ \frac{3}{2}\ldots}\left[\left(\delta_j\delta_{j+1}+\delta_{-j}\delta_{-j-1}\right)-\left(\delta_{j+1}^2+\delta_{-j-1}^2\right)\right]\right\}.$$

Using asymptotics from Lemma 1, we find

$$\left(\sum\nolimits_2\right)_{tr}=2\pi^2T(a,b)^2\left(a^2+3b^2\right)\left(\frac{(k\tilde{r}_0)}{2}\right)^2\left[1+o\left(1\right)\right],\quad k\tilde{r}_0\to 0.$$

Substituting this equation into (29), we have

$$\left(\sum\nolimits_1\right)_{tr}(k\tilde{r}_0)=\pi^2T\left(a,b\right)^2\left(a^2+3b^2\right)\frac{(k\tilde{r}_0)^2}{2}\left[1+o\left(1\right)\right],\quad k\tilde{r}_0\to 0. \tag{31}$$

Hence using (22) and (23), we obtain (26).
From (24)–(26) we see

$$E_F\tau_{tr}/\hbar=\left[\pi^2T\left(a,b\right)^2\left(a^2+3b^2\right)N_i{r_0}^2\right]^{-1}\left[1+o\left(1\right)\right],\quad k_Fr_0\ll 1. \tag{32}$$

And consequently (see (25))

$$\sigma=\frac{e^2}{h}\left[\pi^2T\left(a,b\right)^2\left(a^2+3b^2\right)N_i{r_0}^2\right]^{-1}\left[1+o\left(1\right)\right],\quad k_Fr_0\ll 1. \tag{33}$$

So Theorem 1 is proved.■

3. Discussion

The results found above were obtained in the framework of the model assuming the delta shell form of the potential (2)–(4). For this assumption to be reasonable, the perturbation radius r_0 should be much less than the Compton wavelength $(k_F)^{-1}$ i.e. there should be satisfied the estimate

$$k_Fr_0\ll 1. \tag{34}$$

We see that this physical condition (33) of correctness for the considered δ-shell model also guarantees the correctness of the obtained asymptotics (26), (27). From the point of view of graphene physics, assumption (33) means that the radius of the circle contains no more than one unit cell of the graphene hexagon lattice. So the principal term in our asymptotics describes the physics well enough. For instance the different pairs (a,b) of intensities satisfying the relation

$$T\left(a,b\right)^2\left(a^2+3b^2\right)=C,$$

with the same constant produce the same conductivity.

Consider now the mobility which can be defined as the ratio

$$\mu = \sigma/(en), \tag{35}$$

where the carrier density at low temperature is determined as follows:

$$n = N/S = \frac{1}{2\pi}\left(\frac{E_F}{\hbar v_F}\right)^2. \tag{36}$$

Substituting (33), (36) into (35), we find

$$\mu = \frac{\mu_0}{E_F^2}, \quad \mu_0 = e\hbar v_F^2\left[\pi^2 T\,(a,b)^2\left(a^2+3b^2\right)N_i {r_0}^2\right]^{-1}\left[1+o\,(1)\right], \quad k_F r_0 \ll 1. \tag{37}$$

Notice that the obtained asymptotics for the mobility is in a good agreement with the experimental results published by Bolotin et al. [12].

Consider now the case $m \neq 0$. Following the same procedure that we used for the case $m = 0$, we finally see that the form of asymptotics for mobility greatly differs from that obtained for the case $m = 0$ and from the corresponding experimental results. Thus, it is clear that in the studied suspended monolayer graphene samples $m = 0$ i,e., there is no gap in spectrum.

4. Conclusion

In the present paper, using both the framework of the model suggested in [6, 7] and the exact analytic formula for the S-matrix found in [7], we obtained the asymptotics near the Dirac point for scattering phases, cross-section, conductivity and mobility. We found that these asymptotics are in good agreement with the experimental results in the case $m = 0$, while in the case $m \neq 0$, the theoretical asymptotics are very far from those obtained experimentally . This contradiction means that as a matter of fact, in the samples studied experimentally, $m = 0$. So, the experimental study of the sample compared to our theoretical results clearly indicates whether or not there is a gap in the spectrum.

References

[1] A.N. Castro-Neto, F. Guinea et al. The electronic properties of graphene. *Rev. Mod. Phys.*, **81**, P. 101–162 (2009).

[2] C.W.J. Beenakker. Colloquium: Andreev reflection and Klein tunneling in graphene. *Rev.Mod.Phys.*, **80**, P. 1337–1354 (2008).

[3] D.M. Basko. Resonant low-energy electron scattering in short-range impurities in graphene. *Phys. Rev.B*, **78**, P. 115432–115442 (2008).

[4] D.S. Novikov. Elastic scattering theory and transport in graphene. *Phys. Rev.B*, **76**, P. 245–435 (2007).

[5] A. Matulis, F.M. Peeters. Quasibound states of quantum dots in single and bilayer graphene. *Phys. Rev. B*, **77**, P. 115423–115430 (2008).

[6] N.J.M. Horing, S.Y. Liu. Green's function for a graphene sheet and quantum dotin a normal magnetic field. *J. Phys. A. Math. Theor.*, **42** (22), P. 225301 (2009).

[7] N.E. Firsova, S.A. Ktitorov, P. Pogorelov. Bound electron states in monolayer gapped graphene with the short-range impurities. *Phys. Lett. A*, **373**, P. 525–529 (2009).

[8] N.E. Firsova, S.A. Ktitorov. Electrons scattering in monolayer graphene with the short-range impurities. *Phys. Lett. A*, **374**, P. 1270–1273 (2010).

[9] A. Lherbier, X. Blase et al. Charge Transport in Chemically Doped 2D Graphene. *Phys. Rev. Lett.*, **101**, P. 036808–036811 (2008).

[10] S.A. Ktitorov, V.I. Tamarchenko. About a short-range infusion in the double zone model [in Russian]. *Soviet Phys. (Solid State)*, **19** (7), P. 2070–2074 (1977).

[11] M. Abramowitz, I.A. Stegun. *Handbook of Mathematical Functions with Formulas, Graphs And Mathematical Tables*, National Bureau of Standards, Washington, DC, 1964.

[12] K.I. Bolotin, K.I. Sikesh, Z. Jiang et al. Ultrahigh electron mobility in suspended graphene. *Solid State Communications*, **146**, P. 351–395 (2008).

NANOSYSTEMS: PHYSICS, CHEMISTRY, MATHEMATICS, 2013, 4 (4), P. 545–549

NEGATIVE EIGENVALUES OF THE Y-TYPE CHAIN OF WEAKLY COUPLED BALL RESONATORS

A. S. Anikevich

St. Petersburg National Research University of Information Technologies, Mechanics and Optics, St. Petersburg, Russia

shadowpoos@gmail.com

PACS 02.30.Tb

Spectral properties of a system are strongly associated with its geometry. The spectral problem for the Y-bent chain of weakly-coupled ball resonators is investigated. The Y-bent system can be described as a central ball linking three chains consisting of balls of the same radius. There is a δ -coupling condition with parameter α at every contact point. Specifically, it is assumed that the axis passing through the center of each ball lies in the same plane and the centers of balls that are the closest to the central ball form an equilateral triangle. The transfer-matrix approach and the theory of extensions are employed to solve the spectral problem for this system. It is shown that such system with a certain value of parameter α has at most one negative eigenvalue in the case of δ -coupling in contact points.

Keywords: negative eigenvalue, delta-coupling, operator extensions theory.

1. Introduction

The interrelation between the geometry of a system and its spectral properties is one of the most frequently asked questions that arises during research. For example, such a problem for quantum graphs is widely discussed, see, e.g., [1] – [5] etc. The problem is especially interesting when one deals with a so-called decorated graph (see, e.g., [4]). The subject of the present paper is close to this; namely, a system of coupled balls is considered. More precisely, a Y-type branching chain is studied. We assume that the Neumann Laplacian is defined inside the balls. The coupling is constructed by using of the theory of self-adjoint extensions of symmetric operators ([6] – [11]). The most intriguing question is about the existence of eigenvalues for the system. In the paper, we proved the existence of negative eigenvalues under certain conditions.

Let us describe briefly in general terms the problem under consideration. The geometry of the Y-type chain is shown at figure 1. The elementary cell of this system is a ball of unit radius. So, the system can be described as the "central"ball connected through the contact points with three semi-infinite direct chains that consist of similar balls.

To simplify considerations, we assume that there are no external fields. The system of units with $\hbar = 2m = 1$ is used. To show the method of solving such problem, a simple example of Y-geometry with additional assumptions is discussed:

1. for each branch, there is an axis passing through the centers of the balls forming this branch and all three axes lie in a single plane;
2. balls are numbered as shown at figure 2;
3. centers of the balls No (1,1); (2,1) and (3,1) are the vertices of an equilateral triangle.

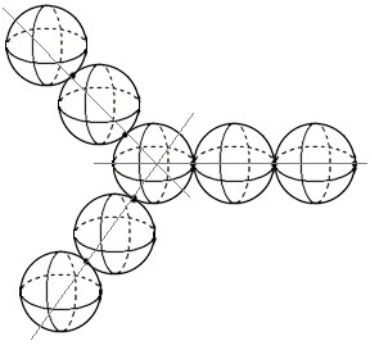

FIG. 1. Scheme of Y-type chain.

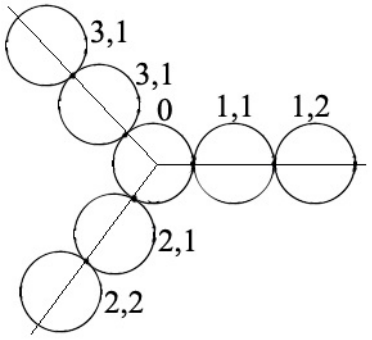

FIG. 2. Basic Y-type chain.

The described geometry of the system will subsequently be called "basic Y-type chain".

The weak coupling between resonators in our case should be considered as follows: all the interactions between elementary cells occur through pinholes (cf, [6] – [13]) at the contact points of resonators.

The wave function $\psi(x)$ of the stationary state of a spinless non-relativistic particle satisfies the stationary Schrödinger equation:

$$\hat{H}(x)\psi(x) = \lambda\psi(x).$$

And it is also considered that the Neumann boundary condition is satisfied at the boundary of the ball:

$$\left.\frac{\partial\psi}{\partial n}\right|_{\partial\Omega} = 0.$$

We use "restriction-extension"procedure, i.e., first, one constructs a symmetric restriction of the initial self-adjoint operator. Then, one considers its self-adjoint extensions, paying attention to those differing from the initial one. We restrict the operator $-\Delta$ on the set of all functions from $D(-\Delta)$ that are equal to zero near the contact points $\mathbf{x}_{i,j}$ (index i refers to chain's number, index j — to ball's number in a chain and the central ball has index 0). Thus, the symmetrical operator $-\Delta_0$ is obtained and its deficiency elements are Green's functions $G(\mathbf{x}, \mathbf{x}_j, \lambda)$ (cf, [14]). In our case, the Green's function written in spherical coordinates has the following form:

$$G\left(r,\theta,\varphi,r_j,\theta_j,\varphi_j,\lambda\right) = \sum_{k=1}^{\infty}\sum_{l=0}^{\infty}\sum_{m=-l}^{l}\frac{\Psi_{klm}\left(r,\theta,\varphi\right)\overline{\Psi_{klm}\left(r_j,\theta_j,\varphi_j\right)}}{\lambda_{lk}-\lambda},$$

where $\lambda_{lk} = x_{lk}^2$ are the eigenvalues, $\Psi_{klm}\left(r,\theta,\varphi\right) = N_{lk}j_l\left(x_{lk}r\right)Y_m^l\left(\theta,\varphi\right)$ are the eigenfunctions of the Neumann problem for the Laplace operator inside the ball, $Y_m^l\left(\theta,\varphi\right)$ are the spherical harmonics, $j_l\left(x\right)$ are the spherical Bessel's functions, x_{lk} is the k^{th} root of the following equation: $j_l'\left(x\right) = 0$, N_{lk} are the normalization coefficients.

As mentioned earlier, operator $-\Delta_0$ is a symmetrical operator, but it is not a self-adjoint operator. Keeping in mind that all self-adjoint extensions of $-\Delta_0$ are restrictions of the adjoint operator, we construct the operator $-\Delta_0^*$.

Any function U, $U \in D\left(-\Delta_0^*\right)$, has the following form:

$$U = U_0 + \frac{a}{|\mathbf{x}-\mathbf{x}_0|} + b,$$

where $U_0 \in D\left(-\Delta_0^*\right)$, $U_0\left(\mathbf{x}_0\right) = 0$; a, b are some coefficients. Henceforth, the following designations will be used: $a_{i,j}^+$, $a_{i,j}^-$ are the coefficients corresponding to pinholes in the ball

boundary with number i, j as you can see at the figure 3 (coefficients $b^+_{i,j}$, $b^-_{i,j}$ are denoted by a similar argument).

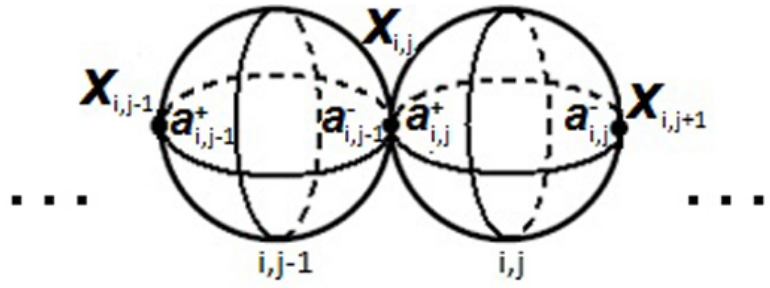

FIG. 3. Scheme of direct chain: coefficient's denotation

Using these notations one can describe a self-adjoint extension by the following relations between the coefficients:

$$\begin{cases} a^+_{i,j} = -a^-_{i,j-1}, \\ b^+_{i,j} = b^-_{i,j-1}. \end{cases} \tag{1}$$

Using these notations, one can describe a self-adjoint extension by the following relations between the coefficients:

$$\begin{cases} a^+_{i,j} = -a^-_{i,j-1}, \\ b^+_{i,j} = b^-_{i,j-1}. \end{cases} \tag{2}$$

We assume additionally that there are point-like potentials at the coupling points.

This letter discusses these results only. Full proofs will be published subsequently in a more detailed paper.

2. δ -coupling

The so-called δ -coupling imposes slightly different requirements for coefficients $a^\pm_{i,j}$, $b^\pm_{i,j}$. Resonators are supposed to be connected at the contact points by δ-coupling with the parameter α, so the following relations for the coefficients (instead of (2)) are considered:

$$\begin{cases} a^+_{i,j} = -a^-_{i,j-1}, \\ b^+_{i,j} - b^-_{i,j-1} = \alpha a^-_{i,j-1}, \end{cases} \tag{3}$$

where coefficients $b^+_{i,j}$, $b^-_{i,j-1}$ have the following form:

$$b^+_{i,j} = a^+_{i,j} \lim_{\mathbf{x}\to\mathbf{x}_{i,j}} \left(G\left(\mathbf{x}, \mathbf{x}_{i,j}, \lambda\right) - G\left(\mathbf{x}, \mathbf{x}_{i,j}, \lambda_0\right)\right) + a^-_{i,j} G\left(\mathbf{x}_{i,j+1}, \mathbf{x}_{i,j}, \lambda\right), \tag{4}$$

$$b^-_{i,j-1} = a^-_{i,j-1} \lim_{\mathbf{x}\to\mathbf{x}_{i,j}} \left(G\left(\mathbf{x}, \mathbf{x}_{i,j}, \lambda\right) - G\left(\mathbf{x}, \mathbf{x}_{i,j}, \lambda_0\right)\right) + a^+_{i,j-1} G\left(\mathbf{x}_{i,j-1}, \mathbf{x}_{i,j}, \lambda\right). \tag{5}$$

$$b^-_{i,0} = a^-_{i,0} \lim_{\mathbf{x}\to\mathbf{x}_{i,1}} \left(G\left(\mathbf{x}, \mathbf{x}_{i,1}, \lambda\right) - G\left(\mathbf{x}, \mathbf{x}_{i,1}, \lambda_0\right)\right) + \sum_{n\neq i} a^+_{n,0} G\left(\mathbf{x}_{n,1}, \mathbf{x}_{i,1}, \lambda\right), \qquad i, n = \overline{1,3}. \tag{6}$$

Matching of equations (3) and (4,5) for different points $\mathbf{x}_{i,j}$ allows one to obtain the discrete spectrum equation.

The relationship between coefficients $a^{\pm}_{i,j}$ and $a^{\pm}_{i,j-1}$ $\forall j \geq 2, i = \overline{1,3}$ can be obtained by substituting expressions (4,5) and the first equation of the system (3) into the second equation of this system:

$$\begin{pmatrix} a^{+}_{i,j} \\ a^{-}_{i,j} \end{pmatrix} = \begin{pmatrix} 0 & -1 \\ \frac{G(\mathbf{x}_{i,j-1},\mathbf{x}_{i,j},\lambda)}{G(\mathbf{x}_{i,j+1},\mathbf{x}_{i,j},\lambda)} & \frac{\alpha+2\left(G(\mathbf{x},\mathbf{x}_{i,j},\lambda)-G(\mathbf{x},\mathbf{x}_{i,j},\lambda_0)\right)|_{\mathbf{x}=\mathbf{x}_{i,j}}}{G(\mathbf{x}_{i,j+1},\mathbf{x}_{i,j},\lambda)} \end{pmatrix} \begin{pmatrix} a^{+}_{i,j-1} \\ a^{-}_{i,j-1} \end{pmatrix} = \mathbf{M_j} \begin{pmatrix} a^{+}_{i,j-1} \\ a^{-}_{i,j-1} \end{pmatrix},$$

where matrix $\mathbf{M}_j$ is a transfer matrix (cf [15]). It is simple to find its eigenvalues $\mu^{\pm}_j$ and the corresponding eigenvectors $\nu^{\pm}_j$. Let us choose unit first components of the eigenvectors. Then, it has the form:

$$\nu^{\pm}_j = \begin{pmatrix} 1 \\ -\mu^{\pm}_j \end{pmatrix}.$$

The relation between coefficients $a^{\pm}_{i,1}$ and $a^{\pm}_{i,0}$ where $i = \overline{1,3}$ can be also obtained by substituting of expressions (4,6) into system (3). Considering now equality (up to a multiplicative constant) of one of vectors (assume for certainty vector $\left(a^{+}_{1,1}, a^{-}_{1,1}\right)^T$) to eigenvector ν and using linear dependence, one obtains the following system:

$$\begin{cases} (\mu^{\pm}_2 - X)c + Aa^{-}_{2,0} + Ba^{-}_{3,0} = 0 \\ Ac + (\mu^{\pm}_2 - X)a^{-}_{2,0} - Ca^{-}_{3,0} = 0 \\ Bc - Ca^{-}_{2,0} + (\mu^{\pm}_2 - X)a^{-}_{3,0} = 0 \end{cases} \tag{7}$$

where c is a constant and the following notations were used:

$$X = \alpha + 2 \lim_{\mathbf{x}\to\mathbf{x}_{i,1}} \left(G\left(\mathbf{x}, \mathbf{x}_{i,1}, \lambda\right) - G\left(\mathbf{x}, \mathbf{x}_{i,1}, \lambda_0\right)\right),$$

$$A = G\left(\mathbf{x}_{2,1}, \mathbf{x}_{1,1}, \lambda\right), B = G\left(\mathbf{x}_{3,1}, \mathbf{x}_{1,1}, \lambda\right), C = G\left(\mathbf{x}_{3,1}, \mathbf{x}_{2,1}, \lambda\right).$$

It is obvious that system (7) has a nontrivial solution relative to c, $a^{-}_{2,0}$ and $a^{-}_{3,0}$ if its determinant equals zero:

$$\left(X - \mu^{\pm}_2 G\right)^3 - \left(X - \mu^{\pm}_2 G\right)\left(A^2 + B^2 + C^2\right) + 2ABC = 0. \tag{8}$$

Equation (8) is the main equation to investigate, but due to our additional assumptions, (namely, $A = B = C$) it can be rewritten in a simpler form:

$$\left(X - \mu^{\pm}_2 G\right)^3 - 3A^2\left(X - \mu^{\pm}_2 G\right) + 2A^3 = 0. \tag{9}$$

It should also be noted that equations (8,9) would be an equation on the discrete spectrum only if the corresponding eigenvalue μ satisfies the condition:

$$\left|\mu^{-}_2\right| < 1 \qquad \Leftrightarrow \qquad \frac{X}{2G} > 1, \tag{10}$$

$$\left|\mu^{+}_2\right| < 1 \qquad \Leftrightarrow \qquad \frac{X}{2G} < -1 \tag{11}$$

Investigating the solutions of equation (9) and keeping in mind conditions (10,11), we can obtain the following theorem (we omit the proof in this letter).

Theorem. *The basic Y-type chain of weakly coupled ball resonators has at most one negative eigenvalue if there is condition of δ -coupling in contact points with a coupling constant α (where $\alpha < -\frac{9}{2}\sum_{k=1,l=0}^{\infty} \frac{N_{lk}}{x^2_{lk}} - \frac{3}{2\pi\lambda_0}$).*

3. Conclusion

The operator extensions theory model for a base Y-type chain of weakly-coupled ball resonators was discussed. The main aim was to find negative eigenvalues for such a system with a certain type of coupling at contact points. For the system with δ -coupling it was proven that it has at most one negative eigenvalue (under certain conditions imposed on the coupling constant).

Acknowledgements

This work was supported by FTP "Scientific and Educational Human Resources for Innovation-Driven Russia"(contract 16.740.11.0030), grant 11-08-00267 of RFBR, FTP "Researches and Development in the Priority Directions Developments of a Scientific and Technological Complex of Russia 2007-2013"(state contract 07.514.11.4146) and grants of the President of Russia (state contract 14.124.13.2045-MK and grant MK-1493.2013.1)

References

[1] P. Duclos, P. Exner, O. Turek. On the spectrum of a bent chain graph. *J. Phys. A: Math. Theor.* **41**, P. 415206 (2008).

[2] N.I. Gerasimenko, B.S. Pavlov. Scattering problems on noncompact graphs. *Theoret. Math. Phys.* **74**, P. 230–240 (1988).

[3] P. Kuchment. Graph models for waves in thin structures. *Wave in random media*. **12** (4), R1-R24 (2002).

[4] E. Korotyaev, I. Lobanov. Schrödinger operators on zigzag graphs. *Ann. Henri Poincaré*. **8** (6), P. 1151–1176 (2007).

[5] I.Yu. Popov, P.I. Smirnov. Spectral problem for branching chain quantum graph. *Phys. Lett. A*. **377**, P. 439–442 (2013).

[6] I.Yu. Popov. The resonator with narrow slit and the model based on the operator extensions theory. *J. Math. Phys.* **33** (11), P. 3794–3801 (1992).

[7] R. Brown, P.D. Hislop, A. Martinez. Eigenvalues and resonances for domains with tubes: Neumann boundary conditions. *J. Diff. Equs*. **115** (2), P. 458–476 (1995).

[8] I.Yu. Popov. Model of point-like window for electromagnetic Helmholtz resonator. *Zeitschrift fur Analysis und ihre Anwendungen*. **32** (2), P. 155–162 (2013).

[9] R.R. Gadylshin. On the vibration amplitude for the Helmholtz resonator. *DAN SSSR*. **310** (5), P. 1094–1097 (1990).

[10] I.Yu. Popov. Operator extensions theory model for electromagnetic fieldelectron interaction. *Journal of Mathematical Physics*. **53** (6), P. 063505/1-8 (2012).

[11] J. Brüning, P. Exner, V. Geyler. Large gaps in point-coupled periodic systems of manifolds. *J. Phys. A, Math. Gen.* **36** (17), P. 4875–4890 (2003).

[12] J. Brüning, G. Martin, B. Pavlov. Calculation of the Kirchhoff coefficients for the Helmholtz resonator. *Russian J. Math. Phys*. **16** (2), P. 188–207 (2009).

[13] A. Laurain, S.A. Nazarov, J. Sokolowski. Singular perturbations of curved boundaries in three dimensions. The spectrum of the Neumann Laplacian. *Z. Anal. Anwend.* **30** (2), P. 145–180 (2011).

[14] N.I. Akhiezer, I.M. Glazman. *Theory of Linear Operators in Hilbert Space.* Vol. I. Translated from the third Russian edition by E. R. Daqson. Translation edited by W. N. Everitt. Monographs and Stidies in Mathematics, 9. London: Pitman (Advanced Publishing Program), 1981. 312 pp.

[15] N. Bagraev, G. Martin, B.S. Pavlov, A. Yafyasov. Landau-Zener effect for a quasi-2D periodic sandwich. *Nanosystems: Physics, Chemistry, Mathyematics*, **2** (4), P. 32–50 (2011).

NANOSYSTEMS: PHYSICS, CHEMISTRY, MATHEMATICS, 2013, 4 (4), P. 550–554

INVESTIGATION OF QUANTUM RANDOM NUMBER GENERATION BASED ON SPACE-TIME DIVISION OF PHOTONS

A. E. Ivanova, V. I. Egorov, S. A. Chivilikhin, A. V. Gleim

St. Petersburg National Research University of Information Technologies, Mechanics and Optics, St. Petersburg, Russia

newiva@mail.ru, egorovvl@gmail.com, sergey.chivilikhin@gmail.com, aglejm@yandex.ru

PACS 03.67.-a

In this paper we investigate a quantum random number generator based on the splitting of a beam of laser emitted light. Statistics of random numbers that depend on a parameter characterizing the symmetry of the beam splitter is theoretically analyzed and simulated. Degree of deviation of the obtained distribution from the uniform random distribution is investigated on a basis of series of statistical tests.

Keywords: quantum random number generation, beam splitter, random number distribution.

1. Introduction

Random numbers are used in many areas of human activity. Historically, two approaches for their generation have been developed. Pseudorandom number generators are based on algorithms implemented on a computing device. Physical generators extract randomness out of a complex physical systems fundamental chaotic behavior, making them suitable for generating truly random sequences. In particular, quantum random number generators (QRNG) belong to the second group. There are different ways to implement QRNG using beam separation [1, 2], entangled photon states [3, 4], processes of photon emission and detection [5, 6, 7], and quantum noise of lasers [8, 9]. Truly random numbers obtained by using a QRNG find many applications requiring higher quality random sequences than pseudorandom, including both classical and quantum cryptography. For example, in quantum cryptography protocols [10], the initial choice of the basis must be truly random.

Initially, simple QRNG was based on photon passage through a beam splitter, where the photon randomly follows one of two possible paths after emission [1, 2]. Similar implementations use several photons and a beam splitter, polarized photons with a polarizing beam splitter, or photons reflected from a diffraction grating (angular measurements are performed). Another type of scheme is based on time delay in one of the arms that photons pass [2]. Detecting the photon's arrival time, we can thus determine which path it has passed, and denote the short way as "0", and the long as "1" to get a sequence of random bits. This approach allows the use of a single detector, but leads to a loss in bitrate.

Such QRNGs are of great interest in the area of optical computation. Indeed, their relatively simple structure and the fact that they consist of only the basic optical elements (light source, detector, waveguide, beamsplitter) make them suitable for implementation as a fully-functional device or 'on-chip' element of a larger setup. However, it is known that imperfectness of actual optical parts may have a large impact on device functionality. In particular, every manufacturing technique is characterized by its own technological limits. Therefore, defining the tolerance of optical element parameters and investigating how they affect random number statistics remain an important task. In this work, we study angular parameters of the beamsplitter.

2. Investigation of random distribution statistics obtained directly from a laser

We consider a system consisting only of a laser, which acts as a radiation source, and a detector. The scheme is shown in fig. 1(a).

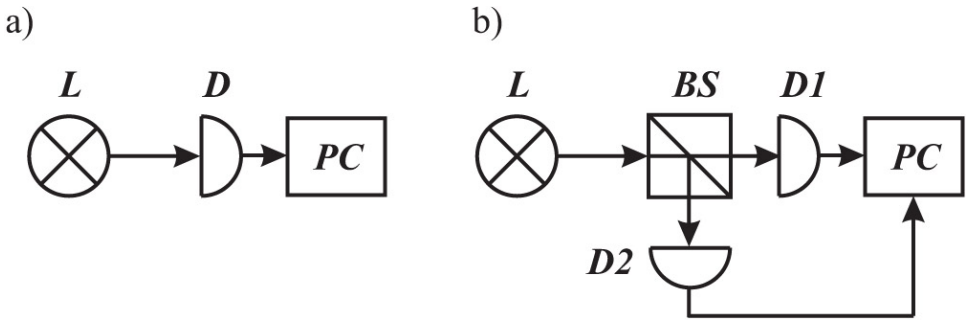

FIG. 1. a) Scheme of random distribution generation obtained directly from the laser, L - Laser, D - detector, PC - computer; b) Scheme of random distribution generation obtained by using a beam splitter, BS - beam splitter, D1, D2 - detectors

To obtain a random sequence, data received from the detector must be processed. A random variable that determines the binary sequence depends on laser radiation, which can be represented as a Poisson process:

$$P(k) = \frac{\lambda^k e^{-\lambda}}{k!},$$

where λ is the parameter of Poisson distribution.

This distribution includes multiphoton states, therefore, additional processing is required to provide binary generation results. We consider empty samples in a given time interval as "0", and samples with any number of photons in it as a "1". The parameter λ in the Poisson distribution should be set to $\lambda = \ln 2$ in order to achieve equal probabilities of zeros and ones in the final sequence. We simulated random sequence vector corresponding to Poisson distribution in Mathcad, using the previously calculated λ optimum value. Simulation results are shown in fig. 2.

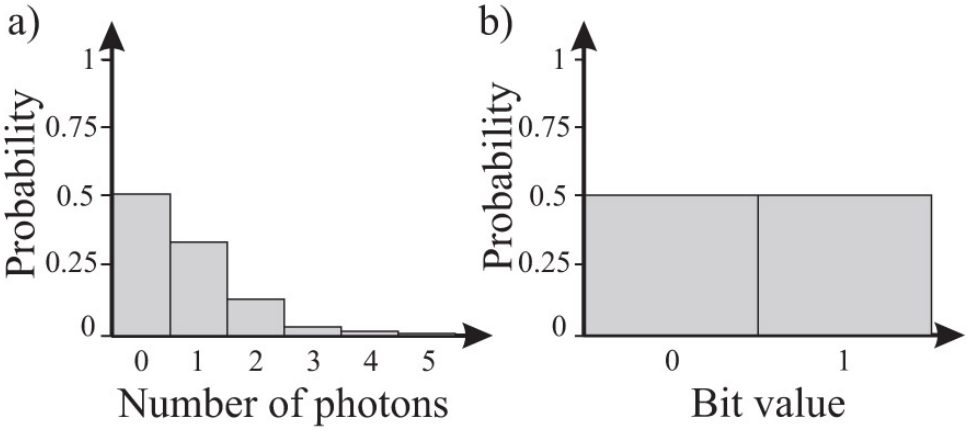

FIG. 2. Probability of occurrence of a) several photons (0-5) in the sequence before processing; b) zeros and ones in the sequence after processing

3. Investigation of distribution statistics obtained by using a beam splitter

We perform the simulation of a probabilistic process by dividing laser radiation with a beam splitter and alternating the obtained data from the detectors. The scheme is shown in fig. 1 b). Taking samples from the two outputs of the beam splitter, we obtain two Poisson distributions, from which, the final (output) binary distribution is generated.

Encoding of random bits from two sequences obtained after separation of the initial laser radiation with the beam splitter is performed as follows: if a non-zero number of photons comes to one of the detectors, and the other detector does not read any photons, such a condition is considered as a binary value 1. The opposite case is considered to be a binary value 0. Situations when both sensors detect or do not detect photons are ignored.

Generation of random numbers was modeled in Mathcad using a symmetric beam splitter. Angle θ of beam splitter in this case was 45°. Thus, the beam splitter output generates two Poisson sequences with the same value λ, which are processed. After modeling and processing, the final binary sequence was obtained. Its probabilities of zero and one bit values are shown in fig. 3(b).

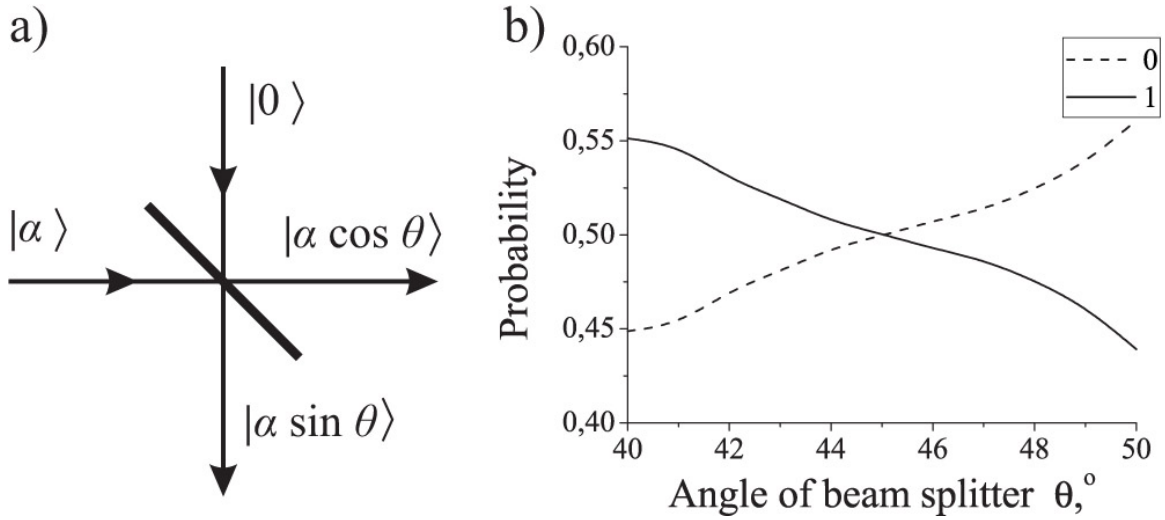

FIG. 3. a) Scheme of a beam splitter b) Probability of occurrence of "0" and "1" in the resulting sequence, depending on the beam splitter angle

4. Investigation of the beam splitter asymmetry influence on the quality of generated sequences

In case of an asymmetrical beam splitter (in practice it's very difficult to achieve perfect symmetry), asymmetry affects the probability of occurrence of ones and zeros in the final sequence of bits. We considered the effect of beam splitter angle on the quality of the generated sequence. The beam splitter scheme is shown in fig. 3(a).

Taking samples from two outputs of the beam splitter, we get two Poisson distributions with parameter values $\lambda_1 = \lambda\cos\theta$, $\lambda_2 = \lambda\sin\theta$. Using these distributions, output binary distribution is generated. Processing of two sequences is the same as in the previous case.

Beam splitter asymmetry affects the quality of the generated sequence. Statistical parameters of the binary distribution obtained with an asymmetric beam splitter are shown in fig. 3(b)). By increasing deviation of the beam splitter angle value from $\theta = 45°$, we increase the difference in zeros and ones generation probability in the final sequence. It is necessary

to calculate tolerance of beam splitter angular deviation from 45°, at which the final binary sequence can still pass tests of randomness.

5. Investigation of detector influence on the quality of generated sequences

Detector parameters affect the quality of generated sequences of random numbers. Let's consider a situation when the percentage of failure of both detectors is equal and detectors do not operate at some random times. Technically, it means that some random samples in two sequences produced by the beam splitter will be forced to zero. In this case, if the beam splitter asymmetry is initially low, the quality of the resulting sequence is not decreased, because the changes are random and the failure percentage is equal for both detectors. If the asymmetry is significant, the difference between the probabilities of zeros and ones remains at the same level, as with perfect detectors.

We also considered a situation when the percentages of failure of the two detectors are different. In this case, one of the sequences produced by the beam splitter will contain more zero samples than the other. Thus, the final sequence quality falls, because changes made by the detectors cause asymmetry in the processing sequences. Fig. 4 illustrates the probability of "0" or "1" bits occurrence depending on the ratio of detection probability on the first detector P_1 to probability of detection on second detector P_2.

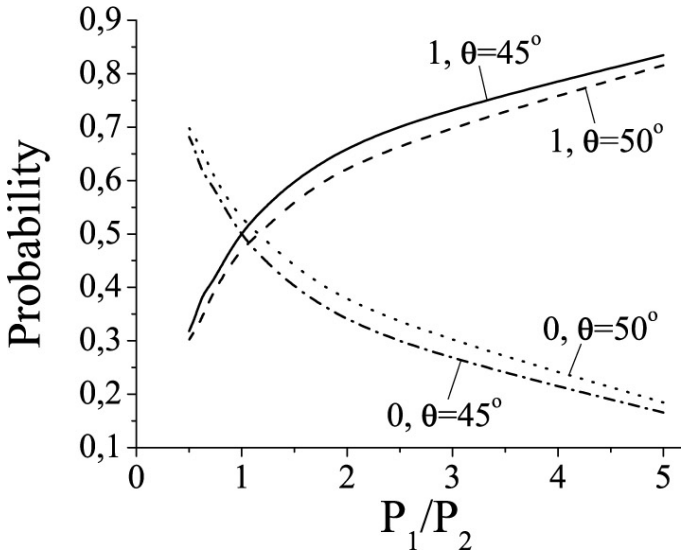

FIG. 4. Probability of zero or single bits occurrence in the sequence obtained by using beam splitters with angles $\theta = 45°$ and $\theta = 50°$, probability of detection of the first detector $P_1 = 10\%$

However, asymmetric detectors can compensate the difference in the probabilities of an asymmetric beam splitter, if their parameters are properly selected. For example, if after the beam division, in one of two resulting sequences the amount of nonzero samples is greater than in the other, but it is detected by a device with a larger number of zero counts, an optimal balance between the probability of occurrence of zeros and ones in the final sequence of bits can be observed.

6. Analysis of obtained results

A series of tests were used for controlling the quality of simulated sequences. These tests allowed the determination of all the continuous sequences of identical bits, and comparing

their distribution with the expected distribution of the series for a truly random sequence. In particular, we used monobit and twobit tests. During the analysis, we received the following results: both the sequence obtained directly from the laser, and the sequence obtained using a symmetric beam splitter, passed all the performed tests of randomness. For an asymmetric beam splitter, the uniformity of the distribution depended on the angle of the beam splitter. The generated sequences passed tests for randomness, if the deviation of the angle $\theta = 45^\circ$ was no more than two degrees.

The detector parameters also affected the generated sequences; with the difference in the frequency of detector responses degrading their quality.

7. Conclusion

A theoretical analysis and modeling of a random number distribution obtained directly from the laser and using the beam splitter, was performed. The influence of beam splitter parameters and parameters of detector to randomly generated sequence were investigated. The generated sequences passed tests for randomness if the deviation of the beam splitter angle $\theta =$ from 45° was less than two degrees. It was found that asymmetric detectors can compensate for the difference in the probabilities of an asymmetric beam splitter.

References

[1] T. Jennewein, U. Achleitner, et al. A fast and compact quantum random number generator. *Rev. Sci. Instrum.*, **71** (4), P. 1675–1680 (2000).

[2] A. Stefanov., N. Gisin, et al. Optical quantum random number generator. *J. Modern Optics*, **47** (4), P. 595–598 (2000).

[3] M. Fiorentino, C. Santori, et al. Secure self-calibrating quantum random bit generator. *Phys. Rev. A.* **75**, P. 032334 (2007).

[4] O. Kwon, Y.-W. Cho, Y.-H. Kim. Quantum random number generator using photon-number path entanglement. *Appl. Opt.*, **48**, P. 1774–1778 (2009).

[5] M. Stipcevic, M.B.Rogina. Quantum random number generator based on photonic emission in semiconductors. *Rev. Sci. Instrum.*, **78**, P. 045104 (2007).

[6] J.F. Dynes, Z.L. Yuan, A.W. Sharpe, A.J. Shields. A high speed, post-processing free, quantum random number generator. *Appl. Phys. Lett.*, **93**, P. 031109 (2008).

[7] M. Furst, H. Weier, et al. High speed optical quantum random number generation. *Optics Express*, **18**, P. 13029 (2010).

[8] B. Qi, Y.M. Chi, H.-K. Lo, L. Qian. High-speed quantum random number generation by measuring phase noise of a single-mode laser. *Optics Letters*, **35**, P. 312–314 (2010).

[9] I. Reidler, Y. Aviad, M. Rosenbluh, I. Kanter. Ultrahigh-speed random number generation based on a chaotic semiconductor laser. *Phys. Rev. Lett.*, **103**, P. 024102 (2009).

[10] V. Scarani, H. Bechmann-Pasquinucci, et al. The security of practical quantum key distribution. *Rev. Mod. Phys.*, **81**, P. 1301–1350 (2009).

NANOSYSTEMS: PHYSICS, CHEMISTRY, MATHEMATICS, 2013, 4 (4), P. 555–558

TUNNELING CURRENT IN CARBON NANOTUBES WITH DEEP IMPURITIES

N. N. Konobeeva[1], M. B. Belonenko[2]

[1]Volgograd State University, Volgograd, Russia
[2]Volgograd Institute of Business, Volgograd, Russia

yana_nn@inbox.ru, mbelonenko@yandex.ru

PACS 73.63.Fg, 71.55.Cn, 73.23.-b

In this paper we study the tunneling contact of carbon nanotubes with deep impurities and metal. The tunneling current in contact nanotube-metal was investigated. The dependence of current-voltage characteristic of such contact on the band gap of the impurity was analyzed. An area with negative differential conductivity was observed.

Keywords: Carbon nanotube, deep impurity, band gap, negative differential conductivity.

1. Introduction

In this paper the tunneling current flowing in contact of carbon nanotubes (CNTs) with deep impurities and metal. A deep impurity is one which creates a deep energy level [1]. It should be noted that research related to the study of such impurities, as well as their influence on the electronic structure and thus the properties of semiconductors is very popular now [2, 3]. Such attention to this problem is primarily caused by the trends of modern opto-, micro- and microwave electronics, and, specifically, more stringent requirements for the quality of semiconductor materials having content of impurities which give rise to deep levels in the band gap. The presence of these impurities impart both positive and negative characteristics. Therefore, to minimize undesirable effects, it is important to study the nature of deep impurities to make the most effective use of positive effects on the functional characteristics of these devices.

At the same time, the attention of researchers is attracted to tunneling, as devices based on the tunneling effect have become a part of the basic elements of modern electronics and are thus of great practical application.

2. Statement of the problem and basic equations

The matrix form of the Hamiltonian of the problem is:

$$H = \begin{bmatrix} 0 & f & \alpha_1 & \beta_1 & \gamma_1 & \Delta_1 \\ f^* & 0 & \alpha_2 & \beta_2 & \gamma_2 & \Delta_2 \\ \alpha_1^* & \alpha_2^* & t_1 & 0 & 0 & 0 \\ \beta_1^* & \beta_2^* & 0 & t_2 & 0 & 0 \\ \gamma_1^* & \gamma_2^* & 0 & 0 & t_3 & 0 \\ \Delta_1^* & \Delta_2^* & 0 & 0 & 0 & t_4 \end{bmatrix} \quad (1)$$

where $|f|$ determines the energy spectrum of the CNT; t_i - the value of the energy level of deep impurities, α, β, γ, Δ - hopping integral between the sublattices and impurity levels.

Hamiltonian (1) can be rewritten by using the structure of the block matrices [4]:

$$H = \begin{bmatrix} 0 & f & \alpha_1 & \beta_1 & \gamma_1 & \Delta_1 \\ f^* & 0 & \alpha_2 & \beta_2 & \gamma_2 & \Delta_2 \\ \alpha_1^* & \alpha_2^* & t_1 & 0 & 0 & 0 \\ \beta_1^* & \beta_2^* & 0 & t_2 & 0 & 0 \\ \gamma_1^* & \gamma_2^* & 0 & 0 & t_3 & 0 \\ \Delta_1^* & \Delta_2^* & 0 & 0 & 0 & t_4 \end{bmatrix} = \begin{bmatrix} H_{11} & H_{12} \\ H_{21} & H_{22} \end{bmatrix}.$$

Considering the electronic system in the long-wave approximation, we can write the effective Hamiltonian of the problem [4]:

$$H_{\text{eff}} = H_{11} - H_{12}H_{22}^{-1}H_{21}. \tag{2}$$

We solve the eigenvalue problem and find:

$$\begin{gathered} \lambda_{1,2}^2 = \frac{R + Q \pm \sqrt{(R-Q)^2 - 4\left(\varepsilon D^* + \varepsilon^* D - |\varepsilon|^2 - |D|^2\right)}}{2}, \\ R = -\left(\frac{|\alpha_1|^2}{t_1} + \frac{|\beta_1|^2}{t_2} + \frac{|\gamma_1|^2}{t_3} + \frac{|\Delta_1|^2}{t_4}\right), \\ Q = -\left(\frac{|\alpha_2|^2}{t_1} + \frac{|\beta_2|^2}{t_2} + \frac{|\gamma_2|^2}{t_3} + \frac{|\Delta 2|^2}{t_4}\right), \\ D = \left(\frac{\alpha_1\alpha_2^*}{t_1} + \frac{\beta_1\beta_2^*}{t_2} + \frac{\gamma_1\gamma_2^*}{t_3} + \frac{\Delta_1\Delta_2^*}{t_4}\right). \end{gathered} \tag{3}$$

Parameters R, Q reflect the probability of a jump from the first (second) CNT sublattice to the impurity, while D reflects the probability of a jump from one CNT's sublattice to another.

We note that the dispersion relation, which describes the properties of CNTs, is [5]:

$$\varepsilon(p,s) = |f| = \pm\gamma\sqrt{1 + 4\cos(ap_x)\cos\left(\frac{\pi s}{m}\right) + 4\cos^2\left(\frac{\pi s}{m}\right)}, \tag{4}$$

where $s = 1, 2, \ldots, m$, the nanotube is of the type $(m, 0)$, $\gamma \approx 2.7$ eV, $a = 3b/2\hbar$, $b = 0.142$ nm is the distance between the adjacent carbon atoms.

Typical band structure of carbon nanotube with deep impurities is presented in Fig. 1.

In the framework of the Kubo theory, the expression for the current density of the contact is the following [6]:

$$\begin{gathered} J = 4\pi e\,|T|^2 \int\limits_{-\infty}^{+\infty} dE\nu_A(E+eV)\nu_B(E)(n_f(E) - n_f(E+eV)), \\ \nu_A(E) = \sum_p \delta(E - E_p^A); \quad \nu_B(E) = \sum_q \delta(E - E_q^B), \end{gathered} \tag{5}$$

where $\delta(x)$ is the Dirac delta function, $\nu_{A(B)}(E)$ is the tunneling density of states, $n_f(E)$ is the equilibrium number of fermions with energy E. Here and below, we use the approach of "rough" contact T (tunneling matrix element between the two states): (in fact, we impose restrictions on the geometry of the contact that is, in what follows we consider the case where the nanotube is perpendicular to the surface of the contact material).

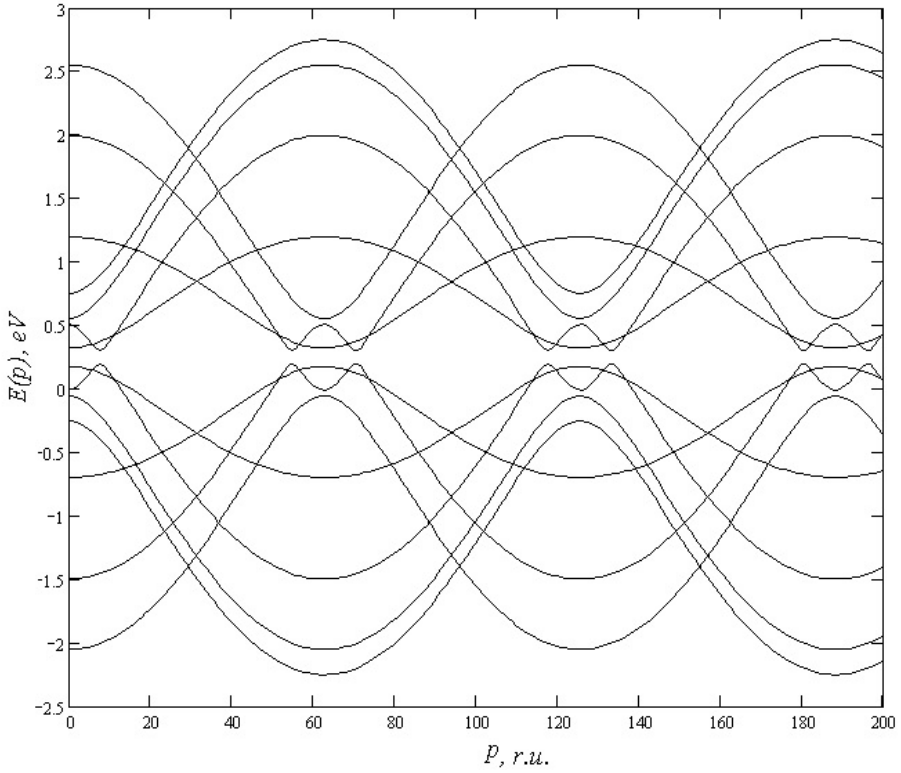

FIG. 1. The band structure of CNT (7,0) with the deep impurities

The metal dispersion law of free electrons in the effective-mass m is:

$$E_q^B = \frac{p^2}{2m}. \tag{6}$$

3. Results

Equation (5) was solved numerically. The current-voltage characteristic (CVC) of the contact is presented in Fig. 2.

A significant influence of the parameters on the behavior of the current-voltage curve can be seen. It should be noted that when R increases, both the current and the area with negative differential conductivity decrease. Also, it should be noted that we have an area with negative differential conductivity (NDC).

The current-voltage characteristic of the contact in the case of different values of D is shown in Fig. 3.

The effect of parameter D appears to weaken of the current, which can be attributed to a stronger bond between the electrons and the impurity levels.

Therefore, we can conclude that the influence of impurities on the tunneling characteristics of CNT-metal contact was investigated. The effect of hopping integrals, and the width of the band gap of deep impurities on the dependence of the tunneling current and the voltage between the contact were also observed. By careful selection of the impurity parameters (D, R, Q), we can control the CVC and the value of the area with NDC. This effect can be used in many practical applications (for example in tunneling diodes).

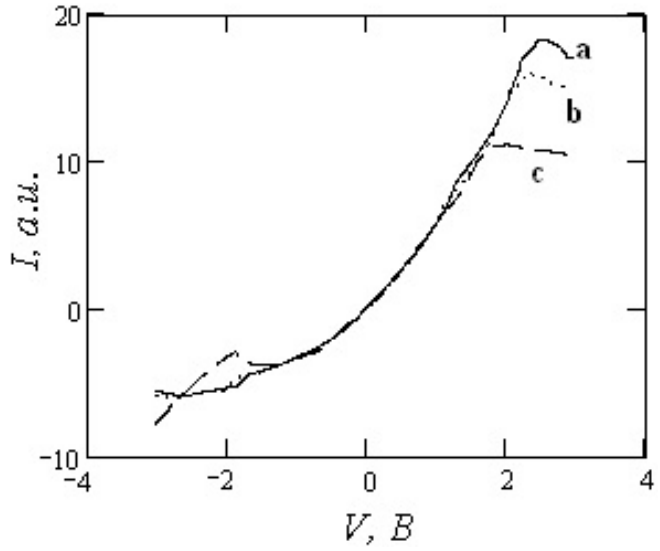

FIG. 2. The current-voltage characteristics of metal-doped CNTs ($Q = 0.03$ eV, $D = 0.05$ eV - fixed): a) $R = 0.02$ eV; b) $R = 0.04$ eV; c) $R = 0.1$ eV

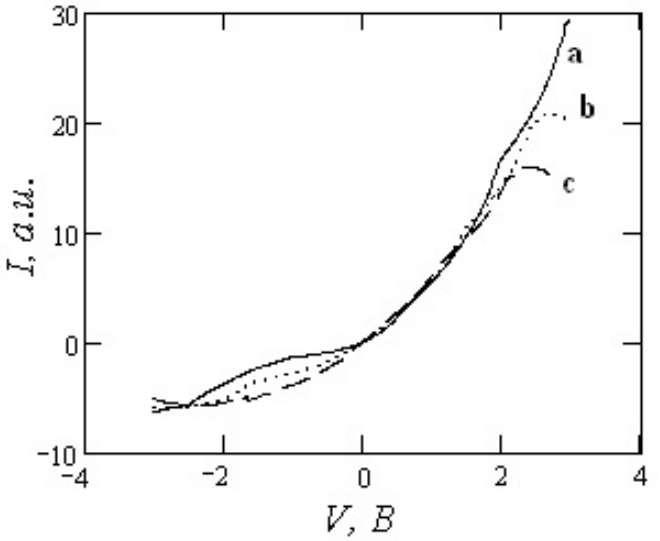

FIG. 3. The current-voltage characteristics of metal-doped CNTs ($R = 0.02$ eV, $Q = 0.03$ eV - fixed): a) $D = 0.01$ eV; b) $D = 0.04$ eV; c) $D = 0.06$ eV

References

[1] A.A. Gvelisiani, E.A. Shelonin. *Behavior and properties of dopped impurities in semiconductors*. IPC MITHT M.V. Lomosov, Moscow: 2004. 80 p.

[2] V.N. Mantsevich, N.S. Maslova. Spatial effects of Fano resonance in local tunneling conductivity in vicinity of impurity on semiconductor surface. *Pis'ma v ZheTF*, **91**, P. 150–153 (2010).

[3] V.N. Mantsevich, N.S. Maslova. The influence of localized states charging of formula nor shown tunneling current noise spectrum. *Solid state communications*, **150**, P. 2072–2075 (2010).

[4] A. Cortijo, F. Guinea, M.A.H. Vozmediano. Geometrical and topological aspects of grapheme and related materials. `arXiv.org 1112.2054v1`, (2011).

[5] P. Harris. *Carbon nanotubes and related structures. New materials of XXI century.* Technosphera, Moscow: 2003. 336 p.

[6] L.S. Levitov,.V. Shitov. *Green's functions. Tasks with solutions*. Fizmatlit, Moscow: 2003. 392 p.

NANOSYSTEMS: PHYSICS, CHEMISTRY, MATHEMATICS, 2013, 4 (4), P. 559–563

HARTREE-FOCK APPROXIMATION FOR THE PROBLEM OF PARTICLE STORAGE IN DEFORMED NANOLAYER

I. F. Melikhov, I. Yu. Popov

St. Petersburg National Research University of Information Technologies, Mechanics and Optics, 49 Kronverkskiy, St. Petersburg 197101, Russia

ivan.melikhov@gmail.com, popov1955@gmail.com

PACS 02.30.Tb, 73.21.Ax, 03.65.Ge

The paper deals with the problem of quantum particle storage in a nanolayered structures. The system of a few electrons interacting via a δ-potential is considered. The particles are placed into a two-dimensional deformed waveguide. From a mathematical point of view, the bound state of the system means that the corresponding Hamiltonian will have eigenvalues. To treat a multi-particle problem, the Hartree-Fock approach and the finite element method are used. Three different types of the perturbation are considered: deformation of the layer boundary, a small window in a wall between two layers and a bent layer. The systems of 2–10 particles with various total spins are studied. The dependence of the minimal deformation parameter, which keeps bound state on the number of particles, is given. Comparison of the storage efficiencies in those cases is made.

Keywords: discrete spectrum, multi-particle problem, waveguide.

1. Introduction

The problem of the existence of the bound states of quantum particles is very important in physics. Its usefulness is demonstrated by the particle storage problem. It is known that a particle can be stored in curved nanolayers. In the terms of math it means the existence of the discrete spectrum of the corresponding Hamiltonian. The single particle system in an undeformed nanolayer has an empty discrete spectrum. But deformation of the layer causes the appearance of an eigenvalue (see, e.g., [1–7]). Increasing the curvature leads to increasing eigenvalue numbers. In many applications it's necessary to store more than one particle and, consequently, to deal with the multi-particle problem [8, 9]. As an example of such an application, the storage of hydrogen in nanolayed structures can be given. This can be used to produce an effective and safe fuel container. In this work, the equations for multi-particle problem are simplified by the Hartree-Fock approach and the eigenvalue problem is solved numerically by the finite element method.

2. Theory background

Consider a number of interacting electrons placed into a nanolayer or a waveguide. Neglecting the spin-orbit interaction, one gets the following form for the Hamiltonian of the multi-particle system:

$$\hat{H} = \sum_k \left(-\frac{\hbar^2}{2m}\nabla_k^2 + U_k \right) + \frac{1}{2}\sum_{\substack{j,k \\ j\neq k}} V_{jk} = \sum_k \hat{H}_k + \frac{1}{2}\sum_{\substack{j,k \\ j\neq k}} \hat{H}_{jk}, \qquad (1)$$

where m is particle's mass, U_k is the external field potential, V_{jk} is potential of the particles' interaction. Solving the multi-particle problem is a Herculean task, so one needs to simplify the equation (1). Application of the *Hartree method* for two particle problem was described in [10]. In this case, the wavefunction of the system is sought in the form

$$\psi(x_1, x_2, \ldots, x_n) = \psi_1(x_1)\psi_2(x_2)\ldots\psi_n(x_n), \tag{2}$$

where ψ_i is the single particle function, x_i represents the set of four coordinates: three spatial ones and a spin one. Substituting (2) into (1) and using the variational principle, one can obtain *Hartree equations* (see [11]):

$$\left[\hat{H}_k + \sum_{\substack{j \\ j\neq k}} \int \psi_j^*(x_j)\hat{H}_{jk}\psi_j(x_j)\,dx_j\right]\psi_k(x_k) = E_k\psi_k(x_k) \qquad (k = \overline{1,n}). \tag{3}$$

The *Hartree method* is easy to implement but this approach has one significant disadvantage; the electronic wavefunction must satisfy the antisymmetry principle, i.e. it must be antisymmetric with respect to the interchange of all (space and spin) coordinates of one fermion with those of another. That is,

$$\psi(x_1, x_2, \ldots, x_i, \ldots, x_j, \ldots, x_n) = -\psi(x_1, x_2, \ldots, x_j, \ldots, x_i, \ldots, x_n). \tag{4}$$

This drawback was avoided by Fock. The idea of the *Hartree-Fock method* is to replace the wavefunction representation (2) by the *Slater determinant*:

$$\psi(x_1, x_2, \ldots, x_n) = \frac{1}{\sqrt{N!}}\begin{vmatrix} \psi_1(x_1) & \psi_2(x_1) & \ldots & \psi_n(x_1) \\ \psi_1(x_2) & \psi_2(x_2) & \ldots & \psi_n(x_2) \\ \ldots & \ldots & \ldots & \ldots \\ \psi_1(x_n) & \psi_2(x_n) & \ldots & \psi_n(x_n) \end{vmatrix}. \tag{5}$$

Again, engaging the variational principle, one can obtain (see [11]) the *Hartree-Fock equations*:

$$\left[\hat{H}_k + \sum_{\substack{j \\ j\neq k}} \int \psi_j^*(x_j)\hat{H}_{jk}\psi_j(x_j)\,dx_j\right]\psi_k(x_k) - \sum_{\substack{j \\ j\neq k}}\left[\int \psi_j^*(x_j)\hat{H}_{jk}\psi_k(x_j)\,dx_j\right]\psi_j(x_k) = \\ = E_k\psi_k(x_k) \qquad (k = \overline{1,n}). \tag{6}$$

To find the discrete spectrum, of the system one has to remember that all eigenvalues $E_1, \ldots, E_n$ must be less than the threshold (the bottom of the continuous spectrum, $E_{bot} = \pi^2\hbar^2/(2mL^2)$, where L is the waveguide width at infinity).

3. Numerical model

For the numerical model, we assume zero external field potential U_k and δ-potential of particles interaction:

$$V_{jk} = U_0\delta(r_j - r_k), \tag{7}$$

where U_0 is a constant which describes the intensity of the interaction, r_j and r_k are spatial coordinates of the particles. We assume every electron has predefined spin $s = 1/2$ or

$s = -1/2$. Applying those assumptions, one rewrites the *Hartree-Fock equations* (6) in simpler form:

$$\left[-\frac{\hbar^2}{2m}\nabla_k^2 + \sum_{\substack{j \\ j\neq k}} U_0 \left|\psi_j(r_k)\right|^2\right] \psi_k(r_k) - \sum_{\substack{j \\ j\neq k}} U_0 \delta_{s_j,s_k} \left|\psi_j(r_k)\right|^2 \psi_k(r_k) = E_k \psi_k(r_k) \qquad (k = \overline{1,n})$$

or

$$\left[-\frac{\hbar^2}{2m}\nabla_k^2 + \sum_{\substack{j \\ j\neq k}} U_0 (1 - \delta_{s_j,s_k}) \left|\psi_j(r_k)\right|^2\right] \psi_k(r_k) = E_k \psi_k(r_k) \qquad (k = \overline{1,n}), \tag{8}$$

where s_j, s_k are spin values of the corresponding electrons. All problems are solved in 2D. Three types of geometries are studied: i) a waveguide with deformed boundary (fig. 1); ii) two layers coupled through window (fig. 2); iii) a bent waveguide (fig. 3). Dirichlet conditions are valid at the waveguide boundaries and Neumann conditions are assumed at the ends of the waveguide. For the first configuration, the deformation is described by an analytical function. Its parameter is H/L (deformation width b is constant). The parameter of the second configuration is a/L. And for the last one is L/R (the length of the curved arc is constant). In all cases, larger geometry parameter values correspond to larger deformations of the waveguide. To find the numerical solution of (8), the FEM is

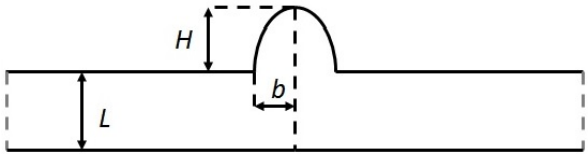

FIG. 1. Deformed waveguide

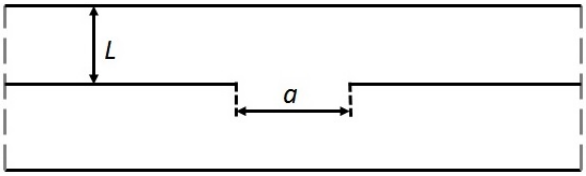

FIG. 2. Window-coupled waveguides

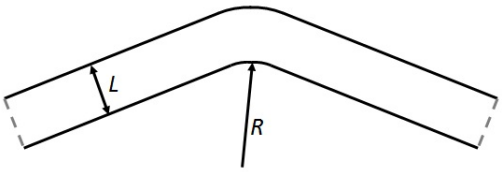

FIG. 3. Bent waveguide

used. The package FreeFEM++ is engaged. The algorithm of the solution is the same as in [10]. First, assume all functions ψ_k to be zero as the first approximation. Then solve the first equation for ψ_1. After that, insert it into the second equation and solve it with respect to ψ_2. The procedure is repeated until the difference between two last approximations becomes small enough.

4. Results

A number of computations for systems with different number of particles and various total spin values were made. While the interaction intensity was constant, the critical value of the geometry parameter was sought. The critical value is the minimal value of the parameter which maintains the bound state of the system. The results are shown at

the figures below. As expected, more particles and bigger total spins lead to increasing deformation which is needed to store the particles. This means that it is more difficult to store these particles. But, one sees an interesting effect which is valid for all geometries. It was shown that to store an even number of particles with zero total spin, the deformation may be the same or even less than that for a system of one less particle. Comparison of the dependencies slopes in figures 4–6 shows the efficiency of the window-coupled type deformation. In contrast, the bent waveguide is the least efficient.

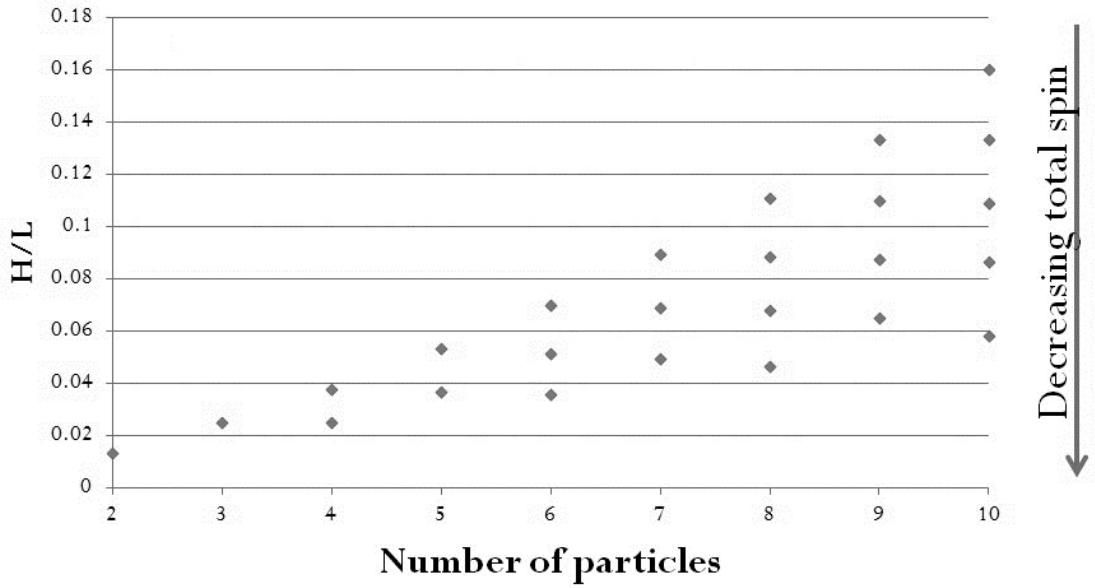

FIG. 4. Deformed waveguide: critical value of the geometry parameter

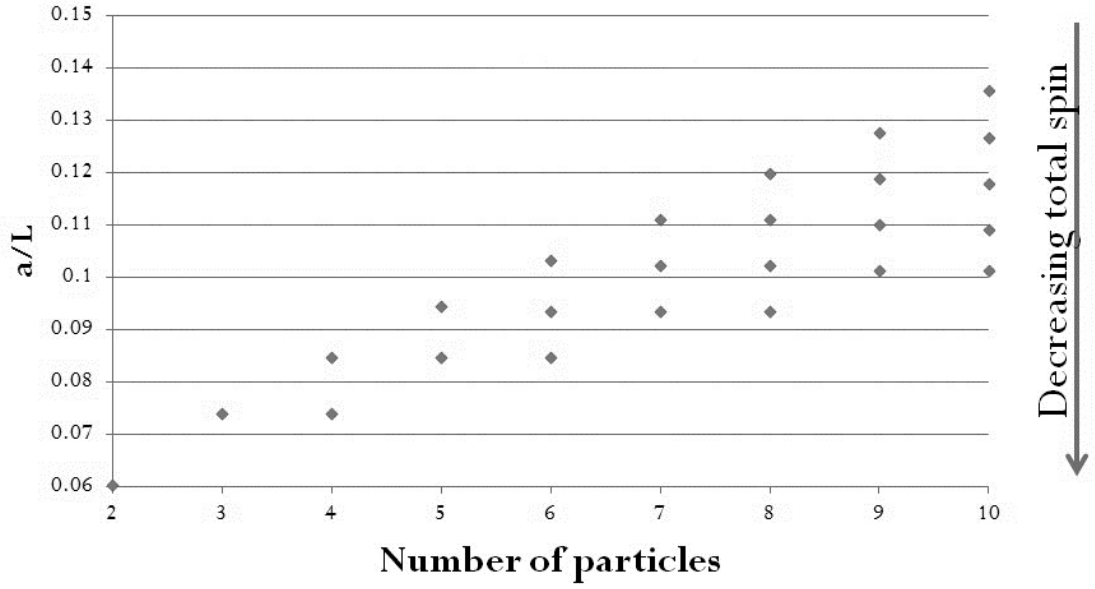

FIG. 5. Window-coupled waveguides: critical value of the geometry parameter

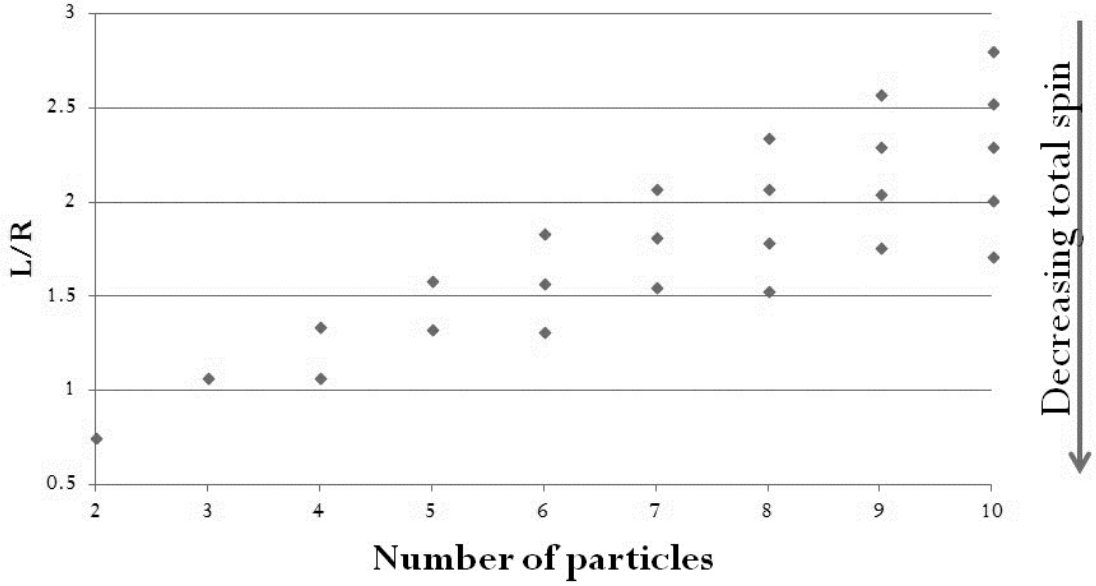

FIG. 6. Bent waveguide: critical value of the geometry parameter

Acknowledgments

Supported by Federal Targeted Program "Scientific and Educational Human Resources for Innovation-Driven Russia" (contracts P689 NK-526P, 14.740.11.0879, and 16.740.11.0030), grant 11-08-00267 of Russian Foundation for Basic Researches and by Federal Targeted Program "Researches and Development in the Priority Directions Developments of a Scientific and Technological Complex of Russia 2007-2013" (state contract 07.514.11.4146) and grants of the President of Russia.

References

[1] P. Duclos, P. Exner, P. Stovichek. Curvature induced resonances in a two-dimensional Dirichlet tube. *Annales de l'I.H.P. Section A*. **62** (1), p. 81–101 (1995).
[2] P. Duclos, P. Exner, D. Krejcirik. Locally curved quantum layers *Ukrainian J. Phys.*, **45**, P. 595–601 (2000).
[3] P. Exner, S.A. Vugalter. Bounds states in a locally deformed waveguide: the critical case. *Lett. Math. Phys.*, **39**, P. 59–68 (1997).
[4] P. Exner, S.A. Vugalter. Asymptotic estimates for bound states in quantum waveguides coupled laterally through a narrow window. *Ann. Inst. H. Poincare*, **65**, P. 109–123 (1996).
[5] P. Exner, P. Seba, M.Tater, D. Vanek. Bound states and scattering in quantum waveguides coupled laterally through a boundary window. *J. Math. Phys.*, **37**, P. 4867–4887 (1996).
[6] I.Yu. Popov. Asymptotics of bound state for laterally coupled waveguides. *Rep. on Math. Phys.*, **43** (3), P. 427–437 (1999).
[7] I.Yu. Popov. Asymptotics of resonances and bound states for laterally coupled curved quantum waveguides. *Phys. Lett. A*, **269**, P. 148–153 (2000).
[8] H. Linde. Geometrically induced two-particle binding in a waveguide. *J. Phys. A: Math. Gen.*, **39**, P. 5105 (2006).
[9] P. Exner, S.A. Vugalter. On the number of particles that a curved quantum waveguide can bind. *J. Math. Phys.*, **40**, P. 4630–4638 (1999).
[10] S.I. Popov, M.I. Gavrilov, I.Yu. Popov. Two interacting particles in deformed nanolayer: discrete spectrum and particle storage. *Phys. Scr.*, **3** (6), P. 17–23 (2012).
[11] A. Messiah. *Quantum mechanics*. V. 2. Moscow.: Nauka, 1979, 583 p.

NANOSYSTEMS: PHYSICS, CHEMISTRY, MATHEMATICS, 2013, 4 (4), P. 564–569

ELECTROPHYSICAL PROPERTIES OF CNT. THE AUGMENTED CYLINDRICAL WAVE METHOD

A. V. Pak[1], M. B. Belonenko[2,3], P. N. Dyachkov[4]

[1] Volgograd State University, 400062, Volgograd, Russia
[2] Entropique Inc., London, N6J 3S2, ON, Canada
[3] Volgograd Institute of Business , 400048, Volgograd, Russia
[4] Institute of General and Inorganic Chemistry named after N.C. Kurnakov RAS, Moscow, Russia

pak.anastasia@gmail.com

PACS 71.10.Fd, 72.80.Vp

Current-voltage characteristics of tunnel contact between semiconducting (and conducting) carbon nanotubes (CNT) of various diameters and system of periodically located quantum dots (and also in contact to metal) was obtained using density of states (DOS) investigation. DOS has been calculated by means of the method of attached cylindrical waves. At certain parameters for quantum dots, the current-voltage characteristics observed testify to the presence of negative differential conductivity.

Keywords: carbon nanotubes, density of the states, current-voltage characteristics.

1. Introduction

In the last few years, the interest of many researchers has been focused on the properties of carbon nanotubes [1]. It is known from classical works that the "Arm-chair" type of nanotube, in Huckel's approximation, are conductors at any temperature [2]. However, using the linear augmented cylindrical wave (LACW) method allows a gap in the band structure of this type of nanotube. This makes it possible to use them in different applications. The simplest method to experimentally verify the change in the state density is to study the tunneling current [3, 4], for example, of the contact with quantum dots. In these papers, the density of states were calculated by the method of Green's functions [5], however, not every system has a density of states for electrons can be determined analytically. For such a system, the more versatile method is based on ab initio calculations .

Theoretically, investigation was done by tight-binding calculations only, but it is known from the band structure theory of solids that the linear combination of atomic orbitals (LCAO) basis is adequate to achieve good results for the valence band, but not for the conduction band. The reason for this is that this basis does not include the delocalized conducting plane-wave type functions. As to the π electron band structure models, they are adequate for calculating the energy curves located in a Fermi level region only. Therefore, we have calculated the complete band structures of metallic armchair (n, n) CNTs with $4 < n < 100$ and zigzag semiconducting $(0, n)$ CNTs with $10 < n < 49$ indivisible by 3 in terms of a LACW method. The LACW method is just a reformulation of the linear augmented plane wave (LAPW) theory for cylindrical multiatomic systems. Its basis functions have both localized and delocalized components. Finally, the main argument for using cylindrical waves is to account for the cylindrical geometry of the nanotubes in an explicit form that offers obvious advantages [6].

2. Basic equations

2.1. Cylindrical muffin-tin potential

Similar to the LAPW technique used in the band structure theory of solids, we apply the muffin-tin (MT) and local density functional approximations for electronic potentials of tubules. However, the potential of a nanotube differs drastically from that of bulk material. Indeed, infinite motion of an electron is possible in any direction in a crystal, but it is obviously limited in the case of nanotubes by their size and cylindrical shape. Therefore, in terms of the LACW method, the atoms of nanotube are considered to be enclosed between two impenetrable cylinder-shaped potential barriers Ω_a and Ω_b, because there are two vacuum regions Ω_v on the outside and on the inside of the tubule. The radii a and b of these barriers are chosen so that the region confined by barriers accommodates a significant portion of the electron density of the tubule. Based on our previous calculations of the CNTs, we take $a = R_{NT}+2.3$ a.u., $b = R_{NT}+2.3$ a.u., where, R_{NT} is radius of the tubule. Finally, the electronic potential is spherically symmetrical in the regions of MT-spheres of atoms α and constant in the interspherical region. Inside these spheres, we calculate the electron potential by means of the local density approximation with Slater exchange. As usually, the radii of the MT spheres were chosen so that the atomic spheres touch, but do not overlap. Outside the MT spheres up to the impenetrable potential barriers Ω_a and Ω_b, the potential is approximated by a constant value taken to be the energy zero point [6,7].

2.2. Solution of the Schrdinger equation

The basis functions called LACWs are solutions of the Schrodinger equation for the interspherical and MT regions of tubule sewn together so that the resulting LACWs are continuous and differentiable anywhere in the system. In the interspherical region, the LACWs are the solutions of the Schrdinger equation for free electron movement in the infinitely long potential well between two impenetrable cylindrical potential barriers. Here, the solutions are the superpositions of the cylindrical Bessel functions of the first and second kinds. In any MT sphere, the solutions are expanded in terms of the spherical harmonic functions and the eigenfunctions of the radial Schrdinger equation. To obtain the basis wave functions, the solutions of Schrdinger equation in these two regions are matched on the surfaces of the MT spheres so that both the basis functions and their normal derivatives are continuous across these surfaces. The eigenfunctions of electrons in the tubule are the linear superpositions of these basis LACWs. The coefficients of the expansions of any eigenfunction in terms of these basis functions and the electron dispersion curves are defined by the variational method.

In this work, we apply the symmetry-adapted version of the LACW method developed previously. In this version, one takes into account that every single-walled CNT can be generated by first mapping only two nearest-neighbor C atoms onto a surface of a cylinder and then using the rotational and helical symmetry operators to determine the remainder of the tubule. With account of these symmetries, the cells contain only two carbon atoms, and the *ab initio* LACW theory becomes applicable to any tubule independent of the number of atoms in a translational unit cell. In the LACW studies, we use only this structural information as input parameters.

The dispersive relation for quantum wells is similar to the band structure of superlattice [8]:

$$E_{QD} = \varepsilon_0 - \Delta\cos(p),$$

where ε_0 is electron energy in quantum well, Δ is tunnel integral, defining by overlap of electron wave functions of nearest wells.

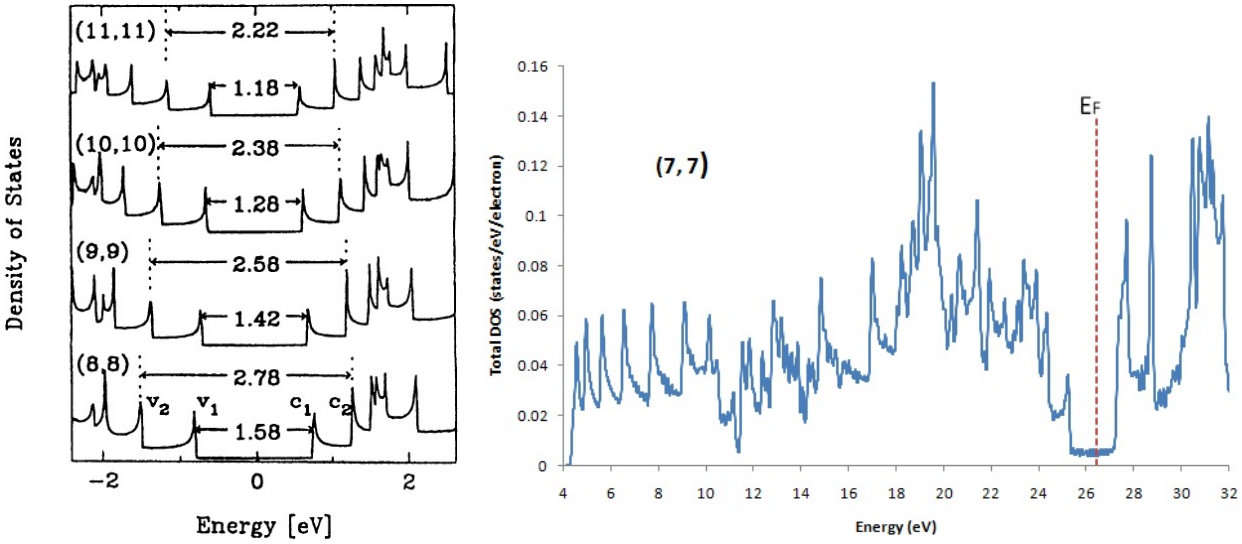

a) b)

FIG. 1. Density of states for CNT arm-chair type: a) Huckel's approximation; b) LACW method

The density of states for arm-chair CNTs, calculated under the π-electron approximation [2], was shown in Fig. 1a. The LACW method allows in the calculation consideration of more deep-seated σ-orbital electrons at very high temperatures ($\sim$ 25–27 eV) to get a gap in the energy spectrum (see Fig. 1b). This fact allowed the calculation of the electrical properties of conductive nanotubes in contact with the quantum dots.

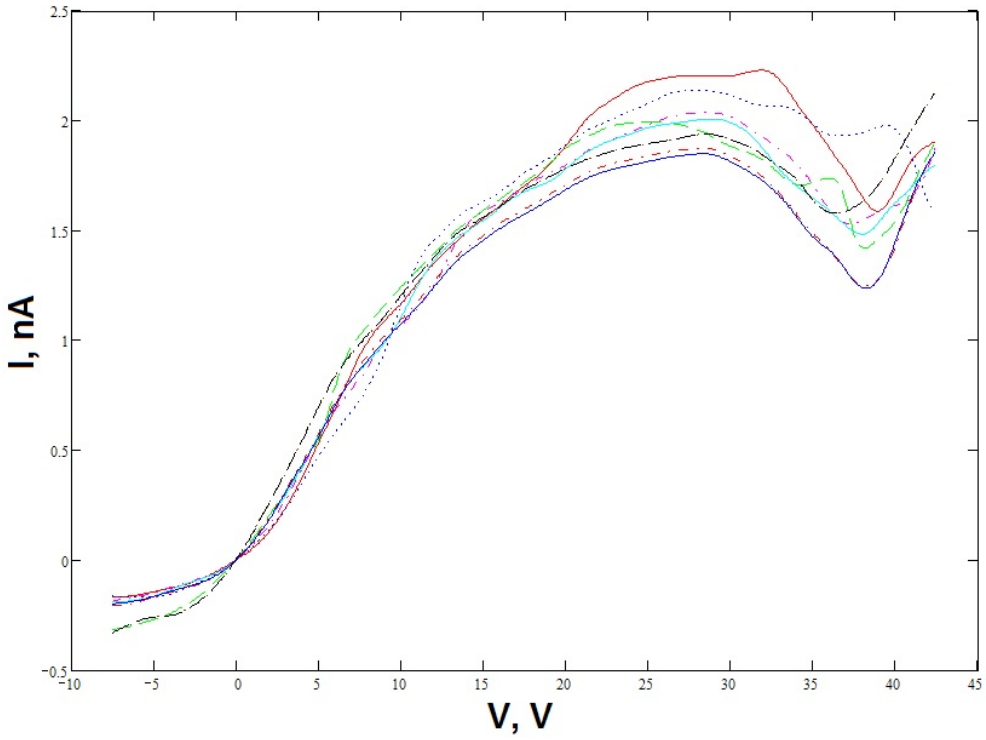

FIG. 2. Current-voltage characterictics for CNT type "zig-zag" of various diameter ((10, 0) – (50, 0)) in contact with quantum dots system

3. Tunnel characteristics

In order to study tunneling effects, we will set Hamiltonian of our model in a form:

$$H = \sum_p \varepsilon_p^A a_p^+ a_p + \sum_q \varepsilon_q^B b_q^+ b_q + \sum_{pq} T_{pq}(a_p^+ b_q + b_q^+ a_q), \tag{1}$$

where a_p^+, a_p - production (annihilation) operators of electrons with a momentum p in carbon nanotubes; ε_p^A - electron energy spectrum of nanotubes (1); T_{pq} - matrix element of the operator of tunneling between conditions p and q; b_q^+, b_q - creation (annihilation) operators of electrons with an momentum q in matter, resulted in contact with carbon nanotubes; ε_p^B - electron energy spectrum of quantum dots. Note, that in (1) p and q are multi-indices. Also, if we consider the external electric field $\vec{E}$ which we will investigate using the gauge: $\vec{E} = -\frac{1}{c}\frac{\partial \vec{A}}{\partial t}$, it is possible to take it into account by means of replacement the corresponding momentum components: $p \to p - eA/c$.

Defining a tunnel current as [5]:

$$J = ie \sum_{pq} \left(a_p^+ b_q - b_q^+ a_p\right), \tag{2}$$

and carrying out calibration transformation [5]:

$$a_p \to S^{-1} a_p S,$$
$$S = \exp\left(ieVt \sum_p a_p^+ a_p\right),$$

where V applied, for definiteness, to CNT voltage, - electron charge, it is possible to reduce formally a problem about calculation characteristic current-voltage to calculation of the response of the operator: $J_t = ie \sum_{pq} \left(a_p^+ b_q e^{ieVt} - b_q^+ a_q e^{-ieVt}\right)$ on external action [5]:

$$H_t = \sum_{pq} T_{pq} \left(a_p^+ b_q e^{ieVt} + b_q^+ a_q e^{-ieVt}\right).$$

Within the framework of Kubo theory, the answer is set by the formula:

$$\begin{gathered} J = 4\pi e \left|T\right|^2 \int\limits_{-\infty}^{\infty} d\varepsilon \nu_A\left(\varepsilon + eV\right) \nu_B\left(\varepsilon\right) \left(n_f(\varepsilon) - n_f(\varepsilon + eV)\right), \\ \nu_A\left(\varepsilon\right) = \sum_p \delta\left(\varepsilon - \varepsilon_p^A\right), \quad \nu_B\left(\varepsilon\right) = \sum_q \delta\left(\varepsilon - \varepsilon_q^B\right), \end{gathered} \tag{3}$$

where $\delta(x)$ - Dirac delta-function, $\nu_{A(B)}\left(\varepsilon\right)$ - tunnel density of states; $n_f\left(\varepsilon\right)$ - equilibrium number of fermions with energy ε. We used the approach of "rough" contact: $T_{pq} = T$ (a nanotube is perpendicular to the quantum dot surface). After integrals calculation entering in (3) it is easy to obtain current-voltage characteristic of the contact presented in Fig. 2–3.

The existence of a descending section of the current-voltage characteristic of the tunneling conductance between the nanotubes and the quantum dots system can be clearly seen in Fig. 2. This indicates the presence of negative differential conduction. The descending section is observed at the same parameters of quantum dots: $\varepsilon_0 = 22$ eV - energy of electrons a quantum

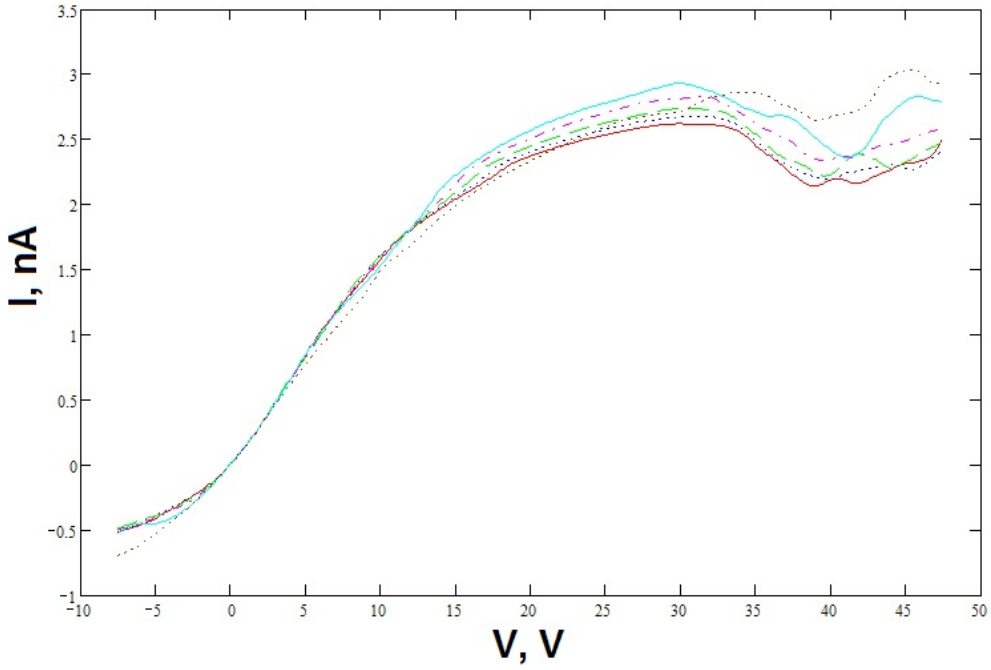

FIG. 3. Current-voltage characteristics for CNT type "arm-chair" of various diameter ((4,4) – (9,9)) in contact with quantum dots system

hole, and $\Delta = 3$ eV - the tunnel integral defined by overlapping of wave electronic functions of the next holes. The size of the resistance obtained in such a system was $R \approx -24$ kOhm.

Similarly, the current-voltage characteristics for semiconducting CNT of various diameters ((10,0)–(50,0)) in contact with systems of quantum dots are represented in Fig. 2. For semiconducting CNT in contact with a quantum dots system, the descending section in the current-voltage, characteristic of tunnel conductivity, was also observed. The resistance obtained for such a system was $R \approx -18$ kOhm (should be -18 kOhm) for the same parameters of the quantum dots system.

It should be noted that the descending section in CVC for system CNT-QD is absent in the case of pi-approximation for CNT DOS.

The obtained dependencies can have the important practical applications for studying noncontact and the design of tunneling diodes based on carbon nanotubes.

4. The conclusion

In summary we will formulate the basic conclusions from the made work.

(1) Current-voltage characteristics of contacts CNT - a superlattice of quantum dots are obtained.
(2) The descending section with negative differential conduction is observed for certain characteristics of quantum dots. This effect can be used to create various frequency amplifiers.

References

[1] E.G. Rakov. Carbon nanotubes in new materials. *Russian Chemical*, **82** (1), P. 27–47 (2013).
[2] P. Harris. Carbon nanotubes and related structures. *New materials of XXI centures*. Tehnosphera, Moscow: 2003. 336 p.
[3] M.B. Belonenko, N.G. Lebedev, A.V. Pak. Tunneling current of the contact impurity Graphene nanoribbon - quantum dots. *Russian Physics Journal*, **55** (6), P. 644–648 (2012).

[4] M.B. Belonenko, A.V. Pak, N.G. Lebedev. Tunnel current between impurity graphene nanoribbons. *Semiconductors*, **47** (5), P. 649–651 (2013).
[5] L.S. Levitov, A.V. Shitov. *Green's functions. Problems with solutions* [In Russian]. Fizmatlit, oscow: 2003, 392 p.
[6] P.N. D'yachkov, H. Hermann, D.V. Kirin. Electronic structure and interband transitions of metallic carbon nanotubes. *Appllied Physics Letters*, **81**, P. 5228–5231 (2002).
[7] P.N. D'yachkov, O.M. Kepp. Science and Application of Nanotubes, D. Tomanek Ed. NY, Plenum, P. 77–82 (2000).
[8] A.P. Silin. Semiconductive superlattice [In Russian]. *Physics-Uspekhi*, **147** (3), P. 485–516 (1985).

NANOSYSTEMS: PHYSICS, CHEMISTRY, MATHEMATICS, 2013, 4 (4), P. 570–576

MODEL OF THE INTERACTION OF POINT SOURCE ELECTROMAGNETIC FIELDS WITH METAMATERIALS

K. V. Pravdin, I. Yu. Popov

Saint Petersburg National Research University of Information Technologies, Mechanics and Optics, Saint Perersburg, Russia

construeman@gmail.com, popov1955@gmail.com

PACS 81.05.Xj, 78.67.Pt

We consider Green's function for layered system. We express it in terms of the well-known scalar s and p ones. For a single NIM layer in vacuum and with a single dispersive Lorentz form for equal electric and magnetic permeabilities $\varepsilon(\omega)$ and $\mu(\omega)$, we obtain an explicit form for Green's function. Also we find Green's function for multilayered system and obtain recurrence relations for its coefficients.

Keywords: metamaterial, point perturbation, refraction, NIM, Maxwell's equations.

1. Introduction

Metamaterials are artificial materials engineered to have properties that may not be found in nature. In particular, they may have negative refractive index. Such materials are called negative index materials (NIMs). In general, a NIM system is defined by the property that for certain frequencies ω the electric permeability $\varepsilon(\omega)$ or the magnetic permeability $\mu(\omega)$ becomes negative. The NIM situation is the case where both at the same frequency $\hat{\omega}$ become negative and are equal –1. Recently, NIMs have come under increased scrutiny (see [1], [2]).

The existence of NIMs has been debated in previous theoretical literature (see [3–8]). In particular, the sign of the index of refraction, which involves taking a square root $n = \pm\sqrt{\varepsilon\mu}$, has been the subject of discussion. Naively it equals +1, in both vacuum and a NIM system but this result is challenged for the NIM situation. The use of the phenomenological Maxwell's equations should solve possible ambiguities.

2. Model

As in [9], where the following model is fully described, the starting point is the set of phenomenological Maxwell's equations for the case where the permanent polarization and magnetization are absent ($\varepsilon_0 = \mu_0 = 1$),

$$\begin{gathered}\partial_t D(x,t) = \partial_x \times H(x,t), \quad \partial_t B(x,t) = -\partial_x \times E(x,t), \\ \partial_x \cdot D(x,t) = 0, \quad \partial_x \cdot B(x,t) = 0,\end{gathered} \tag{1}$$

with the constitutive equations

$$D(x,t) = E(x,t) + P(x,t), P(x,t) = \int_{t_0}^{t} ds \chi_e(x,t-s) \cdot E(x,t),$$

$$H(x,t) = B(x,t) - M(x,t), \quad M(x,t) = \int_{t_0}^{t} ds \chi_m(x,t-s) \cdot H(x,t),$$

where $\chi_e(x,t)$ and $\chi_m(x,t)$ are the electric and magnetic susceptibility tensors. We assume that the system is dispersive, nonabsorptive and use causality and passivity conditions. Causality requires that the susceptibilities $\chi_e(x,t) = \chi_m(x,t) = 0$ for $t \leq t_0$ ($t_0 = 0$). Passivity means

that the electromagnetic energy $\varepsilon_{em}(t) = \frac{1}{2}\int dx \left\{E(x,t)^2 + H(x,t)^2\right\}$ cannot increase as a function of time. We use the Fourier transform,

$$\hat{f}(z) = \int_0^\infty dt \exp[izt]\, f(t), \quad f(t) = \frac{1}{2\pi}\int_\Gamma dz \exp[-izt]\, \hat{f}(t),$$

where Γ is a path running from $-\infty$ to $+\infty$ at some distance $\delta > 0$ parallel to the real axis, $z = \omega + i\delta$, $\delta \to 0$ ($\Im z > 0$). We consider the isotropic system, $\hat{\chi}(x,z) = \hat{\chi}(x,z)U$ where U is the unit matrix 3×3, and we are dealing with a single dispersive Lorentz contribution $\varepsilon(\omega) = \mu(\omega) = 1 - \dfrac{\Omega^2}{\omega^2 - \omega_0^2}$. Then $\hat{\omega} = \sqrt{\omega_0^2 + \dfrac{\Omega^2}{2}}$ is the NIM frequency as $\varepsilon(\pm\hat{\omega}) = \mu(\pm\hat{\omega}) = -1$.

Maxwell's equations (1) can be expressed in terms of Fourier transforms,

$$L^e(z)\cdot\hat{E}(x,z) = g^e(x,z), \quad L^m(z)\cdot\hat{H}(x,z) = g^m(x,z),$$

where

$$\begin{aligned}
L^e(z) &= z^2\varepsilon(x,z) + (\in\cdot p)\cdot\mu(x,z)^{-1}\cdot(\in\cdot p),\\
L^m(z) &= z^2\mu(x,z) + (\in\cdot p)\cdot\varepsilon(x,z)^{-1}\cdot(\in\cdot p),\\
g^e(x,z) &= izE(x,0) + i(\in\cdot p)\cdot\left\{\mu(x,z)^{-1}\cdot H(x,0)\right\},\\
g^m(x,z) &= izH(x,0) - i(\in\cdot p)\cdot\left\{\varepsilon(x,z)^{-1}\cdot E(x,0)\right\}.
\end{aligned}$$

Here $L^e(z)$ and $L^m(z)$ are the electric and magnetic Helmholtz operators, $\in$ is the Levi-Civita symbol, and $p = -i\partial_x$ so $(\in\cdot p)\cdot f = i\partial_x \times f$. Let now

$$R^e(z) = L^e(z)^{-1}, \quad R^m(z) = L^m(z)^{-1}.$$

Then

$$\hat{E}(x,z) = R^e(z)\cdot g^e(x,z), \quad \hat{H}(x,z) = R^m(z)\cdot g^m(x,z).$$

Next we introduce Green's functions

$$\begin{aligned}
G^{e,m}(x,y,z) &= \langle x|R^{e,m}|y\rangle,\\
L^{e,m}(z)\cdot G^{e,m}(x,y,z) &= \delta(x-y)U.
\end{aligned}$$

Then $E(x,t)$ is given by the inverse Fourier transform of

$$\hat{E}(x,z) = \int dy G(x,y,z)\cdot g(y,z),$$

where $g(y,z)$ is some integrable initial field configuration or an external current density.

We only consider the electric Green's function and drop the superscript e. We also assume that the system is layered, and layers are parallel to the X_1X_2-plane and there is the translation invariance in the X_1 and X_2 directions (the three Cartesian axes are denoted by X_1, X_2 and X_3 with corresponding unit vectors e_1, e_2 and e_3). Then the permeabilities only depend on x_3,

$$\varepsilon(x,z) = \varepsilon(x_3,z) = \varepsilon_j(z), \quad \mu(x,z) = \mu(x_3,z) = \mu_j(z).$$

We denote $x = x_3$, $y = y_3$ and let $k = (k_1,k_2,k_3)$, $\kappa = (k_1,k_2,0) = \kappa e_\kappa = k^\perp \perp e_3$,

$$\zeta^2(x,\kappa,z) = z^2\varepsilon(x,z)\mu(x,z) - \kappa^2.$$

We obtain

$$\begin{aligned}
G(x,y,z) &= \frac{1}{2\pi}\int d\kappa \exp[-i\kappa\cdot(x^\perp - y^\perp)]\, G_\kappa(x,y,z),\\
G_\kappa(x,y,z) &= G_s(x,y,z,\kappa) + G_p(x,y,z,\kappa),
\end{aligned}$$

where

$$G_s(x,y,z,\kappa) = G_s(x,y,z,\kappa)\, e_3 \times e_\kappa e_3 \times e_\kappa,$$

$$G_p(x,y,z,\kappa) = \left(e_\kappa + \frac{i\kappa}{\zeta(x)^2}\partial_x e_3\right)\left(e_\kappa - \frac{i\kappa}{\zeta(y)^2}\partial_x e_3\right) G_p(x,y,z,\kappa),$$

s-polarization part G_s and p-polarization part G_p of Green's function are scalar and satisfy

$$\left\{z^2\varepsilon(x,z) - p\frac{z^2\varepsilon(x,z)}{\zeta(x,\kappa,z)^2}p\right\} G_p(x,y,z,\kappa) = \delta(x-y),$$

$$\left\{\frac{\zeta(x,\kappa,z)^2}{\mu(x,z)} - p\frac{1}{\mu(x,z)}p\right\} G_s(x,y,z,\kappa) = \delta(x-y).$$

3. Results

3.1. Single NIM layer

In [9] the simplest layered system, i.e., two half spaces filled with NIM and vacuum was considered and the expressions for Green's function were found. In our investigation we considered the single NIM layer in a vacuum,

$$\varepsilon(x,z) = \begin{cases} \varepsilon(z), & x \in (a,b) \\ 1, & x \notin (a,b) \end{cases}, \quad \mu(x,z) = \begin{cases} \mu(z), & x \in (a,b) \\ 1, & x \notin (a,b) \end{cases}$$

with point perturbation located in a vacuum ($y < a$). For G_s, G_p with frequencies $z = \pm\hat{\omega}$ we find explicit expressions for case $\hat{\omega} > \kappa$ (radiative regime) and expressions in asymptotic form for case $\hat{\omega} < \kappa$ (evanescent regime) the same way [9]. We denote

$$\rho(\hat{\omega}) = \sqrt{\left|\omega^2\left(1 - \Omega^2/\left(\omega^2 - \omega_0^2\right)\right)^2 - \kappa^2\right|}.$$

In the reflection case ($x, y < a < b$), the receiver located in x and the point perturbation located in y are on the one side of the layer (see Fig. 1), and for $\hat{\omega} > \kappa$,

$$G_p(x,y,\pm\hat{\omega}) = \pm\frac{\rho(\hat{\omega})}{2i\hat{\omega}^2}\exp[\pm i\rho(\hat{\omega})|x-y|],$$

$$G_s(x,y,\pm\hat{\omega}) = \pm\frac{1}{2i\rho(\hat{\omega})}\exp[\pm i\rho(\hat{\omega})|x-y|],$$

where the term responsible for reflection is absent, i.e., there is no reflection at the frequencies $\pm\hat{\omega}$ for which $\varepsilon(\pm\hat{\omega}) = \mu(\pm\hat{\omega}) = -1$.

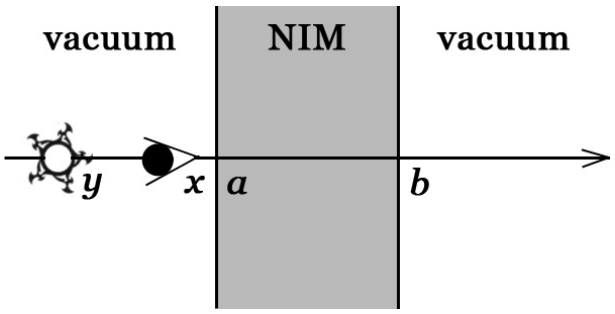

FIG. 1. Reflection case $(x > y)$

For $\hat{\omega} < \kappa$,

$$G_p(x,y,z) \overset{z\to\pm\hat{\omega}}{\sim} \frac{\rho(\hat{\omega})}{2\hat{\omega}^2}\exp\left[-\rho(\hat{\omega})|x-y|\right] + \frac{\Omega^2}{4\hat{\omega}^2\kappa^2}\frac{\rho(\hat{\omega})^3\left(1-4\rho(\hat{\omega})^2\right)}{(z-\hat{\omega})(z+\hat{\omega})}\exp\left[-\rho(\hat{\omega})(a-x+a-y)\right],$$

$$G_s(x,y,z) \overset{z\to\pm\hat{\omega}}{\sim} -\frac{1}{2\rho(\hat{\omega})}\exp\left[-\rho(\hat{\omega})|x-y|\right] + \frac{\Omega^2}{4\kappa^2}\frac{\rho(\hat{\omega})\left(1-4\rho(\hat{\omega})^2\right)}{(z-\hat{\omega})(z+\hat{\omega})}\exp\left[-\rho(\hat{\omega})(a-x+a-y)\right],$$

where the reflection term is still present, but we encounter dampening behavior, typical for the evanescent situation.

In the refraction case ($y < a < x < b$), the receiver is in the NIM layer (see Fig. 2), and for $\hat{\omega} > \kappa$,

$$G_p(x,y,\pm\hat{\omega}) = \pm\frac{\rho(\hat{\omega})}{2i\hat{\omega}^2}\exp\left[\pm i\rho(\hat{\omega})(a-x+a-y)\right],$$
$$G_s(x,y,\pm\hat{\omega}) = \pm\frac{1}{2i\rho(\hat{\omega})}\exp\left[\pm i\rho(\hat{\omega})(a-x+a-y)\right],$$

for $\hat{\omega} < \kappa$,

$$G_p(x,y,z) \overset{z\to\pm\hat{\omega}}{\sim} \frac{\Omega^2}{4\hat{\omega}^2\kappa^2}\frac{\rho(\hat{\omega})^3\left(1+4\rho(\hat{\omega})^2\right)}{(z-\hat{\omega})(z+\hat{\omega})}\exp\left[-\rho(\hat{\omega})(x-y)\right] - \frac{2\rho(\hat{\omega})^3}{\hat{\omega}^2}\exp\left[-\rho(\hat{\omega})(a-x+a-y)\right],$$

$$G_s(x,y,z) \overset{z\to\pm\hat{\omega}}{\sim} -\frac{\Omega^2}{4\kappa^2}\frac{\rho(\hat{\omega})\left(1+4\rho(\hat{\omega})^2\right)}{(z-\hat{\omega})(z+\hat{\omega})}\exp\left[-\rho(\hat{\omega})(y-x)\right] - 2\rho(\hat{\omega})\exp\left[-\rho(\hat{\omega})(a-x+a-y)\right].$$

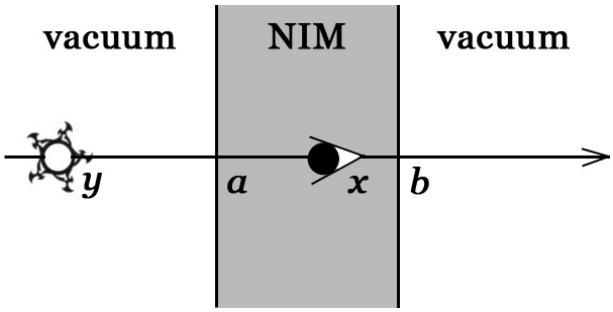

FIG. 2. Refraction case

In the transmission case ($y < a < b < x$), the receiver and point field source are located on different sides the NIM (see Fig. 3), for $\hat{\omega} > \kappa$,

$$G_p(x,y,\pm\hat{\omega}) = \pm\frac{\rho(\hat{\omega})}{2i\hat{\omega}^2}\exp\left[\pm i\rho(\hat{\omega})\left(x-y-2(b-a)\right)\right],$$
$$G_s(x,y,\pm\hat{\omega}) = \pm\frac{1}{2i\rho(\hat{\omega})}\exp\left[\pm i\rho(\hat{\omega})\left(x-y-2(b-a)\right)\right],$$

for $\hat{\omega} < \kappa$,

$$G_p(x,y,z) \overset{z\to\pm\hat{\omega}}{\sim} -\frac{2\rho(\hat{\omega})^3}{\hat{\omega}^2} \exp\left[-\rho(\hat{\omega})\left(x-y-2(b-a)\right)\right],$$
$$G_s(x,y,z) \overset{z\to\pm\hat{\omega}}{\sim} 2\rho(\hat{\omega}) \exp\left[-\rho(\hat{\omega})\left(x-y-2(b-a)\right)\right].$$

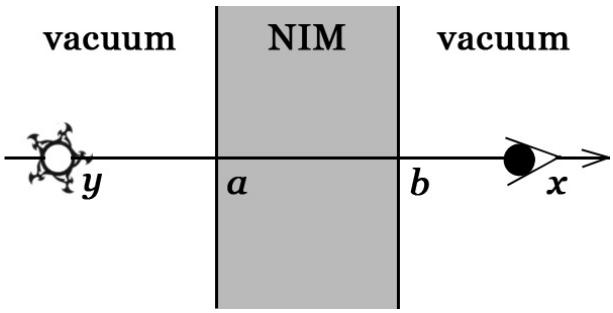

FIG. 3. Transmission case

In retrieving $E(x,t)$, the pole contributions in Green's function give rise to terms that oscillate in time according to $\exp[\pm i\hat{\omega}t]$, so no dampening occurs in a time dependent fashion, a property observed earlier in [2] for the single layer case.

3.2. Multilayered system

Also, we find Green's function for the multilayered system. The point perturbation is located in layer number 0. There are n layers in the positive direction of the x-axis and m layers in the negative, $m+n+1$ layers in total (see Fig. 4).

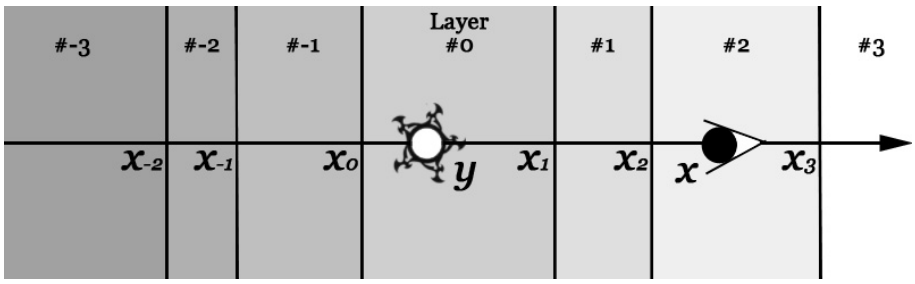

FIG. 4. Multilayered system

Let $\varepsilon(x,z) = \varepsilon_k(z)$ and $\mu(x,z) = \mu_k(z)$ if $x \in (x_k, x_{k+1})$, where $k = -m, \ldots, n$, $x_{-m} = -\infty$, $x_{n+1} = +\infty$. We consider below only the p-polarized part Green's function, omitting subscript p,

$$G(x,y,z) =$$

$$
= \begin{cases}
D_{-m}e^{-i\zeta_{-m}x}, & x \in (-\infty,\ x_{-(m-1)});\\
B_{-(m-1)}e^{-i\zeta_{-(m-1)}x} + C_{-(m-1)}e^{-i\zeta_{-(m-1)}x} + D_{-(m-1)}e^{-i\zeta_{-(m-1)}x}, & x \in (x_{-(m-1)},\ x_{-(m-2)});\\
A_{-(m-2)}e^{-i\zeta_{-(m-2)}x} + B_{-(m-2)}e^{-i\zeta_{-(m-2)}x} + C_{-(m-2)}e^{-i\zeta_{-(m-2)}x} + & \\
+D_{-(m-2)}e^{-i\zeta_{-(m-2)}x}, & x \in (x_{-(m-2)},\ x_{-(m-3)});\\
\dots & \dots\\
A_{-1}e^{-i\zeta_{-1}x} + B_{-1}e^{-i\zeta_{-1}x} + C_{-1}e^{-i\zeta_{-1}x} + D_{-1}e^{-i\zeta_{-1}x}, & x \in (x_{-1},\ x_0);\\
A_0e^{-i\zeta_0x} + B_0e^{-i\zeta_0x} + C_0e^{-i\zeta_0x} + D_0e^{-i\zeta_0x} + E_-e^{-i\zeta_0x}, & x \in (x_0,\ y);\\
A_0e^{-i\zeta_0x} + B_0e^{-i\zeta_0x} + C_0e^{-i\zeta_0x} + D_0e^{-i\zeta_0x} + E_+e^{i\zeta_0x}, & x \in (y,\ x_1);\\
A_1e^{-i\zeta_1x} + B_1e^{-i\zeta_1x} + C_1e^{-i\zeta_1x} + D_1e^{-i\zeta_1x}, & x \in (x_1,\ x_2);\\
\dots & \dots\\
A_{n-2}e^{-i\zeta_{n-2}x} + B_{n-2}e^{-i\zeta_{n-2}x} + C_{n-2}e^{-i\zeta_{n-2}x} + D_{n-2}e^{-i\zeta_{n-2}x}, & x \in (x_{n-2},\ x_{n-1});\\
A_{n-1}e^{-i\zeta_{n-1}x} + B_{n-1}e^{-i\zeta_{n-1}x} + C_{n-1}e^{-i\zeta_{n-1}x}, & x \in (x_{n-1},\ x_n);\\
A_ne^{-i\zeta_nx}, & x \in (x_n,\ +\infty).
\end{cases}
$$

Here coefficients $A_\bullet$ are for waves that come from left outside of current layer, coefficients $B_\bullet$ are for waves reflected from the nearest left interface, coefficients $C_\bullet$ are for waves reflected from the nearest right interface and coefficients $D_\bullet$ are for waves that come from right outside of current layer. Coefficients $E_\pm$ are for waves that come direct from point perturbation located in y. We denote

$$\zeta_i^2(\kappa, z) = z^2\varepsilon_i(z)\mu_i(z) - \kappa^2,$$
$$K_0 = \frac{\zeta_0}{2iz^2\varepsilon_0}, \quad \lambda_{i,j}^{\pm} = \frac{\varepsilon_i\zeta_j \pm \varepsilon_j\zeta_i}{\varepsilon_i\zeta_j}$$

and introduce the Fresnel reflection coefficients

$$r_{i,j} = -\frac{\varepsilon_i\zeta_j - \varepsilon_j\zeta_i}{\varepsilon_i\zeta_j + \varepsilon_j\zeta_i} \quad \text{or} \quad r_{i,j} = -\frac{\lambda_{i,j}^-}{\lambda_{i,j}^+}.$$

As is easy to see $r_{j,i} = -r_{i,j}$. After some calculations, we obtain $E_\pm = K_0e^{\mp i\zeta_0 y}$ that means $E_\pm e^{\pm i\zeta_0 x} = K_0e^{i\zeta_0|x-y|}$ and Green's function is the same for $x \in (x_0,\ x_1)$. Denoting

$$a_k = 2e^{-i\zeta_k x_k}, b_k = \lambda_{k,k-1}^+ e^{-i\zeta_{k-1}x_k}, \quad c_k = 2e^{i\zeta_k x_k}, d_k = \lambda_{k,k-1}^- e^{-i\zeta_{k-1}x_k},$$
$$e_k = 2e^{i\zeta_k x_{k+1}}, f_k = \lambda_{k,k+1}^+ e^{i\zeta_{k+1}x_{k+1}}, \quad g_k = 2e^{-i\zeta_k x_{k+1}}, h_k = \lambda_{k,k+1}^- e^{i\zeta_{k+1}x_{k+1}}$$

we obtain for $k = 1, \dots, (n-1)$,

$$A_k = \alpha_k A_n, \quad B_k = \frac{d_k}{c_k}\gamma_k A_n, \quad C_k = \frac{h_k}{g_k}\alpha_{k+1}A_n, \quad D_{k-1} = \alpha_k A_n,$$

for $k = -(m-1), \dots, 0$,

$$A_k = \alpha_k A_n + \beta_k, \quad B_k = \frac{d_k}{c_k}\left(\gamma_k A_n + \delta_k\right), \quad C_k = \frac{h_k}{g_k}\left(\alpha_{k+1}A_n + \delta_{k+1}\right), \quad D_{k-1} = \alpha_k A_n + \delta_k,$$

but $C_0 = \dfrac{h_0}{g_0}\alpha_1 A_n$ and $A_{-(m-1)} = 0$, where α_k, β_k, γ_k, δ_k satisfy the following recurrence relations

$$\alpha_k = \tilde{\alpha}_k \alpha_{k+1} - \left(\frac{a\,d}{b\,c}\right)_k \gamma_{k+1} \quad \text{and} \quad \alpha_{n-1} = \tilde{\alpha}_{n-1},$$

where

$$\tilde{\alpha}_k = \frac{f_k}{e_k}\left(1 - \left(\frac{a\,d\,e\,h}{b\,c\,f\,g}\right)_k\right),$$

$$\gamma_k = \frac{a_k}{b_k}\left(\frac{h_k}{g_k}\alpha_{k+1} + \gamma_{k+1}\right) \quad \text{and} \quad \gamma_{n-1} = \left(\frac{a\,h}{b\,g}\right)_{n-1},$$

$$\beta_k = \tilde{\alpha}_k \beta_{k+1} - \left(\frac{a\,d}{b\,c}\right)_k \delta_{k+1} \quad \text{and} \quad \beta_0 = K_0\left(e^{-i\zeta_0 y} - \left(\frac{a\,d}{b\,c}\right)_0 e^{i\zeta_0 y}\right),$$

$$\delta_k = \frac{a_k}{b_k}\left(\frac{h_k}{g_k}\beta_{k+1} + \delta_{k+1}\right) \quad \text{and} \quad \delta_0 = K_0\frac{a_0}{b_0}e^{i\zeta_0 y}.$$

Here we use the notation $\left(\frac{a\,d}{b\,c}\right)_k = \frac{a_k d_k}{b_k c_k}$. Hence coefficients $A_\bullet$, $B_\bullet$, $C_\bullet$, and $D_\bullet$ depend on A_n. In our investigation we obtain

$$A_n = -\frac{\beta_{-(m-1)}}{\alpha_{-(m-1)}}.$$

Solving these recurrence relations and finding the explicit expressions for Green's function is the actual problem.

Acknowledgments

The work was supported by Federal Targeted Program "Scientific and Educational Human Resources for Innovation-Driven Russia" (contract 16.740.11.0030), grant 11-08-00267 of Russian Foundation for Basic Researches, Federal Targeted Program "Researches and Development in the Priority Directions Developments of a Scientific and Technological Complex of Russia 2007-2013" (state contract 07.514.11.4146) and grants of the President of Russia (state contract 14.124.13.2045-MK and grant MK-1493.2013.1).

References

[1] V.G. Veselago. The electrodynamics of substances with simultaneously negative values of ε and μ. *Sov. Phys. Usp.*, **10**, P. 509–514 (1968).
[2] J.B. Pendry. Negative refraction makes a perfect lens. *Phys. Rev. Lett.*, **85**, P. 3966–3969 (2000).
[3] G.W. Hooft. A comment on the letter by J.B. Pendry. *Phys. Rev. Lett.*, **87**, P. 249701 (2001).
[4] P.M. Valanju, R.M. Walser. Wave refraction in negative-index media: always positive and very inhomogeneous. *Phys. Rev. Lett.*, **88**, P. 187401 (2002).
[5] N. Garcia, M. Nieto-Vesperinas. Left-handed materials do not make a perfect lens. *Phys. Rev. Lett.*, **88**, P. 207403 (2002).
[6] M. Nieto-Vesperinas. Problem of image superresolution with a negative-refractive-index slab. *J. Opt. Soc. Am.*, **21** (4), P. 491–8 (2004).
[7] D. Maystre, S. Enoch. Perfect lenses made with left-handed materials: Alice's mirror? *J. Opt. Soc. Am.*, **21**, P. 122–131 (2004).
[8] I. Stockman. Criterion for negative refraction with low optical losses from a fundamental principle of causality. *Phys. Rev. Lett.*, **98**, P. 177404 (2007).
[9] B. Gralak, A. Tip. Macroscopic Maxwell's equations and negative index materials. *J. Math. Phys.*, **51**, P. 052902 (2010).

NANO Ф&Х&М

NANOSYSTEMS:

PHYSICS, CHEMISTRY, MATHEMATICS

INFORMATION FOR AUTHORS

The journal publishes research articles and reviews, and also short scientific papers (letters) which are unpublished and have not been accepted for publication in other magazines. Articles should be submitted in English. All articles are reviewed, then if necessary come back to the author to completion.

The journal is indexed in Chemical Abstract Service of the American Chemical Society and in Russian Scientific Citation Index.

Author should submit the following materials:

1. Article file in English, containing article title, the initials and the surname of the authors, Institute (University), postal address, the electronic address, the summary, keywords, MSC or PACS index, article text, the list of references.
2. Files with illustrations, files with tables.
3. The covering letter in English containing the article information (article name, MSC or PACS index, keywords, the summary, the literature) and about all authors (the surname, names, the full name of places of work, the mailing address with the postal code, contact phone number with a city code, the electronic address).
4. The expert judgement on possibility of publication of the article in open press (for authors from Russia).

Authors can submit a paper and the corresponding files to the following addresses: nanojournal.ifmo@gmail.com, popov1955@gmail.com.

Text requirements

Articles should be prepared with using of text editors MS Word or LaTEX (preferable). It is necessary to submit a pdf copy. In the name of files the English alphabet is used. The recommended size of short communications (letters) is 4-6 pages, research articles – 6-15 pages, reviews – 30 pages.

Recommendations for text in MS Word:

Formulas should be written using Math Type. Figures and tables with captions should be inserted in the text. Additionally, authors present separate files for all figures and Word files of tables.

Recommendations for text in LaTex:

Please, use standard LaTex without macros and additional style files. The list of references should be included in the main LaTex file. Single LaTex file of the paper with the corresponding pdf file should be submitted.

References in the article text are given in square brackets. The list of references should be prepared in accordance with the following samples:

[1] N. Surname. *Book Title*. Nauka Publishing House, Saint Petersburg, 281 pp. (2000).
[2] N. Surname, N. Surname. Paper title. *Journal Name*, **1** (5), P. 17-23 (2000).
[3] N. Surname, N. Surname. Lecture title. In: Abstracts/Proceedings of the Conference, Place and Date, P. 17-23 (2000).
[4] N. Surname, N. Surname. Paper title (2010). URL: http://books.ifmo.ru/ntv.
[5] N. Surname, N. Surname. Patent Name. Patent No. 11111, Bul. No. 33, 5 pp. (2010).
[6] N. Surname, N. Surname. Thesis Title. Thesis for full doctor degree in math. and physics, Saint Petersburg, 105 pp. (2000).

Requirements to illustrations

Illustrations should be submitted as separate black-and-white files. Formats of files – jpeg, eps, tiff.

NANOSYSTEMS:

PHYSICS, CHEMISTRY, MATHEMATICS

Журнал зарегистрирован
Федеральной службой по надзору в сфере связи, информационных технологий и массовых коммуникаций
(свидетельство ПИ № ФС 77 - 49048 от 22.03.2012 г.)
ISSN 2220-8054

Учредитель: федеральное государственное бюджетное образовательное учреждение высшего профессионального образования «Санкт-Петербургский национальный исследовательский университет информационных технологий, механики и оптики»

Издатель: федеральное государственное бюджетное образовательное учреждение высшего профессионального образования «Санкт-Петербургский национальный исследовательский университет информационных технологий, механики и оптики»

Отпечатано в типографии «Фалкон Принт»
Адрес: 197101, г. Санкт-Петербург, ул. Большая Пушкарская, 54

Подписка на журнал НФХМ
На 2013 год подписка осуществляется через ОАО Агентство «Роспечать»
Подписной индекс 57385 в каталоге «Издания органов научно-технической информации»